MIT-334-70

EFFECT OF REACTOR IRRADIATION ON SANTOWAX WR:

1. Radiolysis Reaction Order and Fast Neutron Effect

2. Radiopyrolysis

(USAEC Research and Development Report
Contract No. AT(38-1) -334)

Department of Nuclear Engineering
Massachusetts Institute of Technology
Cambridge, Massachusetts 02139

(MITNE-78)

MIT-334-70
Reactor Technology
Standard TID-4500

EFFECT OF REACTOR IRRADIATION ON SANTOWAX WR:

1. Radiolysis Reaction Order and Fast Neutron Effect
2. Radiopyrolysis

by

E. A. Mason

T. H. Timmins

D. T. Morgan

W. N. Bley

DEPARTMENT OF NUCLEAR ENGINEERING

MASSACHUSETTS INSTITUTE OF TECHNOLOGY

CAMBRIDGE 39, MASSACHUSETTS

M.I.T. DSR PROJECT NO. 79819

Work Performed for the Savannah River Operations Office,

U. S. Atomic Energy Commission Under

Contract No. AT(38-1)-334

Issued: October, 1966

(MITNE-78)

ACKNOWLEDGMENT

Research on the effects of radiation on organic coolants has been carried out with an unusual degree of international cooperation in the sharing of preliminary results and planning of future programs. As a result, the activities of the various groups have been highly complementary and the various facilities have thus been most efficiently utilized. The authors of this report wish especially to acknowledge, and express their appreciation for, the contributions and hospitality of the Canadian groups at the AECL Chalk River and Whiteshell laboratories, the Euratom group at the Euratom Research Center (Ispra, Italy) and the French CEA and Progil groups at the CEA Grenoble and Saclay laboratories.

PREVIOUS RELATED REPORTS

MITNE-4	
MITNE-7	(IDO 11,101)
MITNE-9	(IDO 11,102)
MITNE-12	(IDO 11,103)
MITNE-21	(IDO 11,104)
MITNE-22	(IDO 11,105)
MITNE-29	(IDO 11,106)
MITNE-39	(IDO 11,107)
MITNE-41	(SRO-85)
MITNE-48	(SRO-87)
MITNE-55	(MIT-334-11)
MITNE-59	(MIT-334-12)
MITNE-63	(MIT-334-23)
MITNE-66	(MIT-334-33)
MITNE-68	(MIT-334-34)
MITNE-75	(MIT-334-48)

TABLE OF CONTENTS

Page

CHAPTER 3
PHYSICAL PROPERTIES AND HEAT TRANSFER

CHAPTER 4
LOW TEMPERATURE TERPHENYL DEGRADATION

CHAPTER 5
HIGH TEMPERATURE - LOW AVERAGE DOSE RATE IRRADIATIONS OF META-RICH TERPHENYL COOLANTS

LIST OF FIGURES

LIST OF TABLES

ABSTRACT

Santowax WR was irradiated in the M.I.T. In-Pile Loop Facility at 572°F (300°C) and 800°F (427°C). The irradiations were made in a stainless steel irradiation capsule installed in an unfueled sample assembly lined with cadmium in Fuel Position 20 of the MITR. The fast neutron fraction of the dose rate was 0.07 ± 0.01. Both steady-state and transient terphenyl concentration conditions were employed in the irradiations. Steady-state operating conditions were maintained by periodically removing coolant samples from the loop and distilling them to remove the high boilers (HB). The terphenyls and low and intermediate boilers (LIB) were returned to the circulating coolant in the loop along with fresh makeup coolant.

The fast neutron and gamma-ray dose rates were measured with adiabatic calorimeters and foil monitors. The MITR thermal power was raised from about 2 MW to about 5 MW during these irradiations. The average dose rate to the coolant was approximately 0.0066 watts/gram at 2 MW and approximately 0.016 watts/gram at 5 MW. The maximum dose rate to the coolant was 0.15 watts/gram and 0.38 watts/gram at 2 MW and 5 MW, respectively.

Three low temperature (300°C) irradiations of Santowax WR were made at different steady-state concentration levels in order to determine the apparent reaction order for radiolysis. The results of these runs, along with the results of recent Euratom steady-state irradiations of OM-2 coolant, indicated an apparent reaction order of radiolysis of 1.7 with respect to total terphenyl concentration. Using this reaction order, the low temperature irradiation data of M.I.T. and other laboratories were correlated well by a fast neutron effect ratio, G_N/G_γ, of 3.9 ± 0.4 for meta-rich terphenyl mixtures at 320°C. Ortho terphenyl was found to be less stable to gamma rays than meta terphenyl at this temperature.

At high temperatures (above 350°C), irradiated coolant was found to have higher first-order thermal decomposition (radiopyrolysis) rate constants than unirradiated coolant. The radiopyrolysis rate constants were calculated in the range 360°C to 450°C, and were compared with post-irradiation pyrolysis measurements of M.I.T. and other laboratories. The maximum uncertainty on these values appeared to be ±75% at 360°C, ±40% at 400°C, and ±15% at 450°C.

Procedures for estimating coolant makeup rates in organic-cooled reactors are presented and discussed.

Physical property measurements included density, viscosity, melting point and number average molecular weight. Heat transfer measurements showed that standard correlations could be used to determine the heat transfer rate using the bulk physical properties of irradiated coolant. The best correlation for all these data was $Nu = 0.023\ (Re)^{0.8}(Pr)^{0.4}$ ± 10%. No evidence of scale buildup or fouling of heat transfer surfaces was observed.

CHAPTER 1

SUMMARY

1.1 Introduction

The Organic Coolant Project at M.I.T. is a continuing effort to provide information concerning the performance of organic coolants in nuclear reactors. In particular, the radiolytic and pyrolytic degradation rates of terphenyl mixtures over a range of radiation conditions and temperatures have been measured, and the effect of the degradation products on the pertinent physical properties and heat transfer characteristics have been determined.

An in-pile loop is operated under steady-state conditions similar to those of an organic-cooled reactor at constant coolant concentration using batchwise removal of the coolant sidestream which is processed to remove the high boiling degradation products. The treated coolant plus virgin makeup organic coolant are then recharged to the loop. A transient mode of operation is used to lower the terphenyl concentration in the loop from one steady-state level to a lower steady-state level. The degradation rate of the coolant is measured during both the steady-state and transient modes of operation.

During the period May 10, 1965 to June 10, 1966, coolant irradiations were made in the in-pile loop at a fast neutron fraction of the total dose approximately equal to 0.07. The primary objectives of these irradiations were (1) to determine the relative degradation effects of fast neutrons compared to gamma rays by comparing the recent irradiation results at a low fast neutron fraction with earlier results at fast neutron fractions equal to 0.37 and 0.40, (2) to determine the apparent reaction order of radiolysis by measuring the terphenyl degradation rates at three different steady-state terphenyl concentrations, and (3) to determine the relative stabilities of the terphenyl isomers under different irradiation conditions.

An important part of the M.I.T. program has been to correlate the M.I.T. data with the terphenyl irradiation data obtained by other

laboratories. An empirical model has been proposed by M.I.T. for the correlation of organic coolant degradation data. The correlations of the data provided by this model permit the prediction of the rate of degradation of terphenyl coolants used in organic-cooled reactors over any range of feasible operating conditions. Because most of the experimental data obtained to date represent meta-rich terphenyl coolants, the correlations given in this report can be used with greater confidence to predict degradation rates for reactors utilizing such meta-rich coolants. Table 1.1 presents the composition and melting points of the most widely considered terphenyl mixtures for organic-cooled reactors.

An autoclave pyrolysis apparatus has been designed and built at M.I.T. for use in measuring thermal decomposition rates of irradiated and unirradiated organic coolants. Three pyrolysis runs have been completed at temperatures of 780°F and 800°F.

In conjunction with the degradation measurements, physical properties such as density and viscosity, as well as the heat transfer characteristics of the coolant, have been measured. The film formation characteristics of the irradiated coolants were also observed in the experimental program.

1.2 Loop Irradiation Procedure

The in-pile loop at M.I.T. is an all stainless steel system with a total circulating volume of about 5800 cc and is capable of operation to 800°F and 600 psig. A detailed description of the loop has been given by Morgan and Mason (1.1) and modifications of loop equipment are described in later M.I.T. reports (1.2, 1.3) and in Chapter 2 of this report.

The primary emphasis on organic coolant irradiation studies at M.I.T. has been placed on the determination of the terphenyl degradation rates as a function of radiation dose and temperature. Earlier work at M.I.T. (1.3) completed before January 1, 1965, investigated the degradation rates of Santowax WR and Santowax OMP from 425°F to 800°F at 37-40% fast neutron fraction. To determine the relative degradation effects of gamma rays compared to fast neutrons, the loop irradiation position in the MITR was changed in May, 1965, from the central fuel position (Position 1) to a peripheral fuel position (Fuel

Table 1.1

Typical Compositions and Melting Points of Common Organic Coolants

	Santowax OM	Santowax OMP	Santowax WR	OM-2	HB-40
Biphenyl, w/o	3	2	<2	<1	0
O-terphenyl, w/o	65	10	15-20	20	18
M-terphenyl, w/o	30	60	75	76	<0.5
P-terphenyl, w/o	2	28	5	4	<0.5
Hydro-terphenyls, w/o	0	0	0	0	82
High Boiler (HB), w/o	0	0	0	0	0
Melting Point[a] (unirradiated material), °F	178	350	185	185	Liquid at normal room temperatures

[a]Final liquidus point.

Position 20) in order to decrease the fast neutron fraction of the dose rate. To further lower the fast neutron fraction, a cadmium sheath, 24 inches long, was enclosed in an aluminum sample assembly (containing no fuel) before installation of the sample assembly into Fuel Position 20. In-Pile Section No. 3, which had an in-core volume of 280cc, was installed in this irradiation facility. The purpose of this cadmium sheath was to increase the gamma-ray dose rate by the conversion of thermal neutrons into gamma rays through the $Cd^{113}(n,\gamma)$ reaction. The cadmium liner increased the gamma-ray dose rate by a factor of about two and thus a fast neutron fraction, f_N, of 0.07 resulted.

The dose rates to the organic and the fast neutron and gamma-ray contributions were measured by adiabatic calorimetry and by threshold and resonance foil activation measurements. Since space limitations did not permit the insertion of calorimeters into the in-pile section, calorimetry measurements were made in a stainless steel thimble mock-up of the in-pile section, before installation of In-Pile Section No. 3 into Fuel Position 20 and following removal of In-Pile Section No. 3 from Fuel Position 20. During the period of coolant irradiations, foil dosimetry measurements were made approximately once a month (1) inside an aluminum monitor tube attached to the irradiation capsule, and (2) inside a stainless steel monitor tube at the radial center of the irradiation capsule.

The in-pile loop irradiations of Santowax WR in Fuel Position 20 began on May 10, 1965, and ended on June 10, 1966. Three steady-state runs and one transient run at 572°F (300°C) and one steady-state run and two transient runs at 800°F (427°C) were completed during this period. Steady-state conditions were maintained by adjusting the sampling cycle time so that the concentrations of total terphenyl and of high boiler (HB) were kept at constant levels (within 0-2%).

For the steady-state irradiations of Santowax WR in Fuel Position 20, a <u>High Boiler</u> distillation procedure was used in which the distillation temperature cutoff was adjusted so that a trace amount (< 0.2%) of para terphenyl was retained in the distillation pot. For earlier irradiations of Santowax WR in Fuel Position 1, a <u>Bottoms</u> distillation procedure was used. A higher temperature cutoff was

employed in the Bottoms distillation, compared to the High Boiler distillations, which permitted all the para-terphenyl and about 75% of the quaterphenyls to go over in the distillate. Each distillate was mixed with fresh Santowax WR and returned batchwise to the loop. The high boiler (HB) fraction of each sample was thus removed from the loop coolant.

1.3 Terphenyl Coolant Degradation

1.3.1 Major Variables Involved

The major variables which appear to have an effect on the coolant degradation rate are:

1. The coolant composition, including the concentration of the three individual terphenyl isomers and of total terphenyl (OMP) and also the concentrations of high boilers (HB), low and intermediate boilers (LIB) and total degradation products (DP).
2. The average specific dose rate and the local specific dose rate (watts/gram), and the fractions of fast neutrons and gamma rays making up the total dose rate.
3. The total absorbed specific dose and/or the total irradiation time.
4. The coolant irradiation temperature and the temperature profile around the loop.

The weight fraction of each of the terphenyl isomers in a given sample was determined by vapor phase chromatography. The high boiler (HB) concentrations were determined during steady periods of operation by the distillation of 140 or 300 gram samples. By definition, the DP concentration is (100-w/o OMP). LIB concentrations were determined during the steady-state periods by the difference between DP and HB concentrations.

The organic coolant temperature in the irradiation capsule and the temperature profile around the loop were measured by thermocouples spot-welded to various coolant lines and valves, and by immersion thermocouples in the surge tank, test heater, and in the

in-pile section. The temperature variation of the coolant around the loop was approximately 20°F.

1.3.2 Measurement and Calculation of Dose Rates

The MITR normally operates at full thermal power about four days per week and is shut down over the weekend. The nominal power level of the reactor was 1.95 thermal MW before October 15, 1965, and 4.90 thermal MW after November 1, 1965. The megawatt-hours (MWH) of reactor operation was adopted as a convenient scale of radiolytic exposure of the coolant, and the specific dose rate to the coolant (watts/gm) was directly related to the reactor power level by a dose rate factor, F^{SW} (watt-cc/MW-gm). This in-pile dose rate factor was determined by an axial integration of the dose rates to terphenyl calculated from calorimetry or foil dosimetry measurements at thirteen axial positions along the irradiation capsule. Figure 1.1 compares the axial variation of the total, fast neutron, and gamma-ray dose rates measured in Fuel Position 20 with those measured in Fuel Position 1. All data shown in Figure 1.1 were determined by adiabatic calorimetry measurements except the fast neutron dose rates in Fuel Position 20, which, because the neutron dose rates were so low, were determined by combined calorimetry and foil measurements.

Table 1.2 summarizes the dosimetry measurements in Fuel Position 20.

Table 1.2

Summary of Dosimetry Measurements in Fuel Position 20 of the MITR

Total in-pile dose rate factor:	$F_T^{SW} = 20.53 \pm 1.00$ watt-cc/MW-gm
Gamma-ray in-pile dose rate factor:	$F_\gamma^{SW} = 19.08 \pm 0.92$ watt-cc/MW-gm
Fast neutron in-pile dose rate factor:	$F_N^{SW} = 1.45 \pm 0.20$ watt-cc/MW-gm
Fast neutron fraction:	$f_N = 0.071 \pm 0.010$
Average dose rate to coolant:	0.0066[a] watts/gm or 0.016[b] watts/gm
Maximum dose rate to coolant	0.15[a] watts/gm or 0.38[b] watts/gm
Total energy deposition rate:	35[a] watts or 88[b] watts

Note: Error limits are 2σ.

[a]At reactor power level of 1.95 MW.

[b]At reactor power level of 4.90 MW.

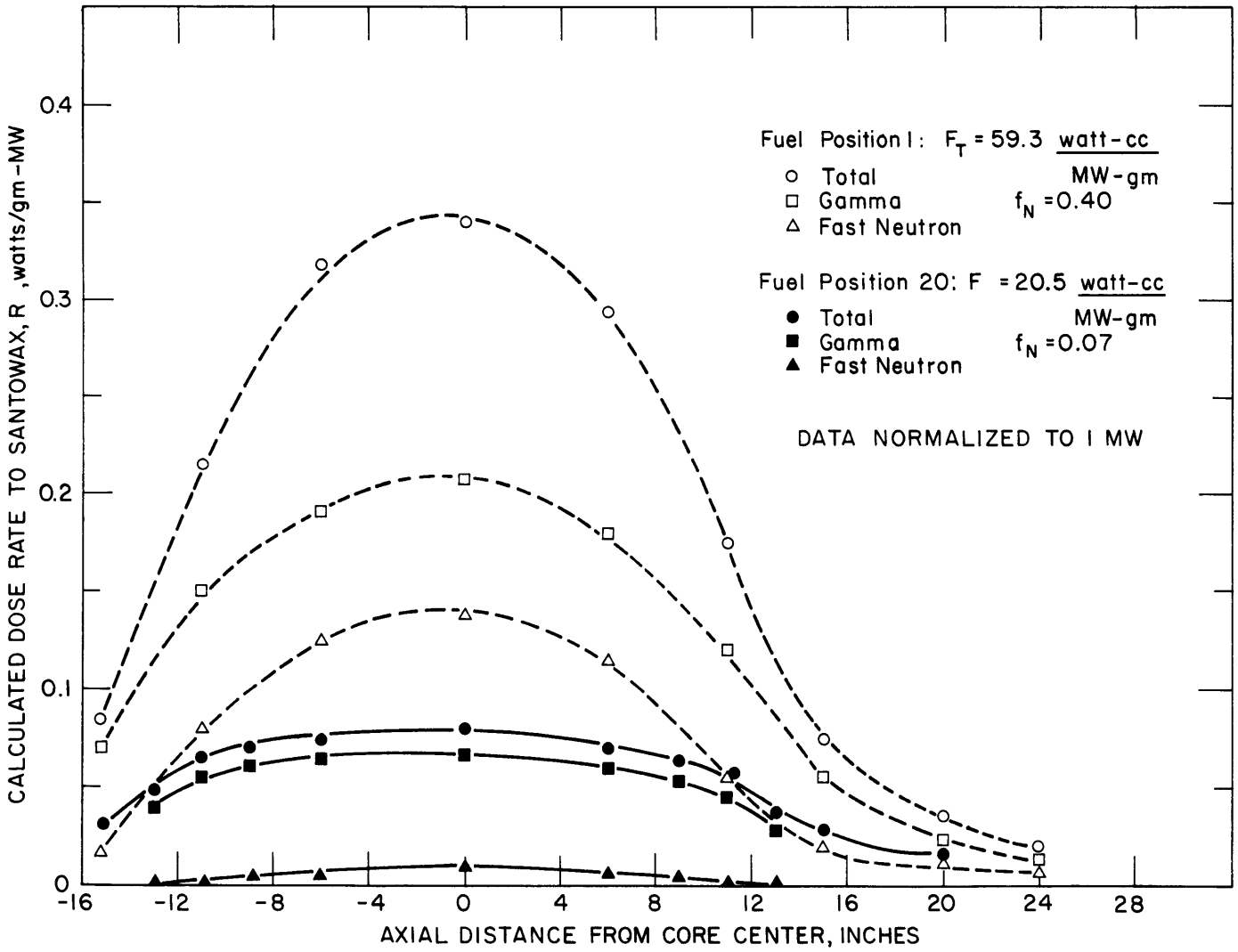

FIGURE I.1 COMPARISON OF DOSE RATES TO SANTOWAX IN FUEL POSITION 1 AND FUEL POSITION 20

No significant variation in the dose rates (normalized to 1 MW) was found during the thirteen-month irradiation period from May 10, 1965, to June 10, 1966. Earlier results (1.2, 1.3) in Fuel Position 1 showed decreases in the dose rates due to fuel burn-up. However, an unfueled sample assembly was the irradiation facility in Fuel Position 20, and fuel burn-up in the other fueled positions did not have a measurable effect on the dose rates in this facility.

1.3.3 Terphenyl Degradation – Theory

The degradation of terphenyl coolants in nuclear reactors results from the combined effect of pile radiations (fast neutrons and gamma rays), designated as radiolysis, and thermal decomposition, designated as pyrolysis when referring to unirradiated coolants or radiopyrolysis when referring to irradiated coolants. Assuming that the rate of degradation of terphenyls from any of these processes depends on the concentration of terphenyls only, and that radiolysis and radiopyrolysis are independent and linearly additive, a general rate equation expressing the total terphenyl degradation rate can be written in units of grams/watt-hour, as (see Appendix A3.1 for derivation):

$$\frac{w_i}{M_L \bar{r}} (C^f_{omp} - C_{omp}) - \frac{dC_{omp}}{d\tau} = k_{R,omp,n} C^n_{omp} + \frac{k_{P,omp,m} C^m_{omp}}{\bar{r}} = \frac{G(-omp)}{11.65} \qquad (1.1)$$

where

w_i = feed rate of organic coolant to the system, grams/hr

M_L = coolant mass in the system (loop), grams

C^f_{omp} = total terphenyl concentration in the feed, weight fraction

C_{omp} = total terphenyl concentration in the well-mixed system (loop), weight fraction

$\bar{r}$ = average specific dose rate to coolant mass M_L, watts/gm

τ = specific dose to coolant mass M_L, watt-hr/gm

$k_{R,omp,n}$ = radiolysis rate constant for total terphenyl for apparent radiolysis kinetics order n, $(\text{watt-hr/gram})^{-1}$

$k_{P,omp,m}$ = radiopyrolysis rate constant for total terphenyl for apparent radiopyrolysis kinetics order m, $(\text{hr})^{-1}$

G(-omp) = total terphenyl degradation rate, molecules terphenyl degraded/100 ev

11.65 = conversion factor, (molecules)(watt-hr)(gram)(100 ev)

For steady-state irradiation runs, $dC_{omp}/d\tau = 0$ in Equation (1.1), and G(-omp) is a constant value for the entire irradiation period. For transient irradiation runs, $w_i = 0$ in Equation (1.1), and G(-omp) decreases throughout the irradiation period (unless both n and m equal zero).

A modified form of Equation (1.1) has been used to describe the disappearance rate of the three individual terphenyl isomers in a mixture of isomers.

$$\frac{w_i}{M_L \bar{r}}(C_i^f - C_i) - \frac{dC_i}{d\tau} = k_{R,i,a+b} C_i^a C_{omp}^b + k_{P,i,c+d} C_i^c C_{omp}^d = \frac{G(-i)}{11.65} \qquad (1.2)$$

where

C_i^f = concentration of terphenyl isomer component i in the feed, weight fraction

C_i = concentration of terphenyl isomer component i in the well-mixed system, weight fraction

$k_{R,i,a+b}$ = radiolysis rate constant for component i for apparent reaction order a+b, (watt-hr)/gram

$k_{P,i,c+d}$ = radiopyrolysis rate constant for component i for apparent reaction order c+d, $(hr)^{-1}$

For pure isomer irradiations (i = omp), Equation (1.2) reduces to Equation (1.1), and a + b = n. This expression takes into account interactions between the terphenyl isomers such that the apparent reaction order for individual isomers in mixtures may be different from the apparent reaction order for total terphenyl. The determination of the reaction order constants for radiolysis (a, b, n) has been a primary objective of the M. I. T. terphenyl irradiations described in this report.

1.3.3.1 Radiolysis Degradation Rate Equations

For terphenyl irradiations below about 350°C (662°F), the radiopyrolysis rate constant, k_P, in Equations (1.1) and (1.2) is negligible and radiolysis effects can be investigated without thermal degradation making a contribution to the total degradation rate. Under these low temperature conditions, the radiolysis rate constant and the radiolysis G value for total terphenyl degradation, $G_R(\text{-omp})$, are related in the following manner

$$G_R(\text{-omp}) = 11.65\ k_{R,\,omp,\,n} C_{omp}^{n} \tag{1.3}$$

where $k_{R,\,omp,\,n}$ and $G_R(\text{-omp})$ may vary with temperature and fast neutron fraction.

Since pile radiations causing damage in organic coolants consist primarily of fast neutrons and gamma rays, a G value may be assigned to each type of radiation. For an irradiation facility in which a fraction, f_N, of the total dose to the coolant is received from fast neutrons, the total radiolysis disappearance rate can be written

$$G_R = G_N f_N + G_\gamma (1 - f_N) \tag{1.4}$$

since generally, for reactor irradiations,

$$f_\gamma = 1 - f_N \tag{1.5}$$

Linear additivity of fast neutron and gamma-ray induced degradation is assumed in Equation (1.4), which appears valid on the basis of available experimental results.

Another stability factor which is used to describe radiolysis yields is $G^*(\text{-omp})$, where

$$G^*(\text{-omp}) = \frac{G(\text{-omp})}{C_{omp}} \tag{1.6}$$

Thus, G^* is a concentration normalized G value. This parameter is useful in comparing the relative stabilities of the individual terphenyl isomers which are present in mixtures at different concentrations.

Equations (1.3) and (1.4) can be combined to give

$$\frac{G_R(\text{-omp})}{11.65} = k_{R,\,omp,\,n} C_{omp}^{n} = \frac{G_\gamma^o}{11.65}\left[\left(\frac{G_N}{G_\gamma} - 1\right) f_N + 1\right] C_{omp}^{n} \tag{1.7}$$

where

G_γ^o = initial degradation rate due to gamma rays, molecules/100 ev
$= G_\gamma / C_{omp}^n$

$\frac{G_N}{G_\gamma}$ = fast neutron effect ratio, assumed to be independent of terphenyl concentration

Equation (1.7) was used to correlate terphenyl irradiation results of M.I.T. and other laboratories to determine the apparent reaction order for radiolysis, n, and the fast neutron effect ratio, G_N/G_γ.

1.3.3.2 Radiopyrolysis Degradation Rate Equations

At temperatures above about 350°C (662°F), thermal decomposition (radiopyrolysis) of the coolant becomes significant in low average dose rate experiments such as the irradiations made to date in the M.I.T. organic loop, where radiopyrolysis was the predominant component of the total degradation rate above about 750°F. However, the separation of the total degradation rate into radiolysis and radiopyrolysis contributions is difficult. The method used at M.I.T. to calculate the radiopyrolysis rate in high temperature runs is to subtract the radiolysis degradation rate measured at low temperature (applying a small activation energy of radiolysis, $\Delta E_R = 1$ k-cal/mole) from the total measured degradation rate, as shown below.

Steady-State Runs

$$k_{P,\,omp,\,m} = \left[\frac{G(-omp)}{11.65\, C_{omp}^m} - \frac{k_{R,\,omp,\,n} C_{omp}^n}{C_{omp}^m} \right] \bar{r} \qquad (1.8)$$

Transient Runs

$$k_{P,\,omp,\,m} = \left[\frac{-dC_{omp}/d\tau}{C_{omp}^m} - \frac{k_{R,\,omp,\,n} C_{omp}^n}{C_{omp}^m} \right] \bar{r} \qquad (1.9)$$

Since the total degradation rate in transient runs, $-dC_{omp}/d\tau$, decreases during the irradiation period, M.I.T. has selected a terphenyl concentration, $\bar{C}_{omp}$, near the middle of the concentration range at which the calculation represented by Equation (1.9) was

made (See Section 5.2.2). The total degradation rate, $-dC_{omp}/d\tau$, is known with the greatest statistical significance near the midpoint of the transient.

1.3.4 Terphenyl Coolant Degradation Results

1.3.4.1 M.I.T. Irradiations

The principal irradiation conditions and results of the irradiations of Santowax WR in Fuel Position 20 of the MITR are presented in Table 1.3, in which the total terphenyl degradation rates for Santowax WR are presented as G values and G^* values. G(→HB) represents the molecules of terphenyl degraded to high boiler per 100 ev radiation energy deposited in the coolant.

1.3.4.2 Apparent Reaction Order for Radiolysis

The apparent reaction order for total terphenyl radiolysis, n, in Equations (1.1) and (1.3) was determined by plotting G(-omp) versus C_{omp}, in logarithmic form (see Equation (1.3)), for the M.I.T. steady-state irradiations at 300°C shown in Table 1.3. The reaction order, n, is the slope of such a plot. For these low temperature runs where radiopyrolysis is negligible, $G(-omp) = G_R(-omp)$. Figure 1.2 shows the data for M.I.T. Runs 14, 16, and 17 plotted in this manner.

Also shown in Figure 1.2 are the data for three series of low temperature (320°C) irradiations of OM-2 terphenyl coolant carried out by Euratom workers in the BLO4 loop in the SILOE reactor (1.4). OM-2 is similar to Santowax WR in terphenyl isomer concentrations (see Table 1.1). These Euratom irradiations were made from July, 1965, to February, 1966, at fast neutron fractions between 12% and 28%. The G values for the Euratom runs shown in Figure 1.2 were calculated at M.I.T. to insure that the different methods used by M.I.T. and Euratom for calculating degradation rates did not produce different values. The average difference between the G values for these Euratom runs by the two methods was only 2.3%.

Figure 1.2 shows that the apparent reaction order for radiolysis, n, for two of the three Euratom steady-state irradiations agrees well with the value for the M.I.T. steady-state irradiations. From these

Table 1.3

Summary of Results of Santowax WR Irradiations in the M.I.T. Loop in Fuel Position 20

Fast Neutron Fraction, $f_N = 0.071 \pm 0.010$ Average Dose Rate, $\bar{r} = 0.0061$ to 0.0166 watts/gram

Run No.	Date mo/day/yr	Reactor Power MW	Method[a] Operation	Temperature[b] °F	°C	Concentration, w/o OMP	DP	HB	G(-omp)[c,d]	G(→HB)[c,d]	G*(-omp)[c]
13	5/10/65-7/12/65	2	Tr	572	300	92-84	6-16	—	—	—	0.189 ±0.035
14	7/15/65-9/30/65	2	SS	572	300	84	16	11	0.163 ±0.016	0.151 ±0.010	0.195 ±0.019
15	10/5/65-10/28/65	2-5	Tr	800	427	82-57	18-43	11-29	—	—	1.64 ±0.16
16	10/29/65-2/24/66	5	SS	572	300	63	37	29	0.100 ±0.012	0.091 ±0.006	0.159 ±0.017
17	2/28/66-4/1/66	5	SS	572	300	90	10	6	0.181 ±0.012	0.168 ±0.012	0.202 ±0.013
18A	4/6/66-4/29/66	5	Tr	800	427	90-54	10-46	6-35	—	—	1.07 ±0.10
18B	5/10/66-6/10/66	5	SS	800	427	52	48	35	0.532 ±0.034	0.489 ±0.032	1.03 ±0.07

[a] Tr = transient, SS = steady-state.

[b] Irradiation capsule temperature.

[c] Error limits are 2σ.

[d] G values are not constant for transient runs.

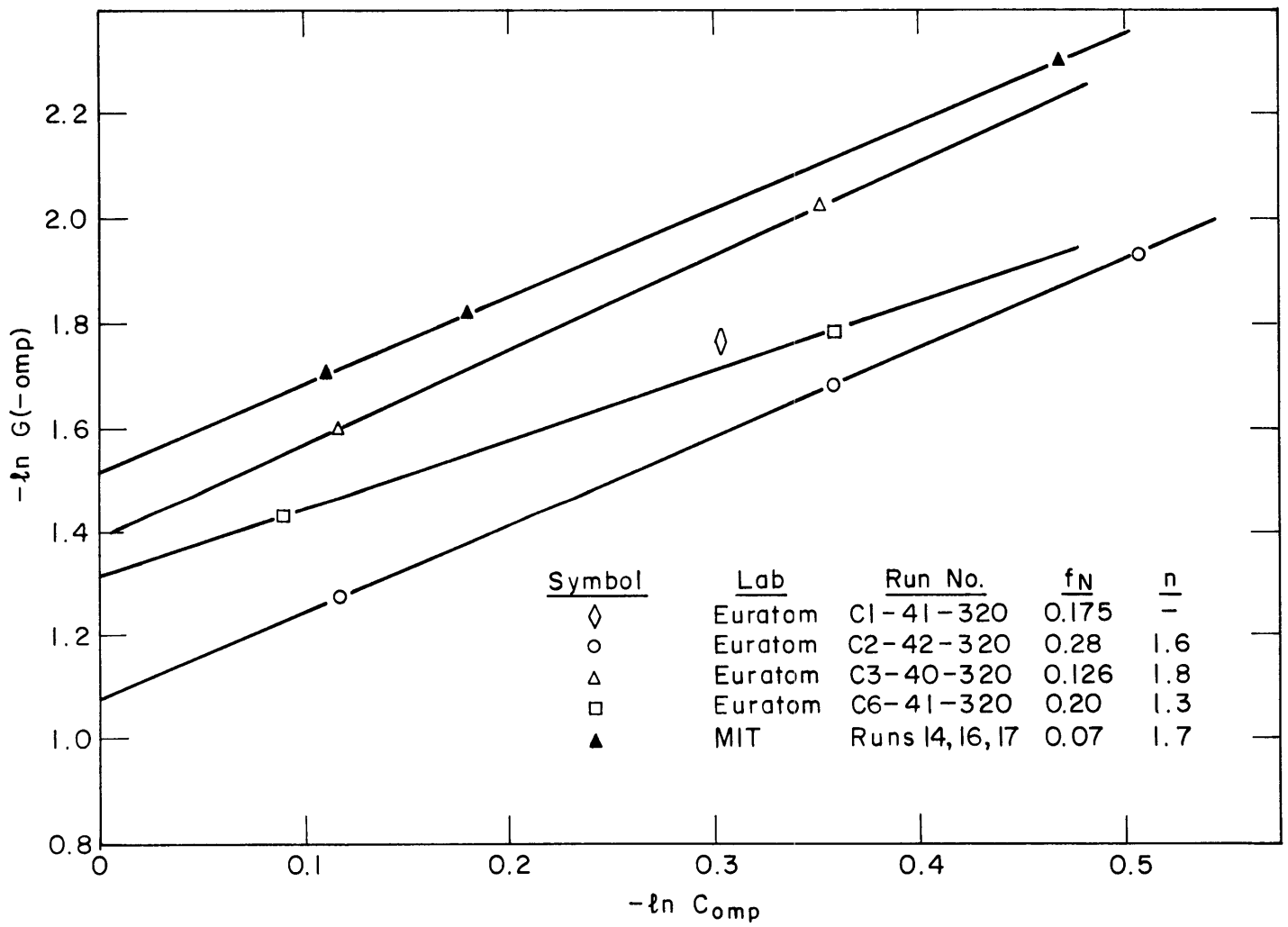

FIGURE 1.2 CORRELATION OF EURATOM (BL04) AND MIT STEADY-STATE IRRADIATIONS AT LOW TEMPERATURE

results, the best value was found to be

$$n = 1.7 \pm 0.2 \quad (2\sigma)$$

The difference in the intercepts of the lines shown in Figure 1.2 is related to the fast neutron fraction employed in the experiments, and to the relative degradation effects of fast neutrons compared to gamma rays (see Equation (1.7)).

Comparison of the relative stabilities of the individual terphenyl isomers for M.I.T. low temperature irradiations of Santowax WR and Santowax OMP at $f_N = 0.07$ and 0.37-0.40 indicated that these relative stabilities did not change significantly with variations in the isomer concentrations or the total omp concentrations at a given fast neutron fraction. This result implies that the values for a and b in Equation (1.2) are approximately

$$a = 1.0$$
$$b = 0.7$$

1.3.4.3 Fast Neutron Effect

The fast neutron effect ratio, G_N/G_γ, can be determined from Equation (1.7) by plotting $k_{R,\,omp,\,n}$ versus f_N for terphenyl irradiations made at varying fast neutron fractions, assuming the reaction order is not a function of f_N. The slope of such a plot is $\frac{G^o_\gamma}{11.65}\left[\frac{G_N}{G_\gamma} - 1\right]$ and the intercept is $\frac{G^o_\gamma}{11.65}$.

Figure 1.3 shows the low temperature irradiation results for meta-rich terphenyls obtained by M.I.T. and other laboratories in the United States, Canada, and Europe plotted in this manner. These data have been normalized to 320°C by an activation energy of radiolysis, $\Delta E_R = 1$ k-cal/mole. The 1.7 order radiolysis rate constant was used in this plot consistent with the recent M.I.T. and Euratom results discussed in Section 1.3.4.2. For steady-state runs, $k_{R,\,omp,\,1.7}$ was found directly from the steady-state G value by Equation (1.3). For transient runs, $k_{R,\,omp,\,1.7}$ was found from Equation (1.1) (with w_i and k_P equal zero) using a computer least-square-error analysis of terphenyl concentration versus dose data.

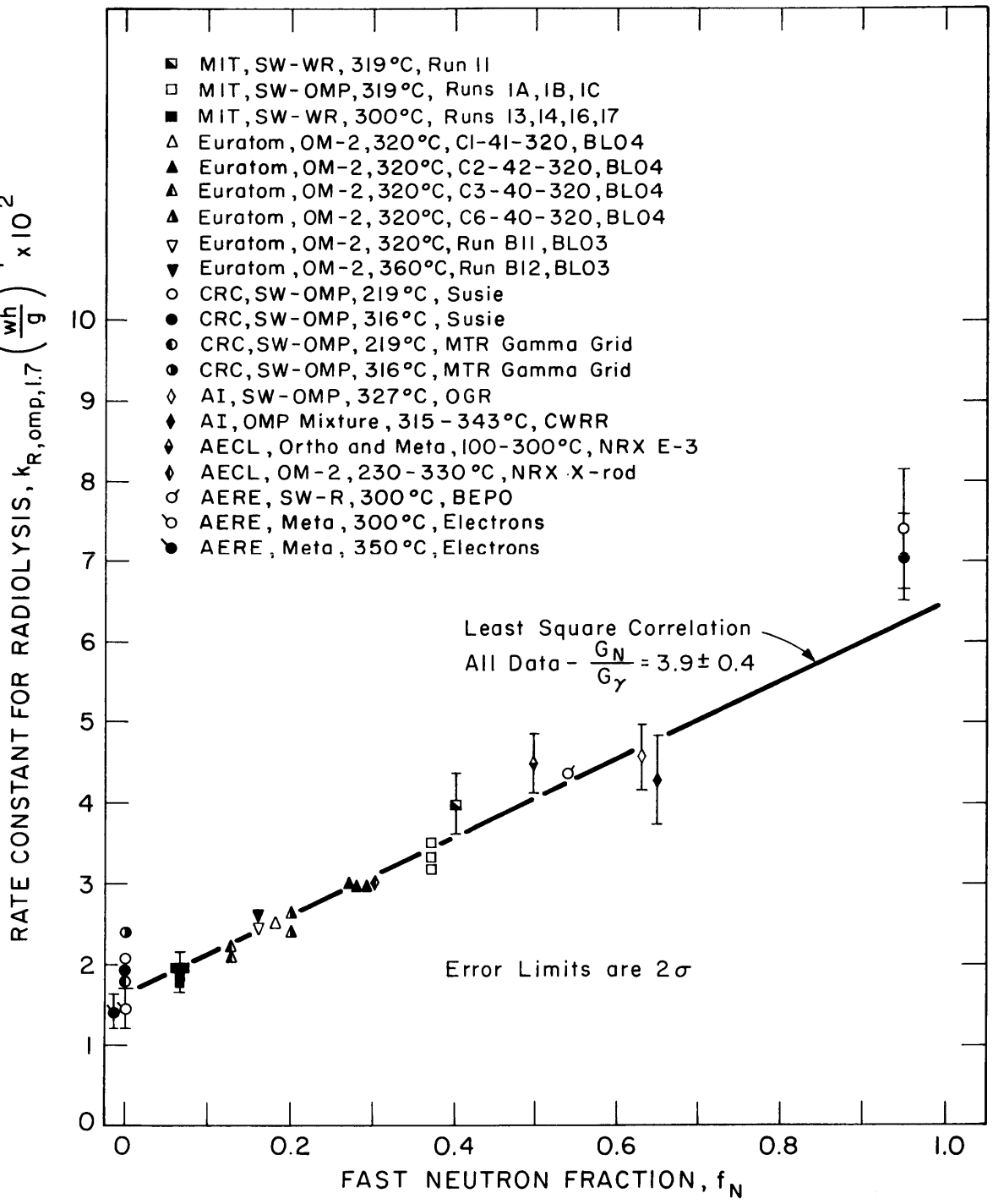

FIGURE 1.3 EFFECT OF FAST NEUTRON FRACTION, f_N, ON THE EMPIRICAL RADIOLYSIS RATE CONSTANT FOR 1.7 ORDER APPARENT KINETICS (NORMALIZED TO 320°C BY ΔE_R = 1K-CAL/MOLE)

Figure 1.3 indicates that all these data are correlated well by Equation (1.7) using n = 1.7, considering that the 95% confidence limits on the measured degradation rates are at least ±8-10%. The correlating line through the data in Figure 1.3 was found by least-square-error analysis with equal weighting for all data. The best values of the fast neutron effect ratio, G_N/G_γ, and the initial gamma-ray degradation rate, G_γ^o, at 320°C are therefore

$$\frac{G_N}{G_\gamma} = 3.9 \pm 0.4 \qquad (2\sigma)$$

$$G_\gamma^o = 0.19 \pm 0.02 \qquad (2\sigma)$$

It should be emphasized that these results were obtained for meta-rich terphenyl coolants for irradiations near 320°C. The values of G_N/G_γ and G_γ^o may be significantly different for ortho-rich terphenyls or for irradiations at higher temperatures.

Comparison of the low temperature G values for ortho and meta terphenyl in M.I.T. irradiations of Santowax WR and Santowax OMP at f_N = 0.07 and 0.37-0.40 gave the following results for the individual terphenyl isomers

	M.I.T.	AECL (1.5)	
Meta	320°C	250°C	300°C
$\frac{G_N}{G_\gamma}$ =	4.5	4.5	3.2
G_γ^o =	0.18	0.15	0.20
Ortho			
$\frac{G_N}{G_\gamma}$ =	2.7	2.7	1.6
G_γ^o =	0.25	0.26	0.42

As indicated, these results agree reasonably well with values recently reported by AECL (1.5) for low temperature irradiations of pure meta and pure ortho terphenyl.

1.3.4.4 Pyrolysis and Radiopyrolysis Rates

Table 1.4 summarizes the results of two pyrolysis experiments with unirradiated Santowax WR and one post-irradiation pyrolysis experiment with irradiated Santowax WR carried out in the M.I.T. autoclave apparatus.

Table 1.4

Summary of M.I.T. Autoclave Pyrolysis Results

Run No.	Coolant	Temperature		Concentration, w/o		First-Order Rate Constant[b]
		°F	°C	OMP	DP	$k_{P,omp,1}$ $(hr)^{-1}$
P1	fresh SW-WR	780	416	95-61	5-39	$8.17 \pm 0.20 \times 10^{-4}$
P2	fresh SW-WR	800	427	94-68	6-32	$1.78 \pm 0.06 \times 10^{-3}$
18P1	irradiated SW-WR[a]	780[c]	416	55-46	45-54	$9.19 \pm 0.56 \times 10^{-4}$

[a]Drained from the loop at the end of Run 18B.

[b]Error limits are 2σ.

[c]Approximately equal to the effective loop temperature in Run 18B.

The pyrolysis rate constants for Runs P1 and P2 agree well with AECL values (1.6) for the pyrolysis rates of unirradiated meta terphenyl (both pure and in Santowax OM), but are about a factor of three higher than Euratom measurements (1.7, 1.8) for unirradiated OM-2. The reason for this discrepancy is not known at the present time.

The post-irradiation pyrolysis rate of irradiated Santowax WR (coolant from Run 18B) determined in pyrolysis Run 18P1 was about 25% lower than the radiopyrolysis rate during Run 18B, calculated by Equation (1.8). This difference may indicate that post-irradiation pyrolysis rates are less than the radiopyrolysis rates occurring during irradiation, or that the radiolysis contribution was underestimated in Equation (1.8) when an activation energy, $\Delta E_R = 1.0$ k-cal/gmole was assumed.

Figure 1.4 is an Arrhenius plot drawn from the first-order radiopyrolysis rates calculated by Equation (1.8) and Equation (1.9) from high temperature irradiation data obtained by M.I.T., Euratom (1.4, 1.7, 1.9), and California Research Corporation (1.10). The pyrolysis rates of unirradiated coolant measured by Euratom (1.7, 1.8) and by AECL (1.6) and M.I.T. (Table 1.4) are shown for comparison. The first-order radiopyrolysis rate constants for irradiated coolants are higher than both sets of values for unirradiated coolant. It is estimated that the maximum uncertainty limits on these values of k_P for irradiated coolants are about ±75% at 360°C, ±40% at 400°C, and ±15% at 450°C. The values of k_P shown in Figure 1.4 are not significantly different from earlier values presented by M.I.T. (1.3) which were based on an assumption of second-order kinetics for radiolysis.

The experimental results available do not provide the basis for a significant test of the reaction order of radiopyrolysis (zero and first-order were tested). First-order dependence of radiopyrolysis on total terphenyl concentration was assumed since first-order kinetics are generally used (1.8) for pyrolysis of unirradiated coolant. However, the first-order radiopyrolysis rate constants at any given temperature generally increase with decreasing terphenyl concentration, or with the increasing concentration of Degradation Products and High Boilers. A possible explanation of the higher rate of thermal decomposition of irradiated coolants, as compared to unirradiated coolants, may be that some of the degradation products are responsible for the increased rate of radiopyrolysis. For example, Electron Spin Resonance (ESR) measurements of terphenyl in the (a) unirradiated, (b) pyrolyzed, and (c) low-temperature irradiated states have indicated no detectable free radical concentrations (1.4). However, heating of the low-temperature irradiated coolant over 400°C caused the formation of free radical species (unresolved spectra resulted). Thus, some of the irradiation degradation products may thermally decompose into "active species" which react with terphenyls to cause the increased rate of radiopyrolysis. Since the true nature of the process and the "active species" is not known, the dependence of the rate equations on these "active species" cannot be formulated now. If this explanation is correct, however, the radiopyrolysis term in Equation (1.1) should include some

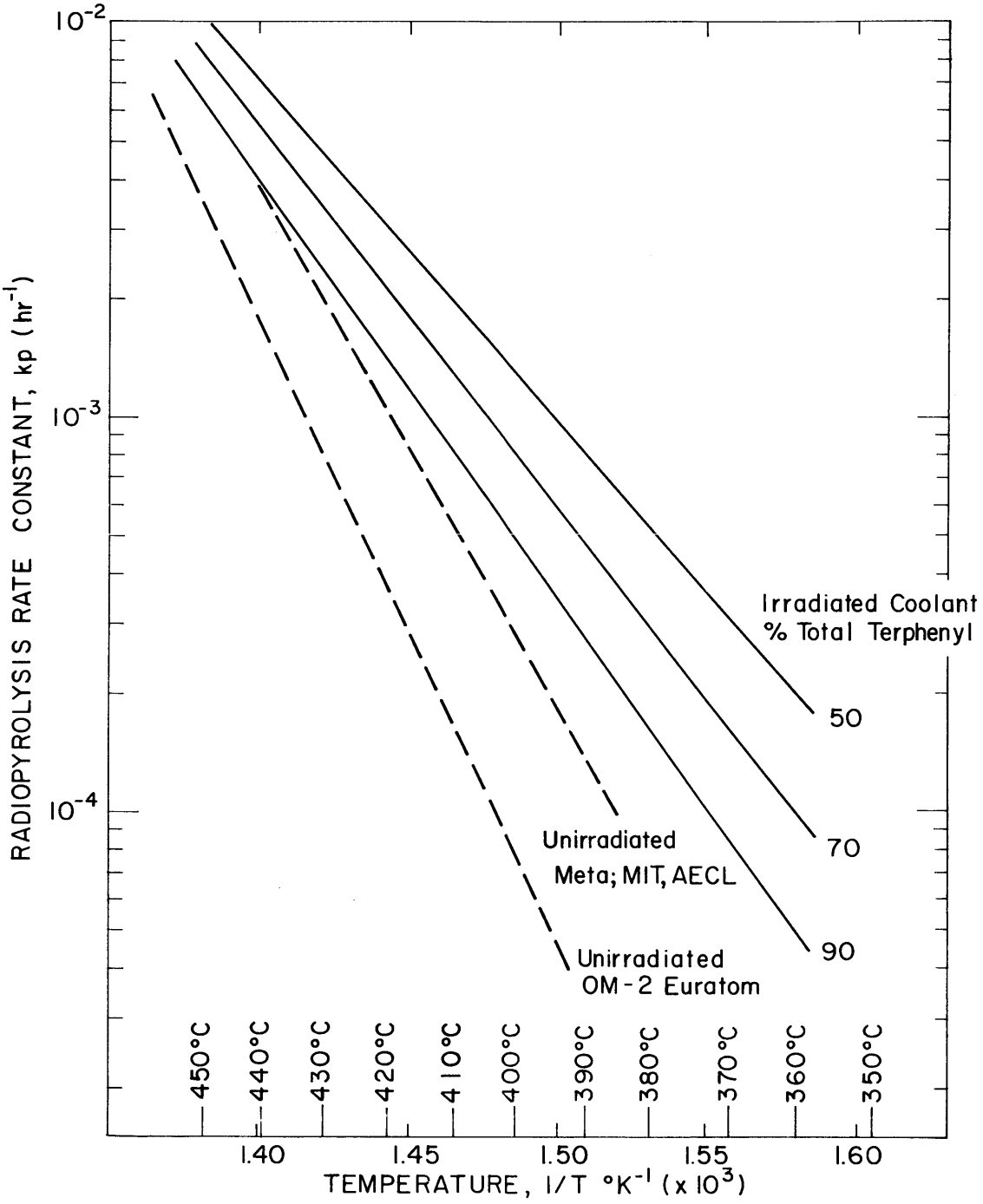

FIGURE 1.4 EFFECT OF TEMPERATURE ON THE PYROLYSIS OF IRRADIATED AND UNIRRADIATED TERPHENYL COOLANT
CLASS I TERPHENYLS: META, SANTOWAX WR, SANTOWAX OMP, OM-2

sort of dependence on degradation products as well as on terphenyl concentrations, in order to explain the differences in radiopyrolysis rate constants obtained with different coolant compositions.

1.3.4.5 Review of High Dose Rate Irradiations

M.I.T. has reviewed the capsule irradiations of pure ortho terphenyl, pure meta terphenyl, and Santowax OM made by AECL (1.5, 1.11, 1.12) at dose rates from 0.1-5 watts/gram and f_N = 0 - 0.60, and the electron irradiations of ortho terphenyl by Atomics International (1.13) at 0.8 watts/gram. Under such high dose rate conditions, the effect of temperature on the radiolysis rate can be measured without large corrections for thermal decomposition. In this review, a second-order radiolysis reaction mechanism was assumed because the degradation results presented by the original workers were determined on this basis. The difference between the rate constants determined by using n = 1.7 and n = 2 is negligible (5-10%) compared to effects of temperature and dose rate on k_R.

Figure 1.5 shows the effects of temperature on the second-order radiolysis rate constants for AECL irradiations of ortho and meta terphenyl at f_N = 0.50-0.60. The rate constants have been normalized to the correlation shown by Figure 1.3 to account for differences in the fast neutron fractions employed in the experiments. The following conclusions can be made from Figure 1.5:

(1) At temperatures above about 320°C, ortho terphenyl is distinctly less stable than meta terphenyl.

(2) There is an apparent dose rate effect for both ortho and meta terphenyl, such that lower degradation rates are obtained (per unit energy deposited) as the dose rate is increased.

(3) The activation energy of radiolysis, ΔE_R = 1 k-cal/mole, assumed in the calculations of k_P in Section 1.3.4.4 appears to be satisfactory for meta-rich terphenyls up to about 400°C. For irradiations at higher temperatures, a substantially higher activation energy of radiolysis is indicated.

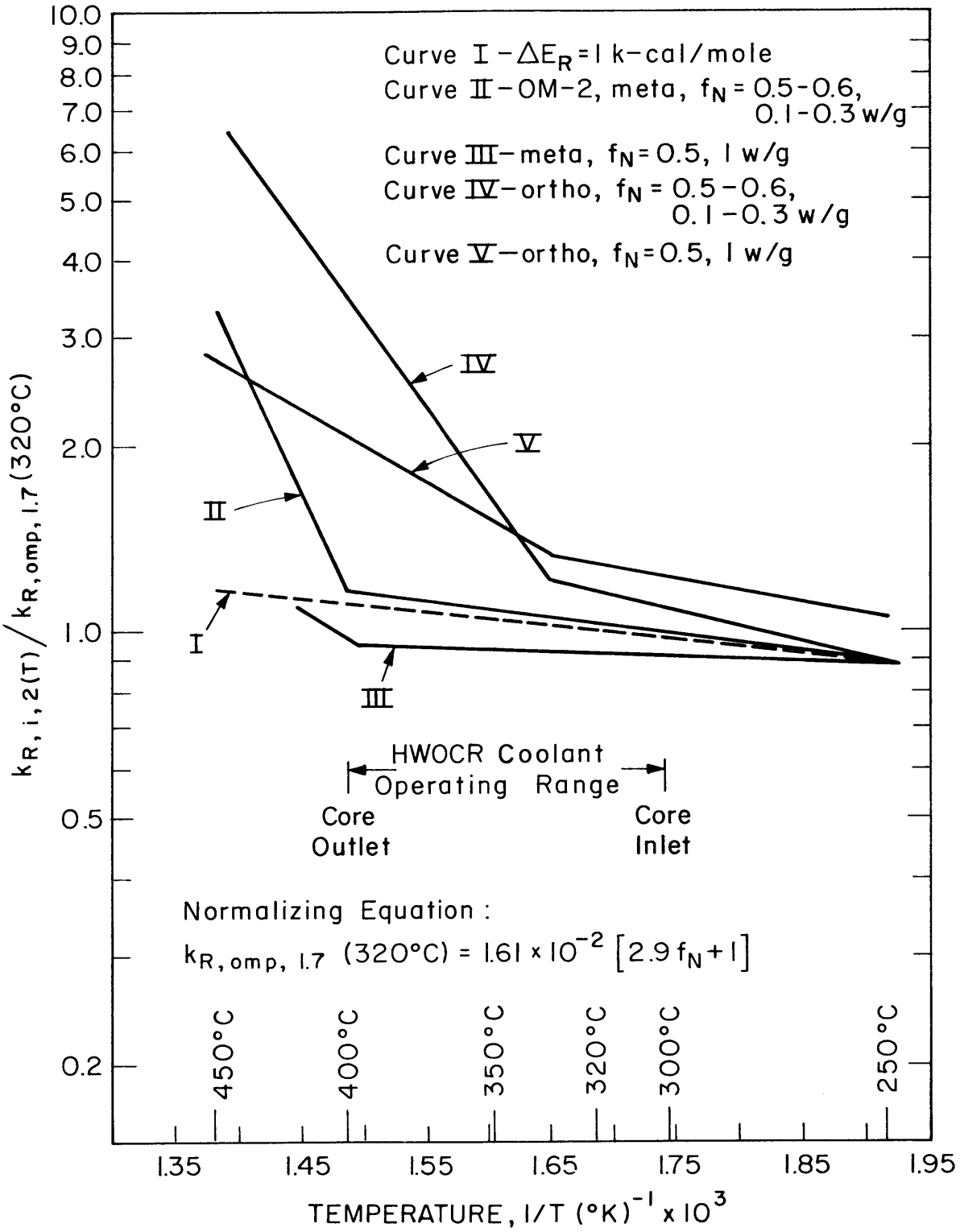

FIGURE 1.5 EFFECT OF TEMPERATURE ON THE RADIOLYSIS RATE OF ORTHO AND META TERPHENAL-MIXED REACTOR RADIATION

Comparison of the G values obtained in AECL high temperature irradiations at $f_N = 0.01$ and at $f_N = 0.50\text{-}0.60$ showed that G_γ increased at a greater rate than G_N at successively higher temperatures, so that the ratio G_N/G_γ decreased and approached unity at about 400°C. This conclusion was made for irradiations of both pure ortho and pure meta terphenyl. Further high dose rate experiments are needed to measure the effect of temperature on G_N/G_γ for terphenyl mixtures.

1.4 Physical Properties and Heat Transfer

Densities of samples of irradiated Santowax WR were measured at M.I.T. over the temperature range 400°F to 800°F with calibrated pycnometers pressurized with nitrogen and immersed in a high temperature fused-salt bath. Viscosities of irradiated Santowax WR samples were also measured in the fused-salt bath at M.I.T. over the temperature range 400°F to 800°F by observing the efflux times in semi-micro capillary viscometers of the Ostwald type. Table 1.5 summarizes these measurements.

Table 1.5

Summary of Density and Viscosity Measurements for Santowax WR Irradiated in Fuel Position 20

% HB	400°F		600°F		800°F	
	ρ, $\frac{gms}{cc}$	μ, cp	ρ, $\frac{gms}{cc}$	μ, cp	ρ, $\frac{gms}{cc}$	μ, cp
0	0.963	0.90	0.868	0.39	0.773	0.20
10	0.972	1.00	0.879	0.43	0.787	0.23
20	0.982	1.20	0.892	0.48	0.802	0.26
30	0.991	1.85	0.903	0.74	0.815	0.39

The densities and viscosities shown in Table 1.5 represent smoothed values obtained from measurements on three or four samples during the steady-state periods of runs at 572°F (300°C). These values are in good agreement with earlier measurements of density and

viscosity reported by M.I.T. (1.2, 1.3). The viscosity of the coolant for Run 18B (800°F, 35% HB) was significantly less than would be expected from the extrapolation of the results shown in Table 1.5 to 35% HB. Earlier M.I.T. results (1.2, 1.3) also indicated that high temperature irradiation produced a coolant with lower viscosity (at the same HB concentration) than that produced by low temperature irradiation.

The densities of irradiated samples from all M.I.T. Santowax WR and Santowax OMP irradiations were found to have a linear temperature dependence, and the density at a given temperature was found to increase with high boiler (HB) concentration. An empirical correlation of the density of irradiated and unirradiated Santowax WR as a function of temperature and HB concentration is given by Equation (1.10)

$$\rho = 1.153 + 0.43 \times 10^{-3}(HB) - [4.75 \times 10^{-4} - 1.23 \times 10^{-6}(HB)]T \qquad (1.10)$$

where

ρ is the sample density, gms/cc

HB is the per cent high boiler, w/o

T is the sample temperature, °F

This correlation predicts the coolant density of all the irradiated Santowax WR and Santowax OMP samples within about ±1%.

Viscosities of all irradiated samples were found to obey the relation

$$\mu = \mu_o e^{-\frac{\Delta E}{RT}} \qquad (1.11)$$

where

μ is the sample viscosity, centipoise

μ_o is a constant for a given sample, centipoise

ΔE is an "activation energy," k-cal/mole

The viscosity constant was found to increase with increasing HB concentrations, and the activation energy, ΔE, ranged from 4.3 to 4.8 k-cal/mole.

Number average molecular weights (MW_N) of samples of irradiated Santowax WR were measured at M.I.T. using an osmometer. The number average molecular weight of the coolant was found to increase

from about 235 ± 5% at 6% HB concentration to about 285 ± 5% at 35% HB concentration. The number average molecular weight of the high boiler fraction of the coolant was found to depend on the irradiation temperature, but in general, this value varied from 450 to 550. High temperature steady-state irradiation gave values of MW_N of the high boiler fraction which were lower than the values for low temperature steady-state irradiations.

The melting points of irradiated Santowax WR samples were measured at M.I.T. by a Fisher-Johns apparatus. The initial and final liquidus points of irradiated Santowax WR samples were found to be significantly lower than the values for unirradiated Santowax WR, which are about 135°F and 185°F, respectively. For irradiated coolant samples containing 6-11% HB, the initial liquidus point was about 115°F and the final liquidus point was about 170°F. For irradiated coolant samples containing 29-35% HB, the samples remained as subcooled liquids at room temperature for several months following irradiation and thus the melting ranges could not be determined.

Heat transfer measurements were made with the aid of an electric test heater installed in the out-of-pile section of the loop. The test heater (TH7) was constructed of stainless steel (1/4-inch OD X 0.020-inch wall) and was heated by the passage of electrical currents of up to 450 amps AC along the tube walls. The coefficients of heat transfer were based on the temperature differences from the inside wall of the test heater to the bulk coolant, as defined by

$$U = \frac{Q/A}{T_{w,i} - T_B} \quad (Btu)/(hr)(ft^2)(°F) \qquad (1.12)$$

where

Q/A is the heat flux into the coolant, $Btu/hr\text{-}ft^2$

$T_{w,i}$ is the average inside wall surface temperature, °F

T_B is the average coolant bulk temperature, °F

The method of Wilson was used to determine that there was no measurable scale buildup on the inside surface of the test heater after thirteen months operation. Therefore, for all of the correlations reported here, the overall coefficient of heat transfer, U, was set

equal to the film coefficient of heat transfer, h_f.

The heat transfer correlations were based on the standard dimensionless parameters (Nusselt Number, Reynolds Number, Prandtl Number) according to a Dittus-Boelter type relation. The heat transfer data for Santowax WR for heat transfer runs with coolant irradiated in Fuel Position 20 were correlated well by the forced convection heat transfer relation of McAdams.

$$Nu_B = 0.023\ Re_B^{0.8}\ Pr^{0.4} \pm 10\% \qquad (1.13)$$

A comparison of the experimental data and the correlation represented by Equation (1.13) is shown on Figure 1.6. These data represent measurements at 572°F (300°C) with coolant velocities from 11 to 21 feet per second and a range of Reynolds numbers from 32,000 to 68,000.

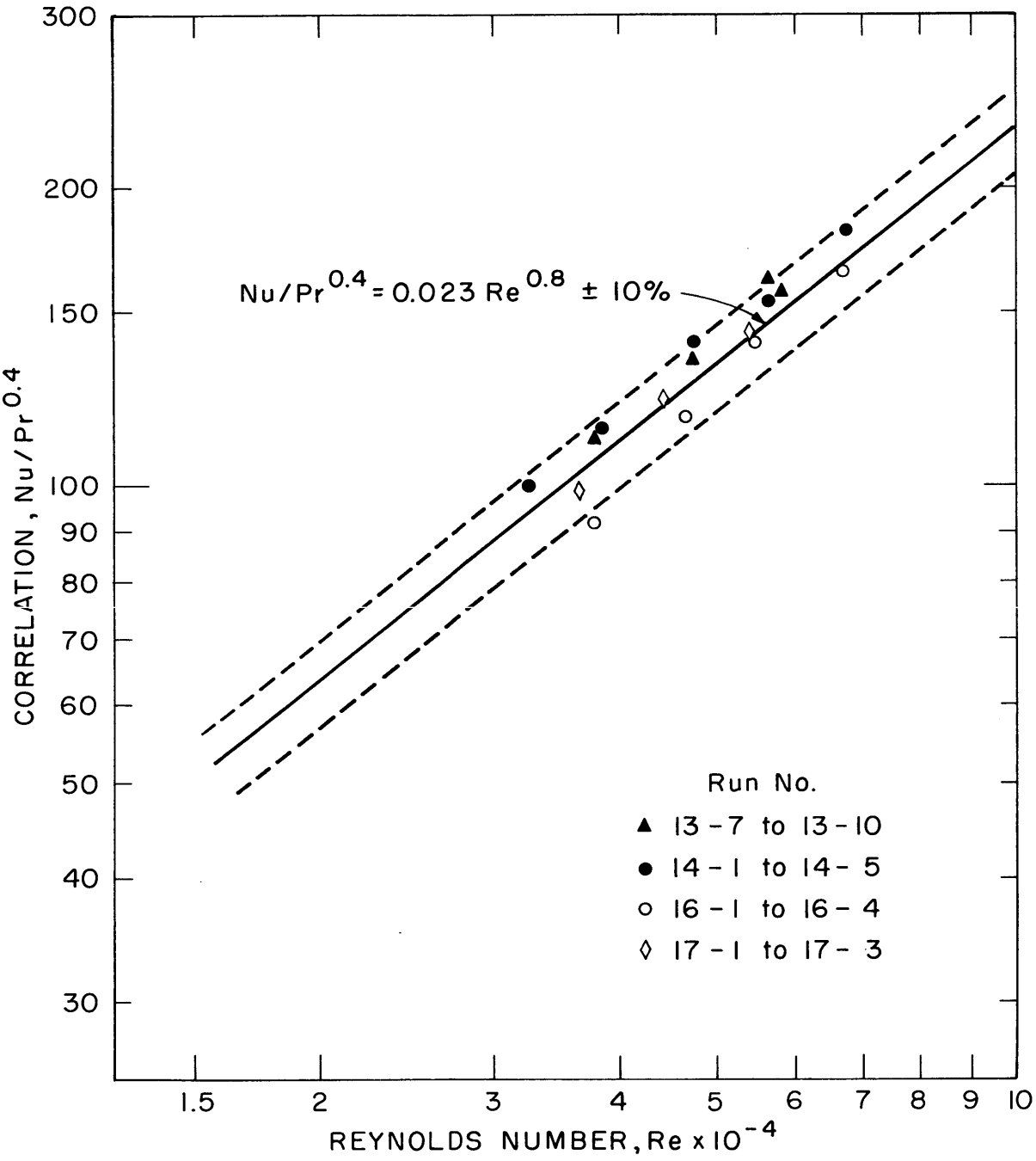

FIGURE 1.6 CORRELATION OF M.I.T. IRRADIATED TERPHENYL HEAT TRANSFER DATA

CHAPTER 2

LOOP AND PYROLYSIS EQUIPMENT AND OPERATION

2.1 Introduction

A complete description of the M. I. T. In-Pile Loop Facility has been given by Morgan and Mason (2.1). Modifications of the equipment during the steady-state irradiations of Santowax OMP and Santowax WR in Fuel Position 1 of the MITR have been presented in later M. I. T. reports (2.2, 2.3). A brief description of the modifications of the irradiation facility used in the irradiations in Fuel Position 20 which were made from May 10, 1965 to June 10, 1966 will be given in this chapter.

Three major changes characterize the irradiations made since May 10, 1965, compared to earlier irradiations:

1. Change of Irradiation Position. The fuel element position in the MITR core in which these irradiations were made was Fuel Position 20, which is on the periphery of the core (see Figure 2.1). Previous irradiations made through September, 1964 were made in the central fuel position of the reactor, Fuel Position 1. The purpose of making irradiations in Fuel Position 20 was to measure the coolant degradation rates with a significantly lower fast neutron fraction of the total dose rate than the 37% and 40% values realized in Fuel Position 1.

2. Cadmium Neutron to Gamma-Ray Converter. In order to increase the gamma-ray dose (and thereby lower the fast neutron fraction), the in-pile irradiation capsule was installed inside a cadmium-lined sample assembly rather than a partial-plate fuel element as used in earlier irradiations. The $Cd^{113}(n,\gamma)Cd^{114}$ reaction was thus utilized to convert thermal neutrons into gamma rays, and the entire sample assembly acted as a gamma-ray converter. This converter increased the gamma-ray dose rate in Fuel Position 20 by a factor of about two. Only about 7% of the

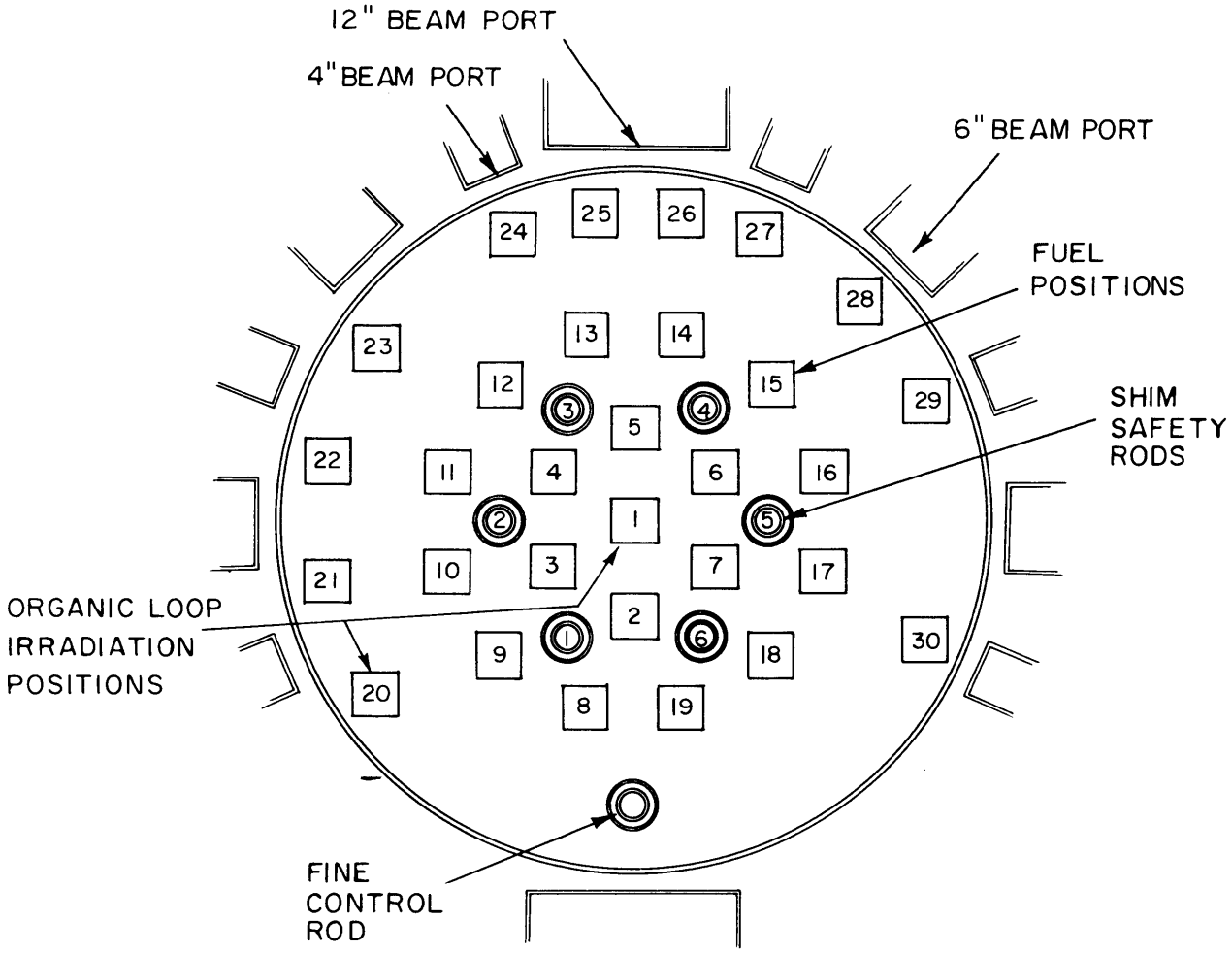

FIG. 2.1 CROSS SECTION OF REACTOR CORE SHOWING FUEL AND CONTROL ROD POSITIONS

total dose rate to the coolant inside the cadmium converter was from fast neutrons; before the cadmium converter was installed, limited measurements indicated the fast neutron fraction in Fuel Position 20 was about 10% to 20%.

3. In-Pile Capsule Modifications. The irradiation capsule used in these irradiations in Fuel Position 20 was a part of In-Pile Section No. 3, which had several modifications not used in the earlier two in-pile sections employed. The most important features of this new in-pile section were: (1) inclusion of a central stainless steel monitor tube (which was used for measuring the neutron and gamma-ray fluxes in the middle of the irradiation capsule and for the insertion of in-pile heaters and thermocouples) and (2) an increase in the in-core coolant volume from about 205 cc to about 280 cc.

A more complete description of these modifications will be presented in Section 2.2.

In addition to the changes made in the irradiation facility, a pyrolysis autoclave has been built. This autoclave is being used to measure the pyrolysis rates of unirradiated terphenyl coolants and the post-irradiation pyrolysis rates of coolants irradiated in the M. I. T. Organic Loop. A description of this equipment is given in Section 2.4.

2.2 Loop Equipment

The loop is constructed entirely of stainless steel and is capable of operation to 800°F and 600 psig. The design and operating specifications are given in Table 2.1 and a schematic flow diagram is shown in Figure 2.2.

In-Pile Section No. 3 was designed to fit in either a partial-plate fuel element or a sample assembly containing no fuel plates. In-Pile Section No. 3 was installed on May 1, 1965 in a cadmium-lined sample assembly in Fuel Position 20. A cross-section diagram in the irradiation zone of this sample assembly, including the in-pile section, is shown in Figure 2.3. The axis of the in-pile section had to be displaced 7/32 inch from the axis of the cadmium-lined sample assembly to accommodate the aluminum monitor tube and leak detector tube running along the side of the in-pile section.

Table 2.1

Design and Operating Specifications of the M. I. T. In-Pile Loop

In-Pile Section No. 3

Bulk temperature	to 800°F
Loop pressure	to 600 psig
Materials of construction	Types 304 and 316 stainless steel
Volume of in-core capsule	280 cc
Circulating volume with 600 cc in surge tank	5800 cc
In-pile to out-of-pile volume ratio	0.05
Maximum circulating flow rate	2.3 gallons/minute
Maximum test heater heat flux	400,000 Btu/(hr)(ft^2)
Test heater wall temperature	to 1000°F
Velocity in test heater	to 23 ft/sec
In-core capsule located along axis of cadmium-lined sample assembly in Fuel Position 20 of MITR	
Specific dose rate at axial center of reactor to Santowax WR in Fuel Position 20	~0.079 watts/gm/MW of reactor power
Average dose rate to all circulating Santowax WR in Fuel Position 20	0.0066 watts/gm[a] or 0.016 watts/gm[b]
Total energy deposition rate from neutrons and gamma interactions	~35 watts[a] or ~90 watts[b]
Fast neutron fraction of total dose rate	0.07

[a] At reactor power level of 1.95 MW.

[b] At reactor power level of 4.90 MW.

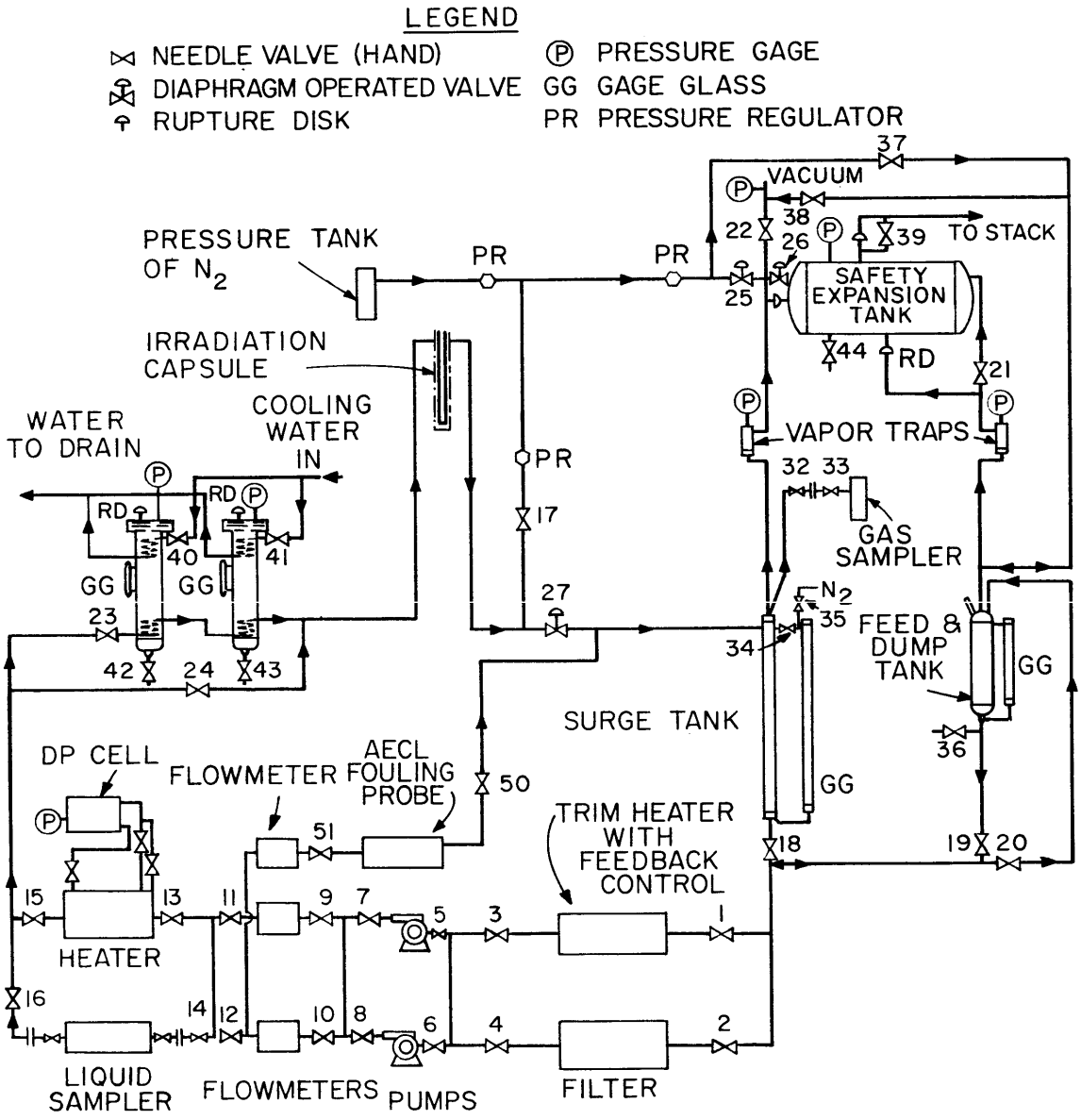

FIG. 2.2 SCHEMATIC FLOW DIAGRAM OF MIT ORGANIC LOOP

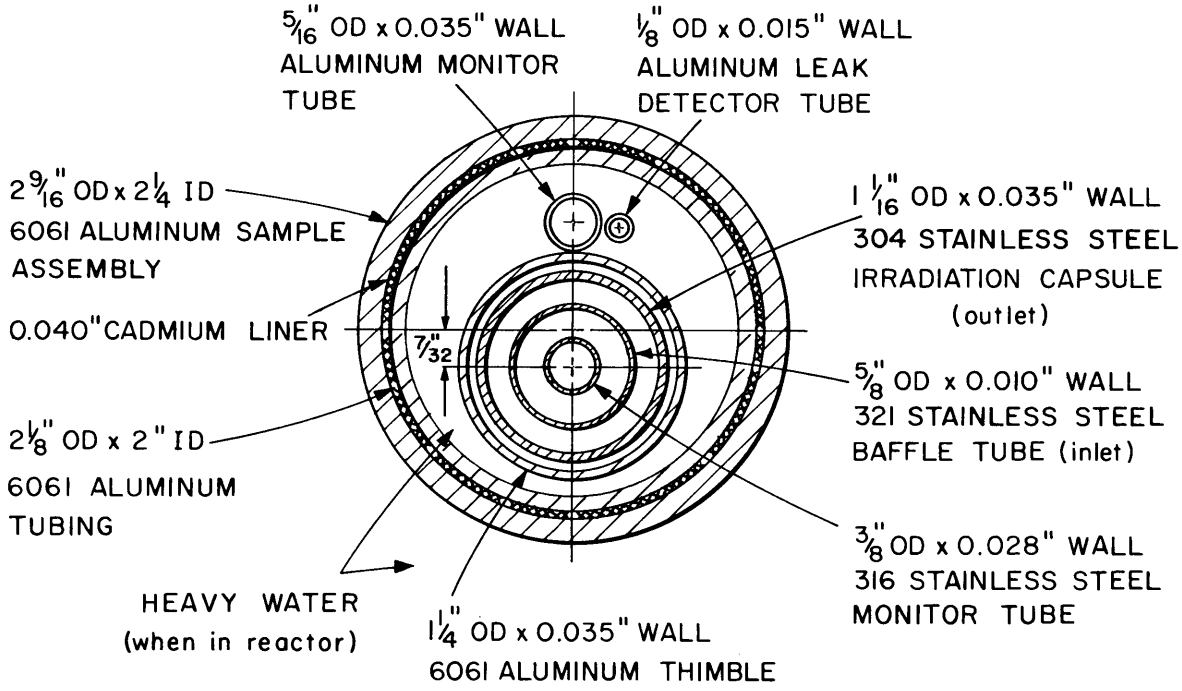

FIGURE 2.3 CROSS-SECTION OF CADMIUM-LINED SAMPLE ASSEMBLY IN FUEL POSITION 20 INCLUDING CROSS-SECTION OF INPILE SECTION NO. 3

In-Pile Section No. 3, shown in cross section in Figure 2.3, consists of a 1-1/4-inch-OD X 0.035-inch-wall aluminum thimble containing a stainless steel irradiation capsule. The aluminum thimble is used to separate the heavy water coolant-moderator of the reactor from the hot organic fluid in the irradiation capsule and inlet-outlet lines. The irradiation capsule consists of three annular stainless steel tubes. The central tube, 3/8-inch-OD X 0.028-inch-wall, is a stainless steel monitor tube which was not included in previous in-pile sections. The purpose of this central monitor tube was to provide an access along the axis of the irradiation capsule which could be used for dosimetry measurements or for the insertion of an in-pile heater. This tube is open at the top, permitting insertion of foils, heaters, or thermocouples from the top of the reactor while irradiations are under way. During the first two irradiation runs in Fuel Position 20, this central monitor tube was used to irradiate threshold and resonance foils for measurement of the neutron flux. For all subsequent runs, a thermocouple was permanently installed in this monitor tube to replace other thermocouples in the in-pile section that had to be disconnected due to leaks at the point where the thermocouples were brazed into the top of the in-pile section. The inlet line for the organic coolant is a 5/8-inch-OD X 0.010-inch-wall, stainless steel baffle tube. The outlet line (or outer wall of the irradiation capsule) is a 1-1/16-inch-OD X 0.035-inch-wall stainless steel tube. At a distance 12-9/16 inches above the core (fuel element) center line, the outer 1-1/16-inch-OD, stainless steel irradiation capsule is reduced to a 7/8-inch-OD X 0.035-inch-wall stainless steel tube. This reduction in the outer tube diameter reduces the volume of irradiated coolant per unit length above this point.

A simplified elevation cut-away view of the lower end of the irradiation capsule of In-Pile Section No. 3 installed in the cadmium-lined sample assembly is shown in Figure 2.4. The cadmium liner is 24 inches long, extending from 12 inches below the core center line to 12 inches above the core center line. A limitation of approximately 1300 millibeta of reactivity per experiment in the MITR required that the amount of cadmium installed in the cadmium liner had to be limited to the dimensions used, rather than extending the whole length of the irradiation capsule. Reactivity measurements made following

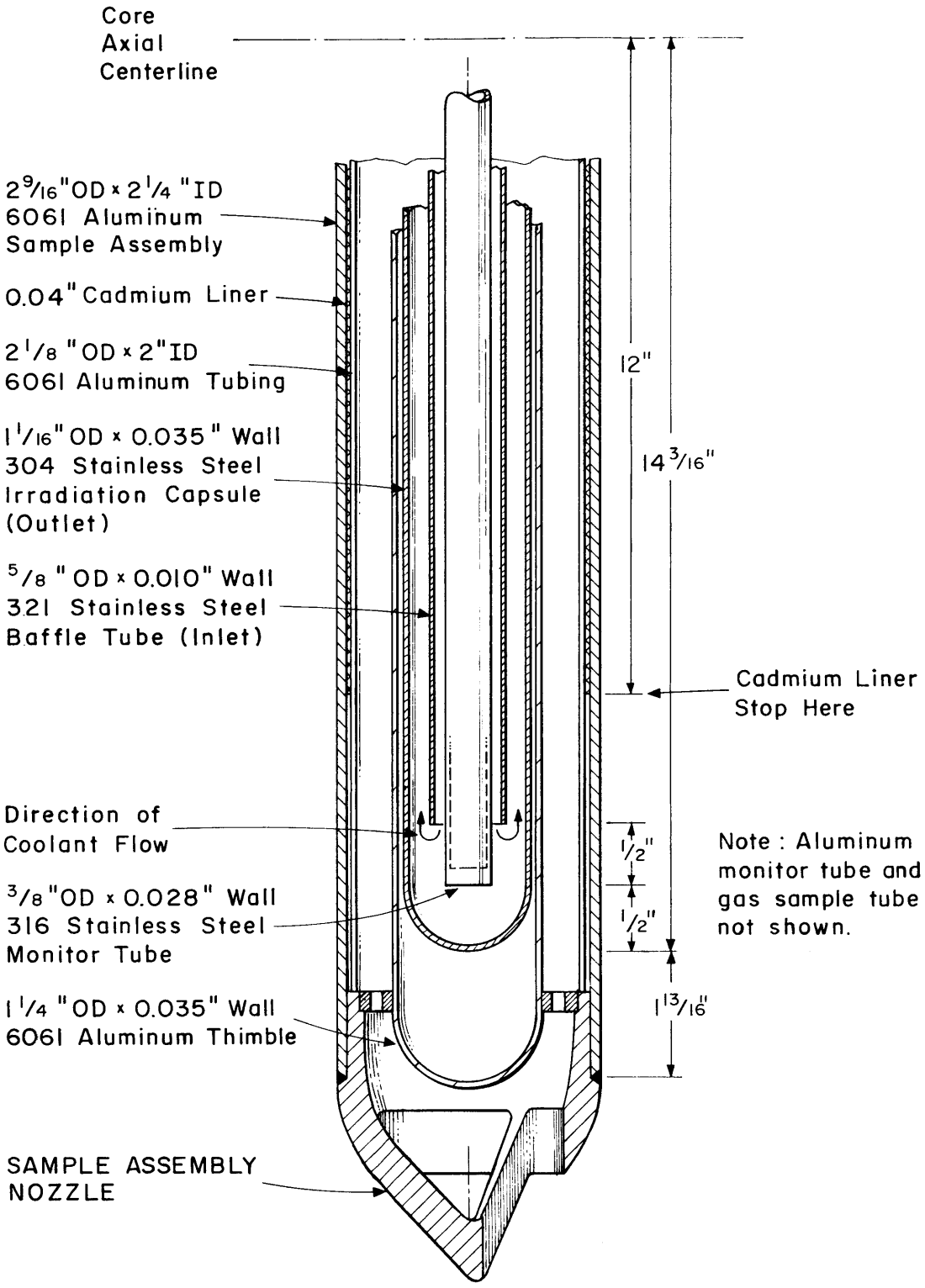

FIGURE 2.4 SIMPLIFIED ELEVATION CUT-AWAY VIEW OF LOWER END OF IRRADIATION CAPSULE OF IN-PILE SECTION No. 3 INSTALLED IN CADMIUM-LINED SAMPLE ASSEMBLY

installation of the cadmium-lined sample assembly and In-Pile Section No. 3 into Fuel Position 20 showed the net reactivity of this experiment was -1075 millibeta. The irradiation zone is considered to extend from 14-3/16 inches below the core center line (bottom of the irradiation capsule) to 25 inches above the core center line where the dose rate becomes negligible. The total volume of coolant in this irradiation zone in In-Pile Section No. 3 is 280 cc. Photographs of the upper and lower ends of In-Pile Section No. 3 are shown in Figures 2.5 and 2.6.

The out-of-pile section (hydraulic console) consists of all loop components containing coolant which are outside the reactor shield. All of these components are enclosed in a sheet metal cabinet equipped with an automatic fire extinguisher because of the flammable nature of the organic coolant. During normal operation, only one of the pumps and one of the flow meters shown in Figure 2.1 are used.

Due to the large effect of temperature on the terphenyl degradation rate at temperatures above 350°C, close temperature control on loop operation is important. Most of the heat used to maintain the loop temperature at the specified level is provided by the test heater (capable of delivering 6 kw) which operates continuously at steady power. All Santowax WR irradiations in Fuel Position 20 were made with Test Heater No. 7 installed in the loop. The additional heat required to maintain the coolant operating temperature is supplied by a trim heater (capable of delivering 2 kw) which is controlled by a proportional controller. The power supplied by the controller is regulated by an immersion thermocouple in the surge tank. A surge tank temperature set point is determined early in each run which corresponds to the specified temperature in the irradiation capsule. The trim heater power is proportional to the difference between the set-point temperature and the measured temperature in the surge tank.

2.3 Loop Operation

2.3.1 General

Normally, the MITR operates for about four days per week at full thermal power (1.95 MW before October 18, 1965 and 4.90 MW after November 1, 1965) and is shut down over the weekend. To match this reactor cycle, the temperature of the coolant in the loop was raised to

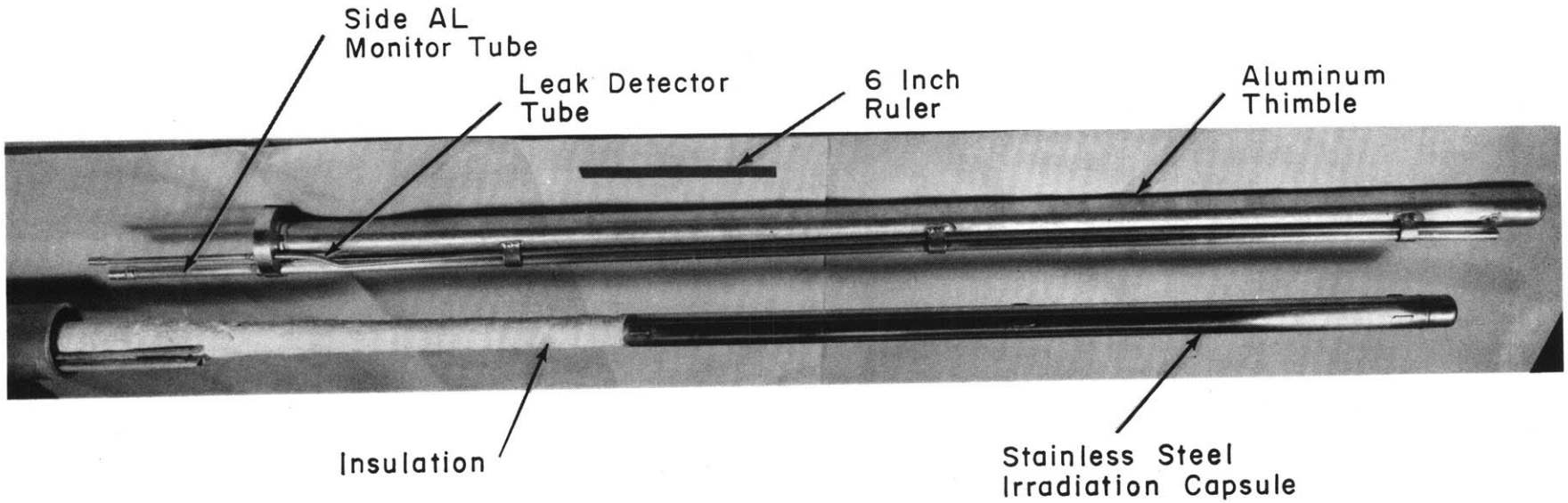

FIGURE 2.5 PHOTOGRAPH OF LOWER END OF IN-PILE SECTION No. 3 SHOWING IRRADIATION CAPSULE AND ALUMINUM THIMBLE BEFORE FINAL ASSEMBLY

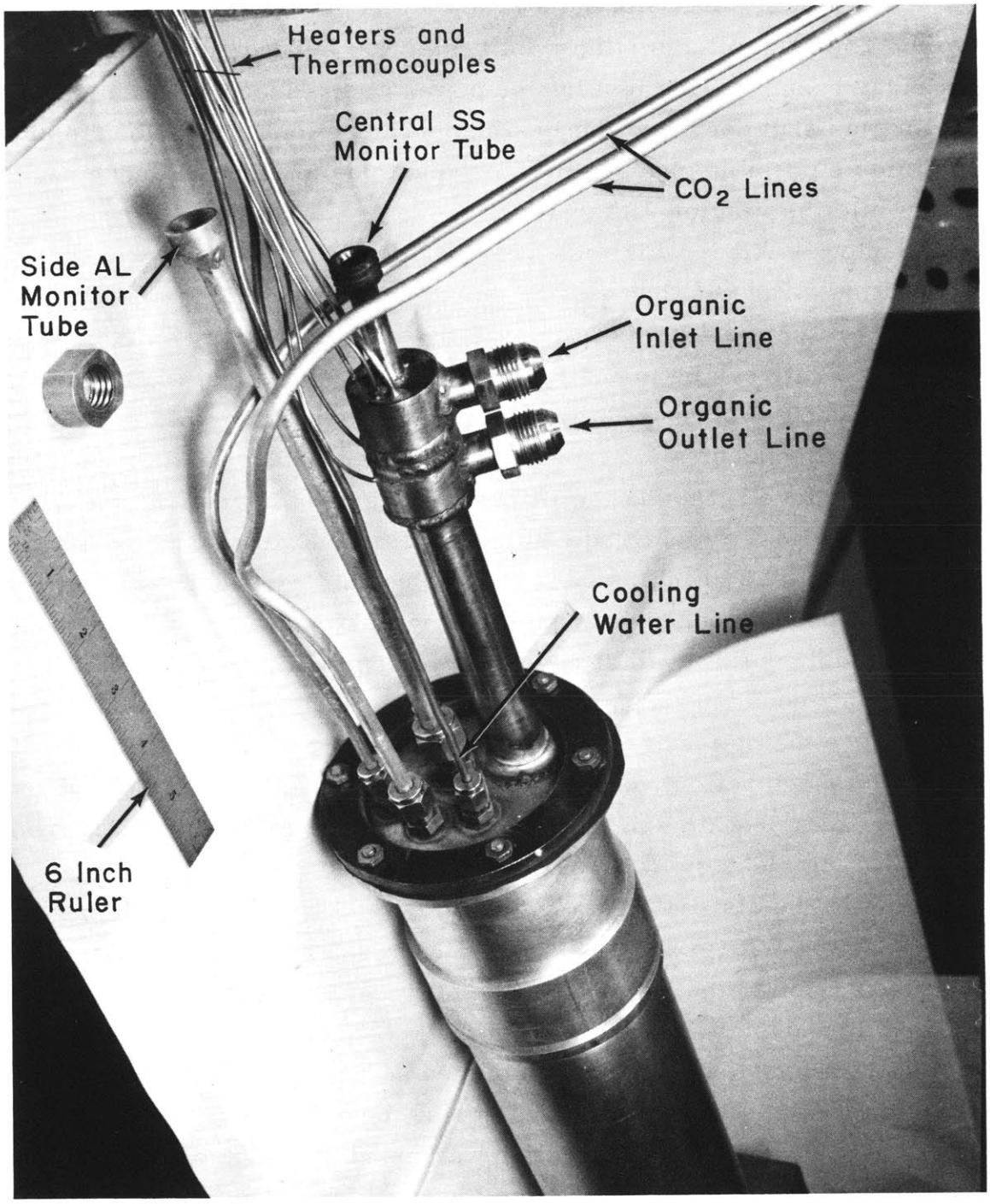

FIGURE 2.6 PHOTOGRAPH OF UPPER END ELBOW OF IN-PILE SECTION No. 3

its operating level Monday mornings by turning up and adjusting the test heater power just before the reactor was brought up to full thermal power. The controller for the trim heater was turned on at this time. On Friday evenings, the test heater power was reduced when the reactor was shut down and the loop temperature lowered to about 450°F to minimize possible changes in the coolant due to thermal decomposition while the reactor was shut down.

Santowax WR irradiations were performed in two different types of operation, transient and steady-state operation. The preferred mode for an irradiation run is the steady-state operation, since the degradation rate can be measured with greater statistical significance for this method of operation. Transient runs were used only to reduce the terphenyl concentration from one steady-state level to a lower steady-state level. During the transient periods of operation, the coolant was allowed to degrade with periodic removal of coolant for sampling (about 25 grams) but no makeup coolant was added. Thus, both the terphenyl concentration and the circulating mass of coolant decreased during this type of operation. During steady-state periods of operation, constant terphenyl and high boiler concentrations in the coolant were maintained (within ±1%). In order to maintain steady-state terphenyl concentration, samples containing about 300 grams of coolant (140-gram samples for Run 16) were removed at regular intervals from the loop in stainless steel capsules and were distilled in a separate laboratory. The distillate obtained from each sample was mixed with fresh Santowax WR (to replace the still bottoms removed) and returned to the loop prior to the removal of the next sample to be distilled. In previous steady-state irradiations in the M. I. T. Organic Loop in Fuel Position 1, the cycle times were adjusted so that the high boiler concentration was at steady-state, and during these "steady-state" periods, the terphenyl concentration was found to be approximately constant (within ±2%). However, the terphenyl analyses were usually not obtained until two or three days after the coolant samples were removed from the loop, and in some cases, accurate terphenyl analyses were not available until the run had been completed. This slight modification of procedure to maintain both terphenyl and high boiler concentration at steady-state was made possible when a digital

integrating system was installed on the chromatograph used for terphenyl analyses. This made it possible to measure the terphenyl concentration in the laboratory about 12 hours after sampling.

A brief description of the two types of distillations used at M. I. T. follows:

2.3.1.1 High Boiler (HB) Distillation

The high boiler (HB) distillation was identical to that reported by Sawyer and Mason (2.2) in describing the Santowax OMP irradiations at 610°F and 750°F. The batch distillations were carried out in Pyrex apparatus at a pressure of approximately 10 mm Hg of nitrogen. During the distillation, the temperature of the distillation bottoms and of the vapor were measured. These temperatures are called, respectively, the pot temperature and the top temperature. For a high boiler distillation, the distillation was concluded when the top temperature reached about 260°C, at which time the pot temperature was about 310°C to 320°C. This temperature cutoff for the distillation permitted the para terphenyl to be carried over to the distillate but left most of the quaterphenyls behind with the high boiler in the pot. The exact cutoff temperature (top temperature) for each run was determined by analyzing the still bottoms by vapor phase chromatography for para terphenyl content. The cutoff temperature was adjusted so that a very small concentration (<0.2%) of para terphenyl remained in the still bottoms after the distillation was completed. Approximately 30 to 45 minutes were required to distill a 300-gram charge in this type distillation. All distillations for the irradiations in Fuel Position 20 were made in this manner.

2.3.1.2 Bottoms Distillation

A distillation procedure called Bottoms distillation was used for Santowax WR irradiations (Run 3 through Run 10) in Fuel Position 1. These irradiations have been described in a recent M. I. T. report (2.3). A distillation pressure of 10 mm Hg of nitrogen was maintained for a Bottoms distillation, just as in the case of a high boiler distillation. However, the top temperature cutoff for a Bottoms distillation was about 319°C, with the pot temperature generally in the range 370°C to 380°C. This type of distillation allowed about 75% of the quaterphenyls

to go over in the distillate and thus be returned to the circulating volume of the loop. No irradiations in Fuel Position 20 utilized this type distillation.

2.3.2 Chronology of Organic Loop Operations – January 1, 1965 through June 30, 1966

The following discussion is a brief description of loop operation and dosimetry measurements during the period of January, 1965 to June, 1966. A summary of operations during this period is shown in Table 2.2.

Five series of calorimetry measurements were made in the cadmium-lined sample assembly in Fuel Position 20 before the in-pile section was installed, but only three of these calorimetry series were used to determine the dose rate in this facility (see Appendix A1). The other two calorimetry series were tests of new calorimeter materials and design models. These calorimetry measurements were made during the period of March 3, 1965 to April 28, 1965.

In-Pile Section No. 3 was installed in the reactor in Fuel Position 20 on May 1, 1965, and the loop was charged with unirradiated Santowax WR. Run 13 (transient) was begun on May 10 at an irradiation capsule temperature of 572°F (300°C) and a reactor power of about 2 MW. Run 13 lasted until July 13 and during this time the total terphenyl concentration decreased from 92% to 84%. Nineteen samples were removed from the loop for analysis during this transient run. On May 12, a series of heat transfer measurements was made. The terphenyl concentration in the coolant at this time was approximately 90%. The total accumulated MWH during Run 13 was 1829.

Run 14 (steady-state) was begun on July 15, 1965 and lasted until September 30. The steady-state terphenyl concentration during this run was about 84%, and the temperature in the irradiation capsule was 572°F. The accumulated MWH during this period was 2200. Two sets of heat transfer data were taken during Run 14 at 820 MWH and 2060 MWH. On September 23, a tritium dilution was made to determine the circulating coolant mass in the loop, which gave 5473 ± 383 gm as the best value (see Appendix A2).

On October 5, 1965, the irradiation capsule temperature was

Table 2.2

Summary of Loop Operations During Period of January 1, 1965 to June 30, 1966

Irradiation of Santowax WR in MITR Fuel Position 20

Operation	Date	Irradiation Capsule Temperature		Reactor Power	Concentration, w/o		
	mo/day/yr	°F	°C	MW	OMP	DP	HB
Calorimetry Series XII	3/3/65						
Calorimetry Series XIII	3/16/65						
Calorimetry Series XIV	4/6/65						
Calorimetry Series XV	4/26/65						
Calorimetry Series XVI	4/28/65						
In-pile section installed in Fuel Position 20	5/1/65						
Run 13, transient	5/4/65-7/12/65	572	300	2	92-84	8-16	–
Run 14, steady-state	7/15/65-9/30/65	572	300	2	84	16	11
Run 15, transient	10/5/65-10/28/65	800	427	2-5	84-62	16-38	11-28
Reactor power raised to 3 MW	10/18/65						
Reactor power raised to 4 MW	10/25/65						
Reactor power raised to 5 MW	11/1/65						
Run 16, steady-state	10/29/65-2/25/66	572	300	5	62	38	28
Run 17, steady-state	2/28/66-4/4/66	572	300	5	90	10	6
Run 18A, transient	4/4/66-5/6/66	800	427	5	90-52	10-48	6-35
Run 18B, steady-state	5/6/66-6/10/66	800	427	5	52	48	35
In-pile section removed from Fuel Position 20	6/11/66						
Calorimetry Series XVIII	6/16/66						
Calorimetry Series XIX	6/22/66						
Calorimetry Series XX	6/29/66						

raised to 800°F (427°C) and Run 15 was begun. This run was a transient irradiation for the purpose of reducing the terphenyl concentration rapidly to 62%, the required concentration for Run 16. On October 18, the reactor power was raised to 2.98 MW. On October 25, the reactor power was raised to 4.00 MW. On November 1, the reactor power was raised to approximately 4.90 MW and was maintained at this level throughout the remaining runs in Fuel Position 20. Run 15 ended on October 28, and approximately 820 MWH were accumulated during the run. Seven samples were removed from the loop for analysis during this run.

Run 16 began on October 29. On November 13, 1965, a routine inspection of the 1/2-inch flare fittings, which connect the in-pile assembly to the lines through the biological shield, was carried out. There were no leaks at the fittings; however, very small leaks had developed where a heater and thermocouple had been brazed into the upper stainless steel elbow assembly (see Figure 2.6). The leaks could be characterized as a "weeping" and very little organic was lost; the critical location of the leaks in the M. I. T. reactor required that they be repaired, however. The loop was drained, and the leaks were repaired by drilling the heater and thermocouple out and by heliarc welding over the holes. A subsequent inspection on November 26, 1965 revealed additional leaks on the remaining heater and thermocouple on the upper elbow. The leaks were repaired as before and subsequent inspection revealed no further leaks. A spare heater and thermocouple were installed in the central monitor tube of the in-pile assembly. On November 25, 1965, it was also necessary to remove the main circulating pump (Chempump No. 1) from the loop, due to a Dowtherm leak in the pump cooling jacket. The pump, itself, was still operating quite satisfactorily and had accumulated approximately 10,000-12,000 hours of trouble-free operation. The pump was removed from the loop, and the alternate pump (No. 2) was used to circulate the coolant for the remaining runs in Fuel Position 20. The loop was recharged with the drained coolant and operation was resumed. Steady-state conditions were reached on December 28. The irradiation capsule temperature during Run 16 was 572°F (300°C) and the steady-state terphenyl concentration was about 62%. The reactor power during this run was 4.90 MW, and the run lasted until February 24, 1966. A series of heat transfer

measurements was made on February 23. The loop was drained on March 1, 1966, and 4432 grams of coolant were removed. A tritium dilution was made on February 17 (Appendix A3), and the mass of coolant circulating in the loop was determined to be 5526 ± 217 grams at the time the loop was drained.

On February 28, 1966, the loop was charged with 5185 grams of unirradiated Santowax WR, and Run 17 was begun. The steady-state terphenyl concentration during this run was about 90% and the irradiation capsule temperature was 572°F (300°C). Run 17 lasted until April 4, when the accumulated irradiation time was 2460 MWH. Thirty-seven samples were removed from the loop during this run (thirty-three in steady-state after the terphenyl concentration of 90% was reached).

On April 4, 1966, the irradiation capsule temperature was raised to 800°F and Run 18A (transient) was begun. This transient run lasted until April 30, when the terphenyl concentration had been reduced to about 52%. Seven samples were removed from the loop during this transient run.

On May 6, 1966, Run 18B was begun. The steady-state terphenyl concentration during this run was approximately 52% and the irradiation capsule temperature was 800°F. This run lasted until June 10, and thirteen samples were removed from the loop during steady-state. On May 17, a tritium dilution to determine the circulating coolant mass in the loop was made, and the best value for this mass was 5384 ± 170 grams.

In-Pile Section No. 3 was removed from the reactor on June 11, 1966, ending the planned irradiations in Fuel Position 20 at a fast neutron fraction of about 0.07. Three calorimetry series of measurements were made in Fuel Position 20 from June 16 to June 29, 1966. Foil dosimetry measurements were made at periodic intervals from March, 1965 to June, 1966, and the results of these foil measurements are given in Appendix A1.

2.4 Autoclave Pyrolysis Experiment

2.4.1 Equipment

An autoclave pyrolysis apparatus has been designed and built at M. I. T. for the purpose of measuring the pyrolysis rate of unirradiated terphenyl mixtures and the radiopyrolysis rate of irradiated terphenyl mixtures from the M. I. T. loop. Photographs of the autoclave and the associated equipment for pyrolysis experiments are shown in Figure 2.7.

The autoclave reactor vessel is the bolted closure type (Model BC-300, Autoclave Engineers, Erie, Pennsylvania). The construction material is 316 stainless steel, and the maximum working conditions are 5000 psi at 650°F and 4900 psi at 800°F. The vessel is 1-13/16 inches ID, 2-9/16 inches OD, and 9-1/4 inches in overall length. The capacity of the vessel is 300 cc. The vessel has three openings (120° apart) in the side shoulder. A 1/8-inch-OD by 1/16-inch-ID, stainless steel, liquid-sampling line enters the autoclave through one of these openings and reaches within 3/4 inch of the bottom of the vessel. Two 1/8-inch-OD, stainless steel clad, chromel-alumel thermocouples are inserted into the autoclave through the other two side connections and positioned in the vessel, 1 inch and 4 inches from the bottom of the autoclave. No provision is made for stirring the sample in the autoclave, but mixing at periodic intervals can be achieved by bubbling nitrogen into the vessel through the liquid sampling line. An opening in the center of the cover allows pressurizing the vessel and removing gas samples.

A schematic diagram showing the liquid and gas sampling lines is shown in Figure 2.8. The autoclave pressure is measured by a Helicoid Chemical Gage (Model 1654, American Chain and Cable Company, Bridgeport, Connecticut) which has a range of 0 - 600 psi. A platinum rupture disc (No. SS4600, Autoclave Engineers) is mounted between the autoclave and the pressure gage. This disc is designed to rupture at 735 psig at 600°F. The stainless steel lines connecting the autoclave with the pressure gage and with Valve 1 are 1/4 inch OD by 1/8 inch ID. All other lines are 1/8 inch OD by 1/16 inch ID, stainless steel. All valves, except that on the gas sampler (Valve 9), are high pressure - high temperature needle stem valves with Ermeto connections (Autoclave Engineers).

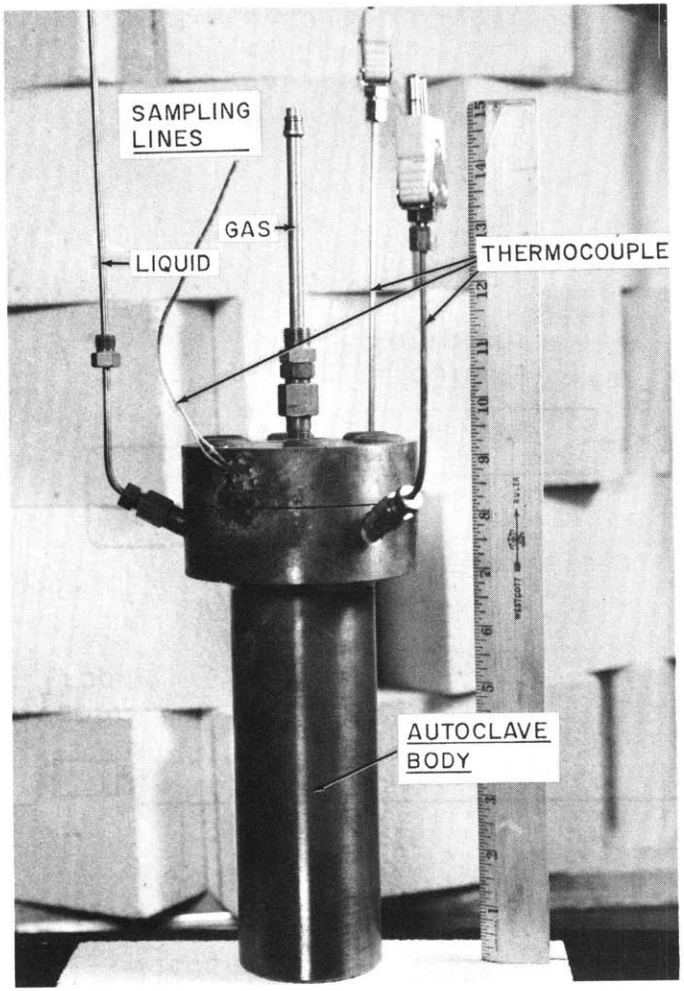

300 cc AUTOCLAVE

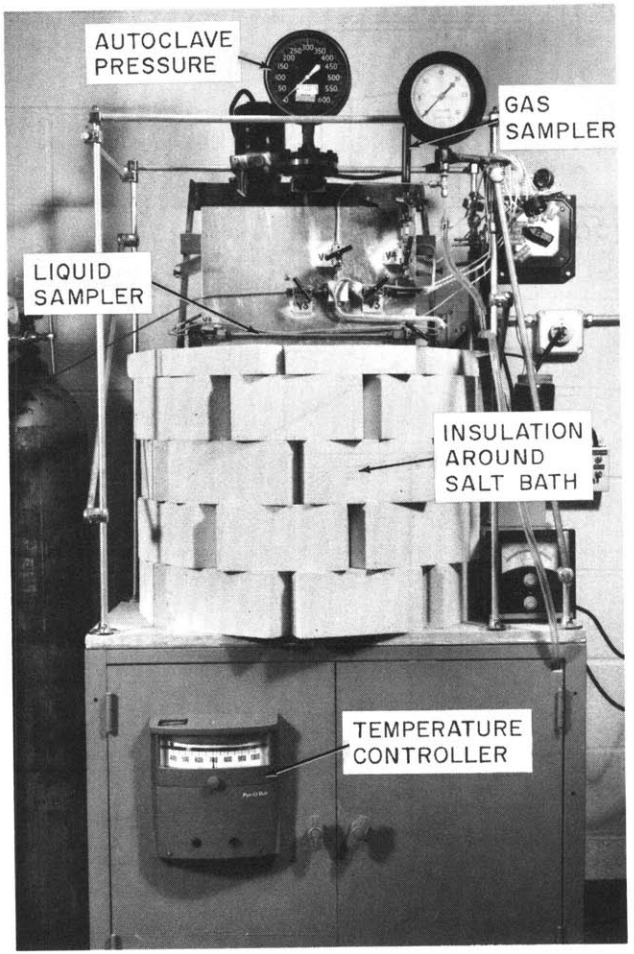

PYROLYSIS EXPERIMENT

FIGURE 2.7 PHOTOGRAPHS OF PYROLYSIS APPARATUS

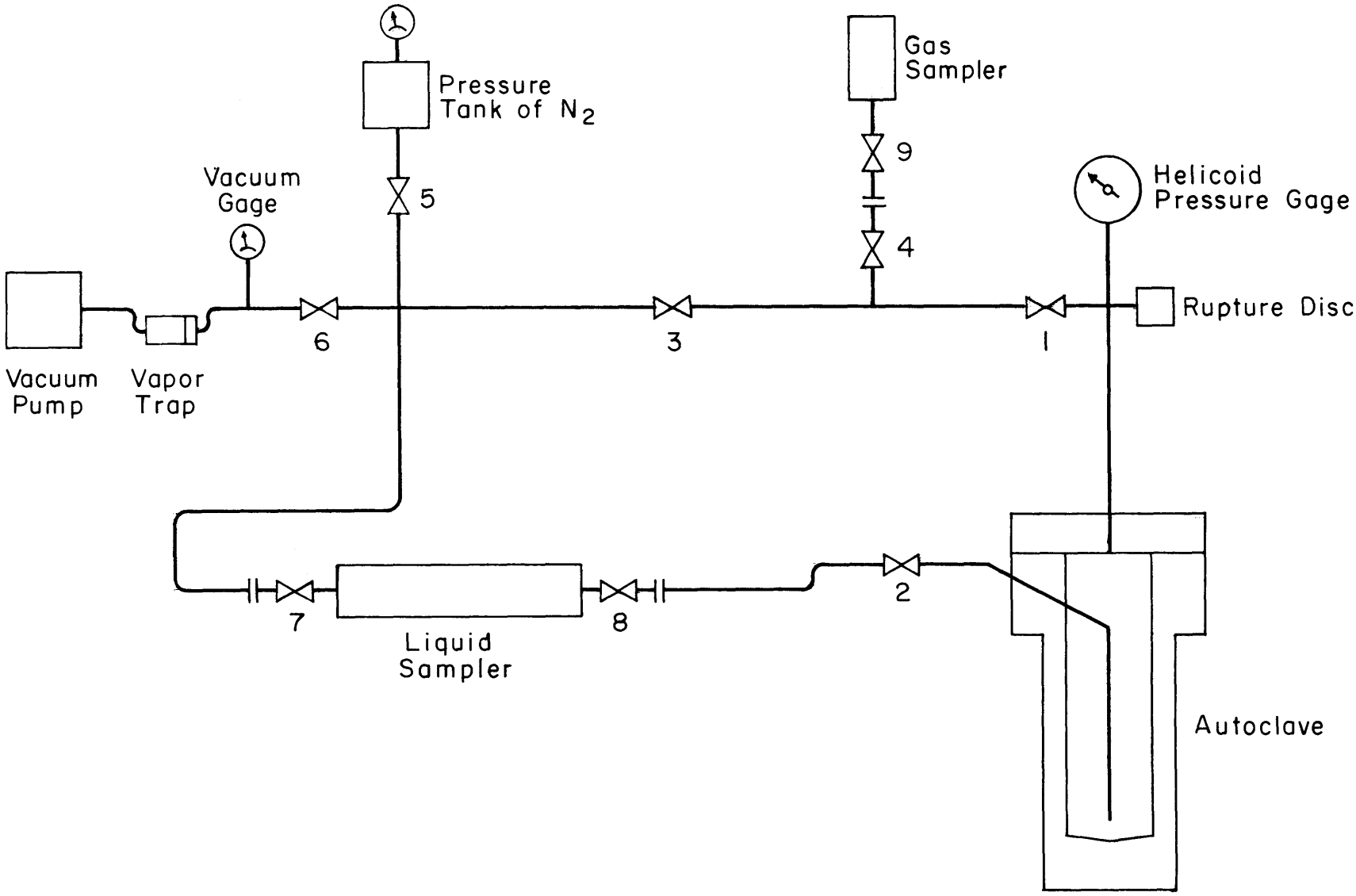

FIGURE 2.8 SCHEMATIC DIAGRAM OF PYROLYSIS APPARATUS

The liquid sampler consists of a 15-inch-long section of 1/4-inch-OD by 1/8-inch-ID stainless steel tubing with high pressure valves on each end. The total volume of the liquid sampler is 3cc. This sampler is mounted on an aluminum panel (see Figure 2.7) heated with a strip heater to help maintain the organic molten during sampling operations. The system can be evacuated with a vacuum pump or pressurized with nitrogen. The vacuum pressure is measured by a standard vacuum gage.

The autoclave rests inside a recessed plate in a salt bath containing a eutectic mixture, 7% $NaNO_3$, 40% $NaNO_2$, 53% KNO_3[1]. The melting point of this mixture is 288°F. The steel containment tank is 20 inches ID by 20 inches high. Four Chromalox heaters (1 kw each) are mounted around the salt bath containment tank. Temperature control is maintained by a Pyr-O-Volt Controller (Honeywell Model No. 105R212-PS-26) connected to the heater near the middle of the bath and controlling from a thermocouple in the salt bath. The temperature in the salt bath and on the autoclave flange are measured by chromel-alumel thermocouples. A temperature safety cutoff is provided by a Sim-Ply-Trol Controller (Model No. 451-C, Assembly Products, Chesterland, Ohio) set about 50°F above the nominal pyrolysis temperature. Temperature control in the autoclave is maintained within ±3°F of the set-point temperature by the temperature controller.

2.4.2 Operation

The autoclave is charged with the organic sample (about 160 grams) after first evacuating and purging the system several times with nitrogen. The vessel is charged with unirradiated terphenyl from a distillation receptacle (graduated cylinder with a stainless steel fitting and stopcock on the drain line) attached to Valve 2. Irradiated coolant is charged directly into the autoclave from airtight, stainless steel sample capsules connected to Valve 2. The system pressure is

---

[1] This salt mixture becomes explosively unstable at temperatures above 1000°F (2.1).

adjusted to 130-150 psi at the operating temperature from the nitrogen bottle.

Liquid samples are taken, after evacuating the liquid sampler, by opening Valve 2 and Valve 8. Since the lines between the autoclave and the sampler contain about 1 cc of organic after the first sample is taken, for all subsequent samples two successive samples are taken and only the second sample is retained for analysis. This procedure insures that the sample taken is representative of the organic liquid in the autoclave. These liquid samples are analyzed by vapor phase chromatography for terphenyl content.

Gas samples are taken after evacuating the system up to Valve 1, including the gas sampler. The gas samples are analyzed by mass spectroscopy (Petroleum Analytical Research, Houston, Texas) and by vapor phase chromatography (M. I. T.).

2.4.3 Chronology of Autoclave Pyrolysis Experiments

The first pyrolysis run to be made in the autoclave was designated Run P1, which began on January 21, 1966 and lasted for 473 hours. The charge material for this run was unirradiated Santowax WR, which had been previously distilled twice. The temperature of the organic in the autoclave was maintained at 780° ± 3°F throughout this run. The total terphenyl concentration during Run P1 decreased from about 95% to about 61%. Nine samples were analyzed during the run.

Due to manpower shortages and modification of the temperature control system on the autoclave, pyrolysis Run P2 was not begun until June 9, 1966. The run was made at 800° ± 3°F with distilled, unirradiated Santowax WR. The experiment lasted 184 hours, and the terphenyl concentration decreased from about 94% to about 67% during this time. Nine samples were removed from the autoclave for analysis during the run.

Pyrolysis Run 18P1 began on June 30, 1966. The charge material for this run was irradiated Santowax WR (Sample 18L-28) removed from the loop at the end of the steady-state period of Run 18B. The sample was removed from the loop in an airtight, stainless steel capsule on June 10 and was charged into the autoclave directly from this capsule. The autoclave temperature for Run 18P1 was 780°F, which was

approximately the effective loop temperature for Run 18B (see Appendix A2). The autoclave reached the set-point temperature on July 1, and the run lasted 222 hours. Twelve samples were removed from the autoclave during this period, and the total omp concentration decreased from about 54% to about 46%.

CHAPTER 3

PHYSICAL PROPERTIES AND HEAT TRANSFER

3.1 Introduction

Physical property measurements on irradiated and unirradiated coolant made at M.I.T. include density, viscosity, melting point, and number average molecular weights of coolant and high boiler samples. No thermal conductivity, specific heat, vapor pressure, or gas solubility measurements on Santowax WR samples irradiated in Fuel Position 20 have been made. Coolant samples removed from the loop at the end of each steady-state run in Fuel Position 20 have been sent to Atomics International (Canoga Park, California) for measurements of carbonyl-bound oxygen, water content, total oxygen content, melting range, and Membrane Stain Test (MST). These analyses have not been completed, but the available results are presented in this chapter. Heat transfer measurements were made at a nominal bulk coolant temperature of 572°F at the end of Runs 13, 14, 16, and 17, at coolant velocities from 11 to 21 feet per second. The data for these measurements were correlated by the Wilson method, which showed no evidence of scale or film buildup in Test Heater No. 7 after approximately 18 months' operation.

A review of physical property measurements made at M.I.T. on irradiated Santowax WR samples from Run 3 through Run 11 has been recently published (3.1). Swan and Mason (3.2) have reviewed heat transfer measurements at M.I.T. from Run 1 to Run 13, and have presented the best correlations for these data. Comparisons of the physical property and heat transfer data obtained during irradiations in Fuel Position 20 with those data reviewed earlier are presented in this chapter.

3.2 Density

The densities of irradiated organic coolants were determined at M.I.T. by use of a pycnometer in which the volume of a known mass of

organic was determined by measuring the liquid height in two capillary tubes connected to a small reservoir of organic. The volume of the pycnometer at different capillary heights was determined by measuring the height in the capillaries when the pycnometer contained a known volume of mercury. All calibrations were made at 25°C. Calculations indicate that the volume change of the pycnometer with temperature due to thermal expansion of the glass can be neglected.

The pycnometer containing approximately one gram of the organic was suspended in a molten salt bath for the high temperature density measurements. The bath was well stirred to insure a uniform temperature and was equipped with a temperature controller which maintained the temperature constant within ±2°F. To prevent boiling of the organic coolant at the higher temperatures, the pycnometer was pressurized with nitrogen to approximately 40 psig. A more detailed description of the equipment and procedure used is given by Morgan and Mason (3.3).

The density data for each sample have been found to closely follow a linear temperature dependence and were fit by the method of least squares to a relation of the form

$$\rho = a + bT \tag{3.1}$$

where

ρ is the sample density, gm/cc
a, b are constants for a given sample
T is the sample temperature, °F.

The variation of the density of irradiated Santowax WR with temperature and high boiler concentration is shown in Figure 3.1. These density measurements are compared with earlier values for Santowax OMP (irradiations with High Boiler distillations) reported by Sawyer and Mason (3.4). The density of unirradiated Santowax WR is also included for comparison. An empirical correlation for the effect of temperature and high boiler (HB) concentration on the density of Santowax WR and Santowax OMP is shown in Equation (3.2).

$$\rho = 1.153 + 0.43 \times 10^{-3}(HB) - [4.75 \times 10^{-4} - 1.23 \times 10^{-6}(HB)]T \tag{3.2}$$

where

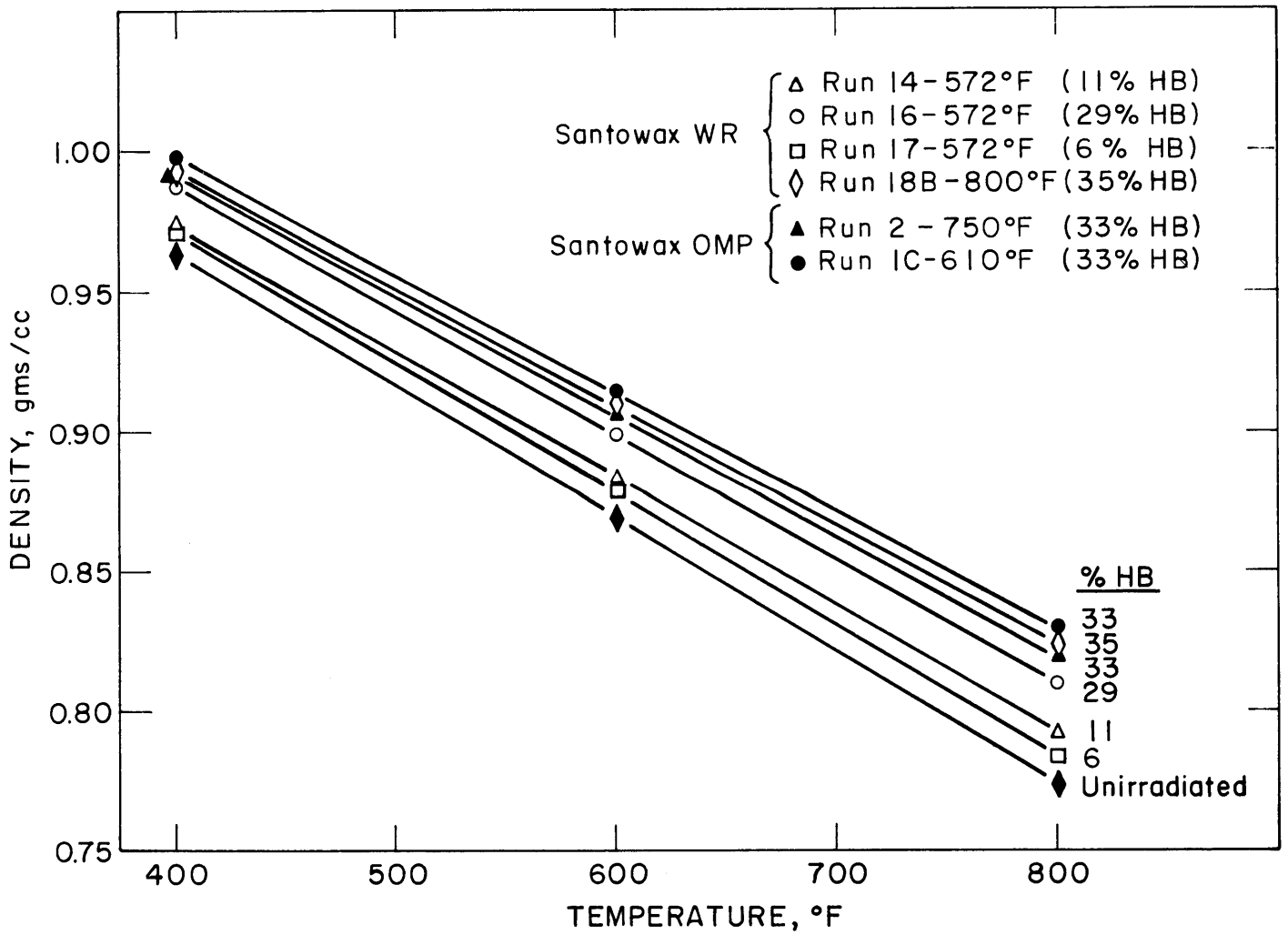

FIGURE 3.1 EFFECT OF TEMPERATURE ON THE DENSITY OF SANTOWAX WR AND SANTOWAX OMP

ρ is the sample density, gms/cc

HB is the per cent high boiler, w/o

T is the sample temperature, °F

This correlation predicts the coolant density of all the irradiated Santowax WR and Santowax OMP samples within 1%.

An earlier correlation has been given by M. I. T. (3.1) which predicts the density of irradiated terphenyl samples as a function of temperature and bottoms concentration (see Section 2.3 for a description of distillation procedures). This correlation is

$$\rho = 1.152 + 0.60 \times 10^{-3}(B) - [4.87 \times 10^{-4} - 1.77 \times 10^{-6}(B)]T \qquad (3.3)$$

where

B is the per cent bottoms, w/o

T is the sample temperature, °F

Since the bottoms distillation provides a deeper cut (i. e., more high boiling components in the distillate) than an HB distillation, the per cent high boiler in a given sample is always larger than the per cent bottoms in the sample. A comparison of the empirical correlations in Equations (3.2) and (3.3) indictes that at 600°F a coolant sample with 30% bottoms has the same density as a coolant sample with 35% HB. Also, if the bottoms and high boiler concentrations are used interchangeably in Equations (3.2) and (3.3), the maximum difference in the predicted density by the two correlations is approximately 1%.

Table 3.1 presents a comparison of density data for Santowax WR and OM-2 (similar to Santowax WR) as (1) obtained by M. I. T. and correlated by Equation (3.2), (2) reported by Mandel (3.5), Atomics International, and (3) reported by Fritz and Elberg (3.6), Euratom, and Chavenal (3.7), Euratom. Mandel's values are based on earlier M. I. T. data (3.8) and represent density versus % degradation products (DP) concentration rather than HB concentration. The Euratom OM-2 density data reported by Fritz and Elberg and by Chavenal et al. appear identical to each other. The densities obtained by M. I. T. are approximately 1-2% higher than the Euratom values at the same HB concentration. Mandel's values generally agree within 1% with the recent M. I. T. density values.

Table 3.1

Comparison of Densities of Santowax WR and OM-2
Reported in Literature

% HB	Density, gms/cc								
	400°F			600°F			800°F		
	MIT[a]	AI[b]	Euratom[c]	MIT[a]	AI[b]	Euratom[c]	MIT[a]	AI[b]	Euratom[c]
0	0.963	0.972	0.952	0.868	0.877	0.860	0.773	0.780	0.756
10	0.972	0.974	0.961	0.879	0.878	0.870	0.787	0.785	0.770
20	0.982	0.976	0.970	0.892	0.883	0.881	0.802	0.792	0.782
30	0.991	0.982	0.980	0.903	0.890	0.893	0.815	0.802	0.794

[a] Calculated by Equation (3.2) for Santowax WR.

[b] Reported by Mandel (3.5), Atomics International, for Santowax WR; values are density vs % DP.

[c] OM-2 densities reported by Fritz and Elberg (3.6), Euratom, and Chavenal et al. (3.7), Euratom.

3.3 Viscosity

The kinematic viscosities of samples of irradiated Santowax WR were determined at M.I.T. by measuring the efflux time in a semi-micro capillary viscometer of the Ostwald type. The details of the M.I.T. viscosity measurements have been presented by Sawyer and Mason (3.4). The viscometer constant was determined as a function of the liquid volume in the viscometer using water as a calibration liquid. An analysis of the change in the calibration constant with temperature due to thermal expansion of the viscometer glass indicated this change was negligible. The viscosity was calculated from the efflux time by means of an appropriate equation of calibration.

The constant temperature bath used for the density measurements was also used for the viscosity measurements; the viscometer was pressurized with nitrogen similar to the pycnometer to prevent boiling of the organic.

The viscosity data obtained for each sample were fit by the method of least squares to the relation

$$\mu = \mu_o e^{\Delta E/RT} \tag{3.4}$$

where

μ is the viscosity of the sample, centipoise

μ_o is a constant, centipoise

ΔE is an "activation energy," k-cal/g-mole

R is the gas constant, k-cal/g-mole-°R

T is the sample temperature, °R

During the steady-state periods of the irradiations (constant high boiler concentration), the coolant viscosity remained constant within the reproducibility of the measurement, which is 3% to 5%. This implies little change in the molecular weight distribution during these periods, which was corroborated in the determination of the number average molecular weight (see Section 3.4).

The viscosity of irradiated Santowax WR and Santowax OMP as a function of temperature and HB concentration is shown in Figure 3.2 for samples removed from the loop during steady-state periods of operation. These data represent smoothed values for viscosity measurements

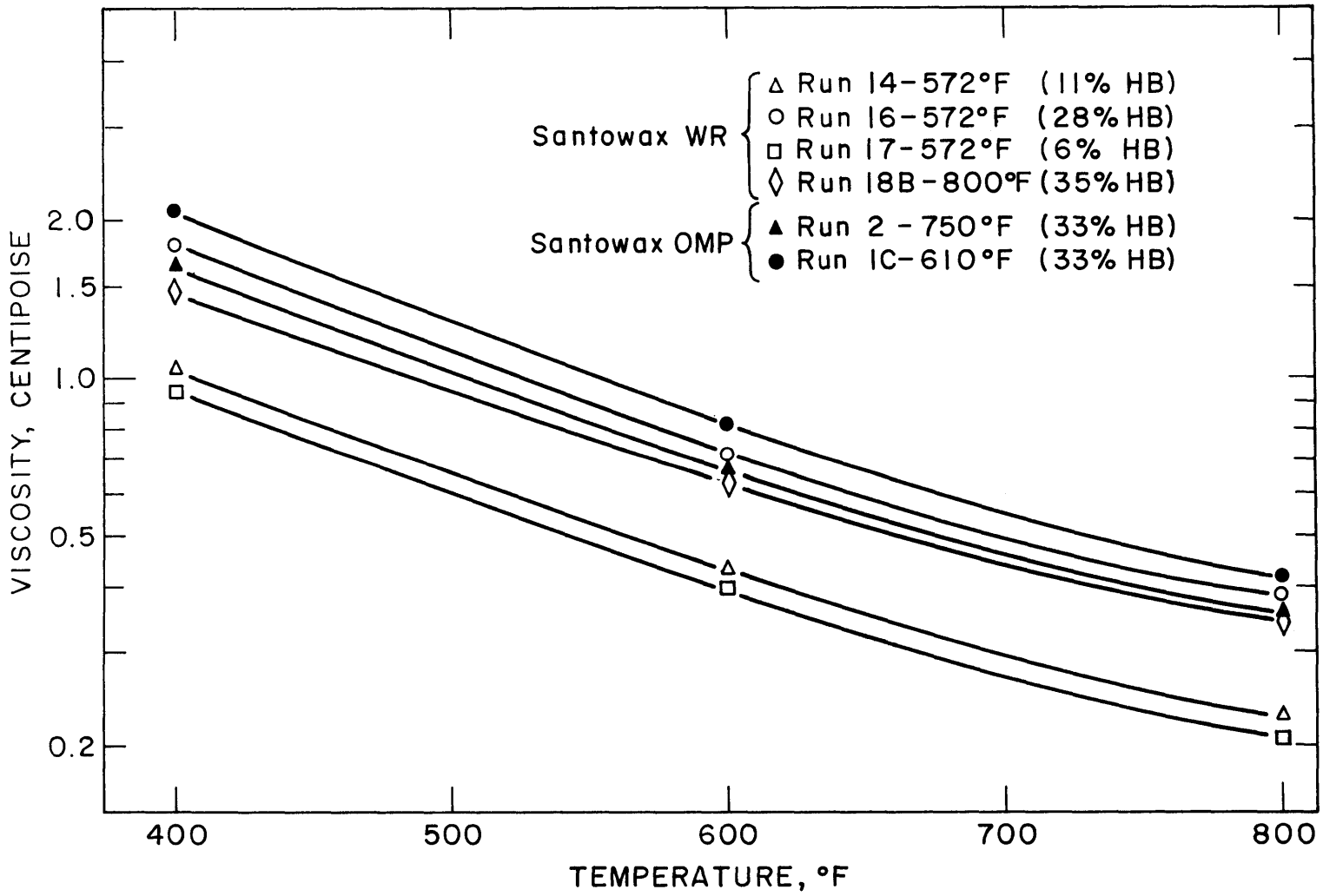

FIGURE 3.2 EFFECT OF TEMPERATURE ON THE VISCOSITY OF SANTOWAX WR AND SANTOWAX OMP.

of 3-4 samples taken at well-spaced intervals during the steady-state period. The computer program VISDEN (3.4) is used to determine the best values of the constants μ_o and ΔE from the viscosity measurements of all samples tested during a steady-state period.

In earlier M.I.T. reports (3.4, 3.1), the viscosity data were correlated by

$$\mu = \mu_1 \exp\left[\frac{\Delta E}{R}\left(\frac{1}{T} - 1.163\times10^{-3}\right)\right] \qquad (3.5)$$

where

T is the temperature, °R

μ_1 is the viscosity constant for a given sample, equal to the viscosity (centipoise) at 400°F.

This same correlation has been used for the Santowax WR viscosity data to determine the effect of HB concentration on the constant μ_1, as shown in Figure 3.3. The open points in Figure 3.3 represent Santowax WR data and the closed points represent Santowax OMP data reported by Sawyer and Mason (3.4). The dashed line in Figure 3.3 is the correlation of μ_1 versus bottoms concentration reported by M.I.T. (3.1) for Santowax WR irradiations in Fuel Position 1 using a Bottoms distillation procedure. The viscosity data obtained from the recent irradiations in Fuel Position 20 at 572°F and 800°F show that at high HB concentrations, the viscosity decreases with increasing irradiation temperature.

The activation energy for the viscosity, ΔE, is shown in Figure 3.4 for the Santowax WR and Santowax OMP irradiations runs with HB distillations. For irradiations at a given temperature (such as 572°F), ΔE appears to increase with increasing HB concentration. The range of ΔE from 4.3 to 4.8 k-cal/mole agrees well with the values reported by M.I.T. (3.1) for the irradiation runs with Bottoms distillation.

Table 3.2 compares the viscosities of Santowax WR and OM-2 samples as (1) measured by M.I.T. for irradiations at 572°F, (2) reported by Mandel (3.5), Atomics International, and (3) reported by Fritz and Elberg (3.6), Euratom, and Chavenal (3.7), Euratom. Mandel's values are based on earlier M.I.T. data (3.8) and represent viscosity versus DP concentration rather than HB concentration. Table 3.2 shows the recent M.I.T. viscosity data agree well with the Euratom data up to

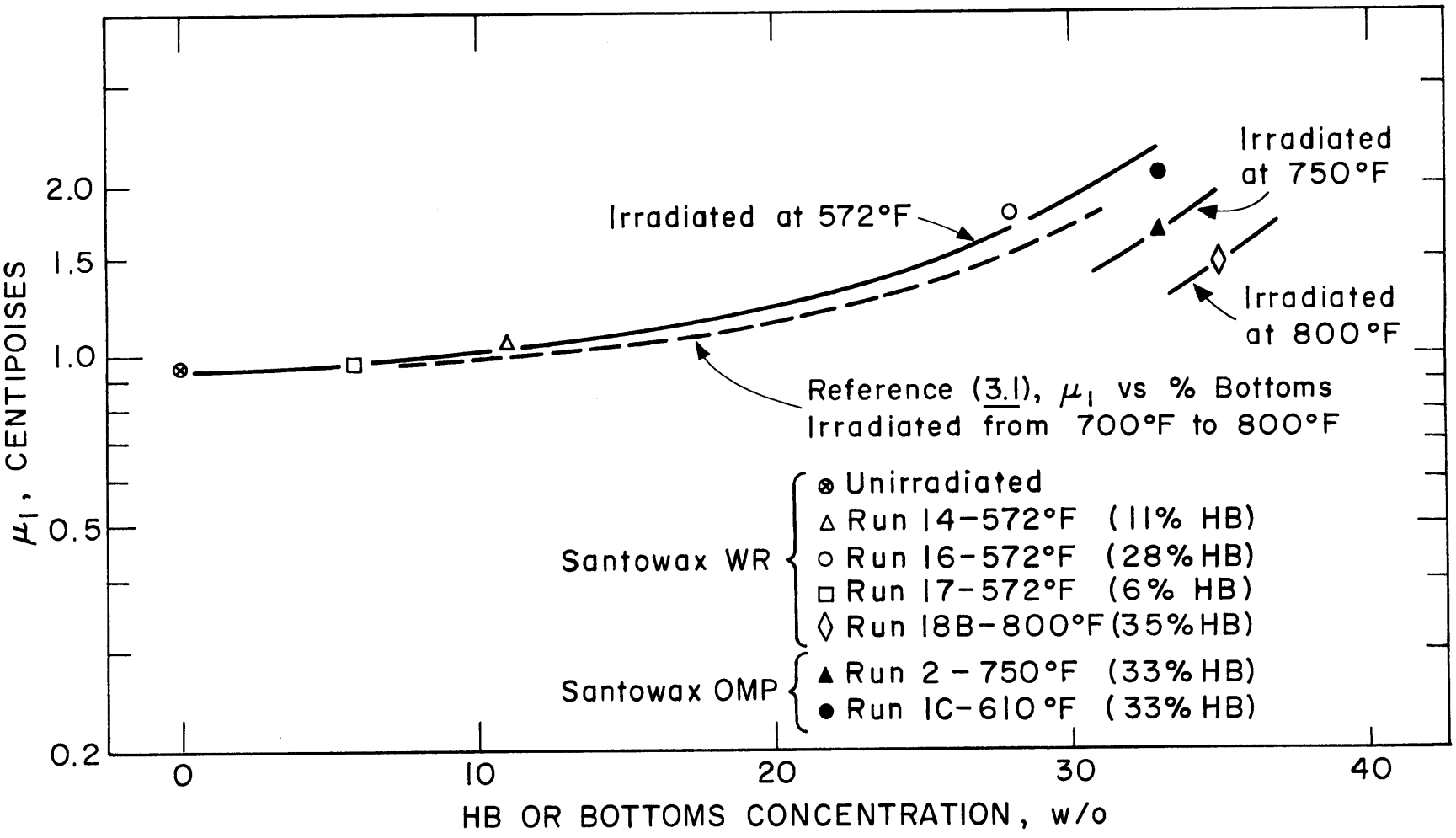

FIGURE 3.3 CORRELATION OF IRRADIATED SANTOWAX WR AND SANTOWAX OMP VISCOSITY WITH HIGH BOILER CONCENTRATION

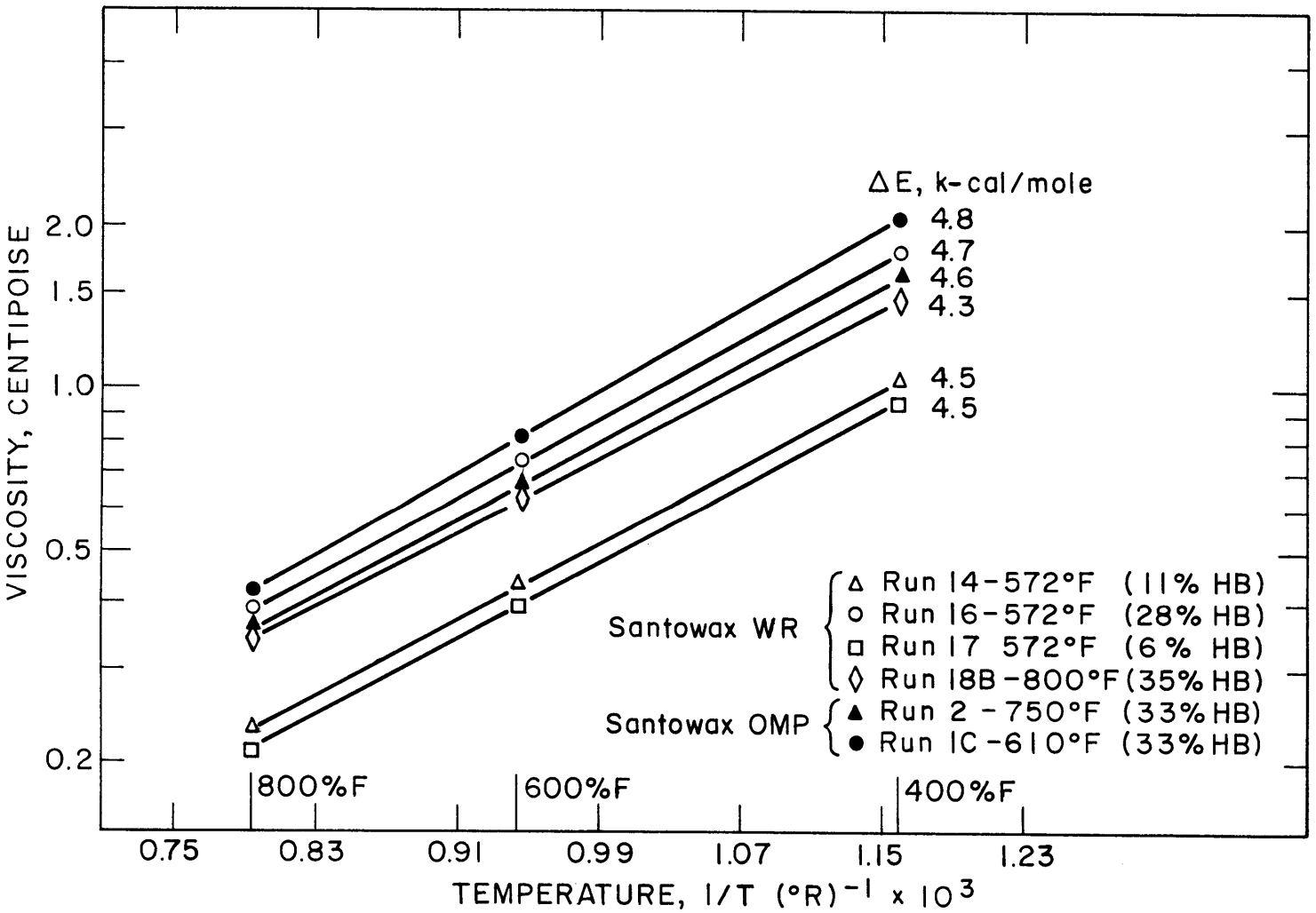

FIGURE 3.4 EFFECT OF HIGH BOILER CONCENTRATION ON VISCOSITY AND ACTIVATION ENERGY

Table 3.2

Comparison of Viscosities of Santowax WR and OM-2

Reported in Literature

% HB	Viscosity, centipoise								
	400°F			600°F			800°F		
	MIT[a]	AI	Euratom	MIT[a]	AI	Euratom	MIT[a]	AI	Euratom
0	0.90	0.78	0.85	0.39	0.33	0.36	0.20	0.17	0.20
10	1.00	0.89	1.00	0.43	0.36	0.43	0.23	0.19	0.23
20	1.20	1.04	1.25	0.48	0.42	0.48	0.26	0.23	0.26
30	1.85	1.22	1.50	0.74	0.50	0.57	0.39	0.27	0.29

[a] Interpolated from Figures 3.2 and 3.4, for Santowax WR irradiated at 572°F.

[b] Reported by Mandel (3.5), Atomics International, for Santowax WR; values are viscosity vs. % DP.

[c] OM-2 densities reported by Fritz and Elberg (3.6), Euratom, and Chavenal et al. (3.7), Euratom.

about 20% HB concentration, but are 20-30% higher than the Euratom values at 30% HB. Since both irradiation temperature and distillation procedures can strongly affect the coolant viscosity at high HB concentrations, this difference between M.I.T. and Euratom values at 30% HB is probably due to different irradiation conditions and operating procedures.

3.4 Number Average Molecular Weight

The number average molecular weight (MW_N) has been determined for irradiated Santowax WR coolant and high boiler samples primarily to (1) determine if steady-state operation was achieved with regard to coolant composition, and (2) investigate the distribution of molecular species as a function of the irradiation temperature and high boiler (HB) concentration. These measurements of MW_N can be correlated with other physical property data (viscosity, density, and vapor phase chromatograph analyses of the high boiler to achieve both the above objectives.

Measurements of the number average molecular weight were made at M.I.T. using a Mechrolab Model 301A osmometer, which compares the lowering of the vapor pressure of a pure solvent by a standard (known molecular weight) and the sample with unknown molecular weight. A detailed description of this procedure is given by Bley and Mason (3.9). The number average molecular weight is defined as

$$MW_N = \frac{\Sigma C_i}{\Sigma \frac{C_i}{A_i}} \tag{3.6}$$

where

C_i is the weight fraction of species i in the mixture

A_i is the molecular weight of species i.

Table 3.3 shows the values of MW_N of the total coolant and the high boiler fraction of the coolant for samples removed from the loop during irradiations in Fuel Position 20. Since a molecular weight measurement was made on almost every sample taken during Run 16, the values of MW_N for this run have been plotted versus irradiation time in Figure 3.5 to determine if the molecular weight distribution remained constant during

Table 3.3

Number Average Molecular Weights of
Steady-State Run Coolant Samples

Sample	Irradiation Temperature, °F	% HB	% Biphenyl	MW_N	
				Coolant	High Boiler
14L-4	572	10.9	–	252	444
14L-8	572	11.0	–	234	450
14L-12	572	10.9	–	251	452
16L-1	572	28.8	3.5	272	473
16L-2	572	29.8	1.4	269	472
16L-3	572	29.7	1.3	291	510
16L-4	572	24.4	1.9	311	530
16L-5	572	24.6	2.2	287	509
16L-6*	572	26.9	2.9	–	517
16L-7*	572	28.9	2.9	297	520
16L-8	572	28.4	2.3	301	–
16L-11	572	28.5	2.9	273	524
16L-12	572	28.7	2.9	278	529
16L-13	572	28.5	2.3	279	533
16L-14	572	28.8	2.5	276	533
16L-15	572	28.5	2.8	281	545
16L-16	572	28.7	2.7	271	–
16L-17	572	28.7	2.7	280	543
16L-18	572	29.0	2.9	285	557
16L-19	572	28.6	2.6	276	533
16L-20	572	28.5	2.7	275	538
16L-21	572	28.7	–	274	540
17L-1	572	6.0	–	240	476
17L-8	572	6.6	1.4	242	476
17L-16	572	6.4	1.5	237	462
17L-24	572	6.4	–	226	457
18L-13	800	36.8	5.2	286	483
18L-18	800	35.1	4.5	284	480
18L-23	800	34.3	5.5	284	469

* Beginning of steady state.

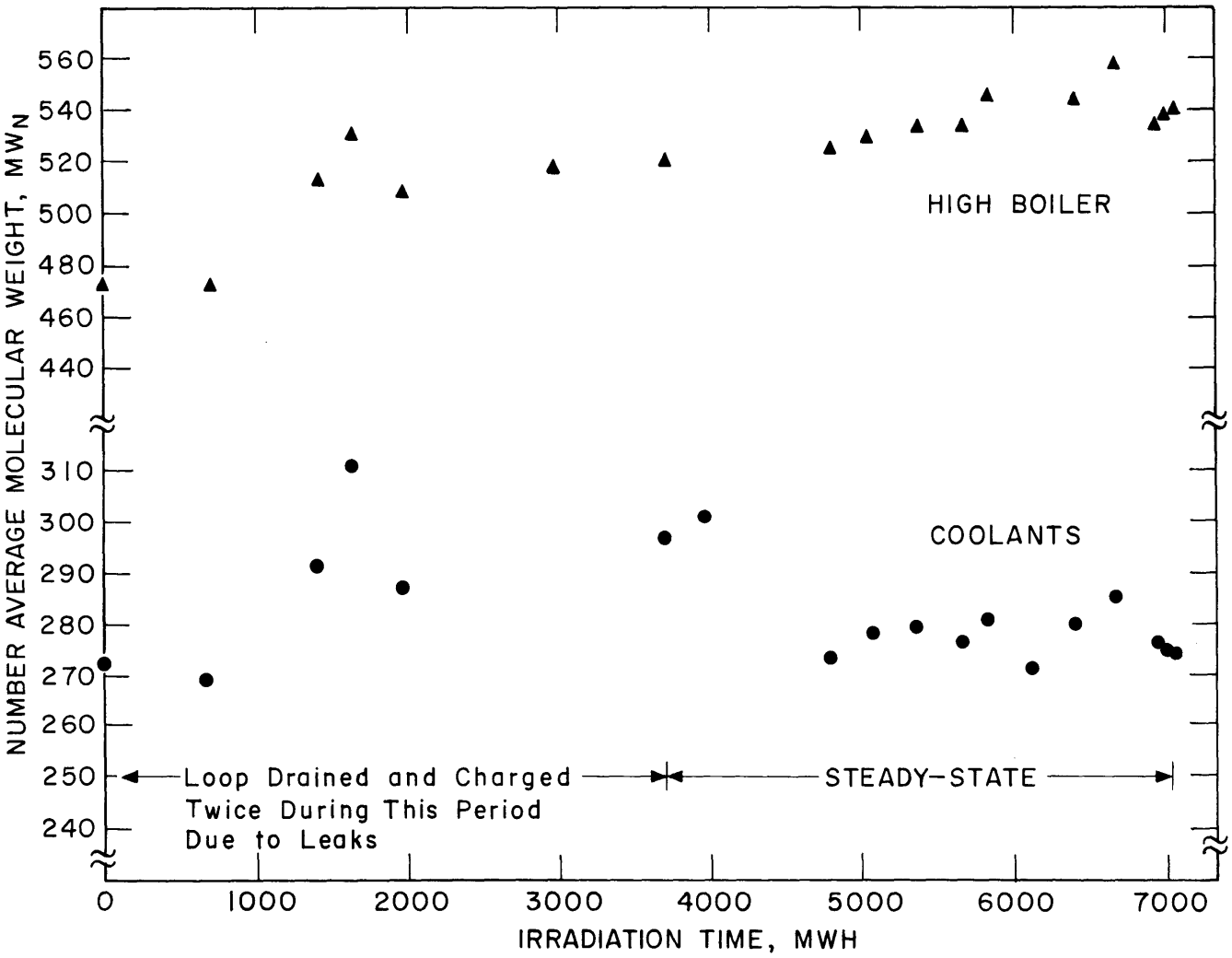

FIGURE 3.5 EFFECT OF IRRADIATION TIME ON THE COOLANT AND HIGH BOILER NUMBER AVERAGE MOLECULAR WEIGHT–RUN 16, 572°F, 29% HB

steady state. This figure indicates that the MW_N of the coolant was constant within the reproducibility limits of the measurements (±5%), but the number average molecular weight of the high boiler may have been increasing slightly during "steady state."

Figure 3.6 is a plot of the number average molecular weight of the coolant and high boiler versus degradation products (DP) concentration. The values of MW_N for the two steady-state irradiations of Santowax OMP are included for comparison. The dashed line in Figure 3.6 represents the coolant MW_N versus % DP reported by Sawyer and Mason (3.4) for Santowax OMP transient runs at 610°F (Runs 1A and 1B). The recent data for Runs 14, 16, and 17 made at 572°F agree well with this curve.

One point of disagreement in Figure 3.6 is the comparison of the number average molecular weight of the high boiler for Run 16 and Run 1. These were both low temperature runs (572°F and 610°F) at high HB concentrations (28% for Run 16 and 33% for Run 1). However, MW_N for the high boiler for Run 1C was 700±35 (3.9) and for Run 16 MW_N for the high boiler was about 540. One possible explanation for this difference is the fact that while Run 1C lasted over one year, Run 16 lasted only two months which may not have been long enough to allow the molecular weight distribution of the high boiler to reach a steady-state value (see Figure 3.5). Also, Run 1C (steady-state) was immediately preceded by a transient run (Run 1B) which reached 60% DP concentration (or about 45% HB). Since high molecular weight species accumulate more rapidly for coolant containing high concentrations of high boiler, the high molecular weight of the HB fraction (MW_N = 700) during Run 1C may reflect products made during the preceding transient run. The run immediately preceding Run 16, on the other hand, was a high temperature irradiation (Run 15 at 800°F) which tends to reduce the MW_N of the high boiler due to thermal cracking of heavy molecules. This latter effect (thermal cracking) is reflected in the relatively low value of MW_N equal 480 for the high boiler during Run 18B (800°F), even though the coolant contained 35% HB. Sawyer and Mason (3.4) and Bley and Mason (3.9) report this same behavior with Santowax OMP irradiated at 610°F (Run 1C) and 750°F (Run 2), as the data points in Figure 3.6 for these runs indicate.

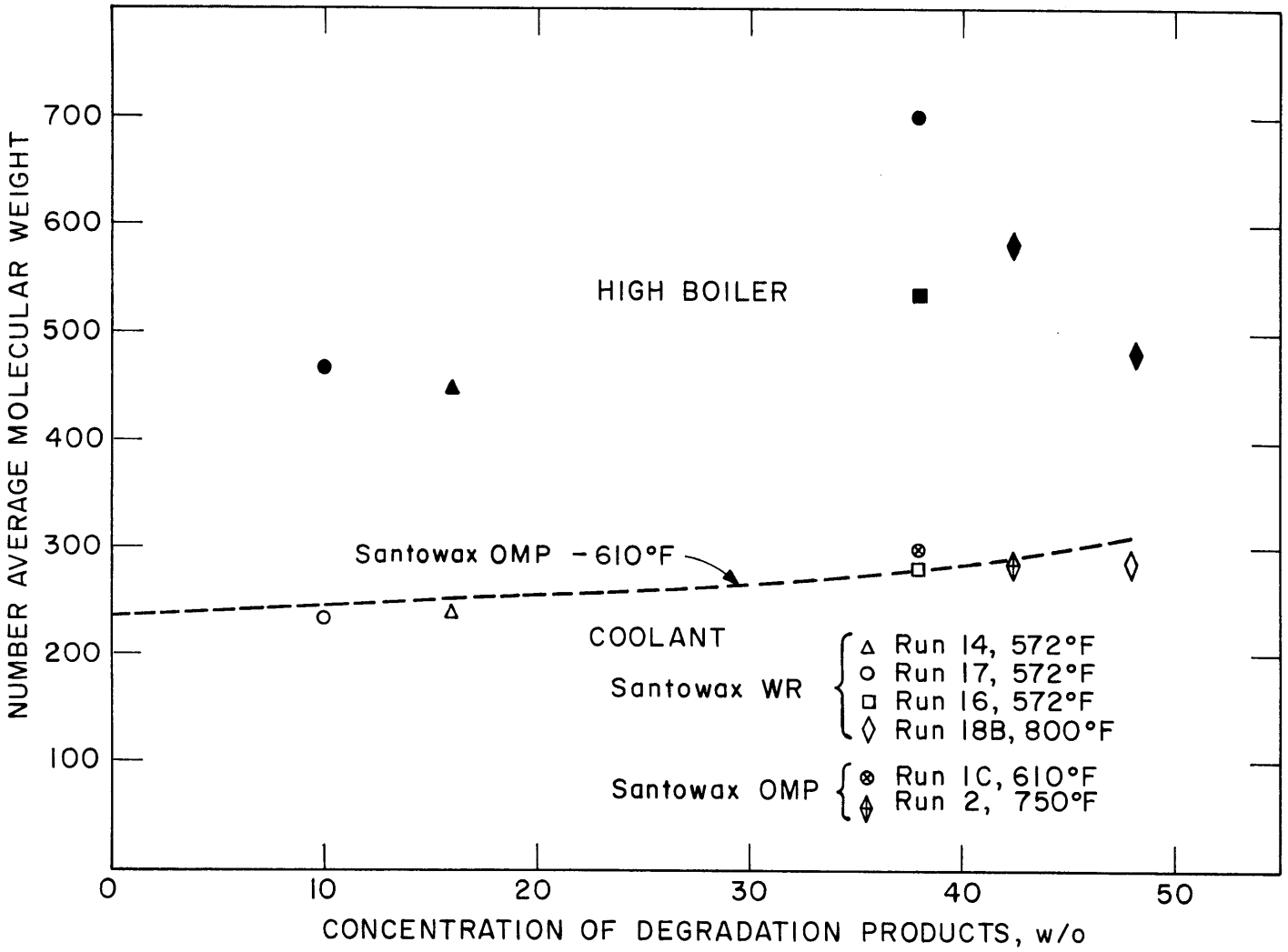

FIGURE 3.6 NUMBER AVERAGE MOLECULAR WEIGHTS OF COOLANT AND HIGH BOILER

3.5 Melting Range

The melting points of organic coolant samples irradiated at M.I.T. were measured by a Fisher-Johns apparatus. Since the coolant is a mixture of terphenyl isomers and degradation products, the melting point is reported over a temperature range from initial liquidus point to final liquidus point. Table 3.4 presents the melting point data for samples irradiated in Fuel Position 20, and compares these data with the melting points of the individual terphenyl isomers and unirradiated Santowax WR.

The coolant samples removed from the loop during Run 16 (38% DP) and Run 18B (48% DP) remained sub-cooled liquids at room temperature since the runs were completed (two to four months) and thus the melting points of these samples could not be determined. The appearance of these samples with high DP concentrations is a viscous black liquid at room temperature. The samples flow easily as the temperature is raised to the range 100°F to 125°F. The flow points of samples from Run 14 (16% DP) and Run 17 (10% DP) appear to be 125°F and 138°F.

3.6 Oxygen, Water, and Membrane Stain Test

Table 3.5 presents the results of analyses of M.I.T. coolant samples performed by Atomics International, Canoga Park, California (3.10). Comparative values for the Santowax OMP coolant from the Piqua organic-cooled and moderated reactor are also shown in this table. These tests included measurements of water content, carbonyl-bound oxygen, and total oxygen, and a Membrane Stain Test (MST). The oxygen and water concentration in the coolant are believed to be related to the degradation rate and fouling tendency of the coolant by some investigators, but quantitative relationships have not been firmly established. The MST is a measure of the concentration of colloids in the coolant which may also be related to the fouling tendency.

3.7 Heat Transfer

Swan and Mason (3.2) have presented the results of heat transfer measurements made on the M.I.T. Organic Loop Project through June, 1965. The two primary conclusions reached in that review were:

Table 3.4

Melting Points of Irradiated and Unirradiated Santowax WR

Sample	Irradiation Temperature °F	Irradiation Temperature °C	% DP	% HB	Initial Liquidus °F	Initial Liquidus °C	Final Liquidus °F	Final Liquidus °C
Pure ortho	–	–	–	–	134	57	135	57
Pure meta	–	–	–	–	189	87	190	88
Pure para	–	–	–	–	410	211	415	213
Unirradiated Santowax WR	–	–	–	–	135	57	194	90
Run 14[b]	572	300	16	11	113	45 (47)[a]	167	75 (87)[a]
Run 16	572	300	38	28	viscous liquid at room temperature			
Run 17[b]	572	300	10	6	115	46	171	77
Run 18B	800	427	48	34	viscous liquid at room temperature			

[a] Measured by Atomics International by differential calorimetry.

[b] Flow point estimated as 125°F to 138°F.

Table 3.5

Analyses of M. I. T. Coolant Samples by Atomics International

	Run 14	Run 16	Run 17	Typical PNPF[a] Value
Sample Number	14L-16	16L-23	17L-37	–
% HB	11	28	6	5-10
Water	213 ppm	477 ppm	77 ppm	50 ppm
Carbonyl-bound oxygen	20 ppm	11 ppm	42 ppm	30 to 50 ppm
Total Oxygen	1295 ± 5 ppm	410 ± 50 ppm	200 ± 90 ppm	~1000 ppm
MST[b]	100 ± 9 $\times 10^{-5}$ A/mg	not available	not available	10 to 20 $\times 10^{-5}$ A/mg

[a] Piqua Nuclear Power Facility.

[b] Membrane Stain Test.

(1) The heat transfer data of Santowax WR and Santowax OMP measured in the M. I. T. loop were correlated well by the forced convection heat transfer relation of McAdams:

$$Nu_B = 0.023\ Re_B^{0.8}\ Pr_B^{0.4} \pm 10\% \qquad (3.7)$$

where

Nu_B = Nusselt number = $\frac{hD}{k}$, using bulk coolant properties

Re_B = Reynolds number = $\frac{\rho VD}{\mu}$, using bulk coolant properties

Pr_B = Prandtl number = $\frac{C_p\mu}{k}$ using bulk coolant properties

(2) Using the method of Wilson to determine the effect of scale or film buildup on the overall heat transfer coefficient, U, it appeared there had been no significant scale buildup on the inside surface of Test Heater No. 6 (TH6) after three years of operation.

Sixteen heat transfer measurements were made during steady-state runs in Fuel Position 20 in order to further test the correlation of heat transfer data by Equation (3.7) and to determine if scale buildup could be detected on the inside surface of Test Heater No. 7 (TH7). The operating conditions and calculated overall heat transfer coefficients, U, for these measurements are given in Table 3.6. The nominal bulk coolant temperature for all these heat transfer runs was 572°F.

Detailed descriptions of the theory and procedures used at M. I. T. to measure the coefficient of heat transfer are given in earlier reports (3.2, 3.3, 3.4). Briefly, U was calculated from

$$U = \frac{Q_{in}}{A(T_{w,i}-T_B)} \quad (Btu/hr\text{-}ft^2\text{-}°F) \qquad (3.8)$$

since the temperature difference between the inside wall and the bulk coolant is constant along the test heater length (except for small local perturbations near the test heater electrodes). The heat input, Q_{in}, is determined from the voltage drop across the test heater resistance, corrected for heat losses along the lugs of the heater.

Table 3.6

Heat Transfer Data from Test Heater No. 7

572°F Irradiation of Santowax WR

Run No.	Velocity (ft/sec)	Heat Flux Q/A ($Btu/hr\text{-}ft^2$)	Heat Transfer Coefficient, U ($Btu/hr\text{-}ft^2\text{-}°F$)	Nusselt No.	Reynolds No.	Prandtl No.	μ/μ_w
13-7	17.7	142,769	1480	391	56,944	9.15	1.35
13-8	14.6	141,107	1227	325	47,151	9.13	1.43
13-9	11.6	139,860	1026	271	37,907	9.04	1.51
13-10	18.1	142,323	1436	380	58,139	9.16	1.36
14-1	20.8	101,896	1665	439	67,590	8.95	1.19
14-2	17.4	100,039	1397	369	56,909	8.91	1.22
14-3	14.5	100,840	1272	336	47,535	8.90	1.25
14-4	11.6	99,986	1030	273	38,554	8.80	1.31
14-5	9.4	99,232	894	238	32,359	8.54	1.35
16-1	20.8	124,547	1512	398	66,800	9.03	1.27
16-2	16.8	121,074	1271	336	54,611	8.96	1.31
16-3	14.3	120,991	1063	281	46,884	8.90	1.38
16-4	11.1	123,859	817	217	37,736	8.65	1.50
17-1	16.6	107,478	1286	339	54,151	8.94	1.27
17-2	13.6	105,848	1116	295	44,303	8.91	1.31
17-3	11.0	106,333	893	237	36,360	8.79	1.40

The film heat transfer coefficient, h_f, is related to U by Equation (3.9):

$$\frac{1}{U} = \frac{1}{h_f} + \frac{1}{h_s} \tag{3.9}$$

The film coefficient is equal to U only when there is no scale resistance, or when h_s is infinite. The method of Wilson has been used to determine that there has been no measurable scale buildup on the inside surface of the test heaters. Therefore, for all of the correlations reported here, U was set equal to h_f.

The relations used to correlate the M. I. T. heat transfer data are the Dittus-Boelter type

$$Nu = a\, Re^b\, Pr^c \tag{3.10}$$

and the Seider-Tate type

$$Nu = a\, Re^b\, Pr^c \left(\frac{\mu}{\mu_w}\right)^d . \tag{3.11}$$

Table 3.7 shows the heat transfer data of Table 3.6 correlated by the Dittus-Boelter relation, and Table 3.8 shows these data correlated by the Seider-Tate relation. The correlations shown in Tables 3.7 and 3.8 have been found by the MNHTR computer program (3.4) in which all the "constants" (a, b, c, and d in Equations (3.10) and (3.11)) can be allowed to vary, or some of the constants can be fixed in order to find the best values for the remaining constants. Comparison of Tables 3.7 and 3.8 reveals that use of the viscosity ratio, μ/μ_w, in Table 3.8 did not improve the data fit, since the root-mean-square (RMS) deviations and correlation coefficients using this term are not quite as good as those shown in Table 3.7. Therefore, the Dittus-Boelter relation was chosen as the best correlating equation. This same choice was made by Swan and Mason (3.2) in correlating earlier M. I. T. data. As shown in Table 3.6, the Prandtl number varied only about 6% for the operating conditions of these heat transfer measurements, so no significant evaluation of the best value of the exponent "c" in Equation (3.10) could be made. Therefore, a value of c equal 0.40 was chosen, consistent with Swan's best value. Table 3.7 shows that using c equal 0.40 gives a best

Table 3.7

Correlation of Heat Transfer Measurements
Using Test Heater No. 7, $Nu = a\,Re^{b}\,Pr^{c}$
(Dittus-Boelter Relation)

(1) Variation of all "constants"		
	$Nu = 0.00166\,Re^{0.77}Pr^{1.72}$	RMS deviation = 6.66% Correlation coefficient = 0.954
(2) c = 0.33		
	$Nu = 0.0147\,Re^{0.86}Pr^{0.33}$	RMS deviation = 6.74% Correlation coefficient = 0.950
(3) c = 0.40		
	$Nu = 0.0133\,Re^{0.85}Pr^{0.40}$	RMS deviation = 6.71% Correlation coefficient = 0.950
(4) b = 0.80, c = 0.40		
	$Nu = 0.0236\,Re^{0.80}Pr^{0.40}$	RMS deviation = 6.59% Correlation coefficient = 0.948

Table 3.8

Correlation of Heat Transfer Measurements

Using Test Heater No. 7, $Nu = a\,Re^{b}\,Pr^{c}\,(\frac{\mu}{\mu_w})^{d}$

(Seider-Tate Relation)

(1) d = 0.14	
$Nu = 0.00197\,Re^{0.82}\,Pr^{1.4}\,(\frac{\mu}{\mu_w})^{0.14}$	RMS deviation = 6.88% Correlation coefficient = 0.947
(2) c = 0.33, d = 0.14	
$Nu = 0.0107\,Re^{0.88}\,Pr^{0.33}\,(\frac{\mu}{\mu_w})^{0.14}$	RMS deviation = 6.82% Correlation coefficient = 0.944
(3) c = 0.40, d = 0.14	
$Nu = -.00955\,Re^{0.88}\,Pr^{0.40}\,(\frac{\mu}{\mu_w})^{0.14}$	RMS deviation = 6.80% Correlation coefficient = 0.945
(4) b = 0.80, c = 0.40, d = 0.14	
$Nu = 0.0227\,Re^{0.80}\,Pr^{0.40}\,(\frac{\mu}{\mu_w})^{0.14}$	RMS deviation = 6.81% Correlation coefficient = 0.941

value for the Reynolds number exponent, b, equal to 0.85. However, the RMS deviation is lower using b = 0.80 rather than b = 0.85, even though the correlation coefficient is not quite as high for b = 0.80. As pointed out by Swan and Mason (3.4), there is no significant difference in the correlations provided by these slightly different values of b over the range of Reynolds numbers realized in the M.I.T. experiments. Using b = 0.80 gives a coefficient "a" consistent with McAdam's value of a = 0.023 (see (4) in Table 3.7).

Figure 3.7 shows the sixteen heat transfer data points of Table 3.6 correlated by the McAdam's relation of Equation (3.7). All but one of these data points agree within ±10% (dashed lines) with the correlating relation. It should be noted, however, that these data cover only a relatively narrow range of Reynolds numbers from 32,000 to 68,000.

Wilson's method to determine scale buildup is based on the fact that for turbulent flow of a fluid, during a period of time when the physical properties are constant, the film coefficient can be expressed

$$h_f = AV^b \tag{3.12}$$

where

A is an arbitrary constant

V is the coolant valocity

b is the exponent on the correlation for forced convection normally taken as 0.8

Combining Equations (3.9) and (3.12), the expression for the overall coefficient is

$$\frac{1}{U} = \frac{1}{h_s} + \frac{A}{V^b} \tag{3.13}$$

Therefore, a plot of $1/U$ against $1/V^b$, when it is extrapolated back to infinite velocity, gives the value $1/h_s$ as the intercept with the $1/U$ axis.

Figure 3.8 is a Wilson plot of the heat transfer data of Table 3.6. The computer program, MNHTR, performs this analysis by fitting the set of data taken at different velocities on a given day to Equation (3.13) by the method of least squares. Considering a possible uncertainty of ±10% in the measurement of U and the necessary extrapolation to obtain the intercepts, the Wilson plot results indicate little or no scale buildup on the inside surface of Test Heater No. 7 after about 18 months' operation.

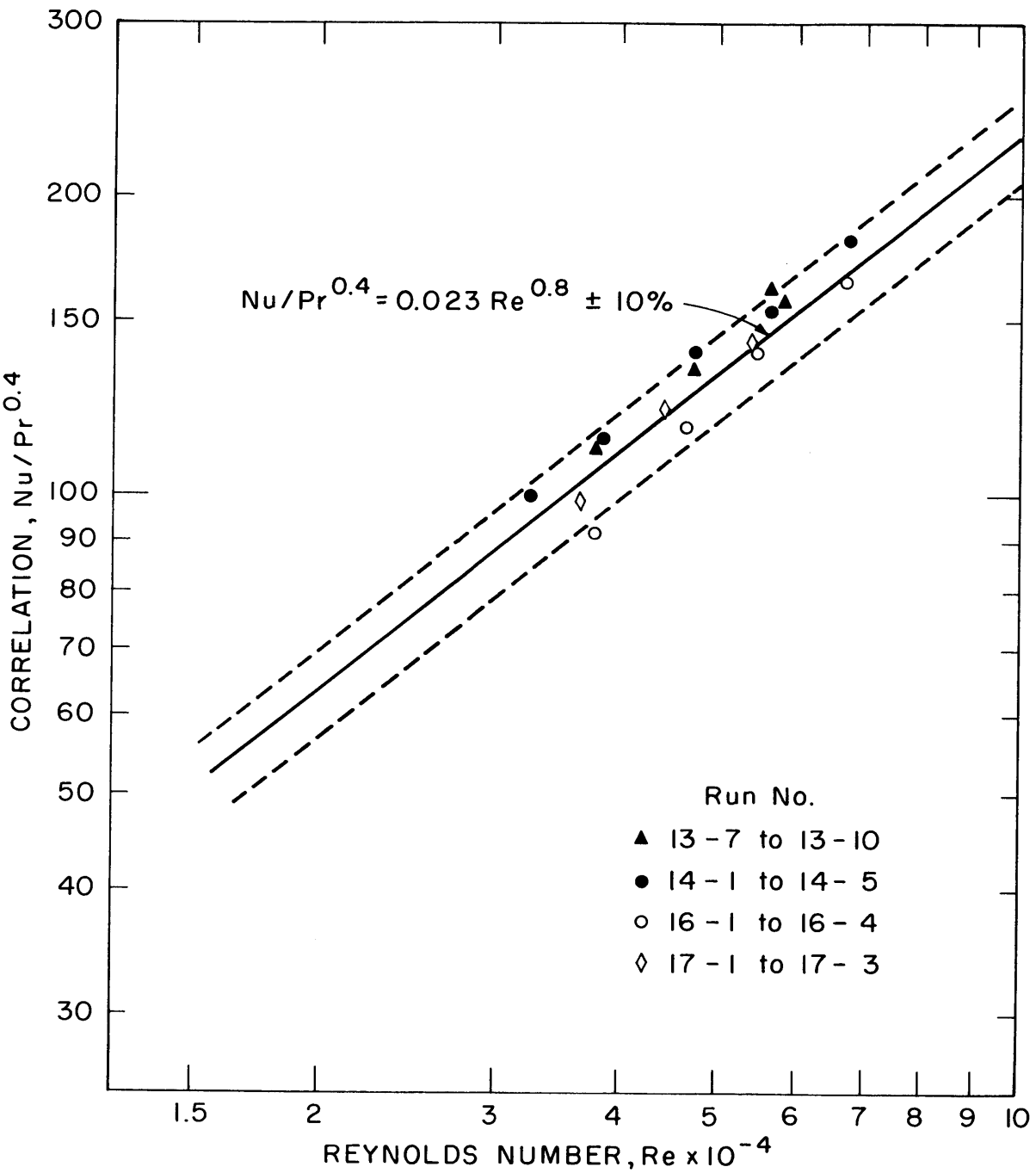

FIGURE 3.7 CORRELATION OF M.I.T. IRRADIATED TERPHENYL HEAT TRANSFER DATA

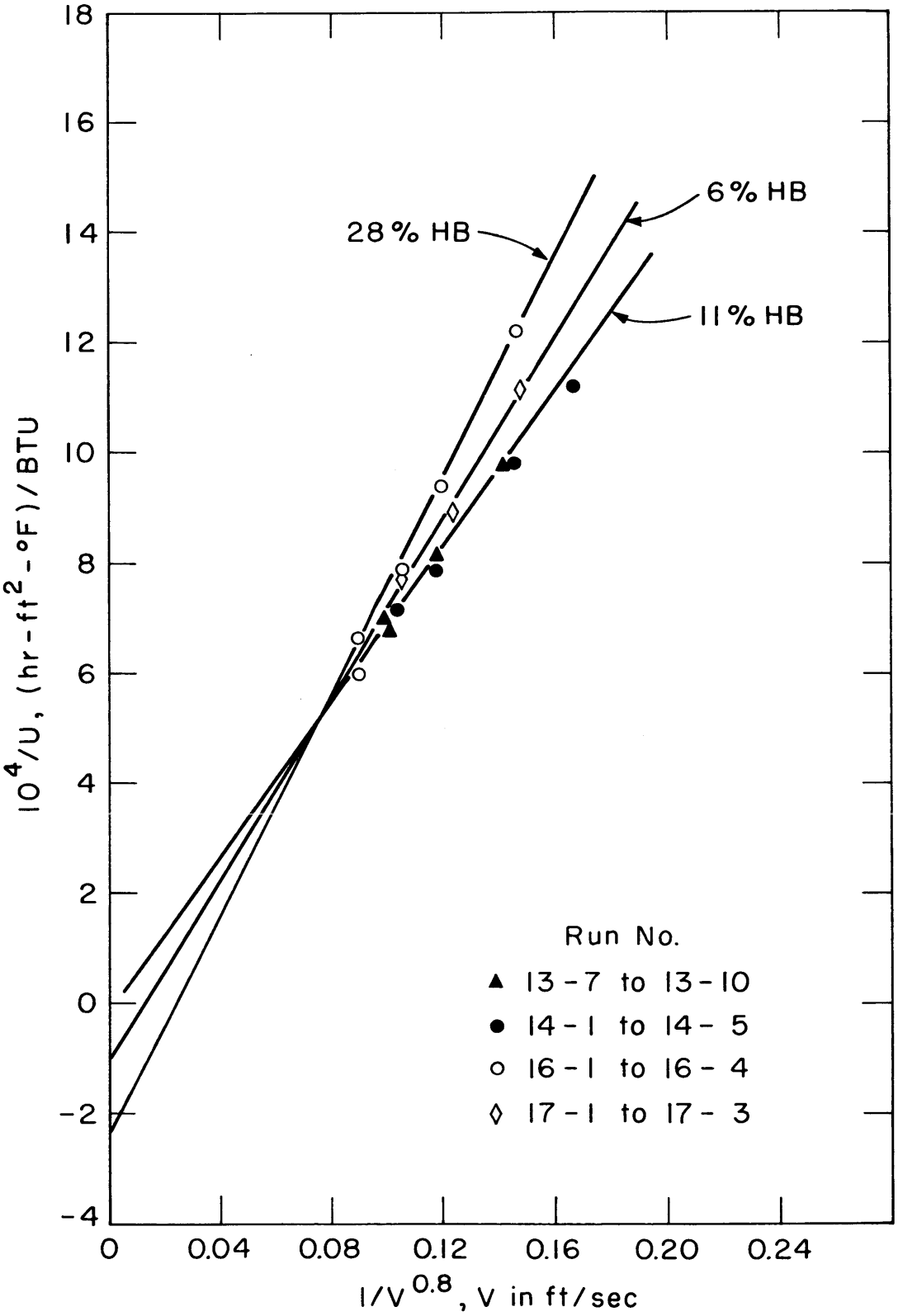

FIGURE 3.8 TYPICAL WILSON PLOT OF SANTOWAX WR, TEST HEATER No.7 DATA

CHAPTER 4

LOW TEMPERATURE TERPHENYL DEGRADATION

4.1 Introduction

The primary emphasis on organic coolant experimental studies at M.I.T., during the period January 1, 1965 – June 30, 1966, has been placed on investigation of radiolysis effects, which are seen at low temperatures (under 320°C) without additional degradation caused by thermal decomposition of the coolant. Three steady-state irradiations and one transient irradiation of Santowax WR have been made at 300°C in Fuel Position 20 at approximately 7% fast neutron fraction (f_N). The objectives of these low temperature irradiations of Santowax WR were:

(1) to determine the apparent kinetics order of radiolysis at these operating conditions by comparing the coolant degradation rates at three different steady-state terphenyl concentrations,

(2) to determine the fast neutron effect ratio, G_N/G_γ, by comparing the coolant degradation rates measured in Fuel Position 20 at $f_N = 0.07$ at 572°F (300°C) with the coolant degradation rates measured in Fuel Position 1 at $f_N = 0.37$ and 0.40 at 610°F (319°C), and

(3) to measure the relative radiolytic stability of the individual terphenyl isomers at $f_N = 0.07$ and compare these values with the relative radiolytic stabilities of the terphenyl isomers at $f_N = 0.37$ and 0.40.

The correlation of M.I.T. terphenyl irradiation results and the results of terphenyl irradiations made by other laboratories in the United States, Canada, and Europe during the past ten years has been a major objective of the M.I.T. program.

4.2 Liquid Degradation – Theory

The degradation of terphenyl coolants in nuclear reactors results from the combined effect of pile radiations (fast neutrons and gamma rays), designated as radiolysis, and thermal decomposition, designated as pyrolysis when referring to unirradiated coolants or radiopyrolysis when referring to irradiated coolants. Assuming the rate of degradation of terphenyls depends only on the concentration of terphenyls and radiolysis and radiopyrolysis are independent and linearly additive, a general rate equation expressing the total terphenyl degradation rate in the coolant can be written (see Section A3.1 for derivation)

$$\frac{w_i}{M\bar{r}}(C^f_{omp}-C_{omp}) - \frac{dC_{omp}}{d\tau} = k_{R,omp,n}C^n_{omp} + \frac{k_{P,omp,m}C^m_{omp}}{\bar{r}} = \frac{G(-omp)}{11.65} \qquad (4.1a)$$

where

w_i = organic coolant feed rate to the system, gms/hr

M = organic coolant mass in the system, gms

C^f_{omp} = concentration of total terphenyl in feed, weight fraction

C_{omp} = concentration of total terphenyl in the system, weight fraction

τ = specific radiation dose, watt-hr/gm

$\bar{r}$ = average dose rate, watts/gm = $d\tau/dt$

n = apparent kinetics order of radiolysis

m = apparent kinetics order of pyrolysis

$k_{R,omp,n}$ = rate constant for radiolysis for specified kinetics order of radiolysis, $(watt\text{-}hr/gm)^{-1}$

$k_{P,omp,m}$ = rate constant for radiopyrolysis for specified kinetics order of pyrolysis $(hr)^{-1}$

G(-omp) = terphenyl degradation rate, molecules degraded/100 ev

11.65 = conversion factor, (molecules)(watt-hr)/(100 ev)(gm)

Some modification of Equation (4.1a) is necessary to express the degradation rate of the individual terphenyl isomers since interactions

between both like and unlike isomers can occur. Equation (4.1b) is a general expression which is useful for the correlation of the degradation rates of the individual isomers.

$$\frac{w_i(C_i^f - C_i)}{M\bar{r}} - \frac{dC_i}{d\tau} = k_{R,i,a+b} C_i^a C_{omp}^b + \frac{k_{P,i,c+d} C_i^c C_{omp}^d}{\bar{r}} = \frac{G(-i)}{11.65} \qquad (4.1b)$$

It should be noted that Equation (4.1b) reduces to Equation (4.1a) where the subscript i refers to total terphenyl. Equation (4.1b) includes terms containing the total terphenyl concentration, C_{omp}, in this empirical expression for the individual isomer degradation rates to account for possible interactions between isomers. For second-order radiolysis kinetics for total terphenyl (n = 2), M.I.T. has recently reported (4.1) correlations for the degradation rates of the isomers at low temperature (610°F), assuming a = b = 1 in Equation (4.1b). This calculational model will be discussed further in Section 4.5 (radiolysis) and Chapter 6 (high temperature effects).

Since both fast neutrons and gamma rays contribute to the radiolysis term in Equations (4.1a) and (4.1b), these expressions inherently assume that fast neutron degradation and gamma-ray degradation follow the same kinetics order, n. The validity of this assumption is discussed with the experimental results in Section 4.4.2. The magnitude of the apparent kinetics order for radiolysis, n, had not been clearly defined at the beginning of this study, due to experimental difficulties. In transient irradiations, the scatter in the data is sufficient to prevent a statistically significant definition of the apparent kinetics order. Long irradiation times are required for the more significant steady-state irradiations at temperatures sufficiently low so that radiolysis can be investigated without radiopyrolysis contributing significantly to the total degradation rate, and thus few low temperature steady-state irradiations have been made. Most investigators report radiolysis degradation yields based on either first- or second-order kinetics (4.1, 4.4, 4.5).

Radiolysis yields for steady-state runs are customarily reported in terms of G(-i), the number of molecules of irradiated substance degraded per 100 ev of radiation energy absorbed. For transient runs

(decreasing terphenyl concentration), the radiolysis yields are usually reported as initial G values (designated G^o or G^*) or integral G values for the entire transient. An alternative method of reporting irradiation results for transient runs is the use of overall rate constants, $K(wh/g)^{-1}$ and $K'(hr)^{-1}$, which are found by computer least-square-error analysis of terphenyl concentration versus dose and/or time data. The equations used to calculate the degradation rates for steady-state and transient runs are described in detail in Appendix A3.

Since pile radiations causing damage in organic coolants consist primarily of fast neutrons and gamma rays, a G value may be assigned to each type of radiation. For an irradiation facility in which a fraction, f_N, of the total dose to the coolant is received from fast neutrons, the total radiolysis degradation yield can be written

$$G_R = G_N f_N + G_\gamma (1-f_N) \tag{4.2}$$

since generally, for reactor irradiations,

$$f_\gamma = 1 - f_N \tag{4.3}$$

Linear additivity of fast neutron and gamma-ray induced degradation is assumed in Equation (4.2) and, on the basis of experimental results available, this assumption will be shown to be valid in Section 4.4.2. The ratio, G_N/G_γ, is called the "fast neutron effect ratio."

The radiolysis rate constant and the G value for total terphenyl radiolysis are related in the following manner:

$$G_R(-omp) = 11.65\ k_{R,omp,n} C_{omp}^n \tag{4.4}$$

where $k_{R,omp,n}$ and G_R may vary with temperature and fast neutron fraction.

An alternative method sometimes used to report coolant radiolysis yields is $G^*(-i)$, which is a concentration normalized G value as shown in Equation (4.5).

$$G^*(-i) = \frac{G(-i)}{C_i} \tag{4.5}$$

The G^* values are useful in comparing the relative stability of the terphenyl isomers.

4.3 Recent M.I.T. and Euratom Low Temperature Terphenyl Irradiation Results in In-Pile Loops

Both M.I.T. and Euratom have recently completed steady-state terphenyl irradiations at low temperature (M.I.T. at 300°C and Euratom at 320°C) in order to measure the apparent kinetics order of radiolysis, n, and the fast neutron effect ratio, G_N/G_γ. Since these results complement each other, the interpretation of these recent M.I.T. and Euratom data will be presented together.

4.3.1 M.I.T. Steady-State and Transient Runs

Table 4.1 presents a summary of results of the M.I.T. steady-state runs made in Fuel Position 20 at 572°F (300°C), and compares these values with the results of steady-state runs in Fuel Position 1 at 610°F (321°C). Detailed descriptions of these irradiations and the degradation calculations for each run are shown in Appendix A3. The radiopyrolysis rate for these irradiations at low temperature is negligible (see Chapter 5), so that the degradation rates shown in Table 4.1 are produced only by radiolysis (fast neutron and gamma-ray interactions with the coolant).

One transient irradiation (Run 13) was made in Fuel Position 20 at low temperature (300°C). The results of this run and of two previously reported (4.3) irradiations of Santowax OMP made in Fuel Position 1 at 321°C and $f_N = 0.37$ are shown in Table 4.2.

4.3.2 Euratom Steady-State Runs

Euratom workers have recently completed low temperature (nominally 320°C) steady-state irradiations of OM-2 coolant (similar to Santowax WR) in the BLO4 loop in the SILOE reactor. Table 4.3 presents the results of these runs as (1) reported by Euratom (4.2), and (2) calculated by M.I.T. using the procedures described in Appendix A3. The purpose of recalculating the Euratom results at M.I.T. was to insure that the differences in calculation procedures used by Euratom and M.I.T. did not produce significantly different G values. Table 4.3 shows that the maximum difference in G(-omp) reported by Euratom and calculated at M.I.T. for these low temperature BLO4 runs is less than 6% and the average difference is only 2.3%.

Table 4.1

Summary of Irradiation Results for Low Temperature Steady State Runs in the M.I.T. Loop

Run No.	Terphenyl	Temperature °F	Temperature °C	Coolant Composition, wt % ortho	meta	para	total omp	HB	G(-i), molecules/100 ev[b] G(-o)	G(-m)	G(-p)	G(-omp)	G(→HB)
Fuel Position 1: f_N = 0.37-0.40													
1C[c]	Santowax OMP	610	321	6.0	37.6	18.3	61.9	32.3	0.0157 ±0.0006	0.0963 ±0.0003	0.051 ±0.003	0.163 ±0.005	0.155 ±0.003
11[d]	Santowax WR	610	321	22.0	56.6	4.8	83.3	9.6[a]	0.087 ±0.004	0.23 ±0.01	0.020 ±0.003	0.34 ±0.02	0.287 ±0.009
Fuel Position 20: f_N = 0.07													
14	Santowax WR	572	300	15.0	63.8	5.0	83.7	11.0	0.034 ±0.001	0.115 ±0.004	0.010 ±0.001	0.163 ±0.008	0.151 ±0.005
16	Santowax WR	572	300	9.7	48.8	4.0	62.6	28.6	0.0189 ±0.001	0.0736 ±0.003	0.0106 ±0.001	0.0998 ±0.004	0.0907 ±0.003
17	Santowax WR	572	300	14.6	70.4	4.7	89.7	6.2	0.037 ±0.001	0.126 ±0.005	0.016 ±0.001	0.181 ±0.006	0.168 ±0.006

[a] Bottoms concentration (see Section 2.3.1.2).

[b] Error limits are 1σ.

[c] f_N = 0.37

[d] f_N = 0.40

Table 4.2

Summary of Irradiation Results for Low Temperature Transient Runs in the M. I. T. Loop

Run No.	Terphenyl	Temperature °F	Temperature °C	Coolant Composition, wt% ortho	meta	para	total omp	$G^*(-i)$, molecules/100 ev-wt fr. i[a] $G^*(-o)$	$G^*(-m)$	$G^*(-p)$	$G^*(-omp)$	K, $(wh/g)^{-1}$ $K_{1.7}(-omp)$[b] $(\times 10^2)$
Fuel Position 1: $f_N = 0.37$												
1A	Santowax OMP	610	321	10.7-6.3	64.8-37.4	24.6-16.2	100.0-59.6	0.34 ±0.09	0.33 ±0.06	0.21 ±0.10	0.30 ±0.05	3.33 ±0.09
1B	Santowax OMP	610	321	6.7-4.1	41.2-25.1	18.7-10.4	66.6-39.6	0.25 ±0.04	0.24 ±0.04	0.26 ±0.05	0.25 ±0.04	3.49 ±0.17
Fuel Position 20: $f_N = 0.07$												
13	Santowax WR	572	300	17.0-15.5	69.8-63.2	5.6-5.1	92.4-83.8	0.22 ±0.02	0.18 ±0.02	0.23 ±0.10	0.19 ±0.02	1.77 ±0.16

[a] First-order kinetics; $G^*(-i) = 11.65\ K_1(-i)$.

[b] 1.7 order rate constant.

Error limits are 1σ.

Table 4.3

Summary of Results of Euratom Steady-State Terphenyl Irradiations

OM-2 Coolant Irradiated at 320°C

Run No.	Facility	Terphenyl[e] Conc. w/o		Temperature[a]	Average[b] Dose Rate	f_N	Euratom Values	Values Calculated at MIT[d]				
		Euratom	MIT	°C	w/g		G(-omp)[c]	G(-omp)	G(-o)	G(-m)	G(-p)	G(→HB)
C1-41-320	BLO4	74.6	73.9	325	1.6 (0.082)	0.175	0.176 ±0.026	0.171	0.044	0.105	0.016	0.161
C2-42-320	BLO4	89.3	89.0	328	2.8 (0.145)	0.28	0.282 ±0.043	0.280	0.036	0.237	-0.004	0.271
		69.7	69.9	328	2.8 (0.145)	0.28	0.185 ±0.027	0.186	0.033	0.140	0.008	0.182
		61.0	60.2	328	2.8 (0.145)	0.28	0.154 ±0.022	0.145	0.024	0.112	0.005	0.138
C3-40-320	BLO4	89.2	89.1	325	0.65 (0.033)	0.126	0.210 ±0.032	0.202	0.042	0.128	0.035	0.201
		70.4	70.4	325	0.61 (0.033)	0.126	0.134 ±0.019	0.132	0.029	0.089	0.009	0.110
C6-41-320	BLO4	92.1	91.5	326	1.4 (0.077)	0.20	0.248 ±0.039	0.239	0.049	0.173	0.027	0.250
		70.6	69.9	326	1.4 (0.077)	0.20	0.168 ±0.024	0.168	0.035	0.117	0.007	0.157

[b] First value is average dose rate in irradiation capsule; second (parenthesis) value is average dose rate to total coolant in loop.

[a] Average temperature in irradiation capsule.

[e] Corrected for intermediate boiler (IB) concentration.

[c] Error limits are reported as 2σ.

[d] Based on degradation produced during entire feed and bleed period.

4.3.3 Apparent Reaction Order

To determine the apparent reaction kinetics order for radiolysis, n, and the fast neutron effect ratio, $G_N/G\gamma$, from low temperature steady-state irradiations, Equations (4.2) and (4.4) can be combined to give

$$\frac{G_R(-omp)}{11.65} = k_{R,omp,n} C^n_{omp} = \frac{G^o_\gamma}{11.65}\left[\left(\frac{G_N}{G_\gamma} - 1\right) f_N + 1\right] C^n_{omp} \qquad (4.6)$$

where

G^o_γ = initial degradation rate due to gamma rays, molecules/100 ev = G_γ/C^n_{omp}

G_N/G_γ = fast neutron effect ratio, assumed to be independent of terphenyl concentration

The reaction order, n, is then the slope of a linear correlation of ln $G_R(-omp)$ versus ln C_{omp}.

Figure 4.1 shows the results of M.I.T. steady-state Runs 14, 16, and 17 plotted in this manner. The three points correlate well, and a least-square-error analysis shows an apparent kinetics order for radiolysis of

$$n = 1.7 \pm 0.3 \quad (2\sigma)$$

for these irradiations at 7% fast neutron fraction.

Figure 4.2 shows the Euratom (BLO4) steady-state irradiations at 320°C (nominal temperature) correlated by Equation (4.6) to determine the reaction order, n. The M.I.T. calculated values of C_{omp} and G(-omp) for these Euratom runs shown in Table 4.3 were used in this correlation. Table 4.4 presents a comparison of the calculated values of n reported by Euratom (4.2) and obtained by M.I.T. for these BLO4 irradiations. The M.I.T. data at 300°C for Runs 14, 16, and 17 are included in Figure 4.2 in order to compare slopes, n, in the correlation. As shown in Figure 4.2 and Table 4.4, the value of n determined in two of the Euratom steady-state runs agree very well with the M.I.T. value. The value of n from Euratom Run C6-41-320 ($f_N = 0.20$) is less than that found in the other runs, but the single measurement of Run C1-41-320 ($f_N = 0.175$) combined with the data of

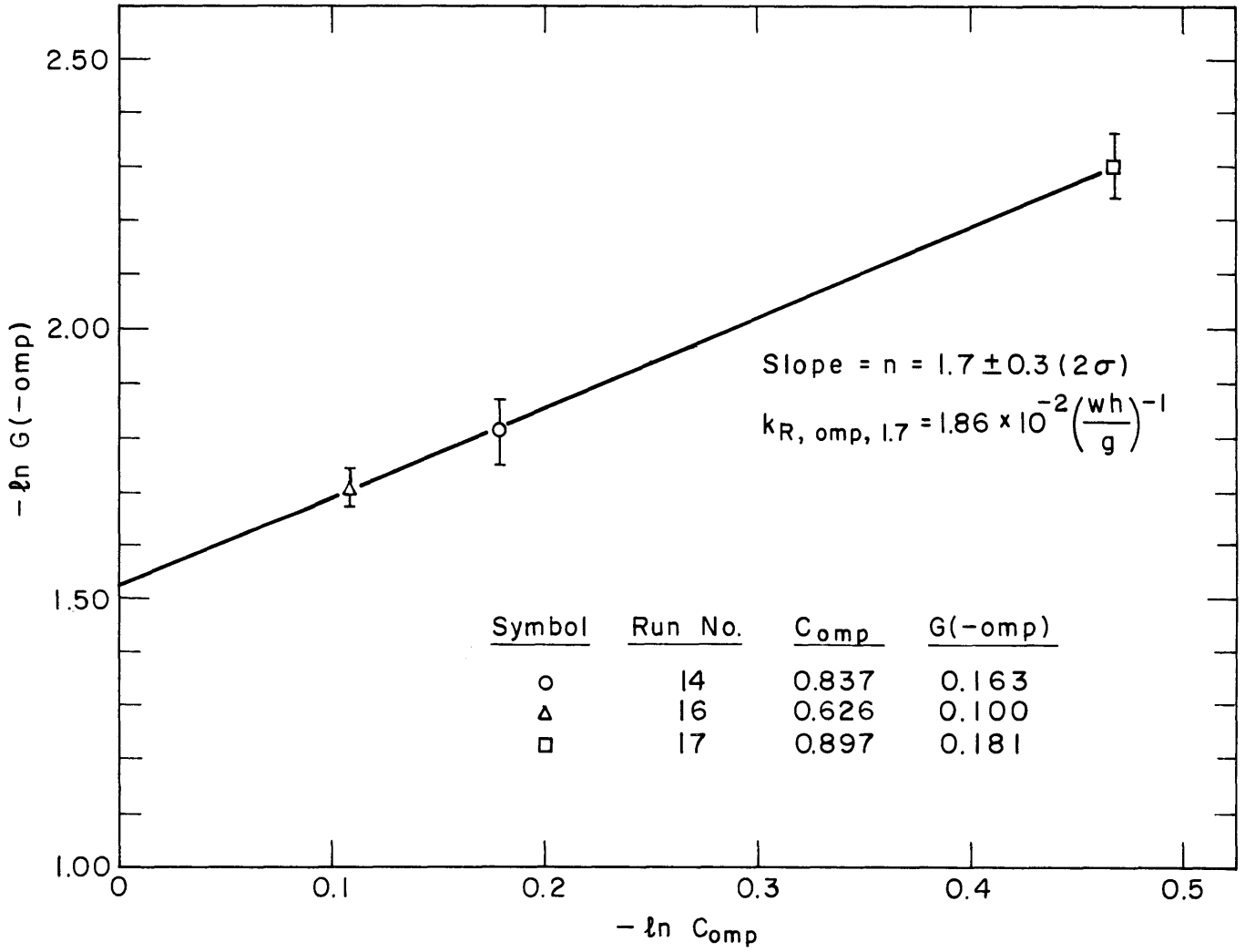

FIGURE 4.1 CORRELATION OF MIT STEADY-STATE IRRADIATIONS AT 572°F (300°C) IN FUEL POSITION 20

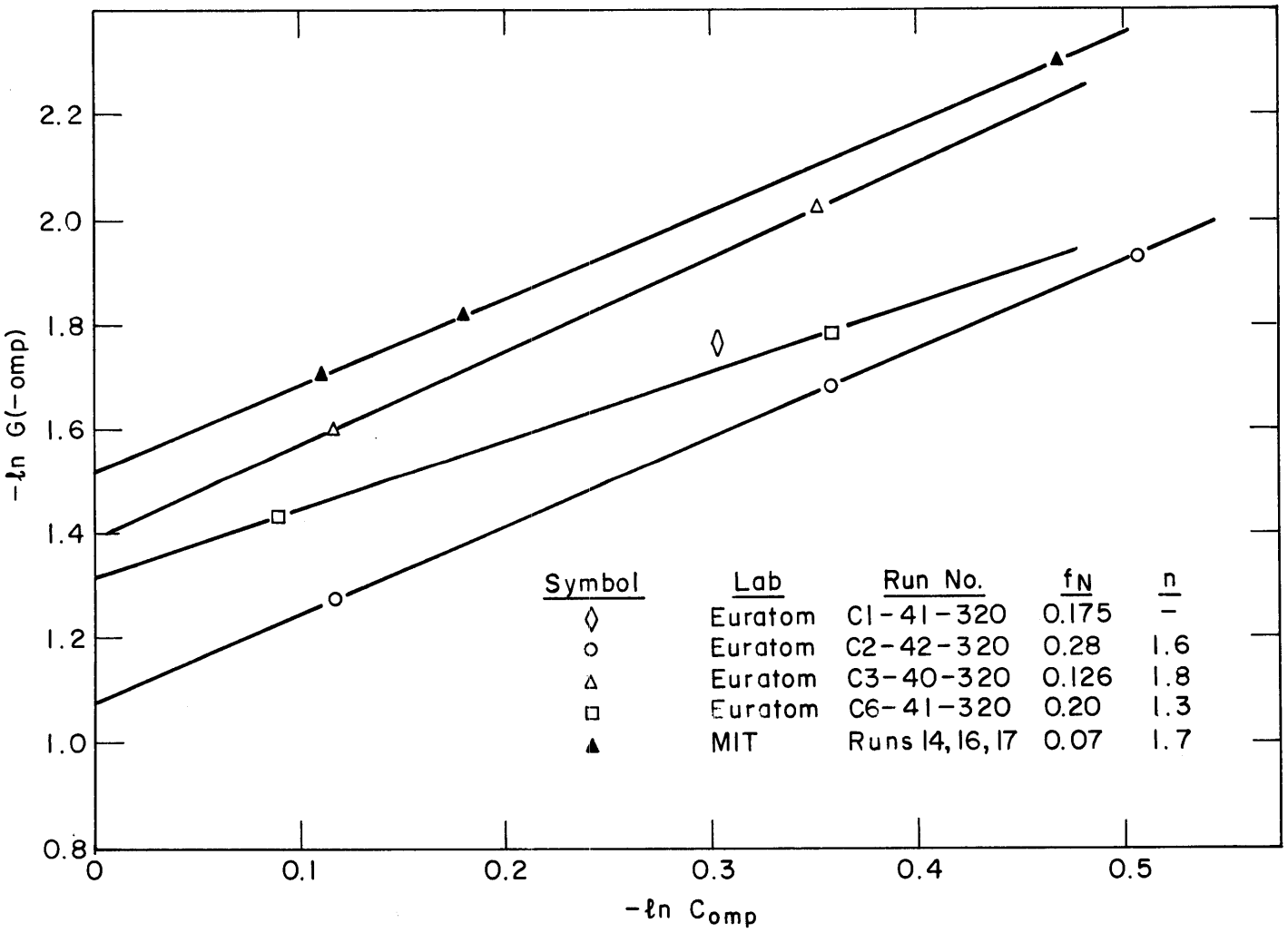

FIGURE 4.2 CORRELATION OF EURATOM (BL04) AND MIT STEADY-STATE IRRADIATIONS AT LOW TEMPERATURE

Table 4.4

Comparison of Calculated Reaction Order for BLO4 Steady-State Runs at 320°C

Run No.	Reaction Order, n	
	Euratom	M.I.T.
C2-42-320	1.4 - 1.7	1.6
C3-40-320	1.9	1.8
C6-41-320	1.5	1.3

Run C6-41-320 indicates that the calculated value of n = 1.3 for Run C6-41-320 may be too low. The best estimate of the apparent kinetics order of radiolysis, n, from the M.I.T. and Euratom data plotted in Figure 4.2 is

$$n = 1.7 \pm 0.2 \quad (2\sigma)$$

Equation (4.6) indicates that the difference in the intercepts of the lines shown in Figure 4.2 are related to the fast neutron fractions employed in the various irradiations; the values of the intercepts are used to determine the magnitude of the fast neutron effect ratio, G_N/G_γ, as discussed in the following section.

4.3.4 Fast Neutron Effect Ratio

The results of M.I.T. and Euratom low temperature steady-state irradiations shown in Tables 4.1 and 4.3 can be used to determine the fast neutron effect ratio. Equation (4.6) shows that the empirical radiolysis rate constant can be written as a function of the fast neutron fraction as follows,

$$k_{R,\,omp,\,n} = \frac{G_\gamma^o}{11.65}\left[\left(\frac{G_N}{G_\gamma} - 1\right) f_N + 1\right] \quad (\text{watt-hr/gram})^{-1} \tag{4.7}$$

Figure 4.3 shows the effect of the fast neutron fraction, f_N, on the empirical radiolysis rate constant for Euratom and M.I.T. steady-state runs, based on a reaction order n = 1.7. The error limits on the data points are $\pm 2\sigma$, or approximately ±14% for the Euratom values (4.2) and

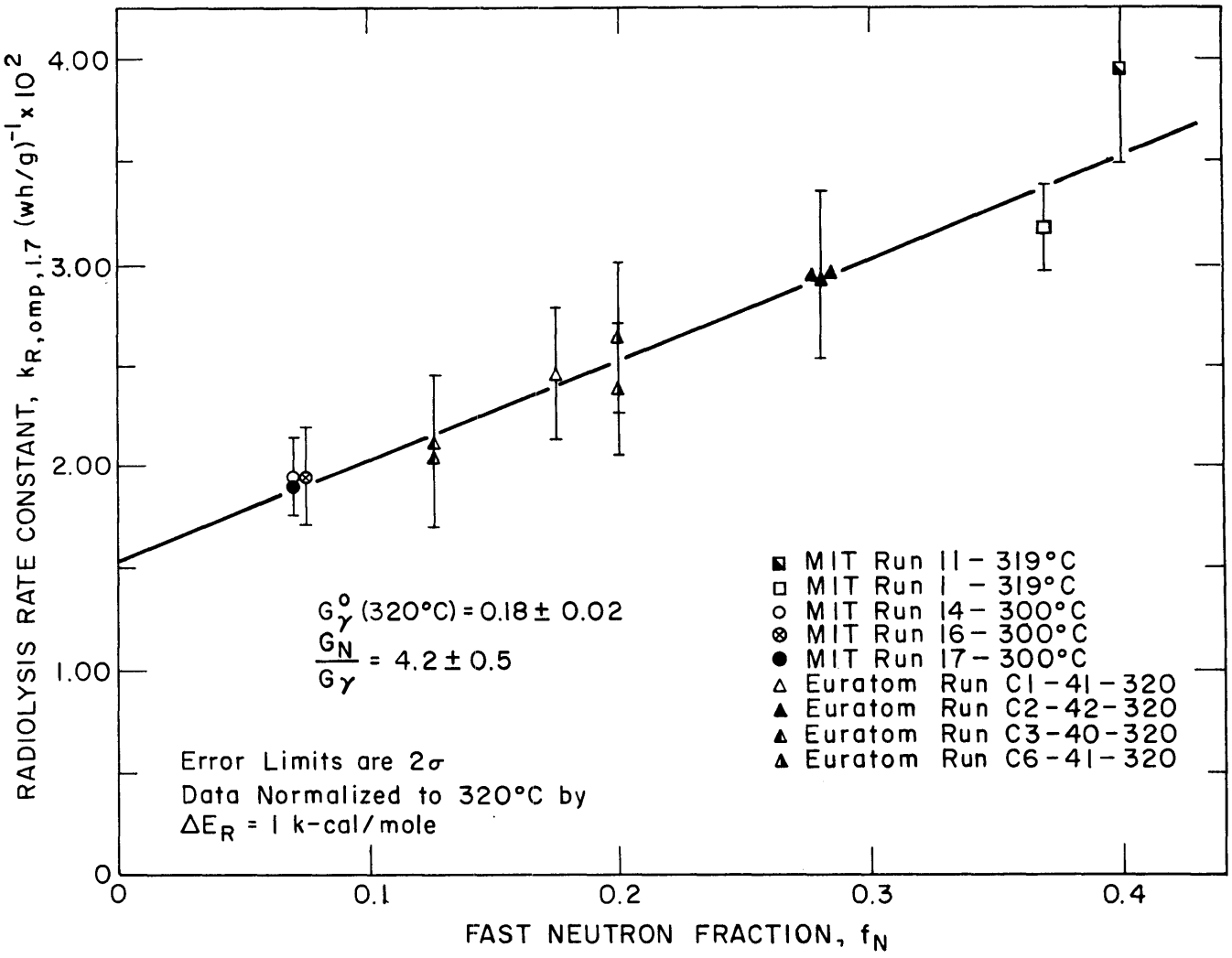

FIGURE 4.3 EFFECT OF FAST NEUTRON FRACTION ON RADIOLYSIS RATE CONSTANT (1.7 order kinetics) MIT AND EURATOM STEADY-STATE RUNS

about ±10% for the M.I.T. values. These data were correlated according to Equation (4.7), using a least-square-error analysis to determine the best straight line through the data. The slope of this line is $\frac{G_\gamma^o}{11.65}\left[\frac{G_N}{G_\gamma} - 1\right]$ and the intercept is $\frac{G_\gamma^o}{11.65}$. The correlation of the steady-state low temperature data shown in Figure 4.3 gives

$$G_\gamma^o(\text{-omp}) = 0.18 \pm 0.02 \qquad (2\sigma)$$

$$\frac{G_N}{G_\gamma} = 4.2 \pm 0.5 \qquad (2\sigma)$$

at 320°C.

4.4 Other Laboratories

M.I.T. has recently presented correlations of the results of terphenyl irradiations at temperatures below 350°C carried out by various laboratories in the United States, Canada, and Europe, based on first-, second- and third-order kinetics (4.1). The data included both loop and capsule irradiations in steady-state and transient modes of operation. In that review where only integer reaction orders were assumed, the best correlation of all data was obtained with second-order kinetics, which gave a fast neutron effect ratio (G_N/G_γ) of 4-5.

These same data, plus the recent M.I.T. and Euratom results given in Section 4.3 have been reinterpreted using a reaction order n = 1.7. Figure 4.4 shows the effect of the fast neutron fraction on the empirical radiolysis rate constant ($k_{R,omp,1.7}$) for these data normalized to 320°C by an activation energy of radiolysis ΔE_R = 1 k-cal/mole. For the transient runs, the rate constant (for n = 1.7) has been found by computer analysis of the concentration versus dose data of the experiments. For the steady-state runs of Euratom and M.I.T. (already shown in Figure 4.3), the rate constant was found by Equation (4.6) using the measured value of G(-omp) at the steady-state total terphenyl concentration. The M.I.T. calculated values of $k_{R,omp,1.7}$ for these data of other laboratories are given in Table A5.1 in Appendix A5.

Figure 4.4 indicates that the best correlation of all these data for low temperature terphenyl irradiations using an apparent reaction order of 1.7 gives

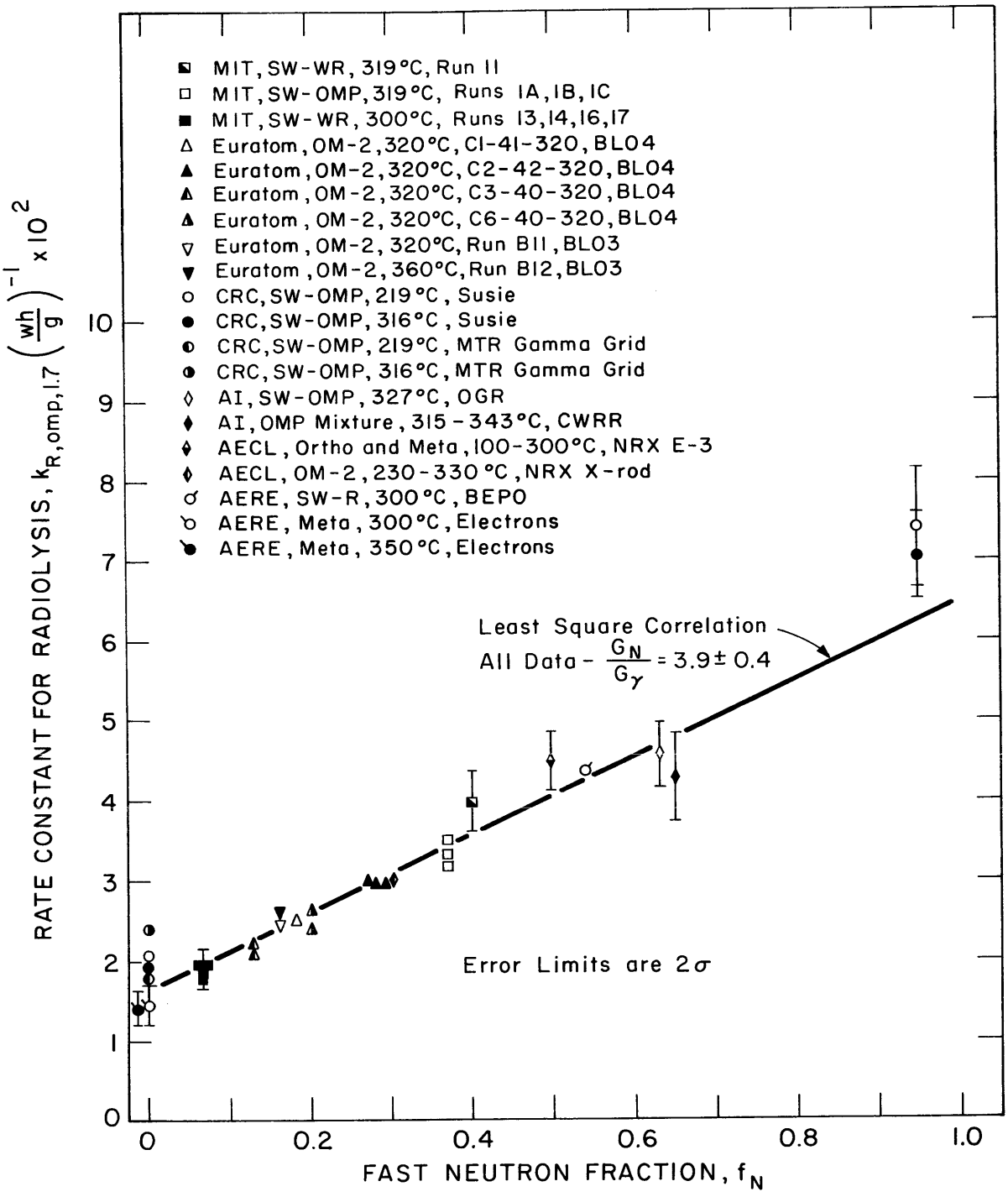

FIGURE 4.4 EFFECT OF FAST NEUTRON FRACTION, f_N, ON THE EMPIRICAL RADIOLYSIS RATE CONSTANT FOR 1.7 ORDER APPARENT KINETICS (NORMALIZED TO 320°C BY ΔE_R = 1K-CAL/MOLE)

$$\frac{G_N}{G_\gamma} = 3.9 \pm 0.4 \qquad (2\sigma)$$

$$G_\gamma^o(\text{-omp}) = 0.19 \pm 0.02 \qquad (2\sigma)$$

at 320°C. These values are in excellent agreement with the values found in the correlation of results of steady-state irradiations of Euratom and M.I.T. in Section 4.3. The values of G_N/G_γ and G_γ^o obtained from the correlation of all the experimental data (Figure 4.4) should be better estimates of these parameters than that obtained from the M.I.T. and Euratom data alone (Figure 4.3). However, the difference between the two correlations is not significant.

Boyd et al. (4.4, 4.5) have recently reported on Canadian experience with radiolysis of ortho and meta terphenyl in transient capsule experiments. These irradiations were made in (1) a mixed neutron and gamma-ray environment (f_N = 0.5 - 0.6) in the E-3 hole of the NRX reactor and (2) in a predominantly gamma-ray environment (f_N = 0.01) in a cadmium annulus in the NRX reactor. One conclusion made from these experiments was that below 300°C fast neutron radiation was about 4.5 times as damaging to meta terphenyl as gamma-radiation and 3 times as damaging to ortho terphenyl as gamma-radiation.

It should be noted that the terphenyl coolant data correlated in Figures 4.3 and 4.4 represent terphenyl mixtures with high meta concentrations. Santowax WR, Santowax OMP, and OM-2 contain 60-75% meta terphenyl in unirradiated coolant (see Table 1.1). The ortho terphenyl concentration in unirradiated Santowax WR and OM-2 is generally 15-20% and the para concentration is about 5%. Including the para terphenyl content with the meta content, an estimate of the fast neutron effect ratio for Santowax WR and OM-2 can be made from the AECL values of G_N/G_γ for pure ortho and meta terphenyl, using the isomer concentrations as weighting factors.

For Santowax WR and OM-2 (essentially same isomeric ratios)

$$\frac{G_N}{G_\gamma} = \frac{(C_m + C_p)}{C_{omp}}\left(\frac{G_N}{G_\gamma}\right)_{meta} + \frac{C_o}{C_{omp}}\left(\frac{G_N}{G_\gamma}\right)_{ortho} \qquad (4.8)$$

or

$$\frac{G_N}{G_\gamma} = \frac{0.75}{0.95}(4.5) + \frac{0.20}{0.95}(3.0) = 4.1 \qquad (4.9)$$

This calculated value of G_N/G_γ for Santowax WR and OM-2 using the AECL results (4.4) for the pure isomers agrees well with the experimental results of Euratom and M.I.T. irradiations (Figure 4.3).

Assumptions were made in the calculational model described in Section 4.2 that fast neutrons and gamma rays followed the same kinetics order, n, and that neutron and gamma ray produced degradations were additive. Since maximum error limits on all these experiments are generally at least ±8-10% (primarily due to uncertainties in dosimetry measurements), Figure 4.4 is considered an extremely good correlation of all these data. Since this correlation is based on the above assumptions, it appears that these assumptions are valid within the limits of experimental uncertainties.

4.5 Relative Stabilities of the Terphenyl Isomers at Low Temperatures

In Appendix A3, the degradation rate of each of the terphenyl isomers is calculated for the irradiations in Fuel Position 20, based on first-order kinetics with respect to the individual isomer concentrations. These values for the individual isomers have been normalized to the degradation rate of total terphenyl so that the relative stability of each isomer could be investigated. For steady-state runs, the ratio of $G^*(-i)/G^*(-omp)$ was calculated and for transient runs, the ratio $K_1(-i)/K_1(-omp)$ was determined. First-order kinetics parameters such as G^* and K_1 provide a measure of the percentage disappearance rate of the individual components, which appears to be an appropriate basis of comparison of isomer stabilities. Table 4.5 compares the relative degradation rates of the terphenyl isomers for transient and steady-state runs in Fuel Position 1 and Fuel Position 20. Since the irradiations with Santowax WR represent coolants containing less than 5% para terphenyl, the relative degradation rates of this isomer calculated for these irradiations are not considered significant.

The following three observations can be made regarding the relative stabilities of the isomers shown in Table 4.5:

Table 4.5

Relative Stabilities of the Terphenyl Isomers at Low Temperature

(M.I.T. Runs at 300°C and 321°C)

Run No.	Terphenyl	Type	f_N	Relative Degradation Rate[a,b] ortho	meta	para	Terphenyl Conc. wt % ortho	meta	para
Fuel Position 1: 321°C									
1A	SW-OMP	transient	0.37	1.11 ± 0.12	1.08 ± 0.06	0.69 ± 0.14	11-6	65-37	25-16
1B	SW-OMP	transient	0.37	1.05 ± 0.05	1.00 ± 0.08	1.05 ± 0.07	7-4	41-25	19-10
1C	SW-OMP	steady-state	0.37	1.00 ± 0.05	1.00 ± 0.05	1.07 ± 0.07	6	37	18
11	SW-WR	steady-state	0.40	0.98 ± 0.06	0.99 ± 0.06	1.04 ± 0.19	22	57	5
Fuel Position 20: 300°C									
13	SW-WR	transient	0.07	1.15 ± 0.13	0.95 ± 0.11	1.22 ± 0.55	17-15	70-63	6-5
14	SW-WR	steady-state	0.07	1.16 ± 0.08	0.92 ± 0.06	1.02 ± 0.12	15	64	5
16	SW-WR	steady-state	0.07	1.22 ± 0.07	0.95 ± 0.05	1.66 ± 0.17	10	49	4
17	SW-WR	steady-state	0.07	1.25 ± 0.06	0.89 ± 0.05	1.68 ± 0.14	15	70	5

[a]Relative to total terphenyl. For steady-state runs, this value represents $G^*(-i)/G^*(-omp)$, and for transient runs the value represents $K_1(-i)/K_1(-omp)$.

[b]Error limits are 1σ.

(1) At f_N = 0.37 and 0.40, there appears to be no significant difference in the relative degradation rates of ortho, meta, and para terphenyl.

(2) At f_N = 0.07, the relative degradation rate of ortho terphenyl appears to be approximately 25-30% greater than meta terphenyl.

(3) The relative degradation rates of ortho and meta terphenyl at f_N = 0.37-0.40 or at f_N = 0.07 do not vary significantly with changes in individual isomer concentration for irradiations at a particular fast neutron fraction.

This last observation can be used to estimate the empirical constants a and b in Equation (4.1b). At low temperatures, where radiopyrolysis is negligible, Equation (4.1b) can be written

$$\frac{w_i(C_i^f - C_i)}{M\bar{r}} - \frac{dC_i}{d\tau} = k_{R,i,a+b} C_i^a C_{omp}^b = \frac{G_R(-i)}{11.65} \tag{4.10}$$

for the individual isomers, and

$$\frac{w_i(C_{omp}^f - C_{omp})}{M\bar{r}} - \frac{dC_{omp}}{d\tau} = k_{R,omp,e+f} C_{omp}^e C_{omp}^f$$

$$= k_{R,omp,n} C_{omp}^n = \frac{G_R(-omp)}{11.65} \tag{4.11}$$

where e + f = n for total terphenyl.

The first-order degradation rates used to calculate the ratios (relative degradation rates) shown in Table 4.5 can be derived from Equations (4.10) and (4.11) as shown below,

$$\frac{w_i(C_i^f - C_i)}{M\bar{r}C_i} - \frac{dC_i/C_i}{d\tau} = k_{R,i,a+b} C_i^{a-1} C_{omp}^b \tag{4.12}$$

where the subscript i represents individual isomers or total terphenyl. Note that for transient runs in which the feed rate (w_i) is zero,

$$-\frac{dC_i/C_i}{d\tau} = K_{1,i} \tag{4.13}$$

by definition of the overall first-order rate constant (see Section A3.3). For steady-state runs in which the concentration is constant (dC_i is zero)

$$\frac{w_i(C_i^f - C_i)}{M\bar{r}C_i} = \frac{G_R^*(-i)}{11.65} \tag{4.14}$$

by the definition of $G^*(-i)$ given in Equation (4.5). The ratio of the degradation rates of the individual isomers to that of total terphenyl is then

$$\frac{K_1(-i)}{K_1(-omp)} \left(\text{or } \frac{G^*(-i)}{G^*(-omp)}\right) = \frac{k_{R,i,a+b} C_i^{a-1} C_{omp}^{b}}{k_{R,omp,e+f} C_{omp}^{e-1} C_{omp}^{f}} \tag{4.15}$$

where e + f = n, the reaction order for total terphenyl. These ratios do not vary significantly with either isomer concentration or total terphenyl concentration (see Table 4.5). This suggests that a = e and b = f. With this assumption, a value of unity is therefore implied for the empirical constants a = e in Equation (4.15). It was shown in Sections 4.3 and 4.4 that the best value of n is about 1.7, and in order to satisfy Equation (4.11), the constants b = f are approximately 0.7. Since the total terphenyl degradation rate is the sum of the degradation rates of the individual isomers, the following expression is implied.

$$\frac{G(-omp)}{11.65} = (k_{R,o,1.7} C_o + k_{R,m,1.7} C_m + k_{R,p,1.7} C_p) C_{omp}^{0.7} \tag{4.16}$$

or

$$\frac{G(-omp)}{11.65} = \left[k_{R,o,1.7}\left(\frac{C_o}{C_{omp}}\right) + k_{R,m,1.7}\left(\frac{C_m}{C_{omp}}\right) + k_{R,p,1.7}\left(\frac{C_p}{C_{omp}}\right)\right] C_{omp}^{1.7} \tag{4.17}$$

where

$k_{R,i,1.7}$ are the empirical radiolysis rate constants for the individual terphenyl isomers, $(wh/g)^{-1}$

By comparing Equations (4.11) and (4.17), it appears that the empirical radiolysis rate constant for total terphenyl, $k_{R,omp,1.7}$, can be considered to be a concentration weighted average of the 1.7 order rate constants for the individual isomers.

$$k_{R,omp,1.7} = k_{R,o,1.7}\left(\frac{C_o}{C_{omp}}\right) + k_{R,m,1.7}\left(\frac{C_m}{C_{omp}}\right) + k_{R,p.1.7}\left(\frac{C_p}{C_{omp}}\right) \quad (4.18)$$

The values of the empirical radiolysis rate constants for the isomers can be estimated from Equation (4.15) and Table 4.5. For this proposed calculational model with a = 1 and b = 0.7, the ratios shown in Table 4.5 and Equation (4.15) are simply $k_{R,i,1.7}/k_{R,omp,1.7}$. Table 4.6 summarizes the calculations of the $k_{R,i,1.7}$, using the experimental values of the relative degradation rates of the terphenyl isomers shown in Table 4.5.

Table 4.6

Calculation of the Radiolysis Rate Constants at 320°C for the Individual Terphenyl Isomers

Fast Neutron Fraction, f_N	$\frac{k_{R,i,1.7}}{k_{R,omp,1.7}}$ [a]		$k_{R,omp,1.7}$ [b]	$k_{R,i,1.7}$ (wh/g)$^{-1}$	
	ortho	meta	(wh/g)$^{-1}$	ortho	meta
0.07	1.19	0.93	0.0199	0.0237	0.0185
0.40	1.00	1.00	0.0357	0.0357	0.0357

[a] Average values from Table 4.5.
[b] From Figure 4.4.

Finally, the calculated values of the $k_{R,i,1.7}$ for ortho and meta terphenyl at $f_N = 0.07$ and 0.40 can be used to calculate the fast neutron effect ratio, G_N/G_γ, for these two isomers using the correlation shown in Equation (4.7). The results of this calculation are:

Ortho Terphenyl

$G_N/G_\gamma = 2.7$ M.I.T. value

$G_N/G_\gamma = 3$ AECL value (4.4)

Meta Terphenyl

$G_N/G_\gamma = 4.5$ M.I.T. value

$G_N/G_\gamma = 4.5$ AECL value (4.4)

The M.I.T. and AECL values of G_N/G_γ for ortho and meta terphenyl are in good agreement.

Using equations of the form of Equation (4.7) for ortho and meta terphenyl and the calculated values of the degradation rate constants shown in Table 4.6, initial gamma-ray G values (G_γ^o) can be determined for the two isomers at 320°C from the M.I.T. irradiations. These calculated values are G_γ^o (ortho) = 0.25 and G_γ^o (meta) = 0.18. AECL has reported (4.5) the following values determined from capsule irradiations of the pure terphenyl isomers:

250°C

G_γ^o (ortho) = 0.26

G_γ^o (meta) = 0.15

300°C

G_γ^o (ortho) = 0.42

G_γ^o (meta) = 0.20

Note that the AECL results indicate a greater increase for G_γ^o (ortho) with increasing temperature than for G_γ^o (meta). Both the AECL and M.I.T. results show that gamma radiation is more damaging to ortho terphenyl than to meta terphenyl at low temperatures. The effects of higher irradiation temperatures on the stabilities of ortho and meta terphenyl are discussed in Chapter 6. The differences between the G_γ^o values reported by AECL and M.I.T. may be due to the fact that AECL irradiated pure isomers while M.I.T. has irradiated isomer mixtures; Section 6.3 discusses differences which have been obtained in isomer stabilities from these two types of irradiations.

CHAPTER 5

HIGH TEMPERATURE - LOW AVERAGE DOSE RATE IRRADIATIONS OF META-RICH TERPHENYL COOLANTS

5.1 Introduction

Figure 5.1 shows the terphenyl degradation rates measured in several irradiation facilities plotted in an Arrhenius diagram. These degradation rates are the values reported by the original authors as initial G values, designated G^*(-omp) or G^o(-omp), which represent the rate of terphenyl degradation at 100% total terphenyl concentration. Since initial decomposition rates must necessarily be estimated by extrapolation of steady-state or transient run data back to 100% concentration, the original authors used correlations by first- and second-order kinetics (as well as smooth curve fitting by eye) to obtain these values. The purpose of presenting this figure is to illustrate the effect of temperature on terphenyl degradation rates measured under a wide variety of experimental conditions and interpreted by the original authors with different techniques.

The interpretation of high temperature terphenyl irradiation data, such as that shown in Figure 5.1, is complicated by the following facts:

(1) Thermal decomposition (radiopyrolysis) becomes significant at temperatures above about 350°C in experiments with low average dose rates (i.e., long irradiation times). The separation of the measured total degradation rates into radiolysis and radiopyrolysis effects is difficult.

(2) As reported earlier by M.I.T. (5.1) and AECL (5.2), the ortho terphenyl isomer appears to be less stable at high temperatures than the meta terphenyl isomer. Thus, the total terphenyl degradation rate may vary with the relative concentration of the isomers.

(3) AECL (5.3) has recently reported dose rate effects in both

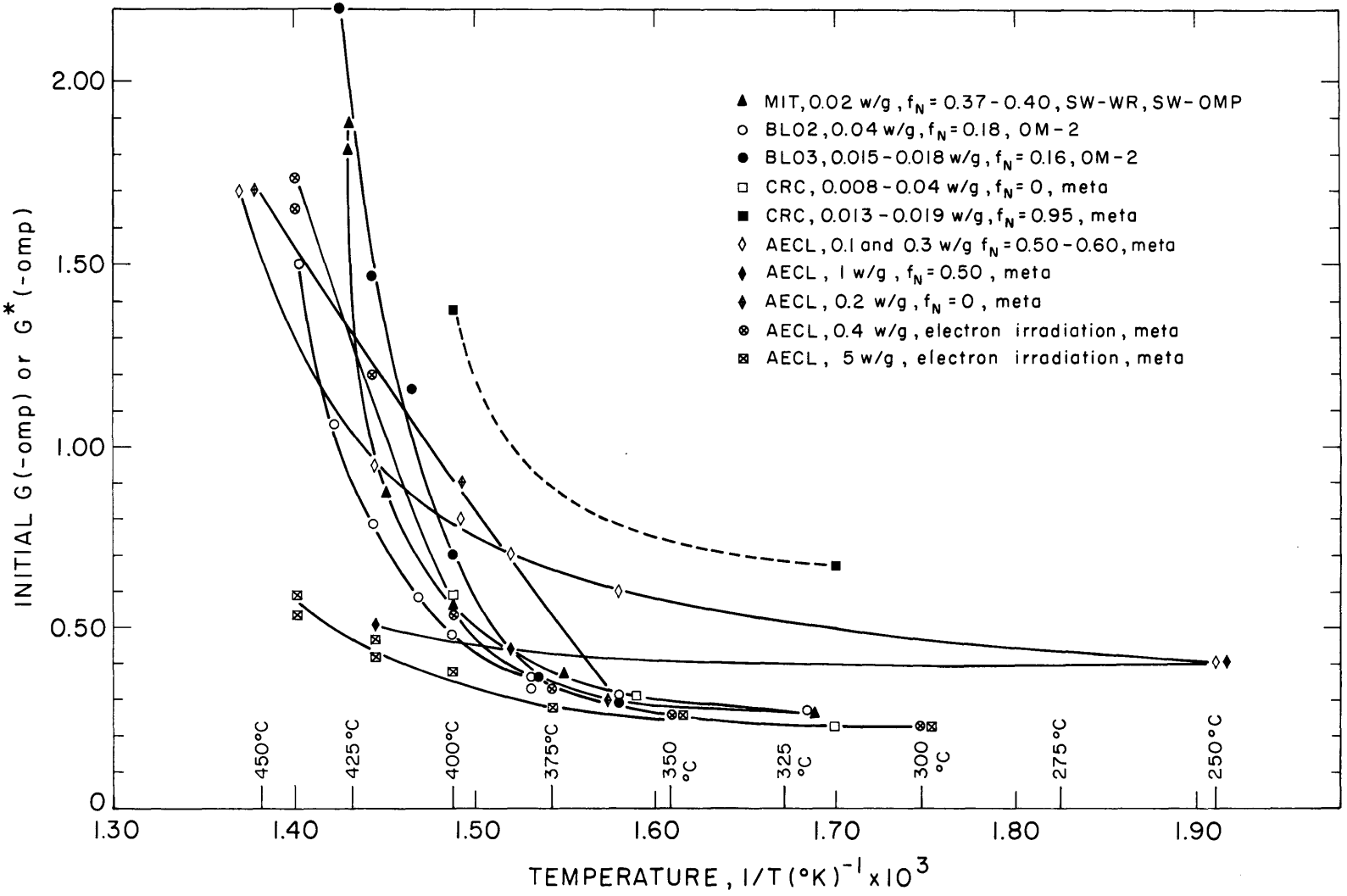

FIGURE 5.1 EFFECT OF TEMPERATURE ON TERPHENYL INITIAL DEGRADATION RATES, META-RICH TERPHENYLS

pile and electron terphenyl irradiations which become significant at temperatures above 350°C for dose rates above 0.3 watts/gram. The amount of degradation occurring under intermittent irradiation has been reported by AECL (5.3) to be different from that occurring under continuous irradiation for electron irradiations of meta terphenyl at 440°C.

A large part of the high temperature terphenyl irradiation data has been obtained in the M.I.T. loop and the Euratom loops (BLO2, BLO3, and BLO4) at low average dose rates (less than 0.1 watt/gm) with meta-rich coolants (Santowax WR, Santowax OMP, OM-2). Available data for high dose rate experiments and for ortho-rich coolants are relatively scarce (no steady-state data are available), and the interpretation of such data should be regarded as tentative at this time. For these reasons, the high temperature terphenyl irradiation data are divided into two sections: (1) low average dose rate experiments of meta-rich coolants (Chapter 5) in which only the total terphenyl disappearance rate is considered, and (2) high average dose rate experiments (Chapter 6) in which the relative stabilities of the ortho and meta isomers are also considered. The concentration of the para isomer is generally so low in practical reactor coolants that accurate measurement and prediction of its degradation rate are not important.

The overall objective of this chapter is to develop an empirical model which can be used to predict the coolant degradation rate in an organic-cooled reactor such as the Heavy-Water Organic-Cooled Reactor (HWOCR), and to show how this model can be applied (Section 5.4). Table 5.1 shows that the average dose rate in the present HWOCR design is expected to be comparable to that found in the M.I.T. loop, and therefore the high dose rate effects discussed in Chapter 6 are probably not important for such a reactor. However, it should be emphasized that the high temperature data reviewed in this chapter represent meta-rich coolants, and ortho-rich coolants (such as Santowax OM) may behave in a different manner.

Table 5.1

Comparison of M.I.T. In-Pile Loop and Conceptual 1000 Mwe HWOCR

Coolant Type	M.I.T. Loop Santowax WR, OMP (10% HB to 40% HB)	Conceptual Design[a] HWOCR Santowax OM (10% HB)
Inlet temperature	400°F - 780°F	575°F
Outlet temperature	420°F - 800°F	750°F
ΔT around coolant loop	~20°F	175°F
Total coolant mass, lbs	~12	~2,400,000
Coolant mass in core, lbs	0.6	23,000
Ratio, $\frac{\text{in-core coolant mass}}{\text{total coolant mass}}$	~0.05	~0.01
Coolant velocity, ft/sec	14 - 22	30 max
In-core residence time, sec	2.4	0.72
Out-of-core residence time, sec	48	77
Average dose rate in core, watts/gm	0.14 - 1.56	1.3
Average dose rate (total coolant), watts/gm	0.007 - 0.072	0.012
Fast neutron fraction, f_N	0.07 - 0.40	0.66[b]

[a]Reference (5.10).

[b]Estimated from preliminary HWOCR core calculations (5.10).

5.2 Theory

The general rate equation given in Chapter 4 for the total terphenyl decomposition rate is

$$\frac{G(-omp)}{11.65} = k_{R,\,omp,\,n} C_{omp}^{n} + \frac{k_{P,\,omp,\,m} C_{omp}^{m}}{\bar{r}} \qquad (5.1)$$

where $k_{R,\,omp,\,n}$ and $k_{P,\,omp,\,m}$ are empirical radiolysis and radiopyrolysis rate constants, respectively. The phenomenon of thermal degradation of irradiated coolant has been called radiopyrolysis to distinguish it from the more thoroughly investigated phenomenon of pyrolysis of unirradiated coolant. In order to use loop and capsule irradiation results to predict coolant degradation rates in organic-cooled reactors, the total measured degradation rates must be separated into radiolysis and radiopyrolysis components (or, alternatively, into in-pile and out-of-pile decomposition). The method used in this report for calculating the radiopyrolysis rates for high temperature irradiations was to employ the form of Equation (5.1) and to subtract the low temperature radiolysis rates correlated in Chapter 4 (applying an activation energy of radiolysis, ΔE_R = 1 k-cal/mole) from the measured total degradation rate, G(-omp)/11.65.

Equation (5.1) can be rearranged to express the radiopyrolysis rate as

$$k_{P,\,omp,\,m} C_{omp}^{m} = \left[\frac{G(-omp)}{11.65} - k_{R,\,omp,\,n} C_{omp}^{n} \right] \bar{r} \qquad (5.2)$$

The term, G(-omp)/11.65, is the measured total degradation rate, which is calculated in two different ways for steady-state and transient runs.

5.2.1 Steady-State Runs

It was shown in Chapter 4 that the best value for the radiolysis reaction order, n, was 1.7 at low temperature (320°C). It will be assumed that this same value of n is applicable at higher temperatures where thermal decomposition occurs. (However, it will be shown in Section 5.3 that the calculated values of $k_{P,\,omp,\,m}$ in Equation (5.2) are not significantly affected by the assumed value of n.) The reaction order for radiopyrolysis, m, is usually assumed to be first order

(m = 1), since the pyrolysis of unirradiated coolant has been shown to follow first-order kinetics (5.4, 5.7). To date, Euratom has completed only two steady-state irradiations in the BLO4 loop at different terphenyl concentrations (C_{omp} = 0.87 and 0.64) and the same high temperature (420°C); a comparison of the results of these two irradiations indicates a value of m = 0.1 ± 0.4 (5.5). More steady-state high temperature runs at varying terphenyl concentrations at a given temperature are needed to more firmly establish the value of m. The important point in this regard is that by subtracting the estimated radiolysis rate at the irradiation temperature (see Section 5.2.3) from the measured total degradation rate, the calculation carried out in Equation (5.2) gives the radiopyrolysis rate in terms of a product, $k_{P,omp,m}C_{omp}^{m}$. Whether m is chosen as zero order or first order affects the calculated radiopyrolysis rate constant, $k_{P,omp,m}$, but it does not affect the product, $k_{P,omp,m}C_{omp}^{m}$, for a given experiment.

For first- and zero-order apparent radiopyrolysis kinetics (m = 1 and 0) and n = 1.7,

m = 1:

$$k_{P,omp,1} = \left[\frac{G(-omp)}{11.65\, C_{omp}} - k_{R,omp,1.7} C_{omp}^{0.7} \right] \bar{r} \qquad (5.3)$$

m = 0:

$$k_{P,omp,0} = k_{P,omp,1} C_{omp} \qquad (5.4)$$

Obviously, the best choice of m in this empirical model depends on the correlation of all experimental data which allows the investigator to interpolate or extrapolate the correlations with the most confidence. It will be shown in Section 5.3 that the correlation of M.I.T. high temperature irradiation data by zero- and first-order radiopyrolysis kinetics does not produce a clear choice of the best correlation, due to the relatively large error limits involved in the calculated k_P. Therefore, in the absence of a basis for a statistically significant choice, the M.I.T. correlation of high temperature data of other laboratories will be based on m = 1, since it has been the generally accepted method in the past.

A procedure for estimating the radiolysis rate constant in

Equation (5.3) at high temperature, using the low temperature correlations in Chapter 4, is discussed in Section 5.2.3.

5.2.2 Transient Runs

Calculation of the radiopyrolysis contribution in transient runs by means of Equation (5.2) is complicated by the fact that both the total terphenyl concentration and the total degradation rate, G(-omp)/11.65, decrease with time and dose. For transient runs with no terphenyl feed, ($w_i = 0$ in Equation 4.1a), the total degradation rate, G(-omp)/11.65 in Equation (5.2), is equal to $-dC_{omp}/d\tau$. Due to experimental scatter in the data, the value of $dC_{omp}/d\tau$ at any concentration is best determined as the derivative of a least-squares correlation of the concentration versus dose data. Thus, for first- and second-order kinetics,

First-Order Kinetics:

$$\left(-\frac{dC_{omp}}{d\tau}\right)_1 = K_1(-omp)\,C_{omp} \tag{5.5}$$

Second-Order Kinetics:

$$\left(-\frac{dC_{omp}}{d\tau}\right)_2 = K_2(-omp)\,C_{omp}^2 \tag{5.6}$$

where the overall degradation rate constants, K_1 and K_2, are determined by a least-squares analysis of the concentration versus dose data. It is usually impossible to show that a particular kinetics order provides the best correlation of the transient run data. However, the M.I.T. transient run curves in Figures A3.3, A3.5, A3.6, and A3.8 show that near the mid-point of the transient, the slopes, $-dC_{omp}/d\tau$, calculated by zero-, first-, and second-order correlation are all approximately equal.

The total degradation rate (i.e., the sum of the radiolysis and radiopyrolysis rates) is expected to follow an intermediate kinetics order between first and second order, depending on the relative roles of radiolytic and thermal decomposition. For this reason, M.I.T. chose to use the total degradation rate for transient runs in Equation (5.2) at the concentration which gives the same value of the

total degradation rate, $-dC_{omp}d\tau$, by both first- and second-order kinetics. In this way, the magnitudes of the total degradation rates used in Equation (5.2) are rendered quite insensitive to the overall kinetics assumed. The concentration at which $\left(-\frac{dC_{omp}}{d\tau}\right)_1 = \left(-\frac{dC_{omp}}{d\tau}\right)_2$ is:

$$\bar{C}_{omp} = \frac{K_1(-omp)}{K_2(-omp)} \tag{5.7}$$

The values of $\bar{C}_{omp}$ for transient runs, shown in Tables A5.1, A5.2, A5.3, and A5.4, confirm that this concentration is near the mid-point of the transient, where the terphenyl concentrations are known with the greatest statistical significance (see Figure A3.1). Using this procedure to define the total degradation rate, $\frac{G(-omp)}{11.65} = -dC_{omp}/d\tau$, at the selected concentration, $\bar{C}_{omp}$, in Equation (5.2), the following expressions for the radiopyrolysis rate constant (assuming n = 1.7) result.

m = 1:

$$k_{P,omp,1} = \left[K_1(-omp) - k_{R,omp,1.7}\bar{C}_{omp}^{0.7} \right]\bar{r} \tag{5.8}$$

m = 0:

$$k_{P,omp,0} = k_{P,omp,1}\bar{C}_{omp} \tag{5.9}$$

5.2.3 Activation Energy of Radiolysis

The effect of temperature on the radiolysis rate constant can be expressed by the Arrhenius relation,

$$k_{R,omp,n}(T) = k_{R,omp,n}(T_o)\exp\left[\frac{-\Delta E_R}{R}\left(\frac{T_o - T}{T_o T}\right)\right] \tag{5.10}$$

where ΔE_R is an activation energy of radiolysis, T and T_o are irradiation temperatures, and R is the gas constant. M.I.T. has recently reported (5.1) that the activation energy of radiolysis is approximately 1 k-cal/mole for meta-rich terphenyl irradiations up to about 350°C. The activation energy, ΔE_R, above 350°C cannot be determined in low average dose rate experiments, due to the onset of thermal

decomposition at these temperatures. It was assumed in the calculations of k_P reported in this chapter that ΔE_R = 1 k-cal/mole at all irradiation temperatures.

AECL high average dose rate experiments discussed in Chapter 6 suggest that ΔE_R may increase to about 20 k-cal/mole for meta-rich coolants above 400°C. This suggested increase in the radiolysis rate with temperature is not important for present operating conditions considered for organic-cooled reactors, since the maximum coolant temperature is about 750°F (399°C). It may be important if higher core outlet coolant temperatures are employed. Also, it will be shown in Chapter 6 that the suggested higher activation energy of radiolysis above 400°C does not significantly affect the values of k_P calculated from low average dose rate experiments at these temperatures. The radiopyrolysis activation energy appears to be approximately 40-50 k-cal/mole (see Table 5.4), and radiolysis is only a small contribution (above 400°C) to the total degradation rate measured in experiments such as the M.I.T. and Euratom loops which have low average dose rates.

In Chapter 4, the radiolysis rate constant for meta-rich terphenyls was determined as a function of the fast neutron fraction (using a 1.7 reaction order) by the following correlation:

$$k_{R,\,omp,\,1.7} = \frac{G_\gamma^o}{11.65}\left[\left(\frac{G_N}{G_\gamma} - 1\right) f_N + 1\right] \qquad (5.11)$$

At 320°C (573°K), the dependent parameters in Equation (5.11) were (see Figure 4.4),

$$G_\gamma^o = 0.19 \pm 0.02$$

$$\frac{G_N}{G_\gamma} = 3.9 \pm 0.4$$

Combining these experimental results at 320°C with Equations (5.10) and (5.11) gives the following relation, which was used to estimate the radiolysis rate constant at high temperatures,

$$k_{R,\,omp,\,1.7}(T) = 1.61 \times 10^{-2}\left[2.9\, f_N + 1\right] \exp\left[\frac{-1 \times 10^3}{1.987}\left(\frac{573 - T}{573T}\right)\right] \qquad (5.12)$$

where T is the irradiation temperature (°K). This relation assumes that the fast neutron effect ratio, G_N/G_γ, is independent of temperature.

5.3 Results – Radiopyrolysis Rates

5.3.1 M.I.T. Autoclave Pyrolysis Results

Table 5.2 gives a summary of results of three autoclave pyrolysis experiments completed at M.I.T. The equipment and operation of this autoclave apparatus have been described in Chapter 2. A more complete description of these pyrolysis tests, along with the zero-, first-, and second-order disappearance rates of the individual terphenyl isomers, is given in Appendix A4.

Figure 5.2 shows a comparison of the first-order pyrolysis rate constants for unirradiated meta-rich terphenyls measured by Euratom (5.4, 5.6), AECL (5.7) and M.I.T. Curve I represents the OM-2 data presented by Houllier (5.6) which combines autoclave and loop pyrolysis results. Juppe's data (5.4) with pure meta terphenyl agree reasonably well with Houllier's correlation, particularly at the higher temperatures shown in Figure 5.2. Curve II represents M.I.T. autoclave data for fresh Santowax WR (and also the disappearance rate of meta terphenyl in Santowax WR) and the AECL (5.7) data for the disappearance rate of the meta terphenyl isomer in Santowax OM and for pure meta. Mackintosh and Miller (5.7) show that the pyrolysis disappearance rate of pure meta is approximately the same as meta in a purified mixture of Santowax OM. The activation energies of pyrolysis for Curve I and Curve II are not significantly different, but the first-order rate constants of M.I.T. and AECL (Curve II) are about a factor of three higher than the Euratom data (Curve I).

It does not appear that the presence of oxygen can explain the large differences shown between Curve I and Curve II in Figure 5.2. The M.I.T. experimental procedure described in Chapter 2 for autoclave tests attempts to remove air from the system by cycles of pressurizing and evacuating the autoclave before the organic is charged. The unirradiated terphenyl is distilled at 10 mm Hg of nitrogen and kept under a nitrogen blanket before charging in the autoclave. However, the organic is not degassed and then frozen to remove the gases after the organic is charged in the autoclave at M.I.T. On the other hand,

Table 5.2

Summary of M.I.T. Autoclave Pyrolysis Results

Run No.	Coolant	Temperature °F	Temperature °C	Range of Concentration, w/o DP	Range of Concentration, w/o Total omp	Total Terphenyl Pyrolysis[b] Rate Constant, $k_{P,omp,m}$ $(hr)^{-1}$ Zero Order	Total Terphenyl Pyrolysis[b] Rate Constant, $k_{P,omp,m}$ $(hr)^{-1}$ First Order
P1	fresh SW-WR	780	416	5-39	95-61	$6.18 \pm 0.20 \times 10^{-4}$	$8.17 \pm 0.20 \times 10^{-4}$
P2	fresh SW-WR	800	427	6-32	94-68	$1.42 \pm 0.06 \times 10^{-3}$	$1.78 \pm 0.06 \times 10^{-3}$
18P1	irradiated SW-WR[a]	780	416	45-54	55-46	$4.64 \pm 0.28 \times 10^{-4}$	$9.19 \pm 0.56 \times 10^{-4}$

[a] Drained from loop at end of Run 18B, initially contained 35% HB.

[b] Error limits are 2σ.

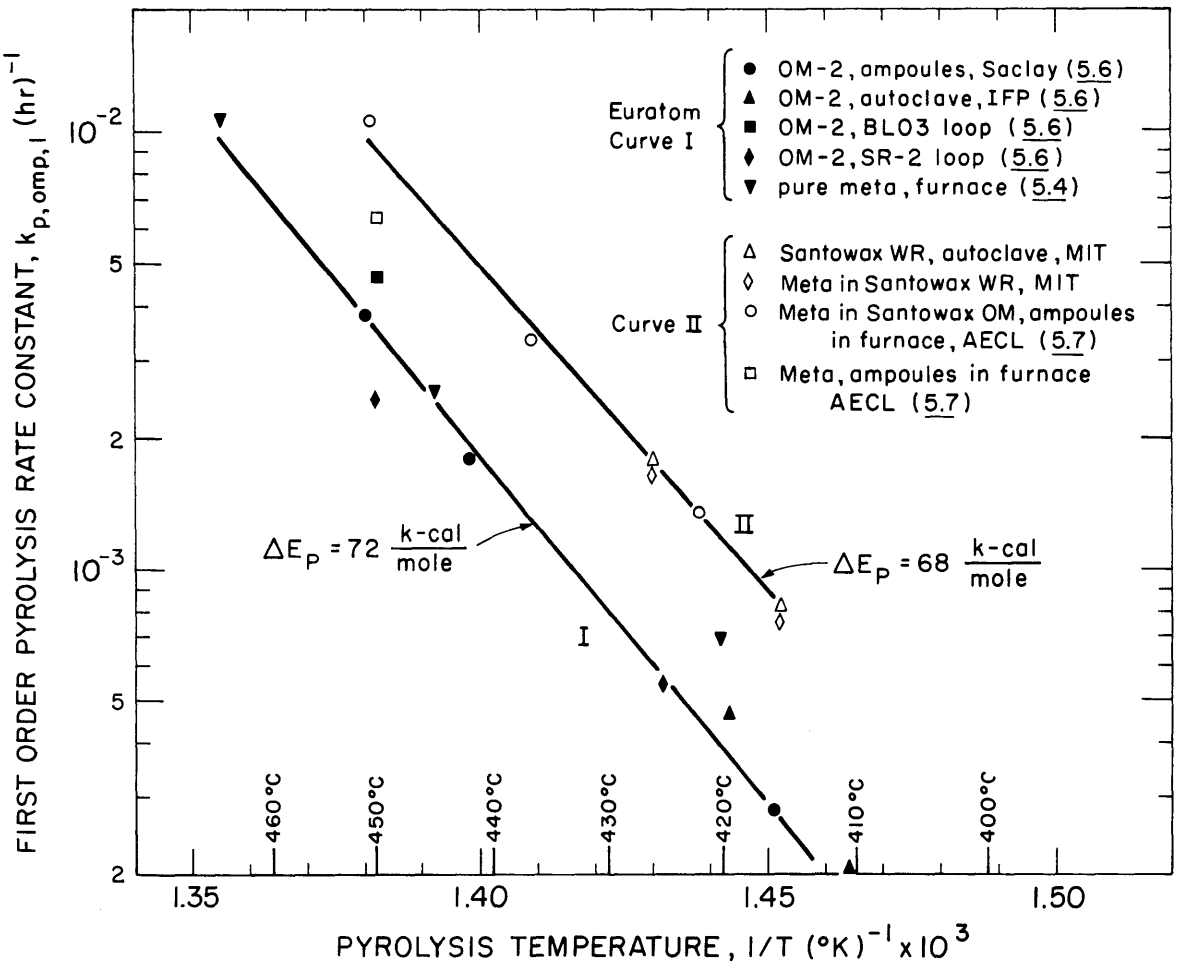

FIGURE 5.2 PYROLYSIS RATES OF META TERPHENYL AND META-RICH TERPHENYL MIXTURES, NON-IRRADIATED COOLANTS

both Juppe (5.4) and Mackintosh and Miller (5.7) report repeated degassing and freezing cycles in an attempt to remove oxygen from the samples before the ampoules are sealed. Also, it does not appear likely that extensive oxygen removal procedures such as degassing and freezing could have been carried out in the BLO3 and SR-2 loop pyrolysis tests shown in Curve I.

The present M.I.T. autoclave pyrolysis data is limited, and in view of the apparent discrepancies between the Euratom, AECL, and M.I.T. data shown in Figure 5.2, further experiments are needed to establish more clearly the pyrolysis rates of unirradiated coolant.

5.3.2 M.I.T. Irradiation Results in Fuel Position 20

A description of the irradiation conditions and experimental results of high temperature irradiations by M.I.T. in Fuel Position 20 is given in Appendix A3. Two transient runs (Runs 15 and 18A) and one steady-state run (Run 18B) were made at an irradiation capsule temperature of 800°F in this fuel position. Plots of the terphenyl isomer concentrations versus specific dose and/or irradiation time for these runs are shown in Figures A3.4, A3.5, A3.7, and A3.12. A summary of results for Runs 15, 18A, and 18B is given in Table 5.3, along with a comparison with earlier runs (Runs 9 and 10) in Fuel Position 1 at an irradiation capsule temperature of 800°F. The first-order radiopyrolysis rate constants have been calculated (see Table 5.3) for each of these experiments, using the relations developed for steady-state and transient runs in Section 5.2. Table A5.2 (Appendix A5) illustrates these calculations of $k_{P,omp,1}$ in detail.

As shown in Table 5.3, the calculated first-order radiopyrolysis rate constants for the runs in Fuel Position 20 at $f_N = 0.07$ are significantly lower than the values found for runs in Fuel Position 1 at $f_N = 0.40$. However, the effective loop temperature was about 780°F for Run 18B compared to 789°F for Run 9. Assuming an activation energy of radiopyrolysis for irradiated coolants of 40 k-cal/mole (see Section 5.3.3), the 9°F difference in the effective loop temperature of Run 9 and Run 18B should cause the radiopyrolysis rate for Run 18B to be approximately 25% less than Run 9. However, as shown in Table 5.3, $k_{P,omp,1}$ for Run 18B is about 50% less than Run 9. The relatively

Table 5.3

Summary of Irradiation Results
for High Temperature Runs in the M.I.T. Loop (800°F)

Run No.	Terphenyl	Type	Temperature, °F		Average Dose Rate	Concentration, w/o			Degradation Rate[a]		Radiopyrolysis[a] Rate Constant, $k_{P,\,omp,\,1}$
			Irradiation Capsule	Loop[c] Effective	(watts/gm)	OMP	DP	HB	G(-omp)	G^*(-omp)	$(hr)^{-1}$ ($\times 10^3$)
Fuel Position 1: $f_N = 0.40$											
9	Santowax WR	SS	800	789	0.0206	52	48	27[d]	0.91 ± 0.06	1.76 ± 0.12	2.56 ± 0.18
10	Santowax WR	SS	800	789	0.0192	65	35	17[d]	1.06 ± 0.08	1.62 ± 0.12	2.10 ± 0.16
Fuel Position 20: $f_N = 0.07$											
15	Santowax WR	Tr	800	780[e]	0.0056-[b] 0.0118	82-57	18-43	11-30	–	1.64 ± 0.16	1.05 ± 0.06
18A	Santowax WR	Tr	800	780[e]	0.0161	90-54	10-46	6-35	–	1.07 ± 0.10	1.20 ± 0.06
18B	Santowax WR	SS	800	780	0.0166	52	48	35	0.53 ± 0.04	1.03 ± 0.08	1.23 ± 0.06

[a] Error limits are 2σ.

[b] Power raised from 2 MW to 4 MW during this run.

[c] Includes temperature fluctuations during run.

[d] Bottoms distillation.

[e] Effective loop temperature assumed same as Run 18B.

low value of $k_{P,omp,1}$ measured in the steady-state run in Fuel Position 20 (Run 18B) was confirmed by the values for the transient runs in this fuel position (Runs 15 and 18A). Also, post-irradiation pyrolysis (see Table 5.2) in an autoclave at 780°F, using the coolant drained from the loop at the end of Run 18B, gave $k_{P,omp,1} = 0.92 \times 10^{-3}$ $(hr)^{-1}$, which is about 25% lower than the value shown for Run 18B in Table 5.3.

In addition to the effective loop temperature difference discussed above, the only other operating conditions which were known to be different in Run 9 and Run 18B were the fast neutron fraction of the total dose and the type of distillation employed. Runs 9 and 10 employed a Bottoms distillation and Run 18B employed a High Boiler distillation. Euratom steady-state runs (5.5) with OM-2 in the BLO4 loop at 420°C (788°F) and $f_N = 0.20$ gave $k_{P,omp,1} = 2.17 \times 10^{-3}$ $(hr)^{-1}$ at $C_{omp} = 0.87$ and $k_{P,omp,1} = 2.66 \times 10^{-3}$ $(hr)^{-1}$ at $C_{omp} = 0.64$ (see Run C5-41-420 in Table A5.2). These results are in good agreement with the M.I.T. values for Runs 9 and 10 at $f_N = 0.40$ shown in Table 5.3. Feed and bleed coolant processing (with no distillation) was used in the Euratom runs. The Euratom results tend to indicate that neither the fast neutron fraction nor the coolant processing method can account for the unexpected low values of k_P seen in Runs 15, 18A, and 18B. However, it should be noted that the fast neutron fraction in the Euratom runs ($f_N = 0.20$) was only a factor of two less than the M.I.T. value ($f_N = 0.40$) for Run 9, while M.I.T. Run 18B employed a fast neutron fraction ($f_N = 0.07$) which was a factor of six less than Run 9.

Recent AECL capsule irradiation data (5.3) for pure ortho and pure meta terphenyl indicate that the fast neutron effect ratio, G_N/G_γ, is not constant with temperature (as assumed in Equation (5.12)) but that G_N/G_γ approached unity at 400°C for both ortho and meta isomers. This change in G_N/G_γ was apparently due to a greater increase for G_γ with temperature than for G_N in pure isomers. Since the k_P calculated for Run 9 and Run 18B were made at different fast neutron fractions (assuming G_N/G_γ was constant with increasing temperature), the radiolysis corrections made for these runs using Equation (5.12) may be incorrect. Further data are needed on the effect of temperature on G_N/G_γ for terphenyl mixtures in order to obtain more reliable radiolysis

corrections than this method shown by Equation (5.12).

Figures 5.3 and 5.4 show the first- and zero-order radiopyrolysis rate constants calculated from M.I.T. high temperature irradiations correlated by the Arrhenius method. Neither zero- nor first-order radiopyrolysis kinetics orders appears to produce a significantly better correlation of these M.I.T. data. In Figure 5.3, the Arrhenius plots of the first-order pyrolysis rate constants for unirradiated terphenyls presented in Figure 5.2 are shown for comparison with the calculated radiopyrolysis rates of Santowax WR irradiated at M.I.T. The radiopyrolysis rates of irradiated coolant are significantly higher than the Euratom values (Curve I) for unirradiated coolants and are slightly higher than the M.I.T. and AECL values (Curve III).

The first-order radiopyrolysis rate constant calculated for M.I.T. Run 2 (Santowax OMP, 59% omp, 33% HB) is about 40% less than the correlating line shown in Figure 5.3 for Santowax WR with 52-55% omp and 27-31% bottoms (Runs 3, 5, and 9). Although this low value of $k_{P,\,omp,\,1}$ for Run 2 may be a result of the lower ortho terphenyl concentration in Santowax OMP compared to Santowax WR, it should be pointed out that a High Boiler distillation was used during Run 2. This comparison may be another indication (in addition to the comparison of Run 9 and Run 18B) that the deep cut distillation (Bottoms) produces higher radiopyrolysis rates for the terphenyl. The effect of the distillation procedure on the radiopyrolysis rate should be investigated in future M.I.T. experiments.

5.3.3 Results of Other Laboratories

The equations developed in Section 5.2 have been used to calculate the first-order radiopyrolysis rate constants for meta-rich terphenyl coolants irradiated in other laboratories. The experimental conditions and results of these experiments are presented in Table A5.2 (both the original author's results and the M.I.T. recalculated values from computer analysis of the data). The calculated values of $k_{P,\,omp,\,1}$ for these irradiations are plotted in Figure 5.5 (along with the M.I.T. high temperature data) as a function of total terphenyl concentration and irradiation temperature. The numbers beside the data points indicate the coolant temperature. The error limits shown on the data points are $\pm 2\sigma$, calculated by M.I.T. A data point with a vertical line through it

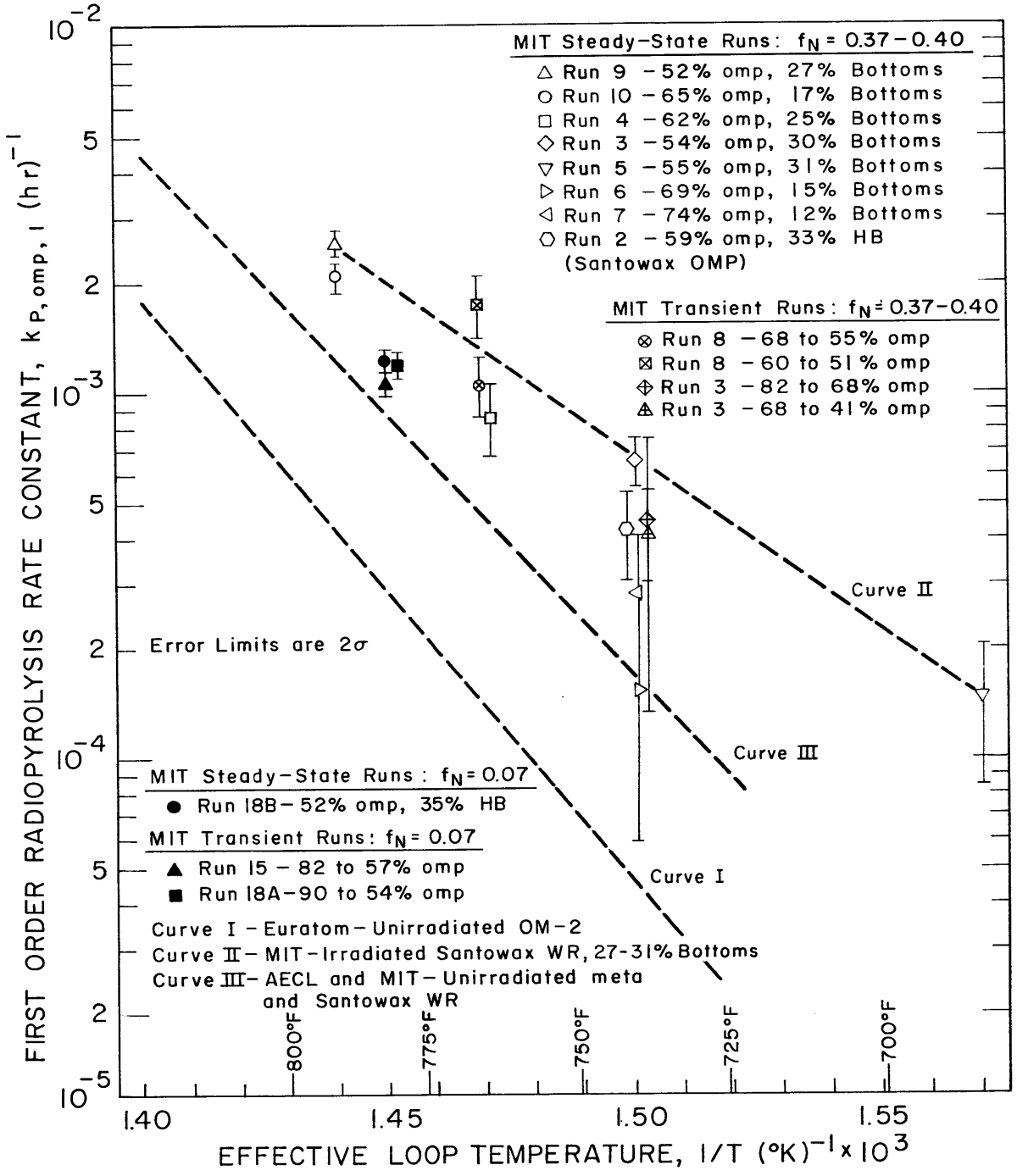

FIGURE 5.3 CORRELATION OF FIRST ORDER RADIOPYROLYSIS RATE CONSTANTS – MIT RUNS

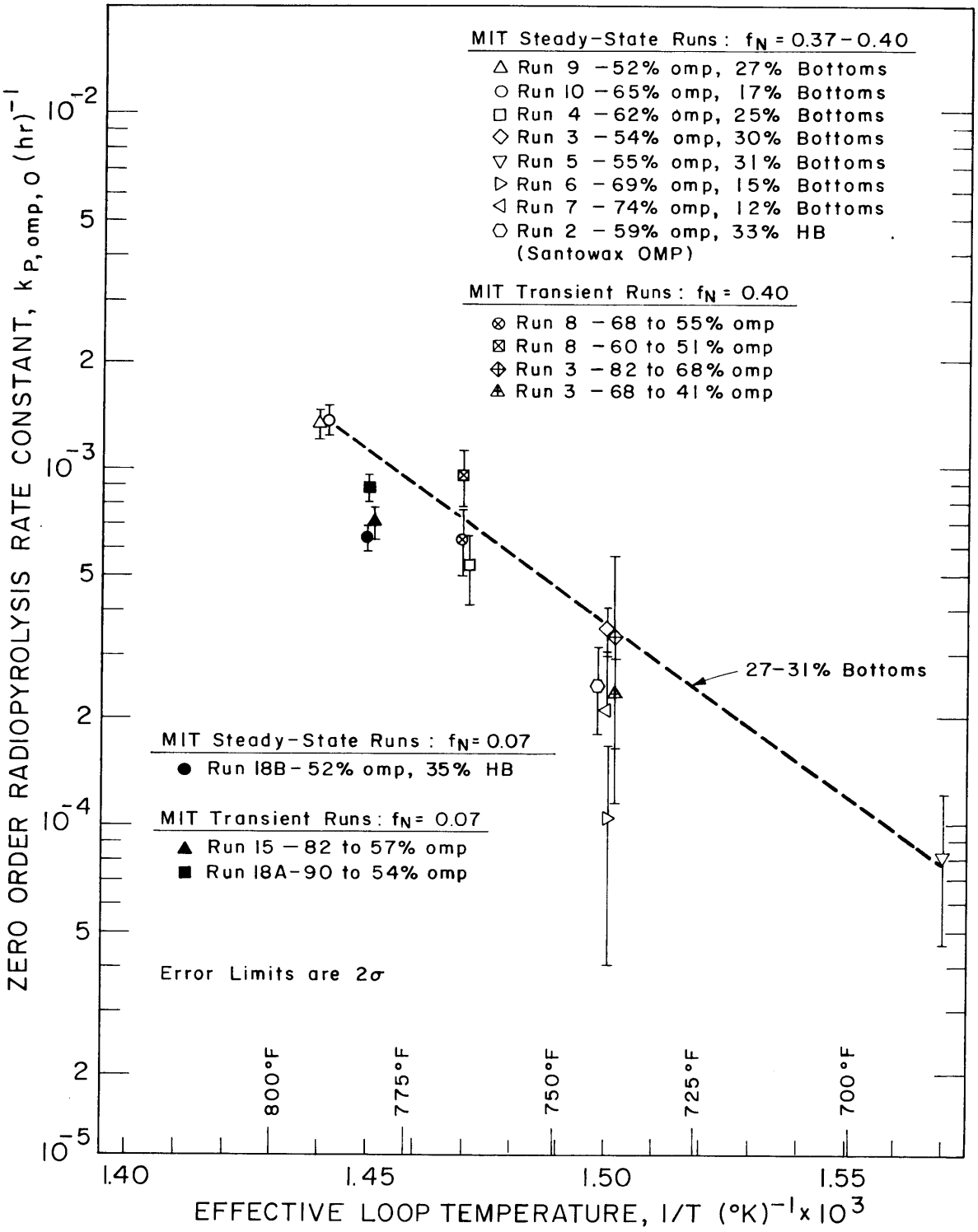

FIGURE 5.4 CORRELATION OF ZERO ORDER RADIOPYROLYSIS RATE CONSTANTS – MIT RUNS

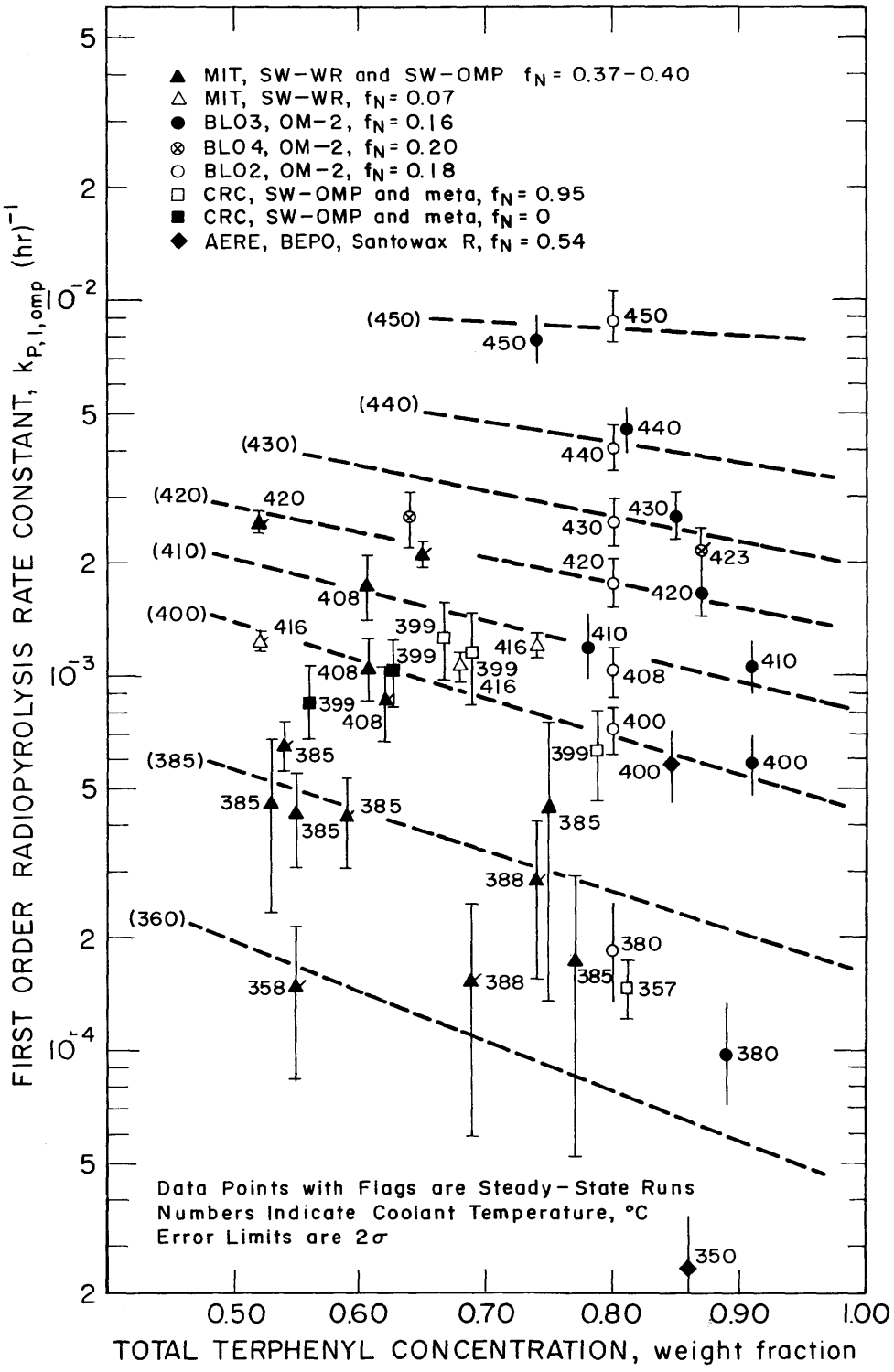

FIGURE 5.5 EFFECT OF TEMPERATURE AND TOTAL TERPHENYL CONCENTRATION ON THE RADIOPYROLYSIS RATE CONSTANT (FIRST ORDER)

(but no bars to indicate error limits) represents an irradiation for which the concentration versus dose data were not available at M.I.T. for computer analysis, and therefore the statistical errors could not be determined. The dashed lines in Figure 5.5 represent isotherms which have been drawn through the data points by eye. Sufficient data are available between 385°C and 420°C to obtain a reasonably good estimate of the slope of the isotherms. At temperatures higher than 420°C and lower than 385°C, the data are insufficient to obtain good estimates of these slopes, and therefore these isotherms were estimated to be similar to the slopes in the region 385°C-420°C.

The following conclusions can be made from the correlation of high temperature - low average dose rate data for meta-rich terphenyl coolants shown in Figure 5.5:

(1) The calculated values of $k_{P,\,omp,\,1}$ from the irradiations in the M.I.T. loop, the Euratom loops (BLO2, BLO3, BLO4) and Cal Research (CRC) capsule experiments and BEPO capsule experiments are correlated well by the empirical equations developed in Section 5.2. However, the recent M.I.T. data at $f_N = 0.07$ (open triangles in Figure 5.5) are significantly lower (by 30-50%) than the isotherms correlating the other data.

(2) The radiopyrolysis rate constants calculated from transient runs agree well with the k_P calculated from steady-state runs (data points with flags in Figure 5.5).

Most of the experimental data shown in Figure 5.5 and Table A5.2 have also been correlated by M.I.T., using second-order radiolysis kinetics (n = 2 in Equation (5.2)) and the following correlating equation for radiolysis presented earlier by M.I.T. (5.1).

$$k_{R,\,omp,\,2}(320°C) = 1.61 \times 10^{-2}\,[3.7\,f_N + 1] \qquad (5.13)$$

The radiopyrolysis rate constants calculated by using the above value of $k_{R,\,omp,\,2}$ and n = 2 in Equation (5.2) gave an average difference of only 4% (for 34 experiments) from the values shown in Figure 5.5 and Table A5.2.* This comparison confirms the fact that the calculated k_P for low average dose rate irradiations is not sensitive to the radiolysis

*where n = 1.7

kinetics order selected.

Figure 5.6 shows measured pyrolysis rates of irradiated and unirradiated terphenyl coolants determined in autoclave and loop post-irradiation and pre-irradiation pyrolysis tests. The isotherms (dashed lines) in Figure 5.5 have been redrawn in Figure 5.6 in order to compare post-irradiation pyrolysis rates with the radiopyrolysis rates calculated from irradiation runs. The post-irradiation pyrolysis data of Euratom have been discussed in an earlier M.I.T. report (5.1). The terphenyl concentration at which the post-irradiation pyrolysis data are plotted are the initial omp concentrations at the beginning of the test (or, equivalently, at the end of the irradiation before post-pyrolysis is begun).

Error limit bands have been drawn on several of the isotherms in Figure 5.6 representing the M.I.T. estimate of the maximum uncertainty in the magnitude of these k_P values. The size of the bands was estimated from the spread of values shown in Figure 5.5. Although drawn at only one coolant composition, it should be understood error limit bands of approximately the same width should apply all along the isotherms. These estimated maximum error limits of the radiopyrolysis rate constants are ±75% at 350°C, ±40% at 400°C, and ±15% at 450°C.

The post-pyrolysis degradation rates shown in Figure 5.6 agree well with the k_P calculated from irradiation tests in most cases. The largest discrepancy is the M.I.T. post-pyrolysis rate for Run 18P1 (coolant drained from loop at end of Run 18B and shown at 52% omp and 416°C). However, the k_P calculated from the irradiation results during Run 18B were also lower than expected (see Figure 5.3), and the irradiation and post-pyrolysis values of k_P for this coolant agree within the error limits described above. The substantial agreement between irradiation and post-pyrolysis k_P suggests that post-irradiation tests are a useful tool in estimating radiopyrolysis rates, particularly at low temperatures (below 400°C) where k_P cannot be calculated accurately from irradiation data because radiolysis is the predominant mode of decomposition.

The M.I.T. and AECL pyrolysis rates of unirradiated coolant (plotted at $C_{omp} = 1.0$) represent Curve II in Figure 5.2, and the

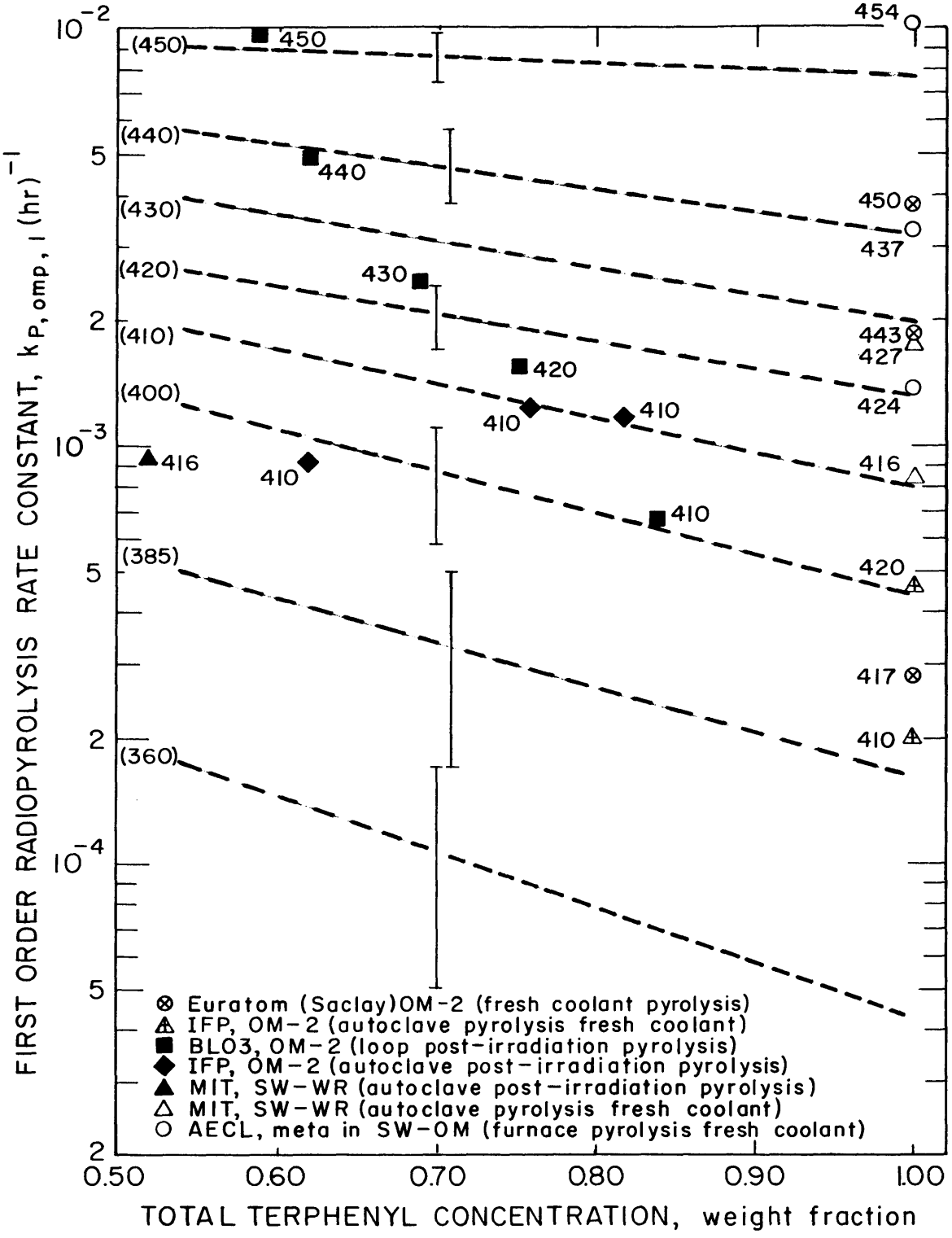

FIGURE 5.6 COMPARISON OF RADIOPYROYSIS RATE CONSTANTS CALCULATED FROM IRRADIATION RUNS AND MEASURED IN POST-IRRADIATION PYROLYSIS TESTS

Euratom (BLO3, IFP, Saclay) pyrolysis rates of unirradiated coolant represent Curve I in Figure 5.2. In general, the M.I.T. and AECL values correspond to linear extrapolations of the calculated isotherms to $C_{omp} = 1.0$, while the Euratom values for unirradiated coolant are significantly lower than the linear extrapolations to $C_{omp} = 1.0$. This discrepancy points out the value of obtaining accurate measurements of k_P for unirradiated terphenyl coolants because values of k_P at high terphenyl concentrations are difficult to obtain from irradiation data, and reliable estimates of k_P at or above terphenyl concentrations of 90% are needed for reactor design purposes. This concentration region is particularly important for predicting thermal decomposition rates in organic-cooled reactors which are currently expected to operate between 85% and 100% terphenyl concentration.

The isotherms of $k_{P,omp,1}$ versus total terphenyl concentration shown in Figures 5.5 and 5.6 have been cross-plotted to construct an Arrhenius diagram for the first-order radiopyrolysis rate constants. This diagram is shown in Figure 5.7 for three different levels of total omp concentration. The dashed lines representing 30% bottoms and 15% bottoms were presented earlier by M.I.T. (5.1), based on second-order radiolysis kinetics. There appears to be no significant difference in the earlier M.I.T. correlation (dashed lines) and the present correlation of the radiopyrolysis rate constants of meta-rich terphenyl coolants as a function of temperature. The Euratom correlation for pyrolysis of unirradiated OM-2 (Curve I in Figure 5.2) is included for comparison in Figure 5.7, as well as the M.I.T. and AECL data for pyrolysis of unirradiated coolant discussed in Section 5.3.1.

Table 5.4 summarizes the activation energies of pyrolysis, ΔE_P, calculated for the curves shown in Figure 5.7.

Euratom has reported (5.5) a value of $\Delta E_P = 38$ k-cal/mole for two steady-state OM-2 irradiations at 395°C and 423°C, assuming zero kinetics order radiopyrolysis.

The dependence of $k_{P,omp,1}$ on the coolant composition as shown in Figure 5.7 indicates that radiopyrolysis is not strictly first-order with respect to total terphenyl concentration, and perhaps the radiopyrolysis term in Equation (5.1) should contain a dependence on the concentration of some degradation products. This matter is discussed in more detail in Section 1.3.4.4.

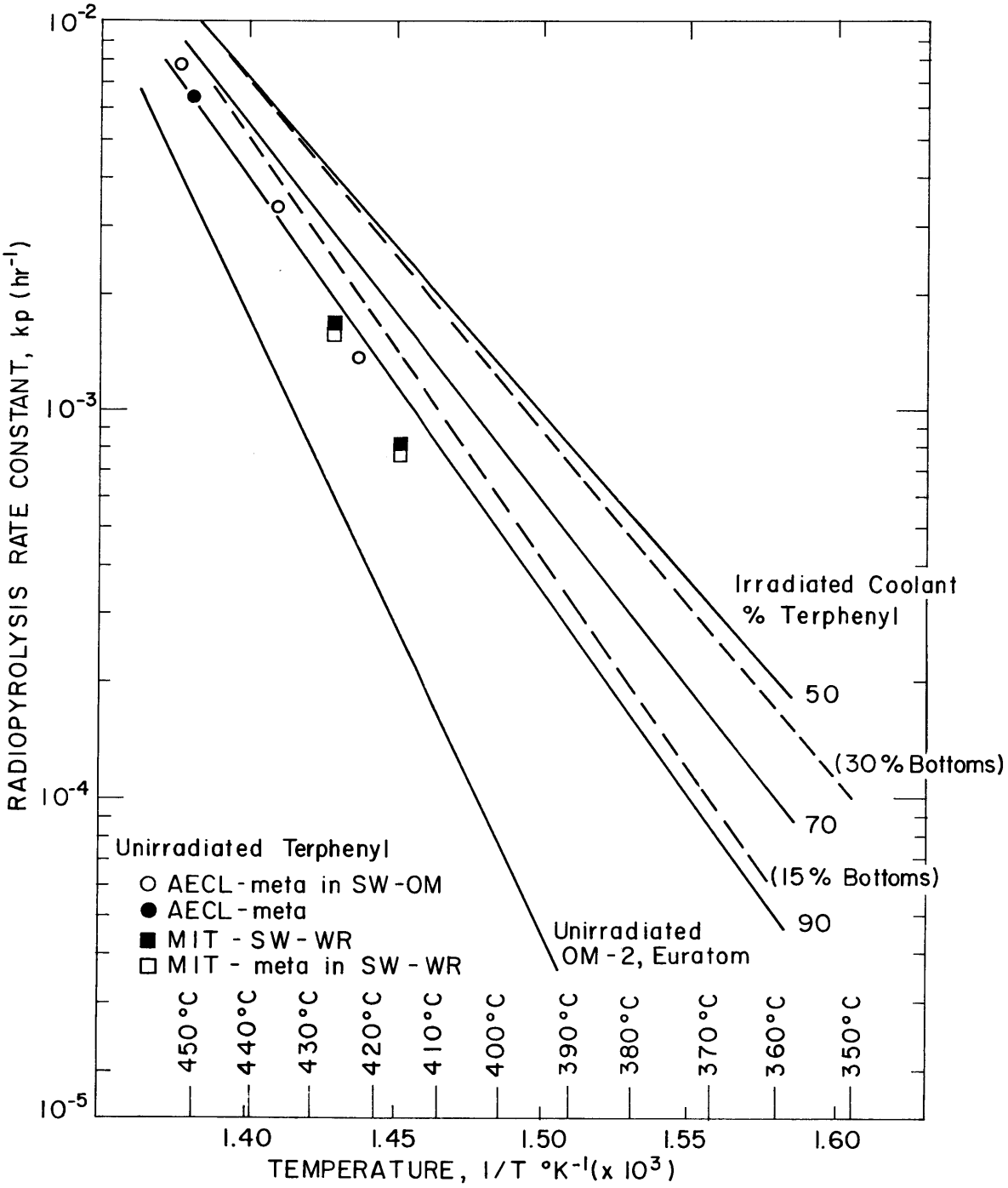

FIGURE 5.7 EFFECT OF TEMPERATURE ON THE PYROLYSIS OF IRRADIATED AND UNIRRADIATED TERPHENYL COOLANT CLASS I TERPHENYLS: META, SANTOWAX WR, SANTOWAX OMP, OM-2

Table 5.4

Activation Energy of Pyrolysis
for Irradiated and Unirradiated Terphenyl Coolants

Percent Terphenyl	ΔE_P, k-cal/mole
50%, irradiated	40
70%, irradiated	45
90%, irradiated	50
Curve I, unirradiated	72

5.4 Prediction of Coolant Makeup Rates for Organic-Cooled Reactors

5.4.1 Introduction

The ultimate use of experimental results of terphenyl irradiations and the correlations developed between the data of different laboratories rests in the use of these data to predict coolant makeup rates and costs, under a variety of operating conditions, for an organic-cooled reactor. This section presents a method for predicting these coolant makeup rates for the present reference design of the Heavy-Water Organic-Cooled Reactor (HWOCR) and investigates the effect of such parameters as coolant composition, temperature and coolant mass distribution around the loop, and fast neutron fraction of the dose rate on the total coolant degradation rate. The experimental data used to predict these coolant decomposition rates represent the meta-rich coolants reviewed in Section 5.3. These data should be used with caution to predict decomposition rates of ortho-rich coolants (such as Santowax OM), since both radiolysis and radiopyrolysis in such coolants may be significantly different from the values calculated in this chapter.

5.4.2 Characterization of the Coolant

The circulating coolant in an organic-cooled reactor will be a complex mixture of terphenyl isomers and low, intermediate, and high boiling degradation products. M.I.T. has found as many as 25 low and intermediate boiling components (LIB) and 16 high boiling components (HB) up to hexaphenyl by vapor phase chromatographic analysis of

irradiated coolant, and undoubtedly there are many more undetected organic species in the coolant. For the purpose of coolant degradation calculations, it should be sufficient to characterize the coolant by estimating the percentage of each terphenyl isomer in the circulating coolant (or by the ratio of isomers), and the percentage of total degradation products (DP) and high boiler (HB). This characterization may be inadequate for other purposes such as estimating fouling rates or designing distillation systems.

For a reactor operating under steady-state coolant operating conditions, the following points apply:

(1) The feed rate of fresh coolant (terphenyl) must equal the disappearance rate of terphenyl in the coolant loop to maintain constant terphenyl composition.

(2) The removal rate of high boiler (plus small amounts of gases and LIB) in the distillation process must equal the feed rate of fresh coolant (terphenyl) to maintain constant coolant mass in the loop.

(3) The production rate of LIB from terphenyl disappearance must exactly equal the disappearance rate of LIB (which is degraded to HB or leaves the coolant loop in the distillation) to maintain constant LIB composition.

From these points, it can be concluded that the ultimate product of terphenyl disappearance is the production of HB (unless terphenyl and LIB are removed in the still) and the coolant makeup rates and distillation processing rates must be based on terphenyl disappearance.

In M.I.T. steady-state irradiations, G(→HB) has always been less than G(-omp). Mass balances of the M.I.T. sampling and distillation operations have repeatedly shown that this difference is due to LIB being removed from the loop and not returned, but retained in the cold trap of the still or in the sample analysis bottles. Thus, there is a net G(→LIB) = G(-omp) - G(→HB) in the M.I.T. loop which is necessary to maintain constant LIB composition. Such a difference would be expected to be less in an organic-cooled reactor removing only HB in the distillation and possibly some low boilers in the degassing system.

Much significance has been attached to the experimental fact (5.2, 5.9) that while the G value for terphenyl disappearance of ortho terphenyl is greater than for meta terphenyl above about 320°C (see Chapter 6), the G(⇒HB) values for the two isomers may be about equal. Mackintosh (5.9) reports that the ortho isomer tends to form biphenyl and triphenylene while the meta isomer tends to produce para terphenyl or polymer (HB). However, these LIB components produced from ortho terphenyl are generally less stable than the terphenyls and are themselves degraded to HB. Again, the final product of ortho terphenyl disappearance in a steady-state operation is the production of HB. The important fact about the tendency of ortho terphenyl to produce LIB is that in a high ortho content coolant (such as Santowax OM), the distribution of degradation products between LIB and HB may be different than that found in a high meta content coolant (such as Santowax WR). At this time, no steady-state Santowax OM irradiations have been made to establish this point.

5.4.3 Coolant Degradation Calculation Methods

The fresh coolant makeup rate is equal to the disappearance rate of terphenyl

$$W_T = w_i(C^f_{omp} - C_{omp}) - \bar{r}M_L\left(\frac{dC_{omp}}{d\tau}\right) = \frac{G(-omp)}{11.65}\,\bar{r}M_L \qquad (5.14)$$

or for steady-state operation, where $dC_{omp}/d\tau = 0$,

$$W_T = w_i(C^f_{omp} - C_{omp}) = \frac{G(-omp)}{11.65}\,\bar{r}M_L \qquad (5.15)$$

where

W_T = total terphenyl degradation rate, gms/hr

w_i = feed rate of fresh coolant, gms/hr

C^f_{omp} = concentration of total terphenyl in the feed, weight fraction

C_{omp} = concentration of total terphenyl in the coolant system, weight fraction

$\bar{r}M_L$ = total energy absorbed in the coolant in the system, watts

Radiolysis and radiopyrolysis degradation are assumed to be independent and additive, since the experimental loop and capsule

irradiation data have been treated in the same manner.

$$\underset{\text{(total)}}{W_T} = \underset{\text{(radiolysis)}}{W_R} + \underset{\text{(radiopyrolysis)}}{W_P} \quad \text{(gms/hr)} \qquad (5.16)$$

The following sections will describe methods for calculating W_R and W_P.

5.4.3.1 Radiolysis Degradation Rate, W_R

Radiolytic degradation is produced by the absorption of fast neutron and gamma-ray radiation energy in the coolant. The radiation energy absorbed in the coolant can be expressed as an average dose rate to all the circulating coolant, $\bar{r}$, or an average dose rate in the irradiation zone (core) r_c.

$$\bar{r}M_L = r_c M_c = Pq_c \quad \text{(watts)} \qquad (5.17)$$

where

Pq_c = rate of radiation energy deposition in the coolant, watts
M_L = total circulating coolant mass, gms
M_c = coolant mass contained in reactor core, gms

The radiolytic degradation rate, W_R, is the product of the degradation per unit radiation energy absorbed (G_R) times the rate of radiation energy absorption in all the coolant (watts). This latter value will be a fraction, q_c, of the total thermal power of the reactor, P(megawatts), depending on the design of the fuel elements and coolant channels. The radiolytic degradation rate can be found by the following expressions, whichever is most convenient. In these equations, G_R is the molecules of terphenyl degraded by radiolysis per 100 ev absorbed in the coolant.

$$W_R = 0.086\, G_R(\text{-omp})\, Pq_c \qquad (5.18a)$$

or

$$W_R = 0.086\, G_R(\text{-omp})\, \bar{r}M_L \qquad (5.18b)$$

or

$$W_R = 0.086\, G_R(\text{-omp})\, r_c M_c \qquad (5.18c)$$

where

$$0.086\, G_R(\text{-omp})M_L = -C_{omp}\left(\frac{dM_L}{d\tau}\right) = k_{R,omp,n}C_{omp}^{n}\, M_L \qquad (5.19)$$

Therefore, by Equations (5.18b) and (5.19),

$$W_R = k_{R,omp,n} C_{omp}^{n} \bar{r} M_L \quad (gms/hr) \tag{5.20}$$

As shown in Chapter 4, the best estimate of the kinetics order of radiolysis is n = 1.7. Figure 4.4 gives a correlation of the radiolysis rate constant versus fast neutron fraction at 320°C. Equation (5.12) can be used to calculate the radiolysis rate constant at other temperatures, assuming an activation energy of radiolysis ΔE_R = 1 k-cal/mole. Since this assumption implies a small effect of temperature of radiolysis, the core average coolant temperature can be used in Equation (5.12).

5.4.3.2 Radiopyrolysis Degradation Rate, W_P

Figure 5.8 is a simplified coolant flow diagram for the HWOCR (5.10), showing the various temperature zones and nominal coolant temperatures. The thermal decomposition or radiopyrolysis rate can be estimated independently from the radiolysis rate, using Equation (5.21) to determine the radiopyrolysis rate of total terphenyl in various zones, N, of the coolant loop.

$$W_P = \sum_N W_P(N) = \sum_N \int_{M_N(T_1)}^{M_N(T_2)} k_{P,omp,1}(T) C_{omp} dM_N(T) \tag{5.21}$$

where

$W_P(N)$ is the radiopyrolysis rate of the total terphenyl in the N^{th} zone of the coolant loop

$k_{P,omp,1}$ is the first-order radiopyrolysis rate constant for total terphenyl shown as a function of coolant composition and temperature in Figure 5.7

C_{omp} is the concentration of total terphenyl isomer in the circulating coolant

$dM_N(T)$ is the coolant mass in zone N between temperatures T and T + dT

T_1 and T_2 are the inlet and outlet temperatures in zone N

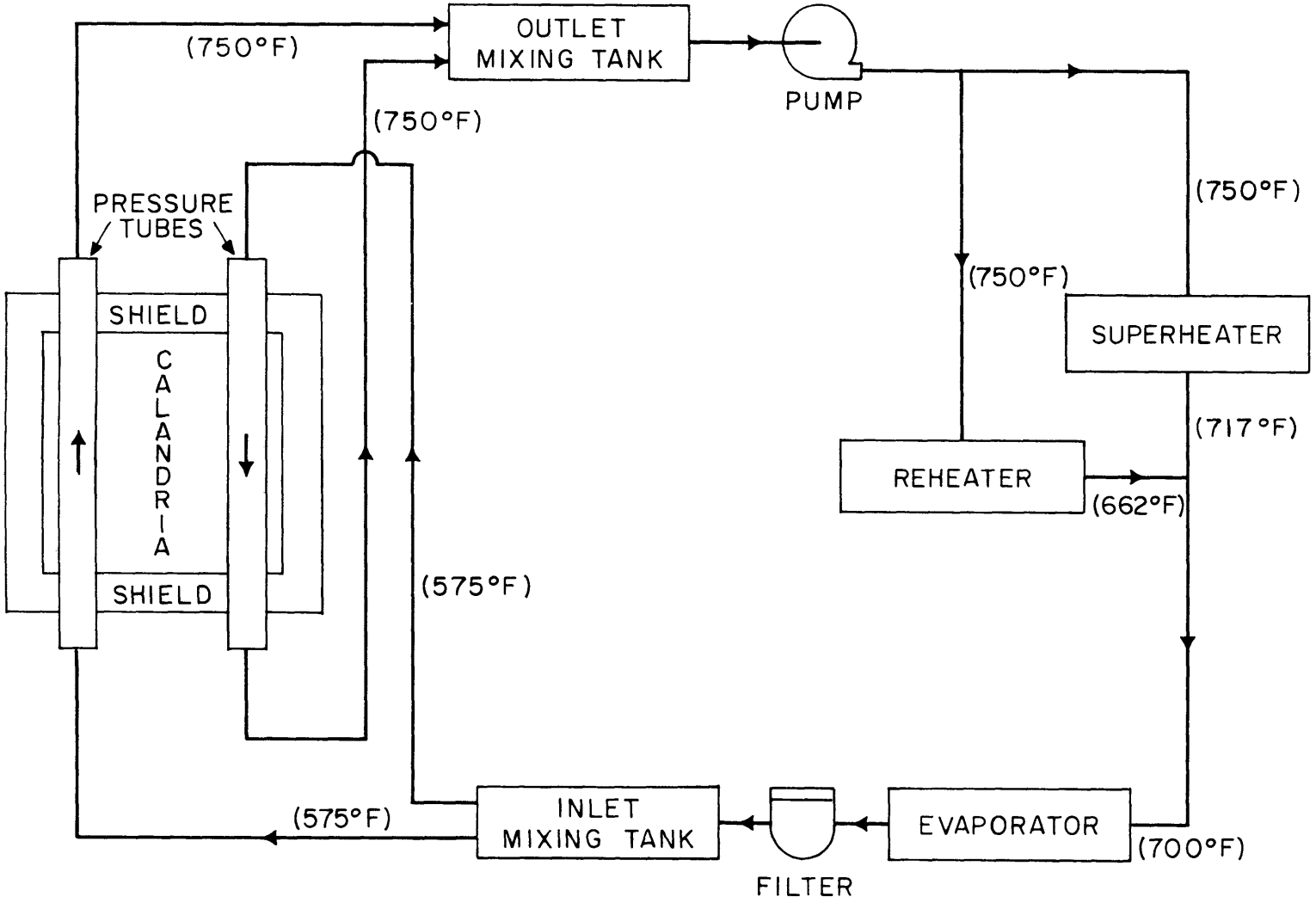

FIGURE 5.8 SIMPLIFIED ORGANIC COOLANT FLOW DIAGRAM - 750 MWE HWOCR

The fraction of coolant, $dM_N(T)$, in zone N with temperature between T and T + dT can be assumed equal to the magnitude of the interval dT divided by the overall temperature change in the zone, as shown below

$$\frac{dM_N(T)}{M_N} = \frac{dT}{T_2 - T_1} \tag{5.22}$$

For constant temperature zones, $dM_N(T)$ is equal to M_N, the total coolant mass in zone N. Substituting Equation (5.22) into Equation (5.21) gives for the radiopyrolysis rate in zone N,

$$W_P(N) = \frac{M_N C_{omp}}{T_2 - T_1} \int_{T_1}^{T_2} k_{P,\,omp,\,1}(T)\, dT \tag{5.23}$$

since C_{omp}, for practical purposes, is constant throughout the coolant loop due to the rapid flow of coolant around the loop relative to the degradation and processing rates, so that the loop behaves as a well-mixed system.

Equation (5.23) can be integrated stepwise using about 10°C steps (ΔT) and the $k_{P,\,omp,\,1}$ from Figure 5.7, as shown below in Equation (5.24).

$$W_P(N) = \frac{M_N C_{omp}}{T_2 - T_1} \sum k_{P,\,omp,\,1}(T)\, \Delta T \tag{5.24}$$

This procedure should be repeated for each variable temperature zone.

For constant temperature zones such as headers and inlet and outlet lines, Equation (5.23) reduces to a simple form.

$$W_P(N) = k_{P,\,omp,\,1}(T)\, C_{omp}\, M_N \tag{5.25}$$

Equation (5.25) can also be used to calculate approximately the radiopyrolysis rate in variable temperature zones by using a value of $k_{P,\,omp,\,1}$ for an effective temperature in the zone. By determining the values of $k_{P,\,omp,\,1}$ in Equation (5.25) which give the same total radiopyrolysis rate as Equation (5.24) for Zones III and V in Figure 5.8, the effective temperatures corresponding to these $k_{P,\,omp,\,1}$ were read directly from Figure 5.7. The effective temperature found in this

manner was about

$$T_{eff} = T_{lower} + 0.65\,(T_2 - T_1) \qquad (5.26)$$

for both variable temperature zones and for all terphenyl concentration levels.

5.4.4 Coolant Degradation Calculations – HWOCR Demonstration Plant

The HWOCR program is presently considering the design and construction of 750 Mwe (design power level) demonstration plant, possibly followed by a 1000 Mwe power reactor (5.10, 5.11). The fuel proposed is slightly enriched UC fuel assemblies (each containing 37 rods) with 0.020-inch SAP cladding. Five fuel assemblies are stacked in each process tube. The core is designed for one coolant pass utilizing bi-directional flow and refueling, with core inlet and outlet temperatures of 575°F and 750°F, respectively.

The primary coolant system consists of two coolant loops, each with an evaporator, superheater, reheater, coolant circulating pump, isolation valves, and interconnecting piping (see Figure 5.8). The loops are connected across reactor inlet and outlet mixing tanks which serve as coolant collection headers. The outlet mixing tank also serves to provide a time delay for the coolant leaving the reactor. The volumes of coolant in each zone of the coolant loops were obtained from Atomics International (5.12).

The values reported (5.10) for the fast neutron and gamma-ray dose rates to the coolant are 10 MW from fast neutrons and 3 MW from gamma rays for the 1000 Mwe plant. The fast neutron dose rate has been modified by Combustion Engineering (5.13) to 5.9 MW for the 750 Mwe demonstration plant. The gamma-ray dose is less well known, but can be estimated as 3 MW. Due to the much greater damaging effects of fast neutrons ($G_N/G\gamma \approx 4$), errors in the estimated gamma dose rate to the coolant should not produce large errors in the calculated degradation rates. Based on the modified values above, the fast neutron fraction of the dose rate is $f_N = 0.66$.

Table 5.5 shows the calculated radiolysis, radiopyrolysis and total degradation rates for a meta-rich terphenyl in HWOCR at

C_{omp} = 0.70 and for core outlet temperatures of 750°F and 800°F. The temperature profile around the coolant loop for the 800°F case was estimated simply by raising all temperatures in the 750°F case by 50°F. No change was made in the mass of coolant in the various reactor zones between the two cases. The values in Table 5.5 indicate that about 90% of the radiopyrolysis for both core outlet temperatures occurs in Zone IV, the outlet header and hot leg of the loop. The advantages in lower coolant makeup rates of reducing the coolant mass held at high temperature in this zone are apparent.

The coolant makeup costs shown in Table 5.5 are based on present estimates (5.10) of the costs of fresh Santowax WR or Santowax OM supplied in large quantities (10 million pounds per year). Although lower priced coolants may be obtained in time with such processing methods as hydrocracking, it should be recognized that the degradation rates of hydrocracked coolant may be substantially different than the values used in this study.

Figure 5.9 shows the effect of coolant composition on the terphenyl degradation rates in HWOCR. The solid lines in Figure 5.9 represent 750°F coolant outlet temperature and the dashed lines represent 800°F outlet temperature. The most important point illustrated in Figure 5.9 is that the decrease in the radiolysis rate with decreasing terphenyl concentration is larger than the increasing radiopyrolysis rates, for both 750°F and 800°F core outlet temperatures. Therefore, lower coolant makeup rates can be achieved by utilizing lower terphenyl (higher DP) concentrations in the coolant. It should be recognized that other factors, such as pumping power costs and possibly film formation or fouling rates, must be considered before an optimum coolant composition is selected.

Table 5.5

Calculated Coolant Makeup Rates for 750 Mwe HWOCR Demonstration Plant

(C_{omp} = 0.70)

Zone	Description	Coolant Mass (lbs)	750°F Core Outlet Coolant Temperature: Temperature (°F)	750°F Core Outlet Coolant Temperature: Total Terphenyl Degradation Rate (lbs/hr)	800°F Core Outlet Coolant Temperature: Temperature (°F)	800°F Core Outlet Coolant Temperature: Total Terphenyl Degradation Rate (lbs/hr)
Radiopyrolysis						
I	Cold leg, inlet header	536,000	575	–	625	–
II	Decay heat loop	43,000	650	2	700	8
III	Reactor core	64,000	575 - 750	8	625 - 800	27
IV	Outlet header, hot leg	690,000	750	392	800	1350
V	Superheater	73,000	750 - 717	27	800 - 767	112
VI	Evaporator	49,000	700 - 574	1	750 - 624	4
VII	Reheater	52,000	750 - 662	11	800 - 712	47
		Sub-total (Radiopyrolysis)		441		1548
Radiolysis				530		565
Total Makeup Rate				971		2113
Coolant Makeup Cost (mills/kwh) $(0.12/lb coolant cost)				0.16		0.35

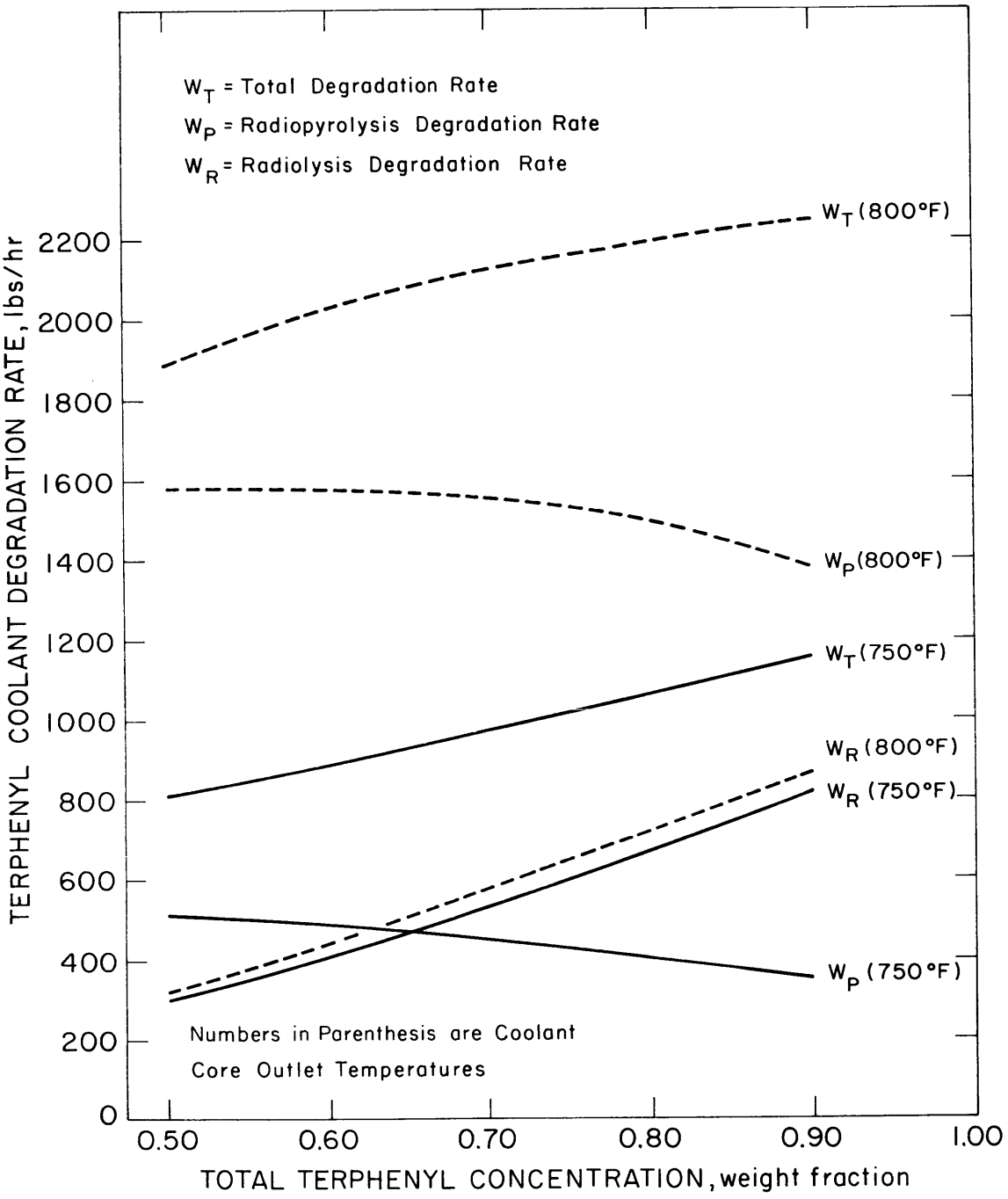

FIGURE 5.9 EFFECT OF COOLANT COMPOSITION AND CORE OUTLET TEMPERATURE ON TERPHENYL DEGRADATION RATE - HWOCR REFERENCE DESIGN

CHAPTER 6

HIGH DOSE RATE IRRADIATIONS AND TERPHENYL ISOMER STABILITIES

6.1 Introduction

The terphenyl irradiation data reviewed in Chapter 5 was restricted to meta-rich terphenyls with low average dose rates primarily because the M.I.T. and Euratom in-pile loop data were obtained under these conditions. By restricting the review of high temperature irradiation results to experiments with low average dose rates (long irradiation times), the analysis in Chapter 5 concentrated on the effect of temperature on the thermal decomposition rates (radiopyrolysis) of meta-rich coolants. The effect of high temperature irradiation on the radiolysis degradation rate cannot be obtained from such experiments because radiopyrolysis decomposition predominates.

AECL has made capsule irradiations of ortho and meta terphenyl in the NRX reactor at $f_N = 0.01$ and $f_N = 0.50\text{-}0.60$ with high dose rates (0.1-1 watts/gram) from 100°-450°C (6.1, 6.7, 6.9). AECL has also made electron (Van de Graaf) irradiations of meta terphenyl in stirred cells at 0.4 watts/gram and 5 watts/gram from 300°-440°C (6.1). Mackintosh (6.2) has reported on the electron irradiation of Santowax OM from 350°C to 450°C and the electron irradiation of ortho and meta terphenyl at 375°C at 73 watts/gram.

M.I.T. (6.3, 6.4) has reviewed the results of AECL irradiations of OM-2 in the NRX X-rod facility at 0.33 watts/gram and $f_N = 0.30$. Scarborough (6.5, 6.6) reports the results of electron irradiations at Atomics International of ortho terphenyl from 752°F to 898°F at an average dose rate of about 0.8 watts/gram.

These irradiations which involved high dose rates at varying temperatures can be used to investigate:

(1) the effect of temperature on the radiolysis rate of terphenyls,

(2) the effect of the dose rate on the terphenyl degradation rate,

(3) the relative stabilities of the ortho and meta terphenyl isomers to radiolysis during irradiations with different fast neutron fractions of the dose rate,

(4) the agreement between the degradation rates observed in electron irradiations and pure gamma-ray irradiations.

M.I.T. has reviewed these high dose rate experiments to determine how the results may affect the method of predicting coolant make-up rates for organic-cooled reactors given in Chapter 5. The conclusions reached in this chapter should be regarded as tentative because (1) in many cases, the experimental data are scarce, and (2) the experiments were made under transient conditions and the application of the results obtained to a reactor operating at steady-state coolant composition is difficult.

6.2 Effect of Temperature on the Radiolysis Rate of Meta-Rich and Ortho-Rich Terphenyls

Figures 6.1 and 6.2 show the effect of temperature on the second-order radiolysis rate constants of meta-rich and ortho-rich terphenyls, respectively, for the high dose rate experiments of AECL (6.1, 6.2, 6.7, 6.9) and Atomics International (6.5, 6.6). Second-order radiolysis kinetics was used in this review (instead of 1.7 order) because recent AECL irradiation results (6.9) were presented as initial G values based on second-order kinetics, and the concentration versus dose data for these experiments are not available at M.I.T. at this time for correlation by other kinetics orders. Since there is only 5-10% difference between $k_{R,i,1.7}$ and $k_{R,i,2}$, the conclusions reached regarding the effect of temperature on the second-order radiolysis rate constant should also apply to the 1.7 order radiolysis rate constant. A description of the calculation methods used to obtain these results is given in Appendix A5.3, and the calculated values of $k_{R,i,2}$ are given in Tables A5.3 and A5.4.

In order to account for the wide variations in fast neutron fraction in these experiments, the calculated values of $k_{R,i,2}$ have been normalized by Equation (6.1).

$$k_{R,omp,1.7}(320°C) = 1.61 \times 10^{-2}[2.9f_N + 1] \qquad (6.1)$$

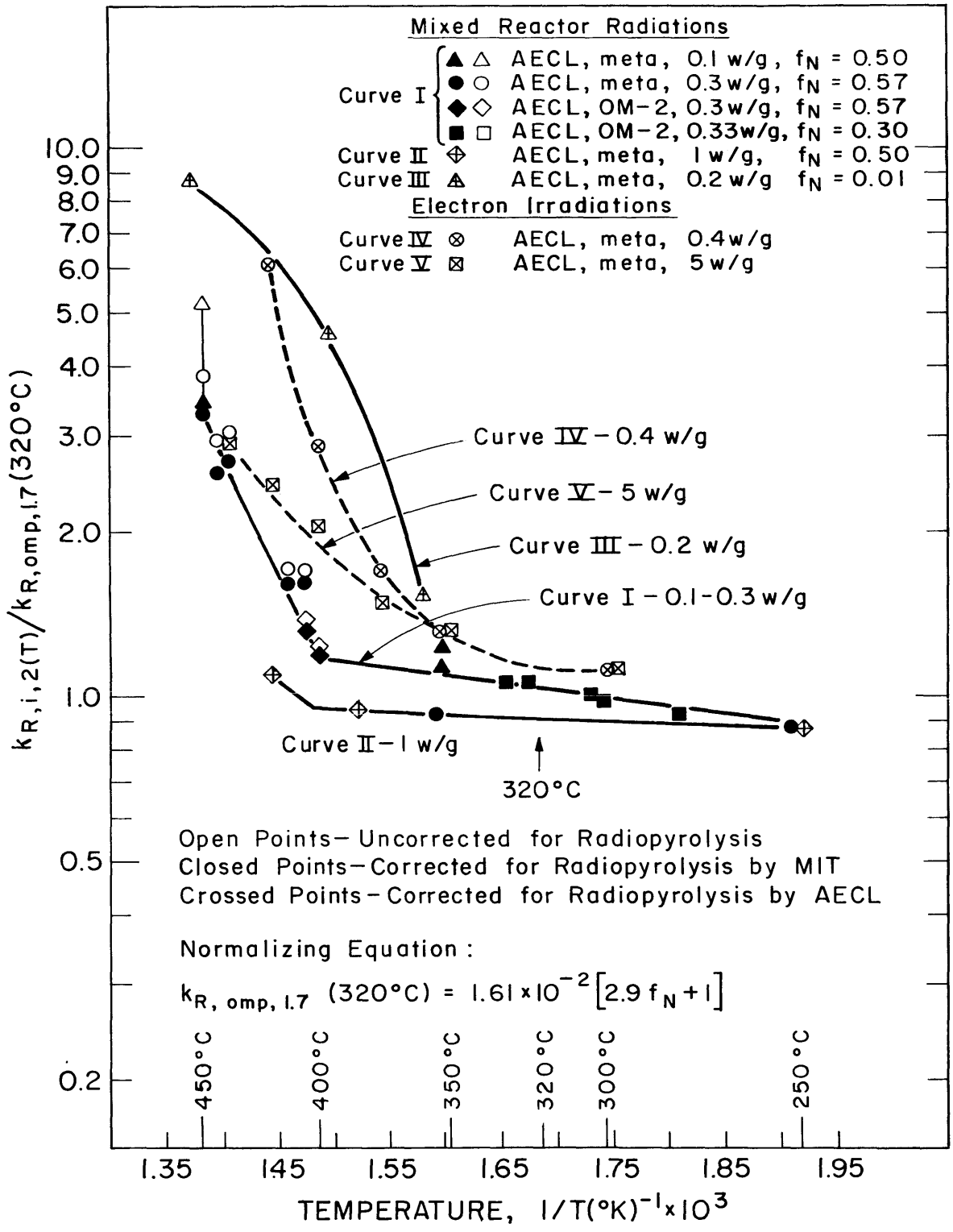

FIGURE 6.1 EFFECT OF TEMPERATURE ON THE RADIOLYSIS RATE OF META-RICH TERPHENYLS (SECOND-ORDER KINETICS)

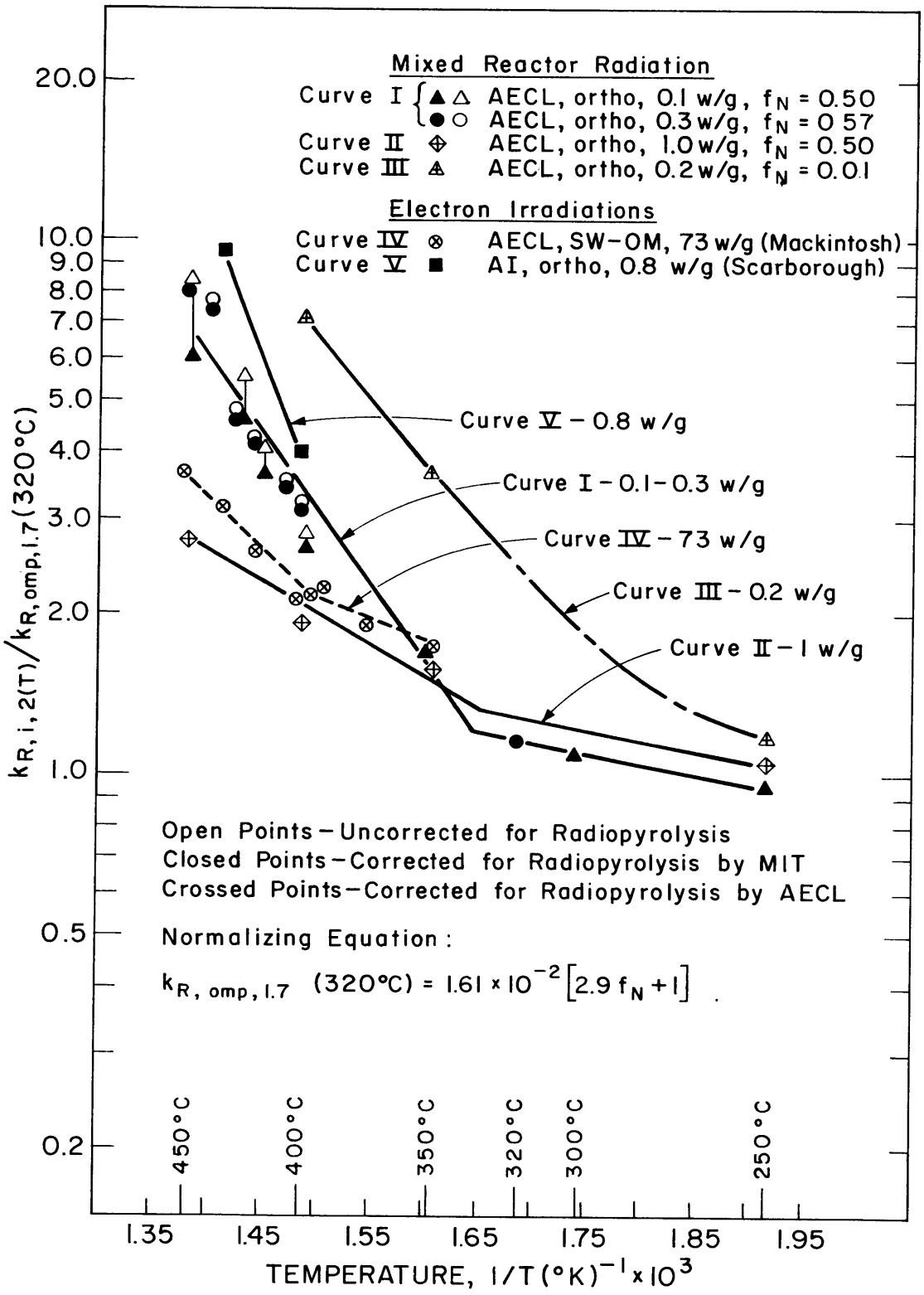

FIGURE 6.2 EFFECT OF TEMPERATURE ON THE RADIOLYSIS RATE OF ORTHO-RICH TERPHENYLS (SECOND-ORDER KINETICS)

which is the correlation shown in Figure 4.4. This normalization was made by dividing the values of $k_{R,i,2}$, shown in Table A5.3, by the value of $k_{R,omp,1.7}$ calculated from Equation (6.1) using the fast neutron fraction, f_N, employed in the experiment.

Equation (6.1) was used in Section 5.4 to predict the radiolysis rate of meta-rich terphenyls in HWOCR by assuming an activation energy of radiolysis ΔE_R = 1 k-cal/mole. Figure 6.1 shows that the correlations of $k_{R,i,2}$ from the AECL high-dose rate irradiations of meta-rich terphenyls agree within ±10% with the normalizing equation at 320°C.

In Figures 6.1 and 6.2, the open data points have not been corrected for radiopyrolysis, the closed data points have been corrected for radiopyrolysis by M.I.T., and the crossed data points have been corrected for radiopyrolysis by AECL. In these corrections, the radiolysis rates were calculated from the experimentally determined value for the total rate of degradation less an estimated correction for the amount of radiopyrolysis occurring during the irradiation. The M.I.T. corrections are based on Figures 5.4 and 5.6, while the AECL corrections used the values of k_P obtained in post-irradiation pyrolysis experiments (6.7), assuming the thermal decomposition rates of irradiated ortho and meta terphenyl were equal. All curves are drawn through data points corrected for radiopyrolysis. Comparison of the open points and closed points show that for most data (except the runs at 0.1 watt/gram at high temperature) the radiopyrolysis correction for these high-dose rate runs is negligible.

The following general conclusions for meta-rich terphenyls can be made from Figure 6.1:

(1) There is a significant increase in the radiolysis rate (Curve I and Curve II) for mixed reactor radiations at temperatures above about 400°C, as observed by Boyd et al. (6.7).

(2) There is a significant increase in the radiolysis rate (Curve IV and Curve V) for electron irradiations at temperatures above about 350°C, as observed by AECL (6.1, 6.2).

(3) There is a dose rate effect on the radiolysis rate (for both mixed reactor radiations and electron irradiations), such that an

increase in the dose rate lowers the radiolysis rate (per unit absorbed energy). Curve I and Curve II show that this effect does not occur for mixed reactor radiations up to 0.3 watts/gram but occurs in the range 0.3-1.0 watts/gram. This dose rate effect becomes more pronounced at high temperatures. Similar conclusions have been drawn from these results by AECL (6.1).

(4) Comparison of Curve III and Curve IV does not offer conclusive evidence on the high temperature radiolysis rate by electron irradiation compared to gamma-ray irradiation. A single curve could represent all these data (crossed circles and crossed triangles) reasonably well. Boyd et al. (6.9) discuss the differences between electron irradiations and gamma-ray irradiations in detail.

(5) Curve III, Curve IV, and Curve V indicate that gamma-ray and electron radiolysis rates increase faster with temperature than the radiolysis rates for mixed reactor radiations (Curve I and Curve II). This is a phenomenon noted by AECL (6.9) as a loss of sensitivity to the quality of the radiation. This result indicates that the fast neutron effect ratio, G_N/G_γ, decreases at high temperature from the value of $G_N/G_\gamma = 3.9$ at 320°C assumed in the normalization.

The following general conclusions for ortho-rich terphenyls can be made from Figure 6.2:

(1) There is a significant increase in the radiolysis rate (Curve I and Curve II) for mixed reactor radiations above about 330°C, as reported by Boyd et al. (6.7).

(2) The electron irradiation data of Scarborough (6.5) for ortho terphenyl (Curve V) is significantly higher than the data of Mackintosh (6.2) for Santowax OM (Curve IV). This difference may be a dose rate effect or due to the fact that Santowax OM contains about 30% meta terphenyl, which is more stable than ortho terphenyl.

(3) There is a dose rate effect for mixed reactor radiations, similar to that seen in meta-rich terphenyls, which occurs between 0.3 and 1 watt/gram. Again, the dose rate effect becomes more pronounced at high temperatures.

In order to compare the radiolytic stability of meta-rich terphenyls and ortho-rich terphenyls for mixed reactor radiations, the appropriate curves from Figures 6.1 and 6.2 have been redrawn in Figure 6.3. The dashed line in Figure 6.3 represents ΔE_R = 1 k-cal/mole, normalized to unity at 320°C. The coolant temperature for the conceptual design of HWOCR (6.8) is included in this figure to show the temperature range which is currently important for organic coolant degradation calculations. For both high dose rates (Curve III, 1 watt/gram) and low dose rates (Curve II, 0.1-0.3 watts/gram), the activation energy of radiolysis assumed in Section 5.4 (ΔE_R = 1 k-cal/mole) for meta-rich terphenyls agrees well with the AECL results up to the maximum coolant temperature of HWOCR (400°C). Table 5.1 shows that the expected dose rate in the core region of HWOCR is about 1.3 watts/gram.

Table 6.1

Comparison of the Activation Energy of Radiolysis of Ortho and Meta Terphenyl

Terphenyl	Dose Rate watts/gram	Curve	Temperature Range °F	°C	ΔE_R, k-cal/mole
meta	0.1-0.3	II	482-752	250-400	1.3
	0.1-0.3	II	752-842	400-450	20
	1.0	III	482-752	250-400	0.4
ortho	0.1-0.3	IV	482-626	250-330	2.5
	0.1-0.3	IV	626-842	330-450	13
	1.0	V	482-626	250-330	2.0
	1.0	V	626-842	330-450	5.5

Figure 6.3 also shows that above 300°C ortho terphenyl has a higher radiolytic degradation rate than meta terphenyl, with the difference between the two isomers depending on the dose rate. Table 6.1 presents a comparison of the activation energy of radiolysis, ΔE_R, for ortho and meta terphenyl in various temperature ranges. These values were calculated from Figure 6.3. Curve II shown in Figure 6.3

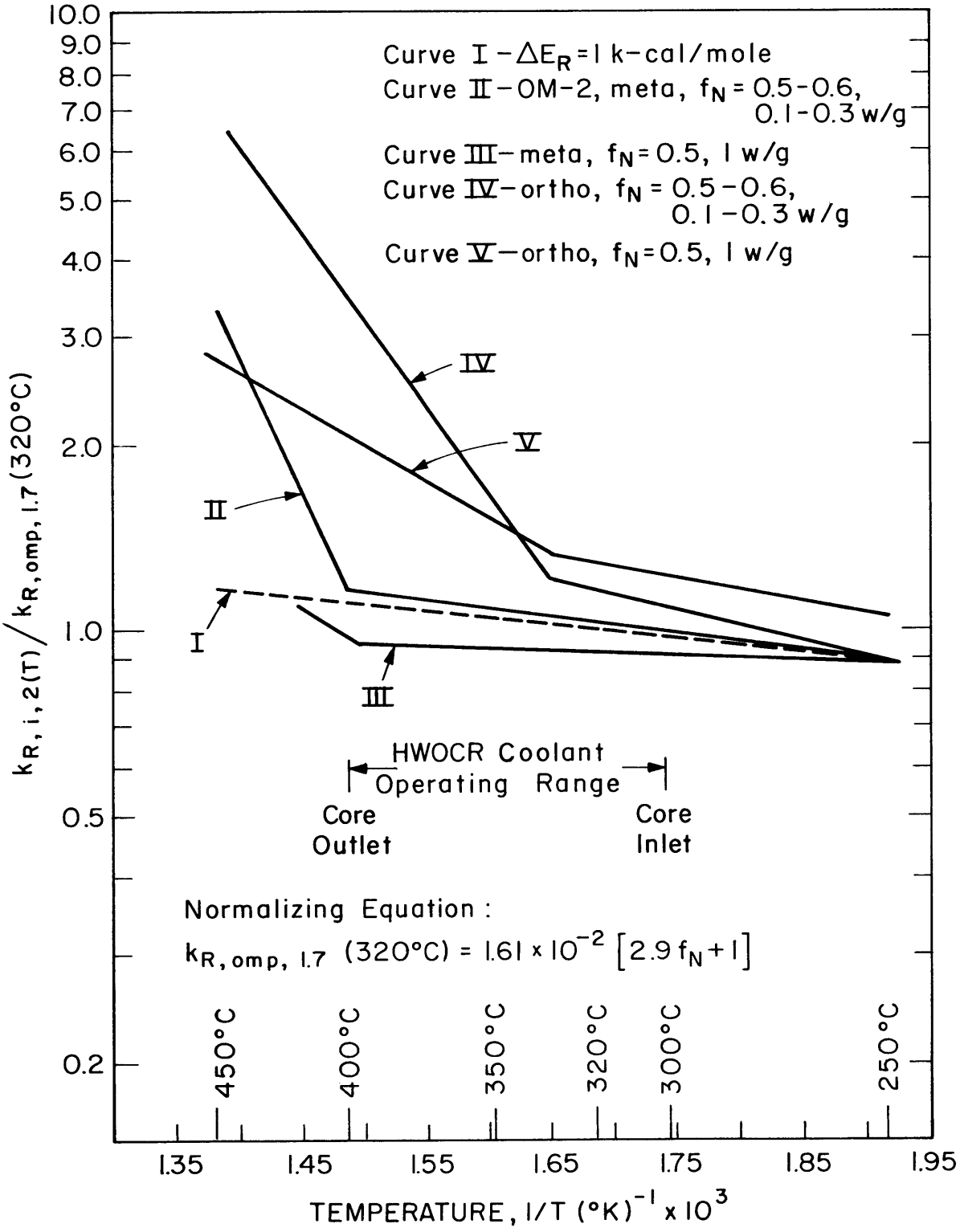

FIGURE 6.3 EFFECT OF TEMPERATURE ON THE RADIOLYSIS RATE OF ORTHO AND META TERPHENAL-MIXED REACTOR RADIATION

represents OM-2 and pure meta terphenyl data up to 400°C, but only pure meta data above 400°C. Curves III, IV, and V represent only pure ortho or meta isomer irradiation data. Terphenyl isomers in mixtures may have different radiolytic stabilities than those depicted in Figure 6.3 for pure isomer irradiations. This may be particularly significant in the case of ortho terphenyl, as will be discussed in Section 6.3. The presence on the Arrhenius diagrams of two regions where the rate constants are correlated by significantly different activation energies suggests that the controlling mechanisms for radiolysis are different at low and at high temperatures. Boyd, Connor, and Miller at AECL (6.9) have proposed a reaction scheme which takes this into account.

6.3 Recalculation of Total Terphenyl Radiopyrolysis Rates – Calculation of Terphenyl Isomer Radiopyrolysis Rates

Although the graphical representation in Figure 6.3 was obtained primarily from pure isomer irradiations, this plot can be used to estimate the effect of temperature on radiolysis in place of the constant activation energy, $\Delta E_R = 1$ k-cal/mole, assumed in Chapter 5 (i. e., Curve I in Figure 6.3). In particular, the effect of rapidly increasing radiolysis rates with temperature on the radiopyrolysis rates shown in Figures 5.5, 5.6, and 5.7 should be reviewed.

From the general rate relation assumed in Equation (4.1b), the radiopyrolysis rate of the terphenyl isomers may be written

$$k_{P,i,c+d} C_i^c C_{omp}^d = \left[\frac{G(-i)}{11.65} - k_{R,i,a+b} C_i^a C_{omp}^b \right] \bar{r} \quad (hr)^{-1} \qquad (6.2)$$

It was shown in Section 4.5 that currently the best values for the constants a and b are

$$a = 1.0$$
$$b = 0.7$$

in the low temperature range near 320°C.

For lack of better information at this time (see Section 5.2.1), it is assumed that radiopyrolysis follows a first-order mechanism, with the rate of radiopyrolysis depending only on the concentration of the component i which is being thermally decomposed. Following these assumptions,

$$c = 1.0$$

$$d = 0$$

and for transient runs, Equation (6.2) can be written

$$k_{P,i,1} = \left[\frac{-dC_i/d\tau}{C_i} - k_{R,i,1.7}C_{omp}^{0.7}\right]\bar{r}\ (hr)^{-1} \qquad (6.3)$$

For steady-state runs,

$$k_{P,i,1} = \left[\frac{G(-i)}{11.65\ C_i} - k_{R,i,1.7}C_{omp}^{0.7}\right]\bar{r}\ (hr)^{-1} \qquad (6.4)$$

This is the same relation used in Chapter 5 (Equation (5.3)) to calculate the radiopyrolysis rate of total terphenyl except the 1.7 order radiolysis rate constant for total terphenyl is the 1.7 order radiolysis rate constant for the terphenyl isomer. The discussion of rate constants given in Section 4.5 indicates that this interpretation is consistent.

Table 6.2 presents values of the radiopyrolysis rate constants for total terphenyl and for the terphenyl isomers calculated for the M. I. T. steady-state runs, using Equation (6.4) and the correlations shown in Figure 6.3 to estimate the radiolysis rate constants, $k_{R,i,1.7}(T)$, as the irradiation temperatures. Since the average dose rate in the irradiation zone for these M. I. T. runs was about 0.5 watt/grams, Curve II in Figure 6.3 has been used to estimate $k_{R,i,1.7}(T)$ for total terphenyl and meta terphenyl in Santowax WR, and Curve IV has been used to estimate $k_{R,i,1.7}(T)$ for ortho terphenyl in Santowax WR. As discussed in Section 5.3.2, this procedure does not account for changes in G_N/G_γ with increasing temperature, but data for the effect of temperature on G_N/G_γ for mixtures of terphenyl isomers are not presently available. Table 6.2 provides a comparison of the radiopyrolysis constants, k_P, calculated for ΔE_R = 1 k-cal/mole (Curve I values, also reported in Chapter 5) and calculated for the higher values of ΔE_R shown on Curve II of Figure 6.3 for the AECL irradiations at high dose rates. The difference between the two values is 10-20% which is within the error limits on $k_{P,omp,1}$ given in Chapter 5. For reactor coolant degradation calculations, the more conservative values are the higher values (i. e., the "Curve I" values which are presented in Figures 5.5 and 5.7).

The calculated radiopyrolysis rate constants for meta terphenyl

Table 6.2

Calculation of Radiopyrolysis Rate Constants for Total Terphenyl, Meta Terphenyl, and Ortho Terphenyl in Santowax WR – M.I.T. Steady-State Runs

Run No.	Temperature		$G^*(-i) = G(-i)/C_i$			First-Order Radiopyrolysis Rate Constant, $k_{P,i,1}(hr)^{-1}$			
						Total OMP		Meta	Ortho
	°F	°C	total omp	meta	ortho	Curve I[a,b]	Curve II[b]	Curve II[b]	Curve IV[b]
9	800	427	1.76	1.65	2.38	2.56×10^{-3}	2.16×10^{-3}	1.97×10^{-3}	1.84×10^{-3}
10	800	427	1.62	1.42	2.18	2.10×10^{-3}	1.63×10^{-3}	1.30×10^{-3}	1.06×10^{-3}
4	780	416	0.87	0.81	1.10	8.60×10^{-4}	6.25×10^{-4}	5.30×10^{-4}	-3.9×10^{-4}
3	750	399	0.63	0.59	1.00	6.50×10^{-4}	5.45×10^{-4}	4.78×10^{-4}	1.0×10^{-4}
6	750	399	0.45	0.45	0.54	1.51×10^{-4}	1.22×10^{-4}	1.22×10^{-4}	-9.3×10^{-4}
7	750	399	0.55	0.53	0.58	2.82×10^{-4}	2.48×10^{-4}	2.22×10^{-4}	-9.3×10^{-4}
2	750	399	0.53	0.52	0.79	4.20×10^{-4}	3.70×10^{-4}	3.52×10^{-4}	-2.2×10^{-4}
5	700	371	0.37	0.35	0.39	1.48×10^{-4}	1.0×10^{-4}	0.65×10^{-4}	-3.9×10^{-4}
18B	800	427	1.03	1.00	1.48	1.23×10^{-3}	1.01×10^{-3}	0.97×10^{-3}	1.02×10^{-3}

[a] ΔE_R = 1 k-cal/mole; values shown in Figures 5.5 and 5.7.

[b] See Figure 6.3.

are generally less than the k_P for total terphenyl.

Table 6.2 also shows that many of the values of k_P for ortho terphenyl calculated from the M.I.T. steady-state irradiations, using Equation (6.4) and Curve IV in Figure 6.3, are negative. In such cases, the total degradation rate (gms/watt-hr) of ortho terphenyl measured in the M.I.T. steady-state runs is less than the radiolysis degradation rate of ortho terphenyl which is predicted from the AECL irradiations (Curve IV) for the conditions of the M.I.T. experiments. This result implies that the radiolysis degradation rate has been overestimated by the use of Curve IV for ortho terphenyl in a mixture of isomers. A possible explanation is that the presence of other terphenyl isomers retards the radiolytic degradation rate of ortho terphenyl in terphenyl mixtures compared to its radiolytic degradation rate in pure ortho terphenyl. However, more steady-state irradiation data for pure ortho terphenyl or ortho-rich terphenyl mixtures are required to confirm this supposition.

6.4 Conclusions

The following conclusions can be made from the review of the results of the irradiations carried out at high dose rates with regard to the reactor coolant degradation calculations in Section 5.4. These conclusions apply to reactor irradiations where the fast neutron fraction is significant.

(1) An activation energy of radiolysis, ΔE_R = 1 k-cal/mole, can be applied to the radiolysis correlation shown in Figure 4.4 for meta-rich terphenyls for organic coolant temperatures up to about 400°C.

(2) Dose rate effects do not appear to be important for meta-rich terphenyls up to about 400°C for the core average dose rates expected in HWOCR (about 1.3 watts/gram). However, any dose rate effects are expected to produce somewhat lower radiolytic degradation rates than predicted in Section 5.4.

(3) The radiopyrolysis correlations for meta-rich terphenyls given in Figures 5.4 and 5.6 appear to be correct within the error limits quoted in Chapter 5.

(4) The radiolytic stability of pure ortho terphenyl is significantly less than that of pure meta terphenyl at temperatures above about 330°C, but the difference between the stabilities of the two isomers in a terphenyl isomer mixture may be much less than the differences indicated for the pure isomers in Figure 6.3.

6.5 Recommendations for Future Work

In Section 5.4, a procedure for calculating the coolant degradation rate in reactors cooled by meta-rich terphenyl coolants was presented, based on the present M.I.T. interpretation of radiolysis and radiopyrolysis. The following effects should be investigated by M.I.T. to check some of the assumptions made in Section 5.4 and modifications in the procedure that may be necessary to calculate properly the degradation expected in ortho-rich coolants. Up to this time, many of these effects have only been investigated in a few capsule experiments, but loop data are needed to establish the results more firmly.

6.5.1 Relative Stability of the Terphenyl Isomers

AECL high dose rate experiments indicate that pure ortho terphenyl is distinctly less stable to mixed reactor radiations above about 330°C than pure meta terphenyl (Section 6.2). M.I.T. low dose rate data tend to indicate that the ortho terphenyl isomer in mixtures does not have the same radiolytic stability characteristics as the pure isomer (Section 6.3). To further study the stability of the terphenyl isomers in isomer mixtures, M.I.T. should irradiate Santowax WR (meta-rich) and Santowax OM (ortho-rich) under identical conditions of dose rate, temperature, and total terphenyl concentration in the coolant. These irradiations should be made at at least two low temperatures (e.g., 572°F, 700°F) to measure radiolysis effects alone, and at at least two high temperatures (e.g., 750°F, 800°F) to measure radiolysis and radiopyrolysis effects. Table 6.3 gives the estimated radiolysis, radiopyrolysis, and total degradation rates for Santowax WR for these experiments.

The purpose of presenting Table 6.3 is to show the relative roles of radiolysis and radiopyrolysis expected in these recommended

Table 6.3

Estimated Santowax WR Degradation Rates for Steady-State Runs in M.I.T. Loop

(In-Pile Section No. 4, Fuel Position 1, 4.9 MW)

Total OMP Concentration %	Irradiation Capsule Temperature °F	°C	Terphenyl Degradation Rate, gms/hr: Radiolysis W_R [a, b, c]	Radiopyrolysis W_P [a, d]	Total W_T [a]	Estimated Percent Radiolysis Degradation
84	572	300	9.8	–	9.8	100
	700	371	10.5	0.3	10.8	97
	750	399	10.8	1.8	12.6	86
	800	427	11.0	7.4	18.4	60
90	700	371	11.8	0.3	12.1	97
	750	399	12.2	1.6	13.8	89
	800	427	12.4	6.9	19.3	64
52[e]	800	427	5.1	7.5	12.6	41
74[f]	750	399	9.1	1.6	10.7	85

[a] Based on M_{loop} = 5500 gms.

[b] Assuming f_N = 0.40, average dose rate, $\bar{r}$ = 70 milliwatts/gm.

[c] Assuming ΔE_R = 1 k-cal/mole.

[d] Assuming the effective loop temperature is about 15°F lower than the irradiation capsule temperature.

[e] Duplicates M.I.T. Run 9 (2 MW) with respect to temperature, terphenyl concentration, and f_N.

[f] Duplicates M.I.T. Run 7 (2 MW) with respect to temperature, terphenyl concentration, and f_N.

experiments, so it will be clear whether the experimental results will show primarily radiolysis or radiopyrolysis effects. The Santowax WR radiolysis degradation rates shown in Table 6.3 were estimated from Equation (5.24), assuming an activation energy of radiolysis, ΔE_R = 1 k-cal/mole. The radiopyrolysis degradation rates were estimated from Equation (5.29), assuming the loop effective temperature will be about 15°F lower than the irradiation capsule temperature.

Sufficient data are not available to estimate the degradation rates of Santowax OM under these conditions, but the radiolysis rate (and perhaps the radiopyrolysis rate) are expected to be higher than the Santowax WR values predicted in Table 6.3. A direct comparison of the G(-omp) and G(-i) values for Santowax WR and Santowax OM will permit the determination of the relative stabilities of the terphenyl isomers in these two terphenyl mixtures.

An important comparison that should be made in the steady-state Santowax WR and Santowax OM runs is the relative distribution of degradation products (DP) into high boilers (HB) and low and intermediate boilers (LIB). AECL capsule irradiations with electrons (6.2) suggest that ortho terphenyl may produce more LIB and less HB than meta terphenyl. Since the HB concentration level will probably be a primary coolant specification for organic cooled reactors, any differences observed between Santowax WR and Santowax OM with regard to distribution of degradation products can affect physical properties and thus be important in coolant selection.

6.5.2 Activation Energy of Radiolysis

As shown in Table 6.3, radiolysis is predicted to be the primary component of coolant degradation for most of these suggested irradiations in Fuel Position 1 at $f_N = 0.40$ and at 4.9 MW reactor power. Therefore, these data can be used to accurately measure the activation energy of radiolysis for Santowax WR and Santowax OM (and for the individual terphenyl isomers in these mixtures) up to at least 750°F. These values of ΔE_R can be compared with the AECL values shown in Table 6.1 for the pure ortho and meta terphenyl isomers. A value of $f_N = 0.40$ was obtained in earlier irradiations (6.4) with a ten-plate fuel element in Fuel Position 1 of the MITR at a power level of 2 MW. However,

radiolysis was not as important in the earlier experiments because the reactor power was lower and the irradiation capsule volume was lower (205 cc in In-Pile Section No. 2 compared to 280 cc in In-Pile Section No. 4 which will be used in the suggested experiments).

In order to calculate the radiolysis rate for these runs (and thus the activation energy ΔE_R), radiopyrolysis corrections must be applied to the total degradation rates. It is recommended that post-irradiation pyrolysis experiments be made in the autoclave with coolant samples from these runs to obtain estimates of k_P. While the post-irradiation pyrolysis rates may be slightly different from the actual radiopyrolysis rates occurring in the loop, this method is probably sufficiently accurate to make the corrections for radiopyrolysis, which are relatively small in most cases.

6.5.3 Radiopyrolysis Rates

In order to lower the uncertainty limits on the radiopyrolysis rate constants (see Figure 5.6), additional values of thermal decomposition rates for high temperature runs are needed. It is particularly important to obtain better estimates of k_P at terphenyl concentrations from about 84% to 90% in the temperature region below 750°F (371°C) where organic coolants for reactors are presently expected to operate. Three additional Santowax WR runs at $C_{omp} = 0.90$ and at 700°F, 750°F, and 800°F are recommended (see Table 6.3).

Radiopyrolysis rates can be calculated from (1) loop irradiation experiments with appropriate radiolysis corrections, and/or (2) post-irradiation pyrolysis experiments. Table 6.3 shows that it will be difficult to calculate accurate values of k_P from M.I.T. loop experiments at an average dose rate of 70 milliwatts/gram (4.9 MW reactor power) because thermal decomposition is expected to be small relative to radiolysis. The relative role of radiopyrolysis could be increased by (1) lowering the reactor power to 1-2 MW long enough to make the necessary runs, or (2) increasing the out-of-pile coolant volume (thus lowering the average dose rate) by adding a heated supplementary surge tank. It will probably not be possible to lower the reactor power for the extended period of time (3-6 months) required to carry out several steady-state runs between 700°F and 750°F for which k_P can be

calculated. Increasing the out-of-pile coolant volume is not attractive because the lower average dose rate which results will require an appreciably longer irradiation time under steady-state conditions to obtain statistically significant G values. For example, Table 6.3 shows that the thermal decomposition rate at 750°F would have to be increased by a factor of six at $C_{omp} = 84\%$ in order to just equal the radiolysis rate. A supplementary surge tank volume five times the coolant volume in the loop would be necessary to accomplish this requirement if its temperature was maintained at the effective loop temperature. Even with this increased rate of radiopyrolysis, the radiolysis correction and the temperature profile around the loop would make it difficult to accurately calculate k_P. The conclusion is that low dose rate loop irradiations alone will not be suitable experiments to accurately calculate radiopyrolysis rate constants below 750°F.

The agreement between post-irradiation pyrolysis rates and the k_P calculated from irradiation experiments shown in Figure 5.6 suggest that autoclave tests can be used to obtain good estimates of k_P. Below 750°F, autoclave post-irradiation tests should provide better estimates of k_P than loop irradiations. However, many more autoclave results are needed to establish that these values are reproducible and that they agree reasonably well with the k_P calculated from low power (2 MW) loop irradiations in Figure 5.5.

The effect of the coolant processing method on the radiopyrolysis rate should be studied. The M.I.T. results discussed in Section 5.3.1 suggest that a High Boiler distillation may produce lower thermal decomposition rates for terphenyl than a Bottoms distillation. This effect can be investigated by (1) making post-irradiation pyrolysis tests on coolant samples for runs in which HB distillations were used and comparing the results with runs in which Bottoms distillations were used, and (2) comparing the post-irradiation pyrolysis rates of distillate samples following both HB and Bottoms distillations. Such tests could be made at high temperatures (800°F) where pyrolysis rates are large enough to be measured accurately.

6.5.4 Dose Rate Effects

The AECL results of capsule irradiations shown in Figures 6.1 and 6.2 indicate that the G values decrease with increasing dose rate above 0.3 watts/gram for irradiation temperatures above approximately 350°C. The increase in the MITR power level from 2 to 5 MW offers an opportunity to investigate this dose rate effect in Santowax WR. It is recommended that an irradiation run be made at 5 MW which duplicates Run 7 at 2 MW (750°F, $C_{omp} = 0.74$) and also a run at 5 MW which duplicates Run 9 at 2 MW (800°F, $C_{omp} = 0.52$) as shown in Table 6.3.

The maximum dose rate at the axial center of the irradiation capsule at 5 MW is expected to be about 1.9 watts/gram, compared to 0.75 watts/gram at 2 MW. This increase by a factor of 2.5 in the maximum dose rate may not be sufficient to observe a dose rate effect, unless this effect is larger than expected from the AECL data. However, even though a dose rate effect may not be seen, this comparison of results at 2 MW and 5 MW will be useful because the experiments will bracket the expected dose rates in the HWOCR core region (see Table 5.1).

6.5.5 Fast Neutron Effect

Although the relationship shown in Figure 4.4 correlates the low temperature irradiation results of many laboratories by indicating a fast neutron effect ratio, $G_N/G_\gamma \approx 4$, more data are needed at a fast neutron fraction above 0.6. Only the limited Cal Research capsule data at $f_N = 0.95$ are available in this region. Since the HWOCR is expected to have a fast neutron fraction of about $f_N = 0.66$, results in this region are important.

M.I.T. should consider the feasibility of redesigning a fuel element to increase the neutron dose rate relative to the gamma-ray dose rate, but only if the fast neutron fraction can be increased significantly above the present obtainable value ($f_N = 0.40$). Since an alteration of the fuel element design will require a change in the MITR operating license (which is now under study), this proposal would probably require at least 1-1/2 to 2 years to become operational.

If a substantial increase in the fast neutron fraction can be achieved with a new fuel element design, M.I.T. should investigate the effect of increasing temperature on the ratio, G_N/G_γ, by comparing

the high temperature degradation rates at $f_N = 0.40$ with the high temperature degradation rates measured in the irradiation facility with higher f_N. It does not appear possible at this time for M.I.T. to measure the effect of temperature on G_N/G_γ by using a lower fast neutron fraction (such as the value $f_N = 0.07$ measured in Fuel Position 20) because the dose rates in such a facility would be too low to measure radiolysis effects at high temperature without a substantial radiopyrolysis contribution.

6.5.6 Prediction of Fast Neutron and Gamma-Ray Dose Rates

Finally, the largest uncertainty in the prediction of coolant degradation rates in organic-cooled reactors is likely to be the prediction of the dose rates in the coolant in large reactors from fast neutrons and gamma rays. A review should be made of existing methods which can be used to predict fast neutron and gamma-ray dose rates in reactors, and the methods should be applied to existing heavy-water reactors (such as the MITR) where extensive calorimetry measurements have been made in order to check the accuracy of the predicted dose rates.

APPENDIX A1

CALORIMETRY AND FOIL DOSIMETRY

A1.1 Introduction

The Organic Loop Project at M. I. T. combines adiabatic calorimetry and foil activation analysis to determine the total dose rate in the irradiation facility, and the fast neutron and gamma-ray fractions of the dose rate. The calorimetry and foil dosimetry theory and procedures have been presented in earlier M. I. T. reports (A1.1, A1.2, A1.3), and a dosimetry report describing these measurements in detail is being prepared (A1.4). A brief description of the dosimetry methods will be given here, along with results of dosimetry measurements in Fuel Position 20. Modifications of (1) dosimetry equipment, and (2) methods of interpretation of experimental results which are unique to the dosimetry measurements in Fuel Position 20 are also given.

The adiabatic calorimetry measurements employ several different calorimeter materials (polyethylene, polystyrene, terphenyl [Santowax OMP], carbon, aluminum, and beryllium), selected to have a large variation in the fast neutron dose rate with a relatively constant gamma-ray dose rate. A statistical least-square error analysis of the measured total dose rate in nine to thirteen axial positions is usually made in order to calculate the total dose rate to the terphenyl coolant, the fast neutron fraction of the total dose rate, and the statistical error limits on these two parameters. However, due to the low fast neutron fraction in Fuel Position 20 (approximately 7% of the total dose rate), it was necessary to compare foil activation measurements in this irradiation facility with calorimetry and foil measurements in Fuel Position 1 (40% fast neutron fraction) to determine the fast neutron dose rate in Fuel Position 20 accurately (see Appendix A1.3). Calorimetry measurements were made inside a special stainless steel thimble (constructed to mock up the perturbation of the neutron spectrum by the in-pile section) installed in Fuel Position 20 before In-Pile Section No. 3 was installed (March - April, 1965) and after it had been removed (June, 1966).

Foil activation measurements were made approximately once a month between March, 1965 and June, 1966, using cobalt, nickel, aluminum, and magnesium foils. Copper and sulfur activations were discontinued, since these measurements did not significantly add to the information received from the other foil activations. The foil measurements were made in the special stainless steel thimble (before the in-pile section was installed and after it was removed from Fuel Position 20) and in the aluminum (side) monitor tube and the stainless steel (center) monitor tube during irradiations in In-Pile Section No. 3. The stainless steel monitor tube was only used three times for foil measurements, since a heater and thermocouple were permanently installed in this tube on November 25, 1965, precluding further foil measurements. In addition to the periodic foil activations with the four foil materials described above, measurements were made using only nickel foils during successive weeks when the reactor power was raised to 2.98 and 4.00 thermal megawatts (Foil Runs 32 and 33), and also to check the reproducibility of nickel foil measurements during a later one-week period (Foil Runs 36A, 36B, and 37).

A1.2 Calorimetry

A1.2.1 Equipment and Procedure

The calorimetry equipment and procedures used in Fuel Position 1 have been described in other M. I. T. reports (A1.1, A1.2, A1.4). Some modifications in this equipment and these procedures were necessary in order to perform calorimetry measurements in Fuel Position 20, due to the smaller access hole in the rotary lid of the MITR above this outer fuel position. Since calorimeters must be lowered into the stainless steel thimble (installed in the fuel position for calorimetry measurements) through the access holes in the rotary lid, a new calorimeter cooling plug and gun barrel shield were constructed.

A simplified diagram of the calorimetry cooling and shielding equipment used in Fuel Position 20 is shown in Figure A1.1. The calorimeter cooling plug fit directly into the MITR rotary lid and provided cooling coils for lowering the calorimeter temperature but did not provide high density concrete or paraffin radiation shielding. The gun barrel was installed on the top of the rotary lid, directly above

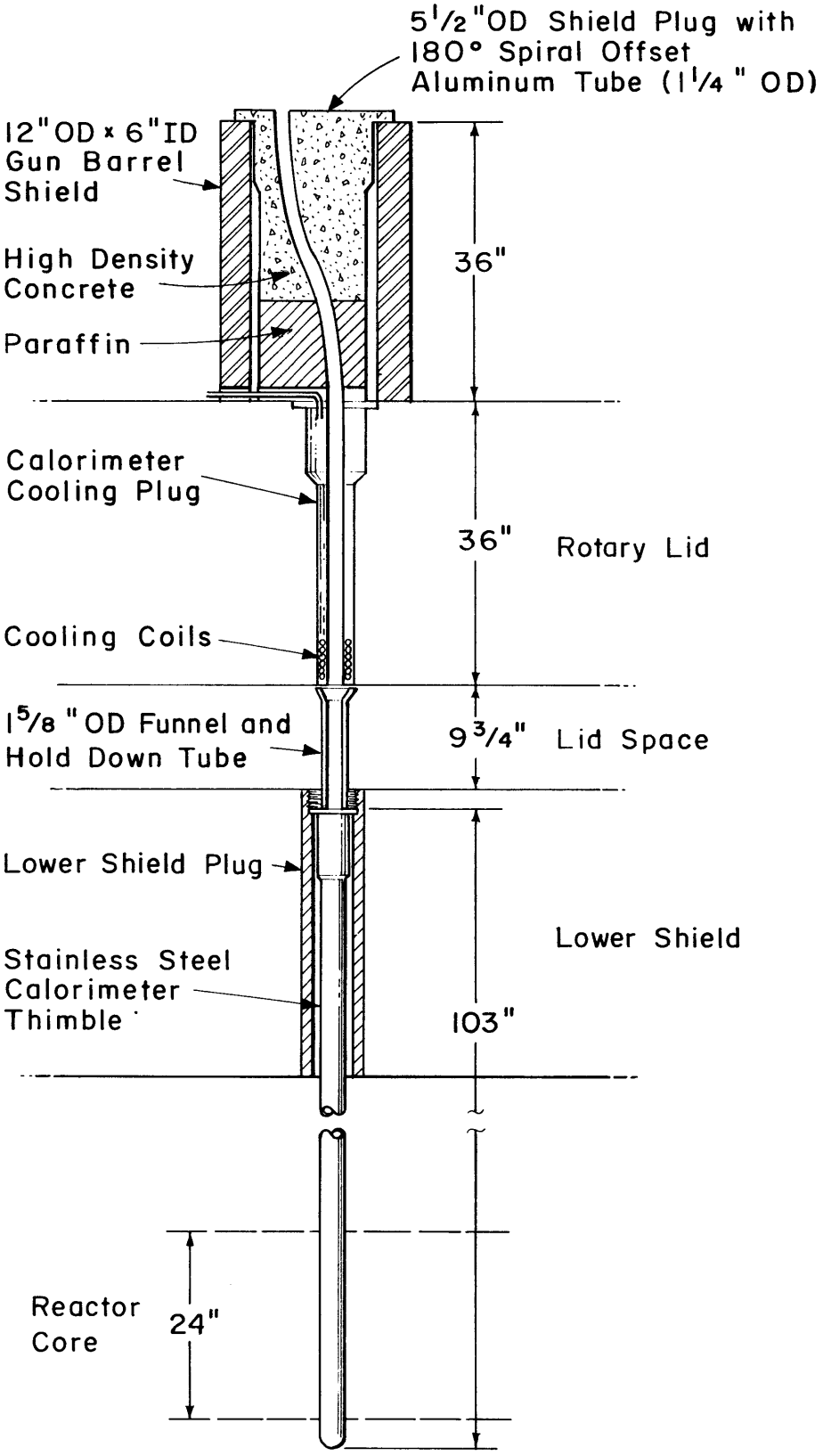

FIGURE A1.1 ARRANGEMENT OF CALORIMETRY EQUIPMENT FOR MEASUREMENTS IN FUEL POSITION 20

the cooling plug in Fuel Position 20; and an aluminum shield plug with a 180° spiral offset access tube (for calorimeter insertion), filled with high density concrete and paraffin, was placed inside the gun barrel. This arrangement prevented radiation streaming from Fuel Position 20. For calorimetry measurements in Fuel Position 1, the calorimeter cooling plug in the rotary lid provided both cooling and radiation shielding (A1.4).

Figure A1.2 is a detailed drawing of the cooling plug used in the 3-inch-OD access hole in the rotary lid above Fuel Position 20. The gun barrel serves as a support for the shield plug and also provides additional gamma-ray shielding. It rests directly on the rotary lid. The shield plug with the 180° spiral offset installed in the gun barrel was the same plug which was used for both cooling and shielding for calorimetry measurements in Fuel Position 1, at which time it was installed in the 6-inch-OD, central access hole in the rotary lid. Detailed drawings of this shield plug are presented in other M. I. T. reports (A1.4, A1.5). The 1-5/8-inch-OD aluminum tube installed in the space beneath the rotary lid in Figure A1.1 serves as a funnel guide for the calorimeters and also as a hold-down ring for the stainless steel thimble.

Figure A1.3 shows an assembly drawing of the Model C calorimeters used for measurements in Fuel Position 20. The cylindrical absorbers, 1-1/2 inches long and 1/2 inch in diameter, were suspended in the aluminum can by means of 1/16-inch-diameter, phenol formaldehyde rods. The rods were glued with plastic glue to the center of phenol formaldehyde discs, 1/32 inch thick and 7/8 inch in diameter, to center the sample in the aluminum can. Two thermocouples were imbedded in each sample, one at the center and one in an upper corner. For the aluminum, polyethylene, and polystyrene samples, 1/8-inch holes were drilled in the sample, 1/8-inch plugs of the sample material were prepared, and the thermocouples were pressed into place in the holes by the plugs of sample material. For the carbon and beryllium samples, 0.05-inch holes were drilled in the sample and the thermocouples were pressed into place, using plugs of aluminum welding rod (type 1100 aluminum with 2% silicon added). For the terphenyl calorimeters, molten Santowax OMP was poured into a 1/2-inch-diameter, cylindrical

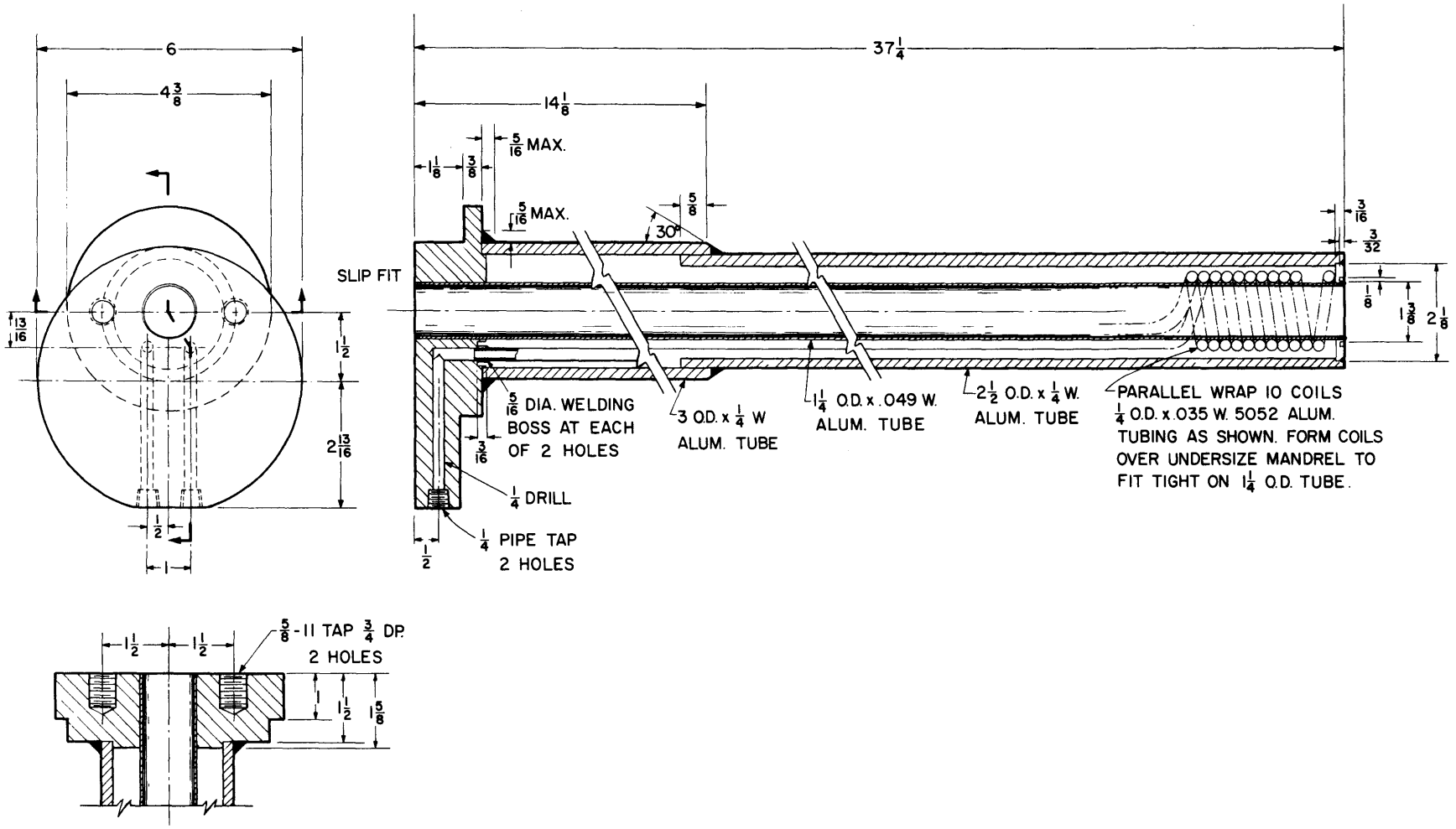

FIGURE AI.2 CALORIMETER COOLING PLUG

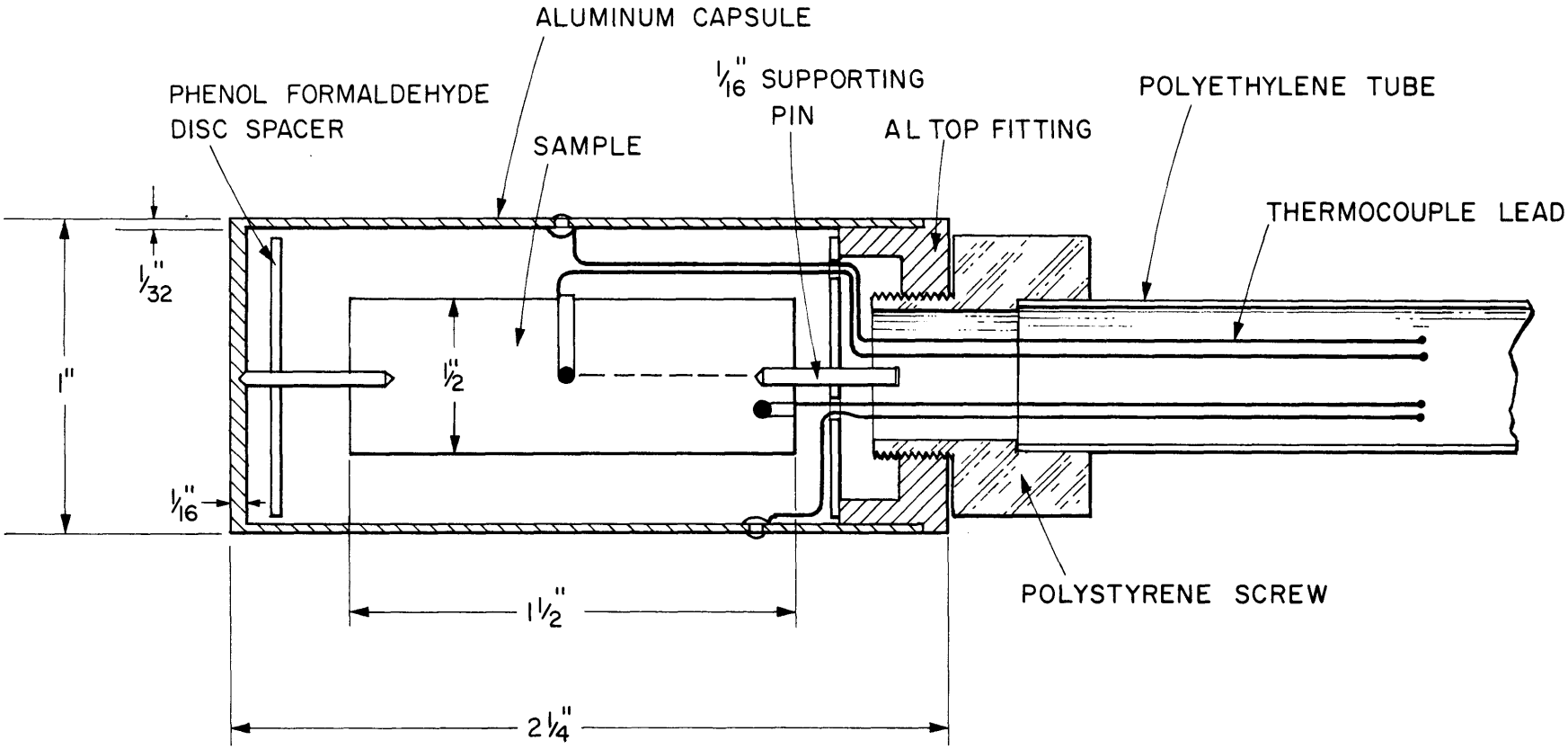

FIGURE A1.3 ASSEMBLY DRAWING OF A MODEL C CALORIMETER

mold with the two thermocouples in place as shown in Figure A1.3.

Three different Model C calorimeters (Models C-2, C-3, C-4) were used in these calorimetry measurements, using different size thermocouple wires. Model E calorimeters were used along with Model C calorimeters for Calorimetry Series XIX and XX, after In-Pile Section No. 3 had been removed from the reactor. Model E was the same basic design as Model C (shown in Figure A1.3), but some slight modifications were made in preparing the thermocouple junctions and installing the thermocouples in the sample. A summary of the calorimeter models used for measurements in Fuel Position 20 is shown in Table A1.1.

A detailed description of the M. I. T. procedure for calorimetry measurements is presented in an M. I. T. dosimetry report (A1.4).

Briefly, this procedure is as follows:

(1) The calorimeter is lowered into the cooling position in the cooling plug (see Figure A1.1) until the aluminum jacket reaches 40° to 50°F and the sample temperature is about 15° to 20°F higher.

(2) The calorimeter is quickly lowered into the desired axial position in the stainless steel thimble, and the rise in the aluminum wall and sample temperatures are recorded on a two-pen temperature recorder (Minneapolis-Honeywell Electrometer 15-Strip Chart, Two Pens Duplex Recorder). Alternatively, the temperature rise of the sample, as measured by the two thermocouples in the sample, may be recorded.

(3) The calorimeter is kept in this position until the wall temperature equals the sample temperature (adiabatic point), and after the temperature crossover is passed, the calorimeter is pulled back up to the cooling position. The wall temperature increases more rapidly than the sample temperature for calorimetry measurements in Fuel Position 20 because the calorimeter wall is in thermal contact with the stainless steel thimble, which has a temperature equal to the temperature of the surrounding heavy water (about 120°F at 5 MW). The procedure is then repeated at other axial positions.

The temperature rise of the sample at the adiabatic point is measured from the strip chart, and the total dose rate in the sample is calculated from Equation (A1.1).

$$R_T^j = KC_p(T)\left(\frac{dT}{dt}\right)_{q=0} \quad \frac{\text{watts}}{\text{gm}} \qquad \text{(A1.1)}$$

Table A1.1

Specifications of Calorimeters Used in Fuel Position 20

Sample Material	Material Source	Date Built (mo/yr)	Model Number	Gauge Thermocouple Wire		Used in Calorimetry Series
				Wall	Sample	
SW	Monsanto	2/65	C-3	24	24	XII, XVI
SW	Monsanto	3/65	C-4	30	30, 36	XIII XIV, XV, XVI, XVIII
SW	Monsanto	6/66	E-1[a]	36	30, 36	XVIII, XIX
PE	B.A.S.F.[h]	12/64	C-3	24	24	XII, XVI
PE	B.A.S.F.[h]	2/65	C-4	36	36	XII, XIII, XIV, XV
PE	Forest Products	6/66	E-1[a]	36	36	XVIII, XIX
PS	Forest Products	9/64	C-2	30	30	XIII, XIV, XVIII, XIX
PS	B.A.S.F.[h]	2/65	C-3	24	24	XII
PS	B.A.S.F.[h]	3/65	C-4	30	30, 36	XIII, XIV, XV, XVI
PS	Forest Products	6/66	E-1[a]	30	36	XVIII, XIX
PS	"	6/66	E-2[a]	30[c]	30, 36	XX
PS	"	6/66	E-3[a]	30[d]	30, 36	XX
C	High Temp. Materials	9/64	C-2[g]	30	30	XII through XIX
C	"	6/66	E-1[b]	30	30, 36	XX
Al	Amer. St. and Al.	9/64	C-2[g]	30	30	XII,XIII,XIV,XVI,XVIII,XIX
Al	"	6/66	E-1[e, g]	30	30, 36	XX
Al	"	6/66	E-2[f, g]	30	30, 36	XX
Be	Nuclear Metals	9/64	C-2	30	30	XII
Be	"	3/65	C-4	30, 36	36	XIII, XIV, XVIII, XIX

(a) Insulation stripped back ~2 inches from junction; bare wires melted into sample.
(b) Carbon press pin used.
(c) Nylon-insulated thermocouple wire to wall.
(d) Glass and asbestos thermocouple wire to wall.
(e) Bare thermocouple wire 1-1/2" from junction.
(f) Nylon insulation to thermocouple bead.
(g) Aluminum press pin used.
(h) Badische Anilin Soda-Fabrik AG, Ludwigshafen an Rhein, Germany.

where

R_T^j is the total dose rate in sample j, watts/gm

K is a conversion factor = 0.0387 (watt)(min)(lb)/(Btu)(gm)

$C_p(T)$ is the specific heat capacity of the sample j at the adiabatic temperature T, (Btu/(lb)(°F)

$\left(\frac{dT}{dt}\right)_{q=0}$ is the adiabatic rate of temperature rise of the sample j, (°F/min)

A1.2.2 Theory

The total dose rate in the calorimeter samples, as calculated by Equation (A1.1), results from the absorption of fast neutron and gamma-ray energy in the sample absorber.

$$R_T^j = R_\gamma^j + R_N^j \quad \frac{\text{watts}}{\text{gm}} \tag{A1.2}$$

The gamma-ray dose rate in each sample can be related to the gamma-ray dose rate in carbon, by Equation (A1.3), assuming Compton interactions are the only significant means of gamma-ray energy deposition in the sample.

$$R_\gamma^j = \frac{(Z/A)_j}{(Z/A)_c} R_\gamma^C \quad \frac{\text{watts}}{\text{gm}} \tag{A1.3}$$

where

Z is the atomic number of sample j

A is the atomic weight of sample j

The fast neutron dose rate in each sample is calculated from Equations (A1.4) and (A1.5), assuming that the energy deposition from fast neutrons in sample j is due to elastic scattering (isotropic) by the absorber nuclei, i, in the sample.

$$R_N^{SW} = \sum_i N_i I_i = \sum_i N_i \left(\frac{I_i}{I_H}\right) I_H \quad \frac{\text{watts}}{\text{gm}} \tag{A1.4}$$

$$I_i = g_i S \int_0^\infty \sigma_s^i(E)\, \phi(E)\, E\, dE \quad \frac{\text{watts}}{\text{atom}} \tag{A1.5}$$

where

N_i is the number of i^{th} atoms/gm in the j^{th} absorber

I_i is the neutron scattering integral for the i^{th} nuclide in the j^{th} absorber (watts/atom) (e.g., I_H = scattering integral for hydrogen).

g_i is the average fraction of energy transferred to the i^{th} nuclide in the absorber, equal to $2A_i/(A_i+1)^2$

S is a conversion factor 1.6×10^{-43} (cm^2)(watt)(sec)/(barn)(ev),

$\sigma_s^i(E)$ is the elastic scattering cross section of the i^{th} nuclide in sample j as a function of the neutron energy E, (barns)

Equations (A1.2), (A1.3) and (A1.4) can be combined to give

$$R_T^j = a_j R_\gamma^C + b_j I_H \quad \frac{\text{watts}}{\text{gm}} \tag{A1.6}$$

For the aluminum absorber, a correction is made for the thermal neutron dose rate, and Equation (A1.6) is modified to give

$$R_T^{Al} - R_{th}^{Al} = a_{Al} R_\gamma^C + b_{Al} I_H \quad \frac{\text{watts}}{\text{gm}} \tag{A1.7}$$

Sawyer and Mason (A1.2) give a method of calculating the thermal neutron dose rate in aluminum as a function of the thermal neutron flux and irradiation time. The values of a_j and b_j used for calorimetry measurements in Fuel Position 20 are shown in Table A1.2 (A1.6).

Table A1.2

Constants a_j and b_j Used for Calorimetry Measurements in Fuel Position 20

Absorber	a_j	b_j, 10^{-22} atoms/gm
Polyethylene	1.142	9.33
Polystyrene	1.076	5.43
Carbon	1.00	0.872
Beryllium	0.888	1.62
Santowax OMP	1.060	4.48
Aluminum	0.965	0.248

The "best" values of R_γ^C and I_H at each axial position in the irradiation facility are determined by a least-square error analysis of the experimental values of the total dose rate in each absorber, R_T^j, with the procedure described by Sawyer and Mason (A1.2).

The total energy deposited in the organic coolant in the in-pile section is found by

$$F_T^{SW} = \int_{L_L}^{L_T} \frac{R_T^{SW}}{P_o} X \, dL \quad \frac{\text{watt-cc}}{\text{MW-gm}} \tag{A1.8}$$

where

F_T is the total in-pile dose rate factor, watt-cc/MW-gm

L_L is the bottom of the in-pile capsule relative to the reactor core center, inches

L_T is the top of the in-pile capsule relative to the reactor core center, inches

P_o is the power level of the reactor at the time of the calorimetry measurements, megawatts

X is the volume per unit length of the irradiation capsule, cc/in

The dose rate to the terphenyl coolant, R_T^{SW}, is calculated by

$$R_T^{SW} = R_\gamma^{SW} + R_N^{SW} = 1.06 \, R_\gamma^C + 4.48 \times 10^{22} \, I_H \quad \frac{\text{watts}}{\text{gm}} \tag{A1.9}$$

where R_γ^C and I_H are the best values from the least-square analysis at each axial position measured. In-pile dose rate factors can also be calculated for fast neutrons, F_N^{SW}, and for gamma rays, F_γ^{SW}, using the values of R_N^{SW} and R_γ^{SW}, respectively, in Equation (A1.7).

The standard deviation of the dose rate factors is determined from the standard deviations of the calculated dose rate, in the following manner (A1.6).

$$\frac{\sigma(F)}{F} = \frac{\sqrt{\sum_i \sigma^2(R_i)}}{\sum_i R_i} \tag{A1.10}$$

Sections A1.2.3 and A1.2.4 present the results of calorimetry measurements made in Fuel Position 20.

A1.2.3 Pre-Irradiation Calorimetry Measurements in Fuel Position 20

Shown in Table A1.3 are the results of calorimetry measurements made in March and April, 1965, in the stainless steel thimble installed in the cadmium-lined sample assembly in Fuel Position 20. These measurements were made before In-Pile Section No. 3 was installed, when the reactor power was 1.95 MW. The calorimeter models (see specifications in Table A1.1) used in these measurements are indicated in Table A1.3. Measurements were made at thirteen axial positions in each calorimetry series (instead of the nine axial positions used in the measurements in Fuel Position 1), in order to more accurately define the dose rates near each end of the cadmium sheath (±12 inches from core center).

The results of Series XII in Table A1.3 are considered to be less accurate than results of the other series because thicker thermocouple wires (24-gauge, 0.02-inch diameter) were used in the Santowax and polystyrene calorimeters (C-3 models) with different results than were obtained with finer thermocouple wires. To obtain the best estimate of the dose rate factors, selected values of the total dose rate in each absorber at each axial position were chosen from Series XII, XIII and XIV (see reference (A1.6)). As shown in Table A1.3, these selected values gave

$$F_T^{SW} = 20.93 \pm 0.33 \quad \frac{\text{watt-cc}}{\text{MW-gm}}$$

and

$$F_\gamma^{SW} = 18.91 \pm 0.18 \quad \frac{\text{watt-cc}}{\text{MW-gm}}$$

Since the fast neutron dose rate was only about 7% of the total dose rate in Fuel Position 20, a more accurate value of F_N^{SW} was determined by foil dosimetry measurements (Section A1.3).

Figure A1.4 shows the graphical representation of the least-square analysis to obtain the best values of R_γ^C and I_H at the axial center of the core, using the selected values of the total dose rate in each absorber.

Table A1.3

Results of Calorimetry Measurements in Fuel Position 20

Before Installation of In-Pile Section No. 3

Calorimetry Series	Date (mo/day/yr)	Calorimeter (Model)	In-Pile Dose Rate Factors, watt-cc/MW-gm	
			Total, F_T^{SW}	Gamma, F_γ^{SW}
XII	3/3/65	SW, PE, PS (C-3)	18.62	17.55
		C, AL, Be (C-2)	±0.40	±0.26
XIII	3/16/65	SW, PE, PS, Be (C-4)	20.50	19.04
		C, AL (C-2)	±0.32	±0.17
XIV	4/6/65	SW, PE, PS, Be (C-4)	20.58	19.36
		C, AL (C-2)	±0.41	±0.28
Selected best values, Series XII, XIII, XIV	—	SW, PE, Be (C-4)	20.93	18.91
		C, AL, PS (C-2)	±0.33	±0.18

Error limits are 1σ.

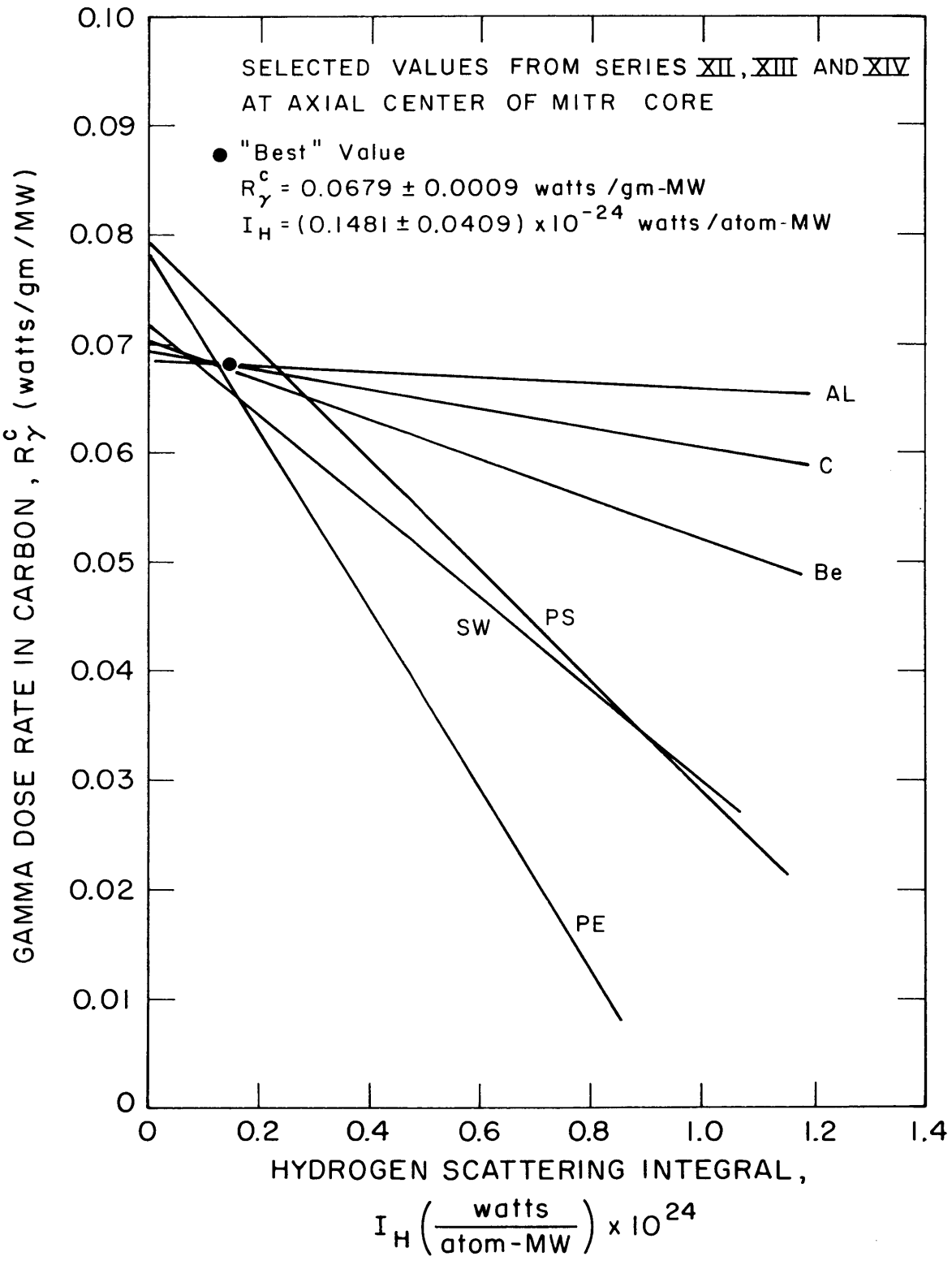

FIGURE A1.4 GRAPHICAL REPRESENTATION OF MEASURED DOSE RATES IN FUEL POSITION 20 - SELECTED VALUES, SERIES XII, XIII, AND XIV

As shown in this figure, the 1σ error limit on the value of I_H, as determined by calorimetric measurement, is ±28%, but the 1σ error limit on R_γ^C is only 1.3%.

Figure A1.5 shows the axial variation of the calculated dose rate to terphenyl, using the selected values of the dose rates in each absorber. The "bumps" seen in the fast neutron dose rates near the edge of the cadmium sheath are probably due to thermal neutron reactions with the glass insulation on the thermocouples, since this behavior was not seen in later calorimetry measurements (Section A1.2.4) where the insulation was removed from the thermocouples. This thermal neutron effect is not significant near the middle of the cadmium sheath because the thermal flux at this position is about a factor of 50 lower than at the edges of the cadmium (Section A1.3).

A1.2.4 Post Irradiation Calorimetry Measurements in Fuel Position 20

Shown in Table A1.4 are the results of calorimetry measurements made in Fuel Position 20 in June, 1966, after In-Pile Section No. 3 had been removed from the cadmium-lined sample assembly. Series XX was a partial calorimetry series using new aluminum, carbon, and polystyrene calorimeters, and the results for this series, shown in Table A1.4, are calculated using the Santowax, beryllium, and polyethylene measurements from Series XIX. The average value of the total in-pile dose rate factor for Series XVIII, XIX, and XX is

$$F_T^{SW} = 19.70 \pm 0.26$$

and the gamma dose rate factor is

$$F_\gamma^{SW} = 19.24 \pm 0.15$$

This average value for F_T^{SW} measured at 4.90 MW agrees within 6% with the best value (20.93 ± 0.33) from the pre-irradiation calorimetry measurements at 1.95 MW. The average gamma dose rate factor, F_γ^{SW}, from these post-irradiation calorimetry measurements agrees within 1.7% with the best value (18.91 ± 0.18) from the pre-irradiation measurements.

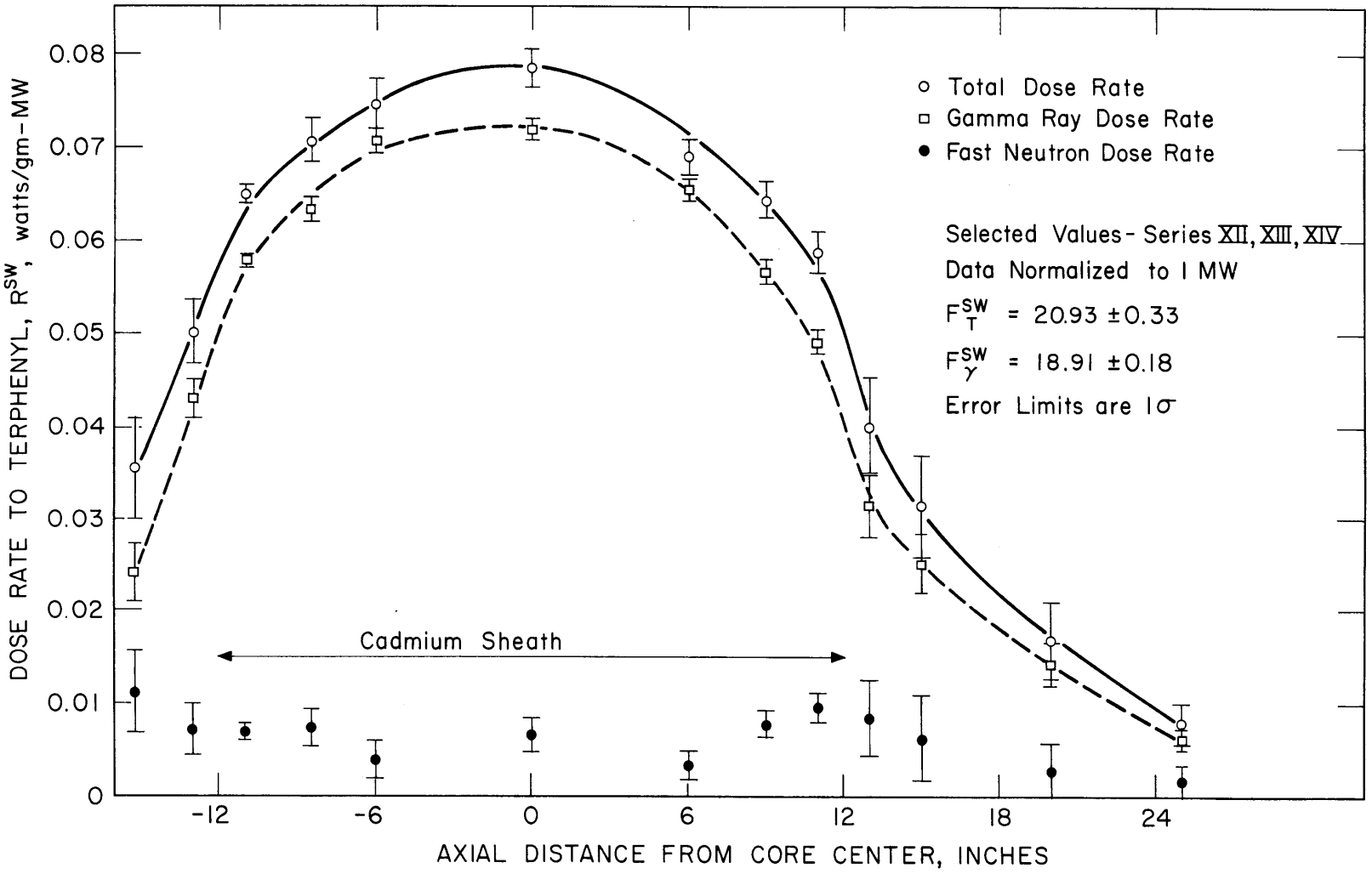

FIGURE A1.5 AXIAL VARIATION OF THE DOSE RATE TO TERPHENYL IN FUEL POSITION 20
SELECTED VALUES FROM CALORIMETRY SERIES XII, XIII AND XIV

Table A1.4

Results of Calorimetry Measurements in Fuel Position 20

After Removal of In-Pile Section No. 3

Calorimetry Series	Date (mo/day/yr)	Calorimeter (Model)	In-Pile Dose Rate Factors, watt-cc/MW-gm[a]	
			Total, F_T	Gamma, F_γ
XVIII	6/16/66	PS, AL, C(C-2)	19.62[b]	19.19
		PE, SW, Be (C-4)	±0.39	±0.21
XIX	6/22/66	PS, AL, C(C-2)	20.20[c]	19.56
		Be (C-4)	±0.33	±0.18
		PE, SW (E-1)		
XX	6/29/66	AL, C (E-1)	19.28	18.98
		PS, AL (E-2)	±0.16	±0.19
		PS (E-3)		

[a] Error limits are 1σ.

[b] F_T^{SW} = 18.01 from Santowax calorimeter only.

[c] F_T^{SW} = 19.33 from Santowax calorimeter only.

Figure A1.6 shows the graphical representation of the least-square analysis of R_γ^C and I_H for Series XIX, and compares the results in individual calorimeters for Series XIX and XX. This comparison shows that the aluminum and carbon results, with different calorimeters having 5-mil and 10-mil thermocouple wires, are in excellent agreement; but the Santowax and polystyrene calorimeters having 10-mil thermocouple wires give measured dose rates 5% to 10% higher than calorimeters with 5-mil thermocouple wires. The effect of thermocouple wire size on calorimetry measurements is being further investigated at M. I. T. For calorimeter Series XIX, Figure A1.6 shows the 1σ error limit on R_γ^C is 2.1% and the 1σ error limit on I_H is about 120%.

Figure A1.7 shows the axial variation of the calculated dose rate to terphenyl for Series XIX. The increases in the neutron dose rate near the edge of the cadmium sheath are not evident for these measurements made without insulation on the thermocouple wires.

These calorimetry results are combined with the foil dosimetry results to give the best estimates of F_T^{SW} and the fast neutron fraction in Section A1.4.

A1.3 Foil Dosimetry Measurements

A1.3.1 Introduction

The procedures used in making foil activation measurements and the cross-section data and calculation techniques used to interpret the experimental results have been presented in detail in other M. I. T. reports (A1.2, A1.3, and A1.4). The foil dosimetry calculations of the fast neutron dose rates for irradiations in Fuel Position 1 were approximately 20% lower than the calorimetry values (A1.3), probably due to uncertainties in the cross-section data, the neutron energy spectrum, and the counter efficiencies. Because of these uncertainties, the foil measurements were primarily used in Fuel Position 1 to (1) measure changes in the fast neutron dose rate with fuel element burnup and refueling operations, and (2) determine the ratios of the neutron scattering integrals relative to the scattering integral for hydrogen (I_i/I_H) for use with the calorimetry absorbers (see Equation (A1.4)). The calorimetry measurements were used to calculate the best values of the fast neutron dose rate to Santowax. However, due to the low fast neutron

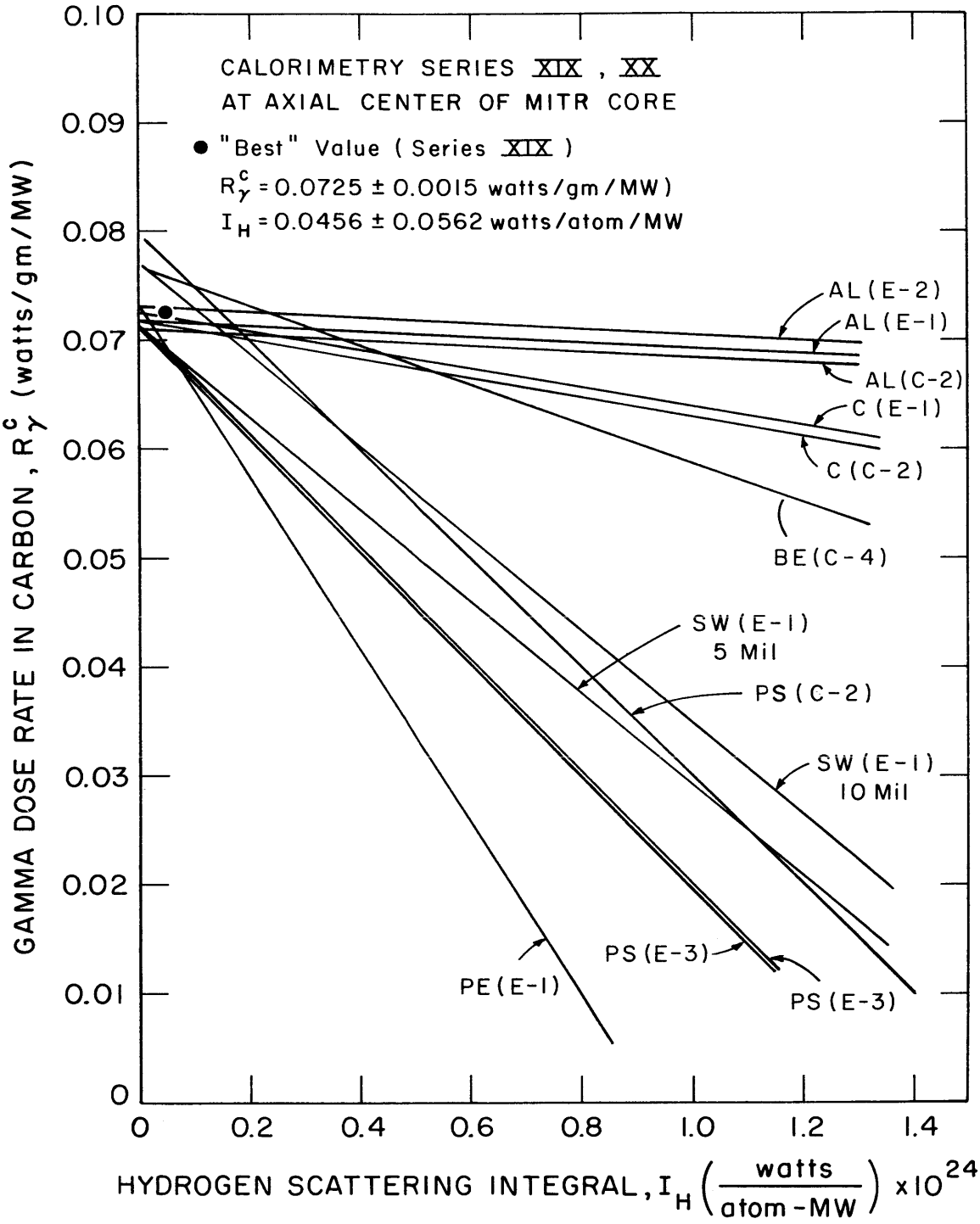

FIGURE A1.6 GRAPHICAL REPRESENTATION OF MEASURED DOSE RATE IN FUEL POSITION 20. SERIES XIX , XX

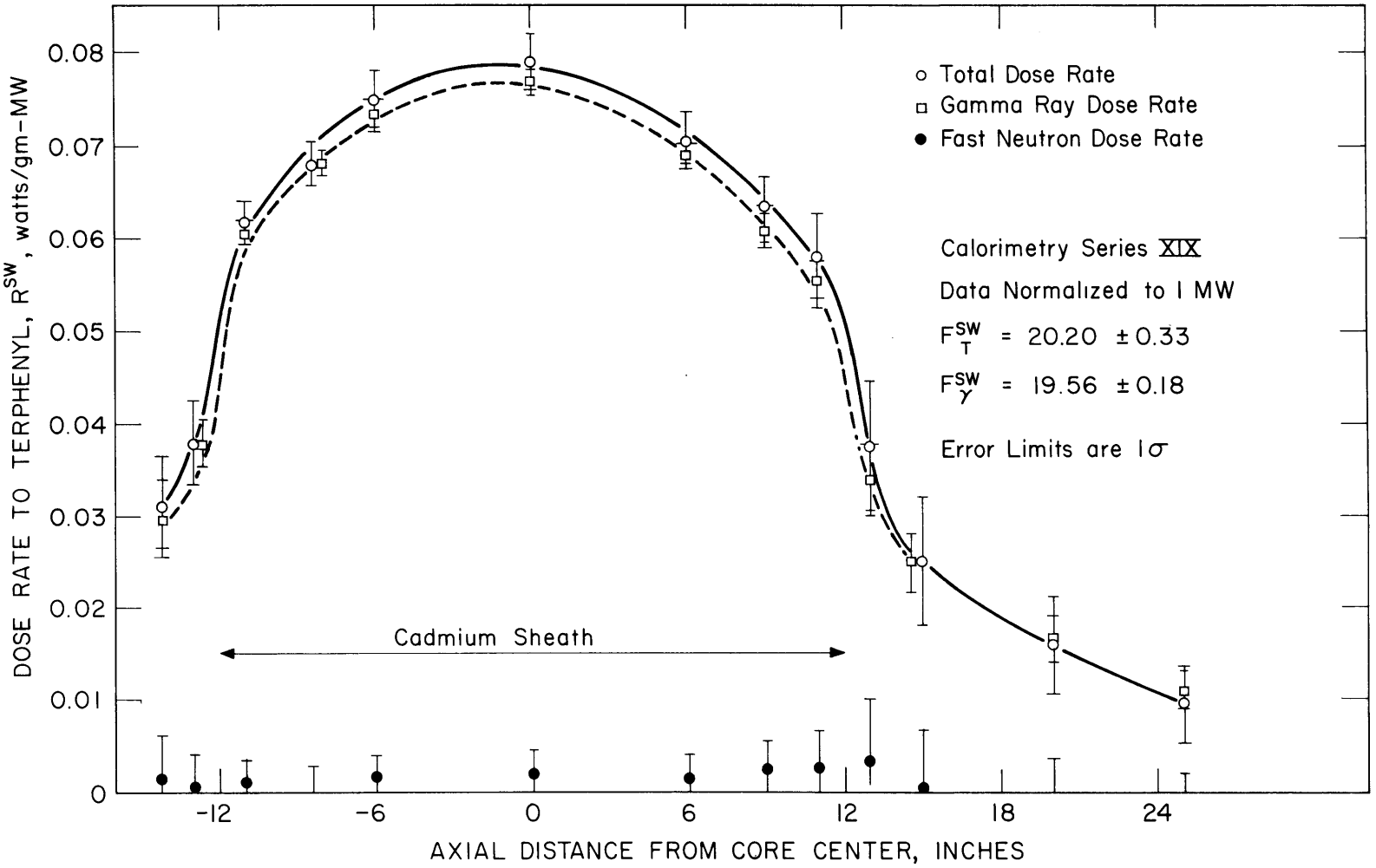

FIGURE A1.7 AXIAL VARIATION OF THE DOSE RATE TO TERPHENYL IN FUEL POSITION 20 CALORIMETRY SERIES XIX

fraction in Fuel Position 20, the calorimetry measurements could no longer be used to give an accurate value of the fast neutron dose rate; and thus the foil measurements have been used to evaluate the fast neutron dose rate factor, F_N^{SW}, for these recent irradiations.

Two procedures have been used to calculate F_N^{SW} from foil measurements:

Method 1. The dose rate to Santowax has been determined from foil activations at six to ten axial positions, using the calculated values of the neutron scattering integral to carbon and hydrogen from Equations (A1.4) and (A1.5). The neutron energy spectrum, $\phi(E)$, in Equation (A1.5) is calculated directly from the foil measurements with the procedure described by Sawyer and Mason (A1.2). The neutron dose rate factor is then calculated from R_N^{SW}, using the axial integration shown in Equation (A1.8).

Method 2. The ratio of the neutron dose rate factors calculated from foil measurements in Fuel Position 20 and Fuel Position 1 has been multiplied by the calorimetry values of F_N^{SW} in Fuel Position 1 to estimate the neutron dose rate factor in Fuel Position 20, as shown below.

$$F_N^{SW}(20) = F_N^{SW}(1)_{CAL}\left[\frac{F_N^{SW}(20)}{F_N^{SW}(1)}\right]_{FOILS} \qquad (A1.11)$$

where

$F_N^{SW}(20)$ is the estimated value of the neutron dose rate factor in Fuel Position 20

$F_N^{SW}(1)_{CAL}$ is the measured value of the neutron dose rate factor from calorimetry measurements in Fuel Position 1

$\left[\frac{F_N^{SW}(20)}{F_N^{SW}(1)}\right]_{FOILS}$ is the ratio of the neutron dose rate factors from foil measurements in Fuel Position 20 and Fuel Position 1.

The advantage of the use of the ratio is that the uncertainties in the magnitude of F_N^{SW} due to uncertainties in cross-section data are reduced

because errors in the cross sections tend to cancel.

Vidal (A1.7) has reported measurements of the resonance integral of Co^{59}, using six different concentrations of cobalt in cobalt-sulfate solutions from 0.5×10^{20} to 4.1×10^{20} atoms cobalt/cm^3. The technique employed by Vidal was the absorber oscillation method in the MINERVA reactor. The purpose of these measurements was to calculate the resonance integral of Co^{59} at infinite dilution by extrapolating the results at finite dilutions back to zero cobalt concentration. These experiments indicated a self-shielding effect in Co^{59} that had not been taken into account in the cobalt cross sections used by M. I. T. in previous calculations (A1.1, A1.2, A1.3). Table A1.5 shows a comparison of the Co^{59} cross-section data of Vidal with that of Dahlberg (A1.8) (used in earlier M. I. T. calculations) and shows the calculated values of the cobalt resonance integral at 0.595 weight percent cobalt, which is the concentration used in CoAl wire foils at M. I. T.

The factor K shown in Table A1.5 is given by

$$K = \frac{\sigma_{2200}}{\int_{E_C}^{\infty} (\sigma_{res}+\sigma_{1/v}) \frac{dE}{E}} \qquad \text{(A1.12)}$$

This factor is used to calculate the differential neutron flux in the slowing-down (1/E) region by

$$\phi_o = \frac{K\phi_{2200}}{(R_{Cd}-1)} \quad \frac{\text{neutrons}}{cm^2\text{-sec}} \qquad \text{(A1.13)}$$

and

$$\phi(E) = \frac{\phi_o}{E} \quad \frac{\text{neutrons}}{cm^2\text{-sec-ev}} \qquad \text{(A1.14)}$$

The foil dosimetry results shown in Section A1.3.2 have been interpreted using K(cobalt) = 0.528 and 0.737, and a comparison of these results is presented.

Table A1.5

Cross Sections for the Resonance Foil Co^{59} [a]

Reference	Cobalt Concentration	$\int_{E_C}^{\infty} \sigma_{res} \frac{dE}{E}$ (barns)	$\int_{E_C}^{\infty} (\sigma_{res}+\sigma_{1/v}) \frac{dE}{E}$ (barns)	σ_{2200} (barns)	K (cobalt)
Dahlberg (A1.7)	0 [c]	55.2 ± 4.5	72.3 ± 4.5	38.0 ± 0.7	0.528
Vidal (A1.6)	0 [c]	50 ± 5	68 ± 5	37.8 ± 0.3	0.556
Vidal (A1.6)	0.595 w/o [d]	35 ± 5 [b]	52 ± 5	37.8 ± 0.3	0.737

[a] 120 ev resonance.

[b] Calculated by $\int_{E_C}^{\infty} \sigma_{res} \frac{dE}{E} = \frac{\hat{\sigma} - g\sigma_{2200}}{\alpha}$ barns, where $\hat{\sigma}$ = Westcott effective cross section = 40.7 barns for Co^{59} at 0.595 w/o

$g = 1.00$

$\alpha = r\sqrt{\frac{T}{T_o}} = 0.083$

[c] Infinite dilution.

[d] $N_{Co} = 1.64 \times 10^{20} \frac{\text{atoms cobalt}}{cm^3}$

A1.3.2 Foil Dosimetry Results

Table A1.6 gives information about the conditions employed in foil dosimetry measurements made in Fuel Position 20. Refuelings during the period from May 10, 1965 to June 30, 1966, made in Fuel Positions 9 and 10 (the closest fuel positions to Fuel Position 20 as shown in Figure 2.1), are also shown in Table A1.6. Previous calculations (A1.3) have indicated that 76% of the neutron dose rate (above about 1 Mev) in Fuel Position 20 comes from fission neutrons from Fuel Positions 9 and 10. The effect of these refuelings on the neutron dose rate factor, F_N^{SW}, will be presented later in this section.

Figure A1.8 shows the differential neutron energy spectrum measured from cobalt, nickel, aluminum, and magnesium foil activations in Foil Run 38, using both the earlier and recent values of the cobalt resonance integral from Table A1.5 (i.e., K = 0.528 and 0.737). Foil Run 38 was selected as a typical example of foil measurements in Fuel Position 20. The spectrum shape used to join the individual foil data points was:

> Spectrum Type I – The flux between 120 ev and 0.71 Mev was assumed to have 1/E behavior. Above 2.81 Mev, the measured fast spectrum was used: $\phi(E) = -de^{c+dE}$. In the region between 0.71 and 2.81 Mev, a joining spectrum of the type $\phi(E) = pE^q$ was used.

An alternative spectrum fit used to interpret foil data in Fuel Position 1 was:

> Spectrum Type II – The flux between 120 ev and 1.51 Mev was assumed to be of the form $\phi(E) = pE^q$ [q = approximately -0.95 near the axial center of the core]. The measured fast spectrum was used above 1.51 Mev.

Spectrum Type I was used in Fuel Position 20 because: (1) it gave a smoother curve fit to the individual foil data; (2) the integrated neutron dose rate to Santowax using this spectrum agreed better with the calorimetry measurements; and (3) the spectrum is expected to be approximately 1/E in the slowing-down region for this fuel position since it is not near a fuel element (see Figure 2.1). It appears from Figure A1.8

Table A1.6

Chronology of Foil Measurements in Fuel Position 20

Foil Run No.	Date day/mo/yr	Reactor Power, MW	Facility	Foils Used
29	3/9/65	1.95	Stainless steel thimble	Co, Al, Mg, Ni, Cu
30	6/4/65 to 6/9/65	1.95	Aluminum monitor tube	Co, Al, Mg, Ni
			Stainless steel monitor tube	Co, Al, Mg, Ni
31	9/28/65	1.95	Aluminum monitor tube	Co, Al, Mg, Ni
			Stainless steel monitor tube	Co, Al, Mg, Ni
Refueling 10/12/65			Fresh (160 grams U^{235}) fuel elements in Fuel Positions 9 and 10	
32	10/22/65	2.93	Aluminum monitor tube	Ni
33	10/29/65	4.00	Aluminum monitor tube	Ni
34	11/24/65	4.90	Aluminum monitor tube	Co, Al, Mg, Ni
			Stainless steel monitor tube	Co, Al, Mg, Ni
35	12/23/65	4.90	Aluminum monitor tube	Co, Al, Mg, Ni
36A	1/4/66	4.90	Aluminum monitor tube	Ni
36B	1/4/66	4.90	Aluminum monitor tube	Ni
37	1/7/66	4.90	Aluminum monitor tube	Ni
38	3/3/66	4.89	Aluminum monitor tube	Co, Al, Mg, Ni
39	4/28/66	4.90	Aluminum monitor tube	Co, Al, Mg, Ni
39A*	6/9/66	4.90	Aluminum monitor tube	Co, Al, Mg, Ni
Refueling 6/11/66			Fresh (160 grams U^{235}) fuel elements in Fuel Position 10	
40	6/16/66	4.90	Stainless steel thimble	Co, Al, Mg, Ni

*Measurements at core axial center only.

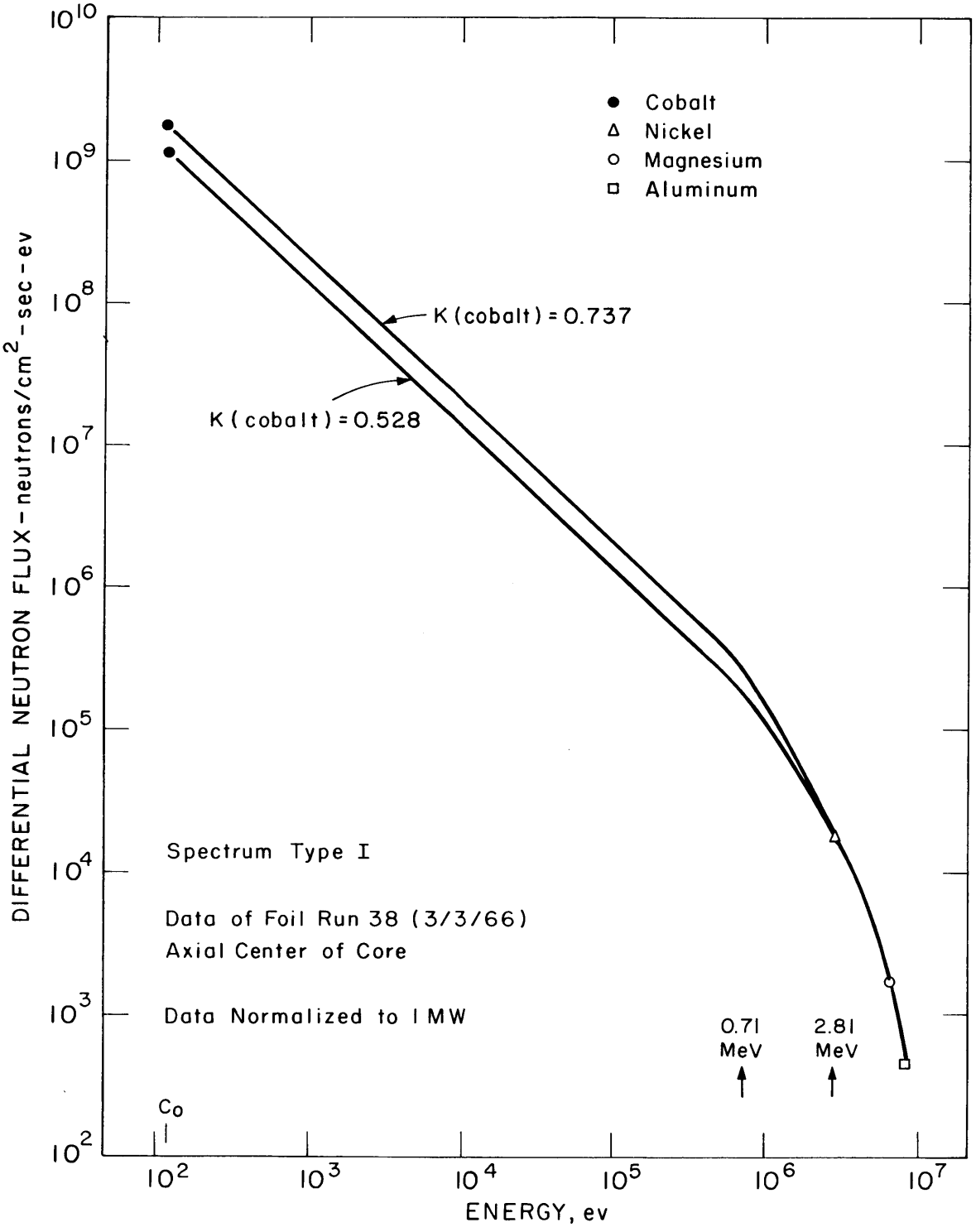

FIGURE A1.8 DIFFERENTIAL NEUTRON SPECTRUM IN FUEL POSITION 20

that either value of K(cobalt) will give a smooth curve spectrum fit for this foil data.

Figure A1.9 shows the effect of the cadmium sheath in the sample assembly on the thermal neutron flux. The 40-mil-thick cadmium liner is essentially "black" to thermal neutrons and causes a reduction of the thermal neutron flux at the axial center of the core by a factor of about 50 compared to the thermal flux beyond the edges of the cadmium.

Figures A1.10 and A1.11 show the axial variation of the fast neutron dose rate to Santowax (calculated by Equations (A1.4) and (A1.5)) from the foil runs shown in Table A1.6, using the two values of K for cobalt. Since the data for these foil measurements agree within about ±8% with the curve fits shown, the following conclusions can be made:

(1) Within the reproducibility limits of these measurements (approximately ±10%), the fast neutron dose rate factor did not change as the reactor power was increased from 1.95 MW to 4.90 MW.

(2) There is no significant difference in the results of foil measurements in the stainless steel thimble, the aluminum monitor tube, and the stainless steel monitor tube.

The values of F_N^{SW} calculated from these foil data are:

K(cobalt) = 0.528

$$F_N^{SW} = 1.12 \frac{\text{watt-cc}}{\text{MW-gm}} \quad \text{from neutrons}$$

K(cobalt) = 0.737

$$F_N^{SW} = 1.45 \frac{\text{watt-cc}}{\text{MW-gm}} \quad \text{from neutrons}$$

Table A1.7 presents the results of the individual foil runs in Fuel Position 20, using the two values of K(cobalt). This table also compares the results of foil measurements and calorimetry measurements in Fuel Position 1 in a fresh ten-plate fuel element (Foil Run 18) and in an aluminum sample assembly (Foil Run 28). It is apparent from these results in Fuel Position 1 that the higher value of K(cobalt), which corrects for self-shielding, gives values of F_N^{SW} which are in better

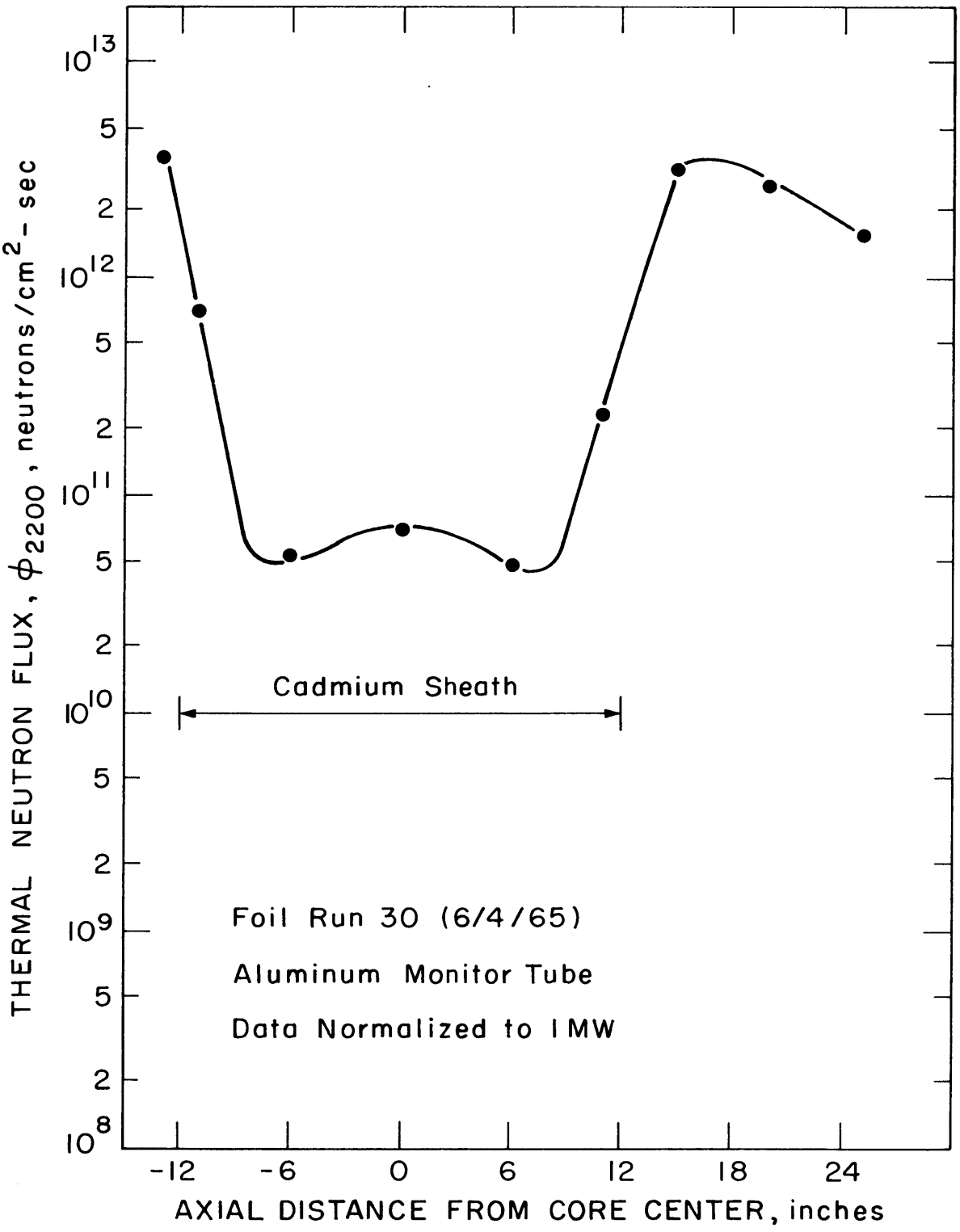

FIGURE A1.9 EFFECT OF CADMIUM SHEATH ON THE THERMAL NEUTRON FLUX IN FUEL POSITION 20

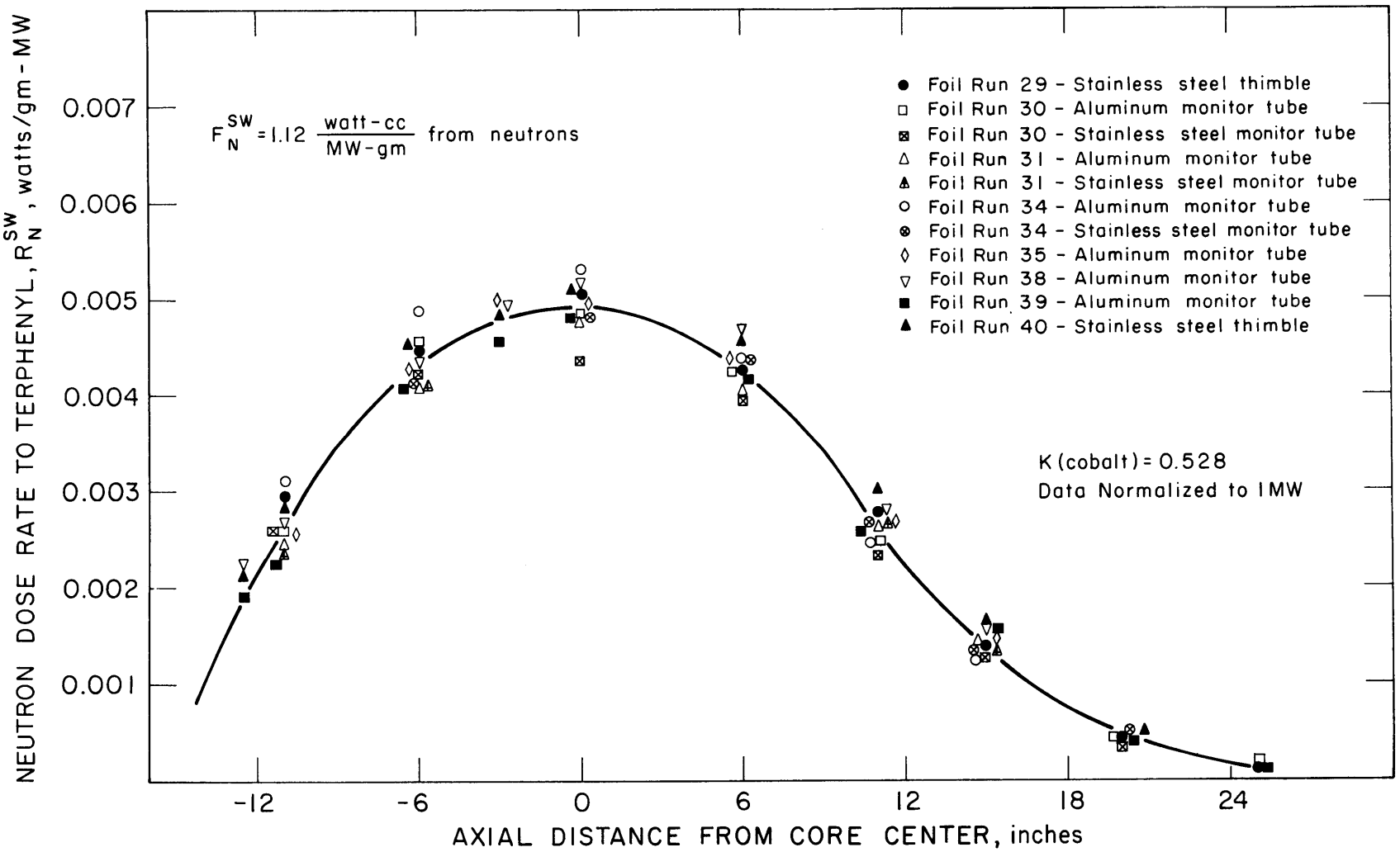

FIGURE A1.10 AXIAL VARIATION OF THE NEUTRON DOSE RATE TO TERPHENYL FROM FOIL MEASUREMENTS USING K (COBALT) = 0.528

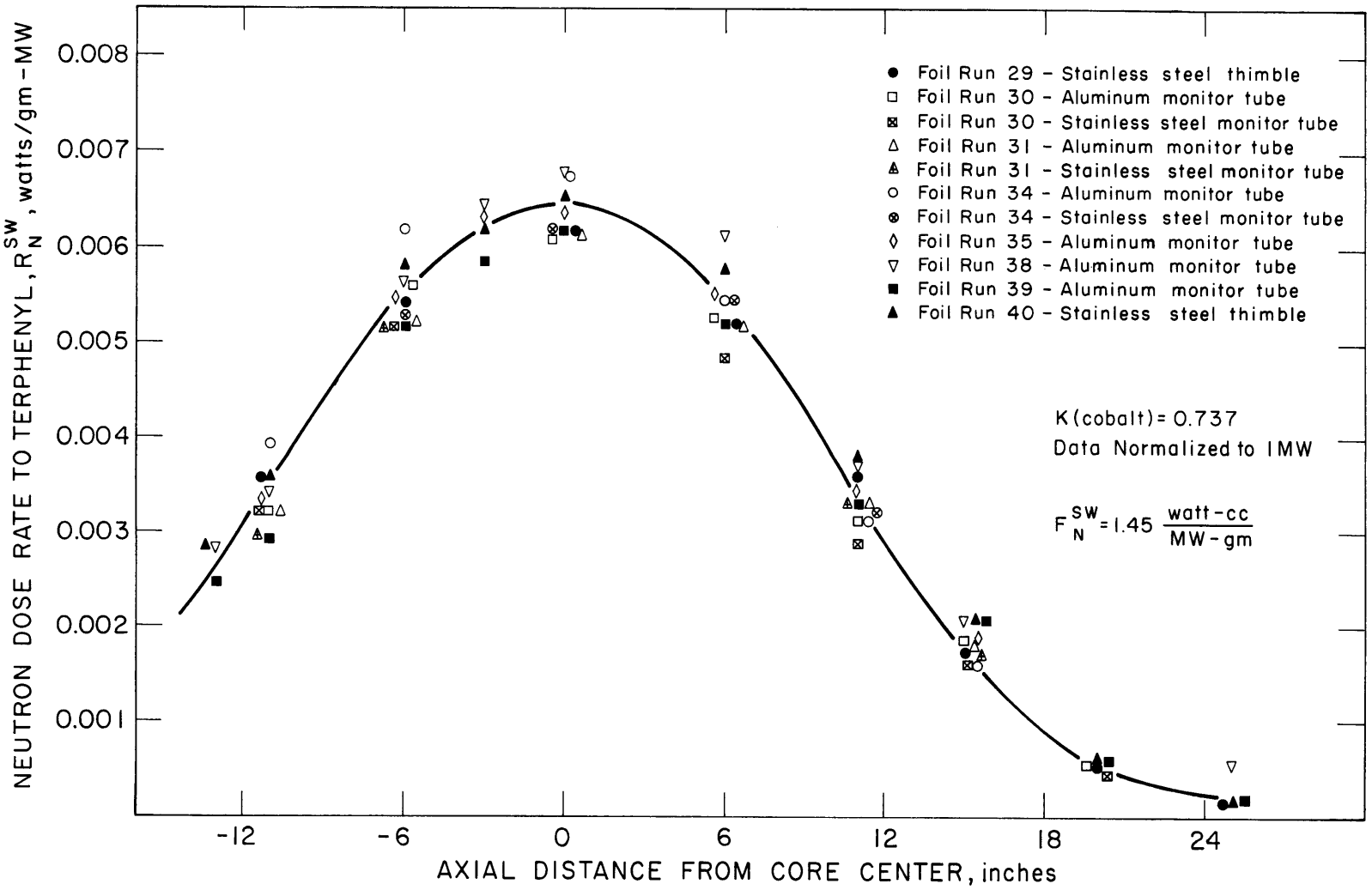

FIGURE A1.11 AXIAL VARIATION OF THE NEUTRON DOSE RATE TO TERPHENYL FROM FOIL MEASUREMENTS USING K (COBALT) = 0.737

Table A1.7

Comparison of Foil Dosimetry and Calorimetry Calculations of the Fast Neutron Dose Rate Factor

Foil Dosimetry				Calorimetry	
Foil Run Number	$F_{N'}$ watt-cc/MW-gm		Date mo/day/yr	Calorimetry Series No.	$F_{N'}$ watt-cc/MW-gm
	K=0.528	K=0.737			
Cadmium-Lined Sample Assembly in Fuel Position 20:					
29	1.15	1.50	3/9/65		
30	1.12	1.47	6/4/65		
31	1.06	1.39	9/28/65		
34	1.19	1.56	11/24/65		
35	1.12	1.47	12/23/65		
38	1.18	1.55	3/3/66		
39	1.07	1.40	4/28/66		
40	1.18	1.55	6/6/66		
Fresh Ten-Plate Fuel Element in Fuel Position 1:					
			6/26/63	IVa	25.6
			7/16/63	IVb	27.8
18	21.0*	22.1*	8/9/63		
Aluminum Sample Assembly in Fuel Position 1:					
			11/17/64	VIII	10.4
28	7.9	9.9	12/4/64		
			12/15/64	IX	11.0

*Spectrum Type II.

agreement with calorimetry results than the earlier infinite dilution values for the cobalt resonance integral.

The refueling operations in Fuel Positions 9 and 10 following Foil Runs 31 and 39 appear to have increased the fast neutron dose rate in Fuel Position 20 by approximately 10% (see results of Foil Runs 34 and 40 in Table A1.7). However, since this increase is about the limit of reproducibility of the foil measurements (due to uncertainties in the counter efficiency), this change is not considered significant. It should be noted that an increase of 10% in the fast neutron dose rate in Fuel Position 20 would result in an increase in the fast neutron fraction, f_N, of less than 1% (absolute).

Table A1.7 indicates that the increase in the value of K(cobalt) from 0.528 to 0.737 gives: (1) an increase of 30% in the calculated value of F_N^{SW} for foil measurements in Fuel Position 20; (2) an increase of 25% in the calculated value of F_N^{SW} in the aluminum sample assembly in Fuel Position 1; and (3) an increase of 5% in the calculated value of F_N^{SW} in a fresh ten-plate fuel element in Fuel Position 1. The smaller effect of the cobalt cross-section data on this latter case is due to the harder spectrum measured in the fuel element in Fuel Position 1, giving a higher fraction of the fast neutron dose rate resulting from higher energy neutrons. Since the cobalt foil measurements are used to calculate the differential neutron flux at low energy (cobalt resonance at 120 ev), changes in K(cobalt) are less important for the harder spectrum. Table A1.8 shows the fraction of the neutron dose rate to terphenyl from different energy regions for the three irradiation facilities where calorimetry and foil measurements have been made. These values were calculated from Equations (A1.4) and (A1.5) by integrating over the energy intervals, ΔE, shown in Table A1.8. The neutron energy spectrums, $\phi(E)$, used in Equation (A1.5) are indicated in this table and shown in Figure A1.12. The calculations shown in Table A1.8 indicate that, in the sample assemblies in Fuel Position 20 and Fuel Position 1, about 65% of the fast neutron dose rate to terphenyl comes from neutrons with energies below 1 Mev. In the fresh ten-plate fuel element in Fuel Position 1, about 47% of the neutron dose rate to terphenyl comes from neutrons with energies below 1 Mev.

Table A1.8

Fast Neutron Dose Rate from Different Energy Regions
(Axial Center of Core)

Irradiation Facility	Energy Region, ΔE (Mev)	Fraction Neutron Dose Rate from Region ΔE
Fuel Position 20: Cadmium-lined sample assembly Foil Run 38 Spectrum Type I	0.01-0.05	.064
	0.05-0.10	.064
	0.10-0.50	.315
	0.50-1.0	.216
	1.0-5.0	.319
	5.0-10.0	.022
	10.0-13.0	.001
Fuel Position 1: Aluminum sample assembly Foil Run 28 Spectrum Type I	0.01-0.05	.062
	0.05-0.10	.062
	0.10-0.50	.302
	0.50-1.0	.209
	1.0-5.0	.337
	5.0-10.0	.028
	10.0-13.0	.001
Fuel Position 1: Fresh ten-plate fuel element Foil Run 18 Spectrum Type II	0.01-0.05	.042
	0.05-0.10	.043
	0.10-0.50	.217
	0.50-1.0	.165
	1.0-5.0	.487
	5.0-10.0	.045
	10.0-13.0	.001

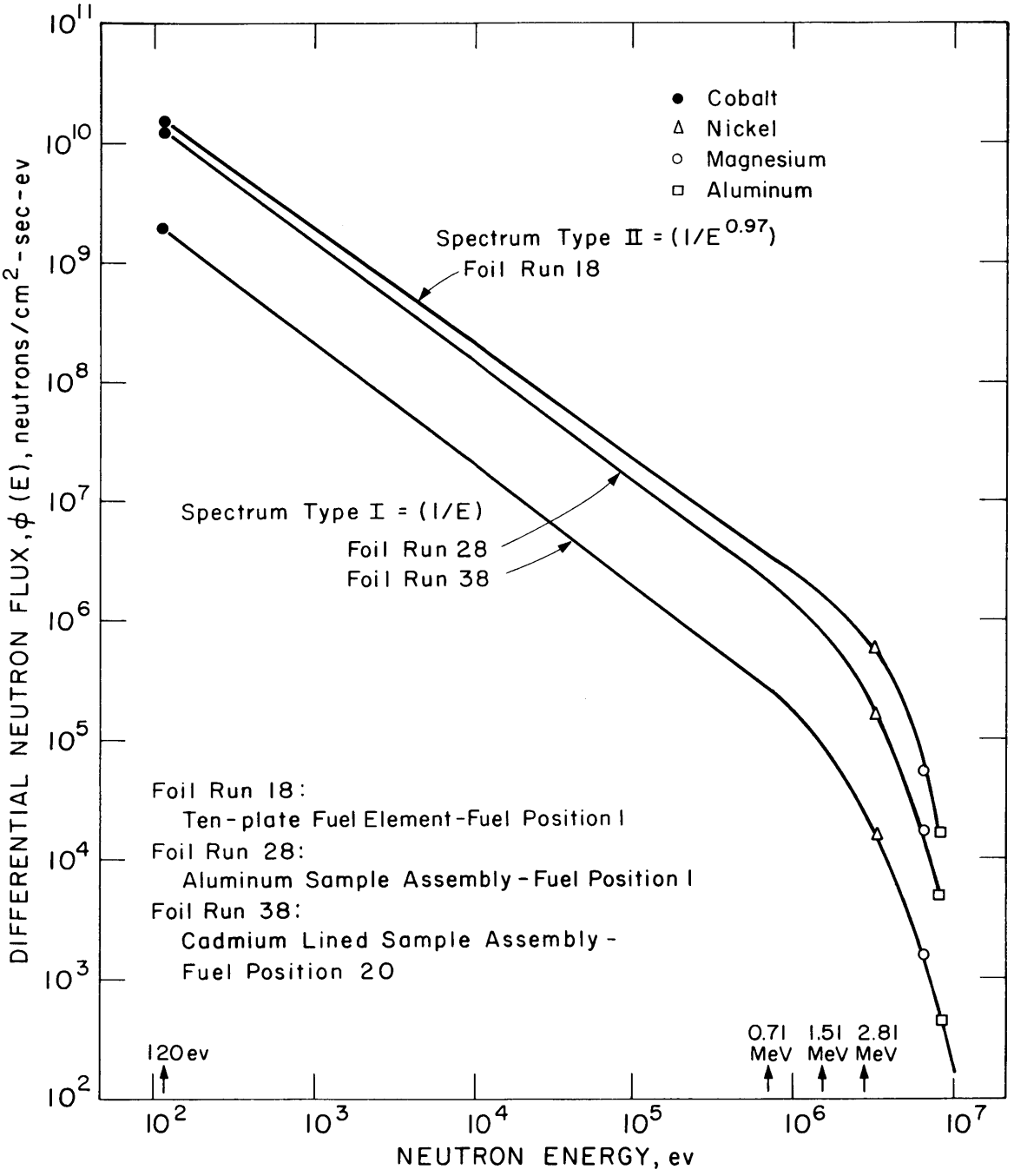

FIGURE A1.12 NEUTRON ENERGY SPECTRUM IN FUEL POSITION 20 AND FUEL POSITION 1

A1.4 Fast Neutron Fraction in Fuel Position 20

The fast neutron fraction of the total dose rate is defined by

$$f_N = \frac{F_N^{SW}}{F_T^{SW}} = \frac{F_N^{SW}}{F_N^{SW} + F_\gamma^{SW}} \qquad \text{(A1.15)}$$

As discussed in Section A1.1, the gamma dose rate factor in Equation (A1.15) can be found directly from calorimetry measurements in Fuel Position 20, but foil activation data were used to determine the fast neutron dose rate.

From the pre-irradiation and post-irradiation calorimetry measurements (see Tables A1.3 and A1.4), the average value of the gamma dose rate factor is

$$F_\gamma^{SW} = 19.08 \pm 0.46 \quad \frac{\text{watt-cc}}{\text{MW-gm}} \qquad (1\sigma)$$

The two methods used to calculate the fast neutron fraction are shown below.

Method 1:

Using the foil measurements alone to calculate the value of F_N^{SW} gives the following results:

K(cobalt) = 0.528 (see Figure A1.10)

$$F_N^{SW} = 1.12 \pm 0.06 \quad \frac{\text{watt-cc}}{\text{MW-gm}} \qquad (1\sigma)$$

$$f_N = \frac{1.12}{(19.08 + 1.12)} = 0.056$$

K(cobalt) = 0.737 (see Figure A1.11)

$$F_N^{SW} = 1.45 \pm 0.10 \quad \frac{\text{watt-cc}}{\text{MW-gm}} \qquad (1\sigma)$$

$$f_N = \frac{1.45}{(19.08 + 1.45)} = 0.071$$

As expected, the value of the fast neutron fraction calculated by this method is extremely sensitive to the cobalt cross-section data used.

Method 2:

The alternate method proposed to calculate the fast neutron dose rate factor in Fuel Position 20 was outlined in Section A1.3.1 (Equation (A1.11)). The values of the fast neutron dose rate factor in Fuel Position 1 are shown in Table A1.7 for calorimetry measurements in the aluminum sample assembly and the ten-plate fuel element. The calorimetry results obtained in both these irradiation facilities were used in this calculation, although the results in the aluminum sample assembly in Fuel Position 1 should be more applicable because the neutron spectrum in this facility was softer (similar to Fuel Position 20) than in the ten-plate fuel element. Table A1.9 presents the fast neutron fraction calculated by this method, using K(cobalt) = 0.528 and 0.737. The values of $F_N^{SW}(20)$ and f_N by Method 2, using both values of K(cobalt), agree much better with the results of Method 1, based on K(cobalt) = 0.737, than with K(cobalt) = 0.528.

In summary, the best values of the dosimetry results in Fuel Position 20 are:

Gamma In-Pile Dose Rate Factor

$$F_\gamma^{SW} = 19.08 \pm 0.46 \text{ watt-cc/MW-gm}$$

Neutron In-Pile Dose Rate Factor

$$F_N^{SW} = 1.45 \pm 0.10 \text{ watt-cc/MW-gm}$$

Total In-Pile Dose Rate Factor

$$F_T^{SW} = 20.53 \pm 0.50 \text{ watt-cc/MW-gm}$$

Fast Neutron Fraction

$$f_N = 0.071 \pm 0.005$$

The error limits shown above are approximately 1σ. The relative statistical error limit on the total in-pile dose rate factor to be used in the degradation calculations of Appendix A3 is

$$\frac{\sigma(F)}{F} = 0.025 \approx 0.03$$

Table A1.9

Calculation of the Fast Neutron Fraction of the Total Dose Rate in Fuel Position 20

K(cobalt)	$F_N^{SW}(1)_{CAL}$	$F_N^{SW}(20)_{FOILS}$	$F_N^{SW}(1)_{FOILS}$	$F_N^{SW}(20)$ [a]	Fast Neutron Fraction, f_N [b]
0.528	10.7 ± 0.3 [c]	1.12	7.9	1.52	0.074
0.528	26.7 ± 1.1 [d]	1.12	21.0	1.42	0.069
0.737	10.7 ± 0.3 [c]	1.45	9.9	1.57	0.076
0.737	26.7 ± 1.1 [d]	1.45	22.1	1.75	0.084

[a] Calculated by Equation (A1.11).

[b] Assuming $F_\gamma^{SW}(20) = 19.08$ watt-cc/MW-gm.

[c] Calorimetry result from aluminum sample assembly.

[d] Calorimetry result from fresh ten-plate fuel element.

APPENDIX A2

COOLANT MASS AND TEMPERATURE PROFILES AROUND LOOP

A2.1 Calculations of Mass of Circulating Coolant in the Loop

In order to determine the average dose rate (watts/gm) to all the coolant in the loop, the mass of circulating coolant must be known. This value (designated M_{loop}) is particularly important in transient runs since the decrease in terphenyl concentration is directly proportional to the average dose rate. In steady-state runs, M_{loop} is only important in the Δ-correction terms in the degradation calculations (see Appendix A3). The mass of circulating coolant in the loop is also important in all high temperature runs because the average dose rate ($\bar{r}$) calculated from M_{loop} is used to calculate the relative rates of radiolysis and radiopyrolysis (see Section 4.2).

Two methods are used at M. I. T. to determine the mass of organic coolant circulating in the loop. These methods are:

1. Calculations based on the known volumes and temperatures of various sections of the loop at some time during the steady-state period of each run, and
2. Calculations based on tritium dilutions in which a known amount of tritiated terphenyl is added to the circulating coolant in the loop.

The primary method used to determine the circulating coolant mass is the tritium dilution method. The results of the tritium dilution made during Run 18B are shown in Table A2.1. In this method, a coolant sample is removed from the loop prior to the addition of the tritiated terphenyl to obtain the background concentration of tritium in the loop. Approximately 100 millicuries of tritium are added to the loop in a weighed sample capsule from which aliquots have been taken for tritium analysis. The tritiated terphenyl sample is allowed to mix with the coolant in the loop for at least two hours, and a sample of the coolant is removed from the loop for analysis. The circulating coolant mass is determined by Equation (A2.1).

Table A2.1

Circulating Coolant Mass in Loop
Tritium Dilution – Run 18B

Sample	Tritium Concentration, (μc/gm)		Circulating Coolant Mass, M_{loop}, (gms)	
	Tracerlab	Isotopes, Inc.	Tracerlab	Isotopes, Inc.
18L-13 (C_o)	1.75 ± 0.02	1.5 ± 0.1		
18L-14 (C_o)	1.74 ± 0.02	1.5 ± 0.1		
18D-8 (C_1)	390 ± 9	314 ± 13		
18L-15 (C_2)	20.7 ± 0.4	17.0 ± 0.7	5384 ± 170	5308 ± 324
18L-16 (C_3)	19.7 ± 0.4	16.3 ± 0.6	5388 ± 190	5267 ± 332

$$M_{loop} = \frac{M_1(C_1-C_2)}{(C_2-C_o)} \qquad (A2.1)$$

where

M_{loop} = circulating coolant mass in the loop before the tritiated terphenyl was added, grams

M_1 = weight of the tritiated terphenyl sample, grams

C_o = background tritium concentration in the loop, $\mu c/gm$

C_1 = tritium concentration in the tritiated terphenyl sample added to the loop, $\mu c/gm$

C_2 = tritium concentration in the coolant sample removed from the loop after mixing, $\mu c/gm$

Normally, the tritium dilution is made in the steady-state period of a run, and after the next makeup sample (which contains no tritium) has been added to the loop, a second coolant sample is removed from the loop for tritium analysis. Since this second sample is taken from 12 to 24 hours after the first sample, a longer mixing time is realized. The analysis of the second sample provides an estimate of the mass of coolant in sections of the loop which have slow mixing times. The circulating coolant mass determined by the second sample is

$$M_{loop} = \frac{M_1(C_1-C_3) - M_2(C_2-C_3) - M_3(C_3)}{(C_3-C_o)} \qquad (A2.2)$$

where

M_{loop} = circulating coolant mass in the loop before the tritiated terphenyl was added, grams

M_2 = weight of the first coolant sample removed from the loop after the tritium dilution, grams

M_3 = weight of the makeup sample added to loop after the first coolant sample was removed, grams

C_3 = tritium concentration in the second coolant sample removed from the loop after mixing, $\mu c/gm$

Analyses of the tritium samples were made by two laboratories — Tracerlab (Waltham, Massachusetts) and Isotopes, Inc. (Westwood,

New Jersey). Approximately 1 gram of sample was analyzed by each laboratory for each tritium-containing sample. Duplicate or triplicate analyses were performed on each sample. Both laboratories used a direct method of analysis, in which the sample was dissolved in a commercial scintillation liquid. Separate aliquots of each solution were analyzed to obtain duplicate or triplicate analyses. The counting efficiency of the system was determined by the use of an internal spike (tritiated toluene) of a known activity in the analyses performed by Tracerlab. The volume of the spike solution was small, relative to the volume of the scintillation solution, so that the addition of the spike did not change the makeup of the solution in any measurable way. The presence of impurities with low energy radiations (in the tritium β-ray energy range) was determined by comparing the relative counting rates in two separate channels with the relative counting rates in these two channels for a tritium standard solution containing no impurities. Isotopes, Inc. used the channels ratio technique to determine the counting efficiency, in which the ratio of counts in two preset channels varies proportionally to a change in efficiency. The relationship was established by comparison of known standards.

A summary of the calculations of the circulating coolant mass in the loop during irradiations in Fuel Position 20 is shown in Table A2.2. For all tritium dilution calculations, the results of Tracerlab agree within ±200 grams of the circulating coolant mass determined by the volume calculation method. For the first two tritium dilutions (Run 14 and Run 16), the results of Isotopes, Inc. are approximately 600-700 grams higher than the Tracerlab results. This discrepancy is believed to be due to the fact that for these two analyses, only 100 milligrams of sample were submitted for analysis, and the weighing errors associated with this small mass of sample (which is a viscous liquid) were relatively large. After the sample size had been increased to about 1 gram, this discrepancy was no longer evident. For the tritium dilution made during Run 16, the first coolant sample was removed from the loop about one-half hour after the tritium dilution, due to faulty closure of a valve on the sample capsule. Since the second coolant sample removed indicated that the circulating coolant mass was about 700 grams larger than the first sample, it was concluded that complete mixing could not be achieved

Table A2.2

Summary of Calculations of Circulating Coolant Mass in Loop

Run Number	Time	Circulating Coolant Mass, M_{loop}, grams		
		Tritium Dilution Method		Volume Method
		Tracerlab	Isotopes, Inc.	
14	After Sample 14L-13 removed	5473 ±383	6130 ±429	5329 ±200
16	After Sample 16L-20 removed			
	First dilution sample	5120 ±116	5664 ±354	5652 ±200
	Second dilution sample	5854 ±143	6435 ±412	5652 ±200
	Before loop drained at end of Run 16	5526 ±217	5508 ±416	5619 ±200
18B	After Sample 18L-14 removed			
	First dilution sample	5384 ±170	5308 ±324	5140 ±200
	Second dilution sample	5388 ±190	5267 ±332	5140 ±200

in one-half hour. Later tritium dilutions indicated no significant difference in the calculated values of M_{loop} after two hours mixing and twenty-four hours mixing. From the summary of results shown in Table A2.2, it appears that the maximum uncertainty in the circulating coolant mass in the loop for irradiations in Fuel Position 20 is approximately ±300 grams. For use in the statistical analysis for transient runs (see Section A3.2), the standard deviation of the coolant mass is estimated to be ±150 grams.

A chronology of the circulating coolant mass in the loop for the irradiations in Fuel Position 20 is shown in Figure A2.1 (May 10 to December 31, 1965) and in Figure A2.2 (January 1 to June 10, 1966).

The coolant masses shown in these figures are based on the tritium dilution results from Tracerlab, since these results appear to be more consistent than those from Isotopes, Inc. and more accurate than the volume calculation results. Comparisons of these masses with the values predicted from the Isotopes, Inc. tritium dilution analyses and the volume method are shown at various points on these figures. The mass of the loop during Run 13, Run 14, and Run 15 was based on the tritium dilution results during Run 14. For Run 16 and Run 17, the basis was changed to the tritium dilution made near the end of Run 16. At the point where the basis of the calculation was changed at the beginning of Run 16 (Sample 16L-1), there is a discrepancy of 224 grams (shown as a dashed line in Figure A2.1) which is within the maximum uncertainty limits of ±300 grams. At the end of the transient part of Run 18 (Sample 18L-6), the basis was again changed to the tritium dilution results obtained during the steady-state part of Run 18. The "best" value of the circulating coolant mass during the transient part of Run 18 (Sample 18L-1 through Sample 18L-6) was based on the volume method of calculation, for the reasons discussed below.

The construction of the liquid samplers used to remove the small samples (about 25 grams) during Run 18A was such that all of the coolant removed from the loop could not be weighed accurately. The decrease in the surge tank level during this transient run indicated that approximately 450 grams were removed from the loop during this transient phase. The volume method of calculation before and after this transient run agrees within the uncertainty limits with the tritium dilution

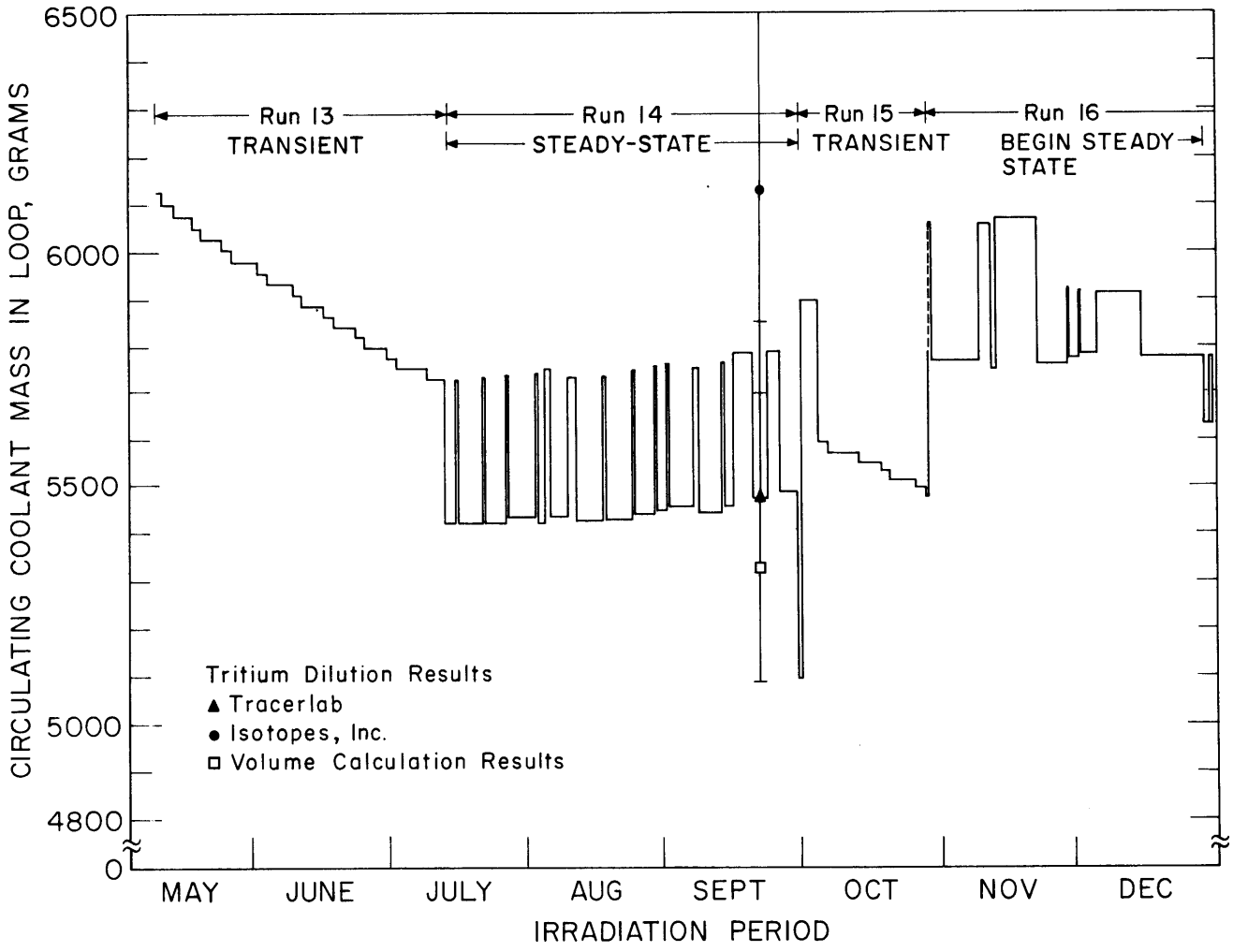

FIGURE A2.1 CIRCULATING COOLANT MASS IN LOOP FROM MAY 10, 1965 TO DECEMBER 31, 1965

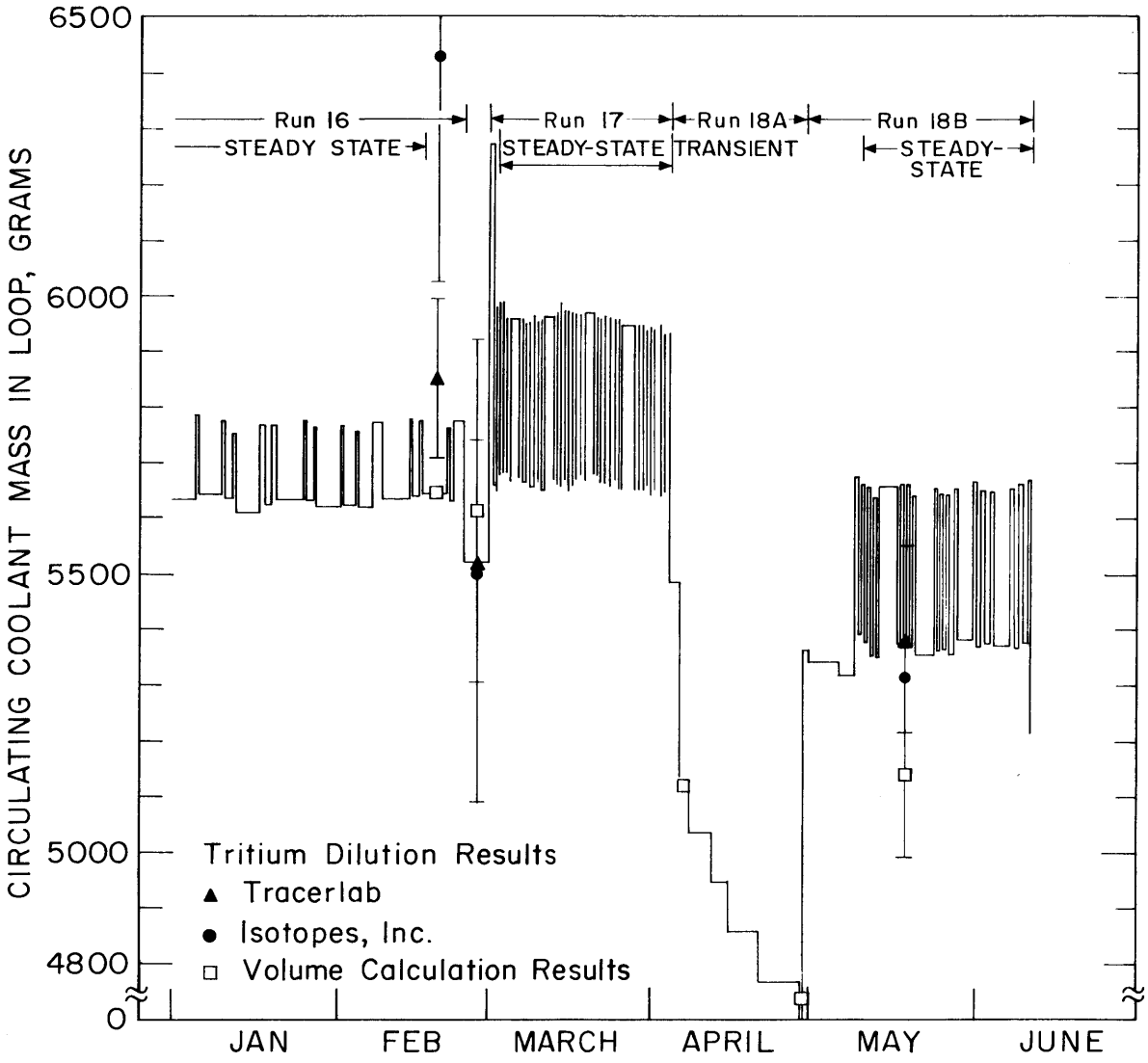

FIGURE A2.2 CIRCULATING COOLANT MASS IN LOOP FROM JANUARY 1, 1966 TO JUNE 10, 1966

results made during Run 16 and Run 18.

The volume method of calculation during Run 18B, at the time of the tritium dilution, is shown in Table A2.3. Morgan and Mason (A2.1) have estimated that the uncertainty in the volume calculation method is ±200 cc, and the results presented in Table A2.2 show that the volume method agrees with the Tracerlab tritium dilution results within this limit.

A2.2 Effect of Coolant Temperature Distribution on Degradation Calculations

A2.2.1 Coolant Temperature Profile Around Loop

The coolant circulating around the loop loses heat to the surroundings. In order to maintain the terphenyl coolant at high temperatures, heat is added to the coolant primarily by a test heater (6 kw) operating at constant power and a trim heater (2 kw) operating at variable power. Heat is also added to the circulating coolant by trace heaters around the surge tank and stainless steel connecting lines, and also by the mechanism of fast neutron and gamma-ray energy absorption in the coolant in the irradiation capsule. Thus, there is a variation in coolant temperature around the loop. It is necessary to determine the temperature profile for the coolant in order to calculate the total circulating coolant mass in the loop from known volumes in the various sections of the loop (Appendix A2.1), and also to determine the "effective" loop temperature for high temperature irradiations where radiopyrolysis causes significant coolant degradation. In addition to this temperature distribution, it is necessary to determine the time-dependent fluctuations in these temperatures due to periodic operating conditions such as adding and removing coolant samples from the loop, loss of power to the test heater, and reactor scrams.

Since the temperature profile of the loop is most important for high temperature runs, the temperature distribution has been extensively investigated for Run 18B, the only steady-state irradiation at high temperature (800°F) made in Fuel Position 20. Run 18B was made under nominally similar conditions of terphenyl concentration and irradiation capsule temperature as Run 9 (made in Fuel Position 1), and a comparison of the temperature profiles for these two runs has been made.

Table A2.3

Volume Calculation of Circulating Coolant Mass in Loop for Run 18

Section	Circulating Volume, cc	Temperature °F	ρ gms/cc	Mass gms
1. In-pile irradiation capsule	796	800	0.81	645
2. Right-angle bend to surge tank	446	775	0.82	366
3. Surge tank above 0" in lower gage glass	$61.1y$[a] $\frac{\rho(GG)}{\rho(ST)}$	GG = 450 ST = 779	ρ(GG) = 0.94 ρ(ST) = 0.82	788
4. 0" lower in surge tank to pump	788	778	0.82	646
4a. Trim heater	300	800	0.81	243
5. Pump impeller section through upstream half of test heater	1320	778	0.82	1082
6. Pump motor section	370	450	0.97	359
7. Downstream half of test heater to coolers	444	806	0.81	360
8. Liquid sample capsule	173 + capsule volume	778	0.83	144
9. Coolers	341	803	0.81	276
10. Coolers to right-angle bend	285	801	0.81	231
			Total[b]	5140

[a] y = 2-1/4" upper gage glass after sample 18L-14 removed from loop.

[b] Does not include liquid sampler capsule volume.

Table A2.4 shows a comparison of the temperature profiles around the loop for Run 9 and Run 18B (see Figure 2.2 for schematic flow diagram of loop, including valve numbering scheme).

In Table A2.4, only the immersion thermocouples (indicated by an asterisk) directly measure the temperature of the coolant. All other thermocouples are spot-welded to the specified lines, valves, etc. and therefore measure the metal temperature at that point. Such measurements are useful in comparing relative coolant temperatures at these positions between two different runs but cannot be used as an absolute measurement of the organic coolant temperature at that position.

The most important temperature in this profile is that of the irradiation capsule. Although in both In-Pile Section No. 2 (Run 9) and In-Pile Section No. 3 (Run 18B) there were initially at least three immersion thermocouples in the irradiation capsule, at the time of these runs all but one of these thermocouples had been removed (see Section 2.3.2). For Run 9, the irradiation capsule temperature was 804°F, and for Run 18B, the irradiation capsule temperature was 800°F. During Run 18B, a thermocouple was installed in the central monitor tube of In-Pile Section No. 3 which extended down to the center of the irradiation capsule. This thermocouple measured 812°F with the reactor at 5 MW, but previous measurements had shown that this thermocouple read approximately 12°F high with the reactor at 5 MW, due to the radiation dose in the thermocouple. Since this thermocouple was installed in the central monitor tube, it was not cooled by the organic coolant.

Comparison of the temperatures measured by the immersion thermocouples at the test heater inlet and outlet indicate that, in this section of the loop, the coolant temperature was 6° - 7°F higher for Run 9 than for Run 18B. Comparison of the temperature measurements of the immersion thermocouples in the surge tank indicate that the temperature in this section of the loop was about 2°F higher for Run 9 than for Run 18B. In general, Table A2.4 indicates that the organic coolant temperature in various sections of the loop was 2° - 12°F lower for Run 18B than for Run 9. An exception to this is found in the temperatures measured on the lines through the main biological shield, which are higher for Run 18B than for Run 9. Since these lines were replaced when In-Pile Section No. 2 was removed from the reactor and In-Pile

Table A2.4

Comparison of Temperature Profile Around Loop for Run 9 and Run 18B

Section	Temperature, °F	
	Run 9 (July 2, 1964)	Run 18B (June 7, 1966)
Surge tank	782*	779*
Pump		
Inlet	794	767
Outlet	768	766
Test heater		
Inlet	785*	778*
Outlet	815*	809*
Console exit line	786	777
Console inlet line	765	754
Irradiation capsule		
Immersion thermocouple	804*	800*
Central monitor tube	–	812
Outlet line, elbow in-pile section	–	791
Lines through biological shield		
Inlet (valve 24 to in-pile section)	789	800
(valve 24 to in-pile section)	778	796
Outlet (in-pile section to valve 27)	762	784
(in-pile section to valve 27)	765	785
(in-pile section to valve 27)	765	778
Outlet valve 27	771	759
Line from valve 27 to surge tank	786	–
Pump impeller section	–	772
Trim heater	800	800
Cooler bypass	781	778
Outlet valve 24	809	803
Outlet valve 1	786	774
Outlet valve 9	752	578

* Immersion thermocouple.

Section No. 3 was installed, these measurements probably indicate that better heating and insulation of these connecting lines were obtained with In-Pile Section No. 3. The effect of this difference in the temperature profile around the loop on the "effective" loop temperature for these two runs is given in the following section.

A2.2.2 Calculation of the Effective Loop Temperature

Terrien and Mason (A2.2) have described a method used to determine the effective loop temperature for M. I. T. runs at high temperature with a temperature distribution around the loop. This method assumes that the experimentally determined radiopyrolysis rate constant for m^{th}-order kinetics, $\bar{k}_{P,i,m}$, is a mass-average value resulting from the absolute values of $k_{P,i,m}$ for different sections of the loop which are at different temperatures. The radiopyrolysis rate for each approximately isothermal section j of the loop is assumed to fit an Arrhenius-type relation, as shown in Equation (A2.3).

$$k_{P,i,m} = k^{o}_{P,i,m} \exp\left[- \frac{\Delta E_{P,i}}{RT_j} \right] \tag{A2.3}$$

where

$k^{o}_{P,i,m}$ = radiopyrolysis reaction rate constant, (hr^{-1})

j refers to a section of the loop

T_j = the average temperature in section j

$\Delta E_{P,i}$ = the radiopyrolysis activation energy of irradiated component i, k-cal/mole

R = gas constant

The experimental mass-average $\bar{k}_{P,i,m}$ can then be expressed in the following manner,

$$\bar{k}_{P,i,m} = \frac{\sum_j M_j C_{i,j} k^{o}_{P,i,m} \exp\left[- \frac{\Delta E_{P,i}}{RT_j} \right]}{\sum_j M_j C_{i,j}} \tag{A2.4}$$

where

M_j = total mass of coolant in section j
= $V_j \rho_j$ (V_j being the volume of section j and ρ_j the coolant density in section j)

$C_{i,j}$ = concentration of component i in section j, which is assumed equal in all sections so that the $C_{i,j}$ terms in Equation (A2.4) cancel out.

In applying this technique, values of $k^o_{P,i,m}$ and $\Delta E_{P,i}$ are assumed and, using known values of M_j and T_j in Equation (A2.4), a value of the mass-average $\bar{k}_{P,i,m}$ is calculated and compared to the experimental value. An iteration procedure is employed to obtain successively better estimates of the constants $k^o_{P,i,m}$ and $\Delta E_{P,i}$ until the calculated value of $\bar{k}_{P,i,m}$ equals the experimental value. The iteration converges in two or three steps. Finally, the best values of $k^o_{P,i,m}$ and $\Delta E_{P,i}$ from the iteration and the experimental value of $\bar{k}_{P,i,m}$ are used in Equation (A2.3) to calculate a temperature, T_j, which is designated the "effective" loop temperature.

This procedure is particularly useful when irradiations at various high temperatures (e.g., Run 5 at 700°F, Run 3 at 750°F, and Run 9 at 800°F, all in Fuel Position 1 at $f_N = 0.40$) have been made at similar coolant compositions and fast neutron fractions because initial estimates of $k^o_{P,i,m}$ and $\Delta E_{P,i}$ (which are presumed to apply to all runs at these similar conditions) can be made easily. However, in Fuel Position 20, only one steady-state high temperature irradiation was made (Run 18B at 800°F) and a modification of this procedure was used to determine the effective loop temperature. This modified procedure is described below.

Equation (A2.3) can be written in a slightly different form,

$$\frac{k_{P,i,m}(T_j)}{k_{P,i,m}(T_o)} = \exp\left[-\frac{\Delta E_{P,i}}{R}\left(\frac{T_o - T_j}{T_o T_j}\right)\right] \qquad \text{(A2.5)}$$

to give the radiopyrolysis rate in section j and temperature T_j relative to the radiopyrolysis rate at a selected temperature, T_o, which is near the average coolant temperature in the loop. A mass-averaging procedure, similar to Equation (A2.4), is then performed, as shown in Equation (A2.6), using Equation (A2.5) and assuming only a value of

$\Delta E_{P,i}$ and a temperature basis, T_o. It should be noted that the temperature basis for the calculation, T_o, can be any temperature, but it is convenient to select T_o near the average loop temperature.

$$\frac{\overline{k_{P,i,m}(T_j)}}{k_{P,i,m}(T_o)} = \frac{\sum_j M_j \frac{k_{P,i,m}(T_j)}{k_{P,i,m}(T_o)}}{\sum_j M_j} \qquad \text{(A2.6)}$$

The mass-averaged value of the relative radiopyrolysis rate constant shown in Equation (A2.6) is then used in Equation (A2.5) to calculate T_j, the "effective" loop temperature associated with the experimentally determined radiopyrolysis rate constant, $\overline{k}_{P,i,m}$.

The advantage of this modified procedure is that only one constant, $\Delta E_{P,i}$, must be assumed and the calculation of the effective loop temperature does not depend on the measured radiopyrolysis rate. The activation energy of radiopyrolysis for various coolant compositions has been determined under a wide variety of operating conditions (see Chapter 5) and does not appear to be particularly sensitive to the fast neutron fraction employed. On the other hand, the absolute value of the radiopyrolysis rate constant, which is determined by the constant, $k^o_{P,i,m}$, may vary significantly with fast neutron fraction. Another advantage of this modified procedure is that the effective loop temperature of two runs under similar conditions of coolant composition and nominal temperature (such as Run 9 and Run 18B) can be compared, simply by assuming that the radiopyrolysis rate for each run varies with temperature in the same way ($\Delta E_{P,i}$ assumed to be the same for each run). Since the temperature, T_o, is selected near the average loop temperature, small errors in $\Delta E_{P,i}$ do not significantly affect the calculation of the effective loop temperature.

This modified procedure has been used to compare the effective loop temperature for Run 9 and Run 18B, and the results are shown in Table A2.5. For each of these runs, the temperature, T_o, was selected as the surge tank set-point temperature for Run 9, 782°F. An activation energy of radiopyrolysis, $\Delta E_{P,i}$, of 40 k-cal/mole was assumed for these irradiations at 52% terphenyl (see Table 5.4). As shown in

Table A2.5

Calculation of Effective Loop Temperature for Run 9 and Run 18B

Section	Temperature T_j, °F		$\frac{k_{P,i,m}(T_j)}{k_{P,i,m}(T_o)}$ [a,b]		Circulating Coolant Mass, M_j, grams		$\frac{k_{P,i,m}(T_j)}{k_{P,i,m}(T_o)} \frac{M_j}{\sum M_j}$	
	Run 9	Run 18B	Run 9	Run 18B	Run 9	Run 18B	Run 9	Run 18B
1. In-pile section	804	800	1.72	1.59	415	645	0.156	0.199
2. Right-angle bend to surge tank	786	775	1.15	0.89	338	366	0.085	0.063
3. Surge tank above 0" in lower gage glass	782	779	1.00	0.96	511	788	0.112	0.147
4. 0" lower in surge tank to pump	785	778	1.12	0.94	646	646	0.158	0.118
4a. Trim heater	800	800	1.59	1.59	243	243	0.084	0.075
5. Pump impeller section through upstream half of test heater	785	778	1.12	0.94	1082	1082	0.265	0.198
6. Pump motor section	450	450	—	—	359	359	—	—
7. Downstream half test heater to coolers	812	806	2.08	1.80	360	360	0.164	0.126
8. Liquid sample capsule and capsule lines	785	778	1.12	0.94	144[c]	144[c]	0.035	0.026
9. Coolers	809	803	1.94	1.74	276	276	0.117	0.093
10. Coolers to right-angle bend	806	806	1.80	1.65	203	231	0.080	0.074
				TOTAL	4577	5140	1.261	1.119
				EFFECTIVE LOOP TEMPERATURE, °F[d]			790	784

[a] T_o = surge tank set-point temperature for Run 9, 782°F.

[b] Assuming $\Delta E_{P,i}$ = 40 k-cal/mole at 52% total omp concentration.

[c] Does not include mass in sample capsule.

[d] Calculated from Equation (A2.5).

Table A2.5, two basic differences exist in the temperature profile around the loop for Run 9 and Run 18B. In most sections of the loop, the temperature for Run 9 was 2°-12°F higher than for Run 18B. However, the mass in the in-pile section during Run 18B was about 417 gms greater than for Run 9, due to the increased size of the stainless steel coolant lines in In-Pile Section No. 3 (Run 18B) over that used in In-Pile Section No. 2 (Run 9). The mass-averaged values of the relative radiopyrolysis rate constants for the two runs are shown in the last two columns on the right in Table A2.5. Equation (A2.5) was used to calculate the effective loop temperatures, which are 790°F for Run 9 and 784°F for Run 18B, using ΔE_P = 40 k-cal/mole.

A2.2.3 Effect of Temperature Fluctuations During Steady-State Operation

Shown in Figures A2.3, A2.4, and A2.5 are the measured fluctuations in the surge tank coolant temperature (measured by an immersion thermocouple) during one week of Run 9 and two weeks of Run 18B. The coolant temperature was maintained at the specified level by a trim heater (2 kw) which was controlled from the immersion thermocouple in the surge tank (see Section 2.3.2). Figure A2.3 shows that, during a typical week for Run 9, most of the drops in the surge tank temperature were caused by adding or removing coolant samples from the loop. Two momentary temperature drops were caused by loss of power to the test heater. It should be noted that, during Run 9, the trim heater caused the coolant temperature in the surge tank to "overshoot" the set point by 2°-9°F. The fluctuations in the surge tank temperature are shown for two weeks during Run 18B, one a typical week (Figure A2.4) and the other a week in which there was a loss of power to the test heater twice due to blown-out fuses in the voltage regulator (Figure A2.5). After each loss in power to the test heater during this week (May 16 - May 20, 1966), the voltage regulator was bypassed and the test heater power was reduced. The effect of these incidents was that the temperature in the surge tank did not reach the set point until about 15 hours after the incident occurred in each case. Notice in Figures A2.4 and A2.5 that, during Run 18B, the "overshoot" caused by the trim heater was much less than that measured during Run 9 because the controller on the trim heater power had been modified

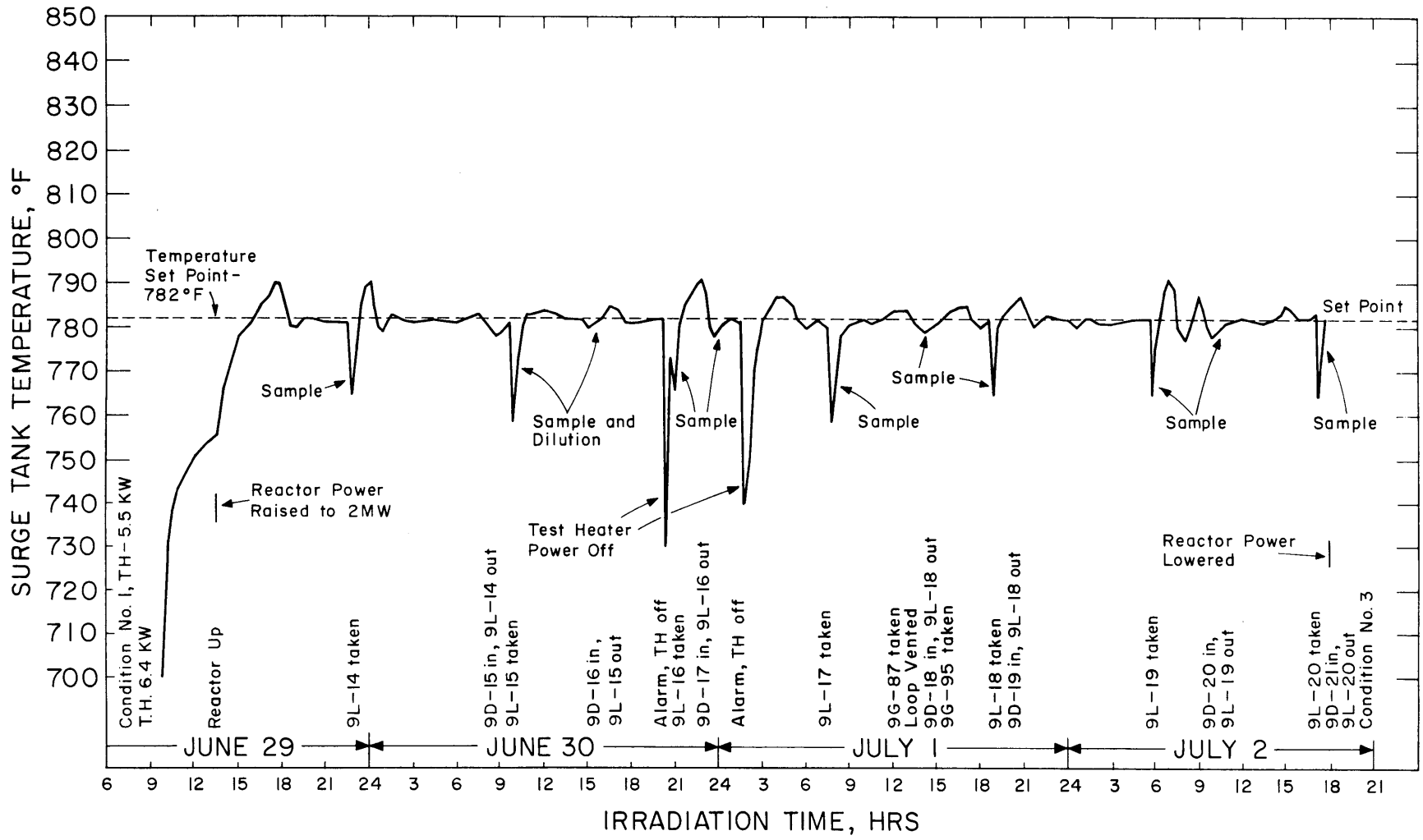

FIGURE A2.3 SURGE TANK TEMPERATURE PROFILE - WEEK OF JUNE 29 - JULY 2, 1964
RUN 9 IRRADIATION CAPSULE AT 804°F

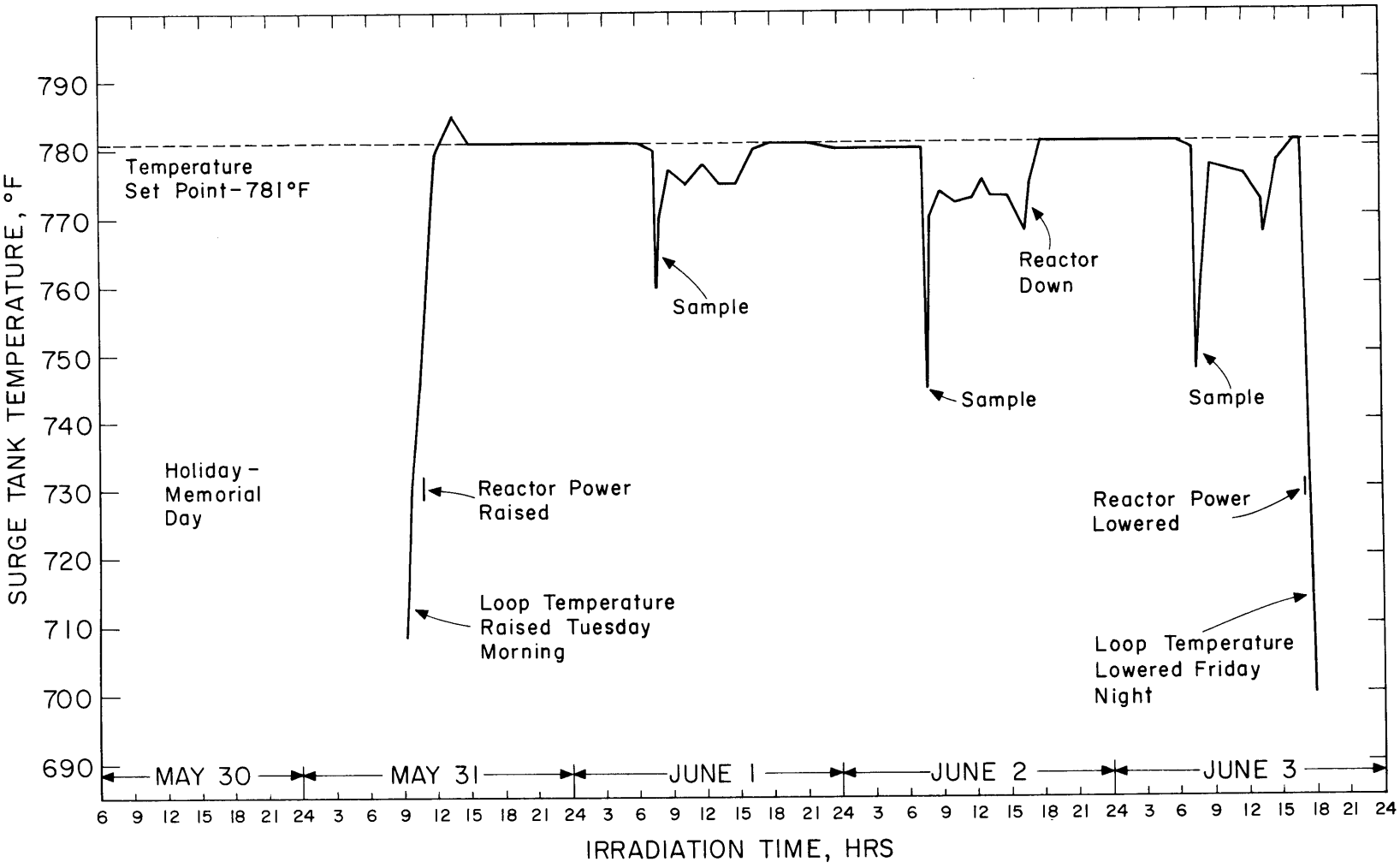

FIGURE A2.4 SURGE TANK TEMPERATURE PROFILE – WEEK OF MAY 30 – JUNE 3, 1966
RUN 18B IRRADIATION CAPSULE AT 800°F

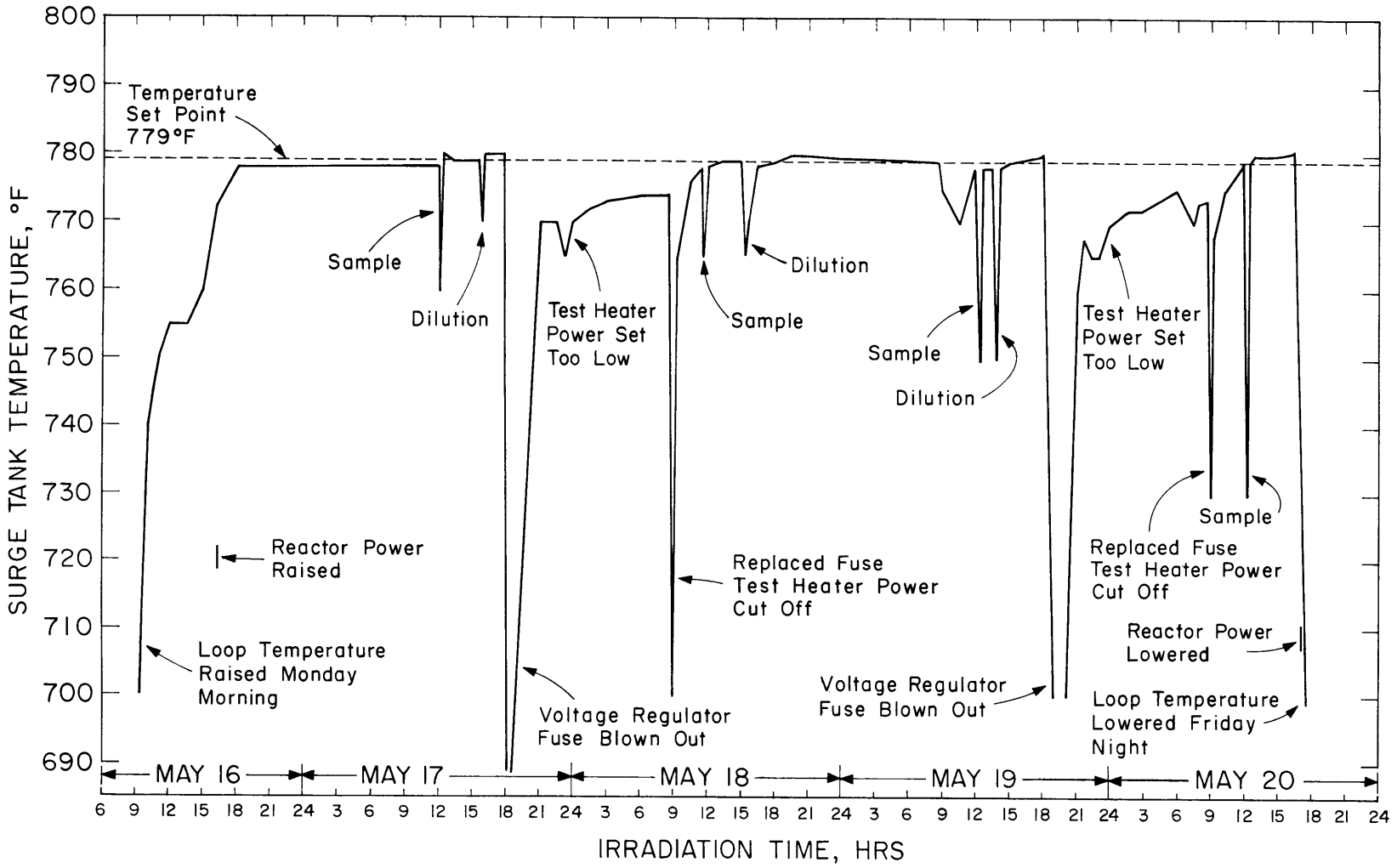

FIGURE A2.5 SURGE TANK TEMPERATURE PROFILE, WEEK OF MAY 16 - MAY 20, 1966
RUN 18B - IRRADIATION CAPSULE AT 800°F

to prevent such overshoots.

The fluctuations in the organic coolant temperature during Run 9 and Run 18B, as measured by the immersion thermocouple in the surge tank (shown in Figures A2.3, A2.4, and A2.5), have been analyzed to determine the effect of these fluctuations upon the radiopyrolysis rate (or the "effective" loop temperature) during these steady-state irradiations. The method used to evaluate the effect of temperature fluctuations on the radiopyrolysis rate was the following:

(1) The temperature profiles in the surge tank during the periods investigated for Run 9 and Run 18B were divided into temperature intervals of 2°F, and the percent of time ($\Delta t_i/t$) the surge tank temperature, T_i, spent in each interval was determined.

(2) The radiopyrolysis rate constant (relative to the radiopyrolysis rate constant at the set point for Run 9, 782°F) was determined for the mid-point temperature of each 2°F temperature interval. An activation energy of radiopyrolysis for total terphenyl, ΔE_P, of 40 k-cal/mole for these irradiations at 52% terphenyl was assumed (see Table 5.4).

(3) These relative radiopyrolysis rate constants ($k_P(T_i)/k_P(T_o)$) were weighted with the percent of time spent within each interval ($\Delta t_i/t$), and these time-weighted rate constants were summed over all intervals. The overall effect of the temperature fluctuations can then be expressed as a factor, f, defined as

$$f = \sum_i f_i = \sum_i \left[\frac{k_{P,i,m}(T_i)}{k_{P,i,m}(T_o)} \frac{\Delta t_i}{t} \right] \qquad \text{(A2.7)}$$

The radiopyrolysis rate constant over the total time interval considered would be the same as if the surge tank temperature had remained at a set point of 782°F for the whole interval if the factor, f, was found to be unity.

Table A2.6 shows the effect of these temperature fluctuations caused by sampling operations and test heater power failures during Run 9 and

Table A2.6

Effect of Fluctuations in Coolant Temperature on the Radiopyrolysis Rate Constant

Temperature Interval	$T_i - T_o$ (°F)	$\frac{k_{P,i,m}(T_i)}{k_{P,i,m}(T_o)}$	Run 9 June 29-July 2, 1964 $\frac{\Delta t_i}{t}$ [d]	Run 9 June 29-July 2, 1964 f_i [e]	Run 18B May 16-May 20, 1966 $\frac{\Delta t_i}{t}$ [d]	Run 18B May 16-May 20, 1966 f_i [e]	Run 18B May 30-June 3, 1966 $\frac{\Delta t_i}{t}$ [d]	Run 18B May 30-June 3, 1966 f_i [d]
Above set point:								
790-792	+9	1.20	0.006	0.007	--	--	--	--
788-790	+7	1.15	0.030	0.035	--	--	--	--
786-788	+5	1.10	0.044	0.048	--	--	--	--
784-786	+3	1.06	0.065	0.069	--	--	--	--
Below set point:								
778-780	-3	0.93	0.081	0.075	0.457	0.425	0.064	0.059
776-778	-5	0.88	0.009	0.008	0.114	0.100	0.095	0.084
774-776	-7	0.85	0.013	0.011	0.067	0.057	0.078	0.066
772-774	-9	0.80	0.013	0.010	0.121	0.097	0.105	0.084
770-772	-11	0.77	0.010	0.008	0.080	0.062	0.030	0.023
768-770	-13	0.73	0.010	0.007	0.042	0.031	0.021	0.015
766-768	-15	0.70	0.010	0.007	0.019	0.013	0.005	0.004
764-766	-17	0.66	0.006	0.004	0.014	0.009	0.005	0.003
762-764	-19	0.63	0.006	0.004	0.004	0.003	0.005	0.003
760-762	-21	0.60	0.004	0.002	0.004	0.002	0.005	0.003
758-760	-23	0.58	0.002	0.001	0.002	0.001	0.003	0.002
below 758[a]		0.33	0.011	0.004	0.075	0.025	0.017	0.006
At set point (T_o):								
780-784		1.00	0.680	0.680	0.0[b]	0.00	0.573	0.573
	$f = \sum_i f_i$			0.988		0.825		0.925

[a] Average temperature assumed 740°F.
[b] Set point for this week was 779°F.
[c] Assuming an activation energy $\Delta E_P = 40$ k-cal/mole.
[d] Fraction of time in specified temperature interval.
[e] $f_i = \frac{k_{P,i,m}(T_i)}{k_{P,i,m}(T_o)} \frac{\Delta t_i}{t}$

Run 18B on the relative radiopyrolysis rate constants. For Run 9, the factor f is approximately 0.99, indicating that the temperature fluctuations shown in Figure A2.3 cause a negligible overall effect on the radiopyrolysis rate. This results from the fact that the temperature overshoots partially compensated for the temperature drops and also from the fact that the trim heater was able to bring the surge tank temperature back to the set point rapidly. For the week of May 16 - May 20, 1966, during Run 18B, the factor f is about 0.83, indicating that there was a substantial reduction in the radiopyrolysis rate during this week, caused primarily by the blown fuses in the voltage regulator and the resulting power failure to the test heater. For the period of May 20 - June 3, 1966, during Run 18B, the factor f is about 0.93, indicating that the effective radiopyrolysis rate during this period was about 6% lower than during the period investigated for Run 9. This fact results from a slightly lower set-point temperature for Run 18B (781°F) and the longer time required for the temperature to return to the set point following sampling operations.

APPENDIX A3

CALCULATION OF DEGRADATION RESULTS AND STATISTICS FOR M.I.T. IRRADIATIONS IN FUEL POSITION 20

A3.1 General Degradation Rate Equation

The total terphenyl degradation rate can be obtained from a terphenyl material balance of the coolant system under consideration. This material balance is illustrated in the following diagram:

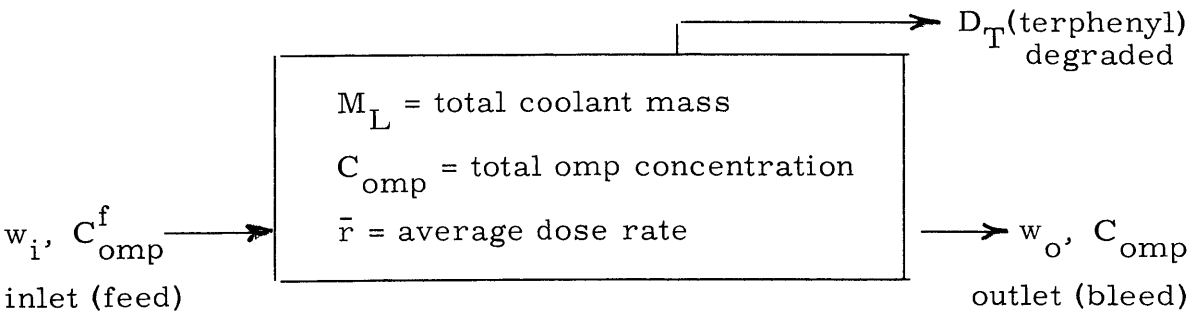

Coolant System

where

w_i = inlet coolant feed rate, gms/hr

w_o = outlet coolant bleed rate, gms/hr

C^f_{omp} = total terphenyl concentration in the feed, wt. fraction

C_{omp} = total terphenyl concentration in the coolant system, wt. fraction

The coolant system is assumed to be well mixed so that the terphenyl concentration in the bleed stream is equal to that in the system.

For terphenyl, the material balance is

$$\text{Accumulation} = \text{Feed Rate} - \text{Bleed Rate} - \text{Degradation} \tag{A3.1}$$

or

$$\frac{d(M_L C_{omp})}{dt} = M_L\left(\frac{dC_{omp}}{dt}\right) + C_{omp}\left(\frac{dM_L}{dt}\right) = w_i C^f_{omp} - w_o C_{omp} - D_T \quad \text{(gms/hr)} \tag{A3.2}$$

The terphenyl degradation rate, D_T, is the sum of the radiolysis and radiopyrolysis contributions in grams/hr and can be expressed as

$$D_T = \left[k_{R,omp,n} C^n_{omp}\left(\frac{d\tau}{dt}\right) + k_{P,omp,m} C^m_{omp}\right] M_L \tag{A3.3}$$

or in terms of a G value

$$\frac{D_T}{\bar{r} M_L} = \frac{G(-omp)}{11.65} \quad \text{(gms/watt-hr)} \tag{A3.4}$$

where

$G(-omp)$ = molecules of terphenyl degraded/100 ev

11.65 = conversion factor, (molecules)(watt-hr)/(gram)(100 ev)

$\bar{r}$ = average specific dose rate in M_L = $d\tau/dt$, watts/gm

τ = specific dose, watt-hr/gm

M_L = coolant mass in the system, grams

$\bar{r} M_L$ = rate of energy deposition in the total coolant, watts

Neglecting the small amount of terphenyl converted into gases, a material balance on the total mass requires that

$$w_i - w_o = \frac{dM_L}{dt} \tag{A3.5}$$

Combining Equations (A3.2), (A3.3), (A3.4), and (A3.5), the following relation is obtained

$$\frac{w_i}{\bar{r} M_L}(C^f_{omp} - C_{omp}) - \frac{dC_{omp}}{d\tau} = k_{R,omp,n} C^n_{omp} + \frac{k_{P,omp,m}}{\bar{r}} C^m_{omp} = \frac{G(-omp)}{11.65} \tag{A3.6}$$

which is the general degradation rate equation for total terphenyl.

For steady-state runs, $dC_{omp}/d\tau$ is zero and

$$\frac{w_i}{\bar{r}M_L}(C^f_{omp}-C_{omp}) = k_{R,omp,n}C^n_{omp} + \frac{k_{P,omp,m}}{\bar{r}}C^m_{omp} = \frac{G(-omp)}{11.65} \tag{A3.7}$$

For transient runs, w_i is zero and

$$-\left(\frac{dC_{omp}}{d\tau}\right) = k_{R,omp,n}C^n_{omp} + \frac{k_{P,omp,m}}{\bar{r}}C^m_{omp} = \frac{G(-omp)}{11.65} \tag{A3.8}$$

A3.2 Method of Calculating Degradation Rates for Steady-State Runs

A3.2.1 Method of Calculating G and G^* Values

The G and G^* values for steady-state runs at M.I.T. are determined by Equations (A3.9) and (A3.10):

$$G(-i) = \frac{11.65W_i}{F\rho(MWH)} \frac{\text{molecules of i degraded}}{\text{100 ev absorbed in total coolant}} \tag{A3.9}$$

$$G^*(-i) = \frac{G(-i)}{C_i} \frac{\text{molecules of i degraded/100 ev absorbed in total coolant}}{\text{weight fraction i in coolant}} \tag{A3.10}$$

where

$G(-i)$ = G value for the disappearance of total terphenyl, terphenyl isomer, or for the production of HB

W_i = total mass of terphenyl or terphenyl isomer degraded, or HB produced, gms

F = total in-pile dose rate factor, watt-cc/MW-gm

ρ = density of coolant at irradiation temperature, gms/cc

(MWH) = length of steady-state irradiation, reactor megawatt-hours

C_i = average concentration of total terphenyl or terphenyl isomer, or HB, weight fraction

During steady-state loop operation, coolant samples are removed from the circulating coolant mass in the loop and distilled to remove the high boiling constituents. Fresh makeup terphenyl, approximately equal to the weight of high boiler removed, is added to the distillate and the distillate plus fresh makeup is returned to the circulating mass of coolant in the loop. Sampling cycle times and sample sizes are adjusted in order to maintain, as nearly as possible, a constant terphenyl concentration and coolant mass throughout the run. Each coolant sample removed from the loop and each returned to the loop is analyzed at least four times by vapor phase chromatography (VPC) for the biphenyl, ortho, meta, and para terphenyl concentrations. The concentration of high boiler (HB) in the samples removed is determined by distillation. The LIB concentration is then defined as (100 - % omp - % HB).

The total mass of terphenyl (or any terphenyl isomer) degraded, or HB produced, is the sum of the net terphenyl mass (net makeup) added or HB removed during the steady-state period and the change in the terphenyl mass or HB (Δ) circulating in the loop as expressed by Equation (A3.11) (see also Equation (A3.2)).

$$W_i = (\text{net makeup})_i + (\Delta)_i$$

$$= \int w_i\left(C_i^f - C_i\right) dt + \int \frac{d(M_L C_i)}{dt}\, dt \qquad \text{(A3.11)}$$

For the case where coolant feed and removal is not continuous but is accomplished by intermittent sampling, the net makeup is determined by the terphenyl or HB concentration and mass of the samples removed from the loop and returned to the loop.

$$(\text{net makeup})_i = \sum_j M_j C_{i,j}(\text{samples returned})$$

$$- \sum_j M_j C_{i,j}(\text{samples removed}) \qquad \text{(A3.12)}$$

where

M_j = mass of the j^{th} sample removed from or returned to the loop, gms

$C_{i,j}$ = concentration of the i^{th} component in the j^{th} sample, weight fraction

An exact steady-state condition may not be achieved during a finite "steady-state" period, and the Δ correction is required to account for small changes in the coolant composition in the loop during these periods. The Δ correction is determined from the circulating coolant mass in the loop at the beginning and end of steady-state and the respective terphenyl, or HB, concentrations at these times.

$$\Delta_i = M_{loop}\, C_i(\text{beginning steady-state}) - M_{loop}\, C_i(\text{end steady-state}) \qquad \text{(A3.13)}$$

Since the circulating coolant mass and terphenyl concentration do not vary appreciably during the run, the following approximation may be made:

$$\Delta = M_{loop}(\delta C) + C(\delta M)_{loop} \qquad \text{(A3.14)}$$

where

M_{loop} = average circulating coolant mass in the loop during steady-state, gms

δC = change in terphenyl concentration $(C_1 - C_2)$ during steady-state, weight fraction

C = average terphenyl concentration during steady-state, weight fraction

δM = change in circulating coolant mass $(M_1 - M_2)$, in the loop, gms

Subscript 1 denotes beginning of steady-state.
Subscript 2 denotes end of steady-state.

Under ideal steady-state conditions, both δC and δM are zero and there is no Δ correction. The approximation shown by Equation (A3.14) is not used in calculations of the Δ correction, but this approximation is useful in establishing the statistical errors associated with the Δ correction in Section A3.2.2.

The concentrations of terphenyl used in Equations (A3.12), (A3.13), and (A3.14) are calculated by a least-square fit of all vapor phase chromatograph (VPC) analyses for coolant samples removed from the loop by the following equation:

$$C_{i,j} = a_i + b_i X_j \qquad \text{(A3.15)}$$

where

$C_{i,j}$ = calculated concentration of the i^{th} component of the j^{th} sample determined by least-square-error analysis

X_j = accumulated megawatt-hrs since the beginning of the run at which the j^{th} sample was removed

This least-square fit is employed because the sampling cycle time used may permit a small change in the terphenyl concentration during supposed steady-state operation, and the calculated concentrations using Equation (A3.15) present the best estimate of the sample concentration at any time during the run. The best values of the HB concentration in the coolant samples are also determined by a similar least-square fit of the type shown in Equation (A3.15).

There are two possible methods for determining the best value of the terphenyl concentration, $C_{i,j}$, in the return (distillate plus fresh makeup) samples in Equation (A3.12). A least-square fit of all VPC concentration analyses of return samples (identical to the method used for coolant samples removed from the loop) utilizing Equation (A3.15) can be made. However, since each return sample is prepared independently and the relative proportions of distillate and fresh makeup vary to some extent, a least-square fit of all concentrations does not account for real variations in return sample compositions. Therefore, in this report, the values of $C_{i,j}$ of return samples in Equation (A3.12) are determined from the average concentration of at least four VPC analyses of each individual return sample. In an earlier M. I. T. report (A3.3), the first method described was used.

A3.2.2 Statistical Errors in G Values for Steady-State Runs

The statistical errors in the determination of G values are due to uncertainties in the mass of coolant degraded, W_i, and the dose rate factor, F. (The errors in the coolant density, ρ, and the irradiation time in megawatt-hrs are negligible compared to errors in W_i and F.) Consequently, the variance of G may be expressed by Equation (A3.16).

$$\frac{\sigma^2(G)_i}{G_i^2} = \frac{\sigma^2(W)_i}{W_i^2} + \frac{\sigma^2(F)}{F^2} \qquad \text{(A3.16)}$$

Since the uncertainty in the G value is much greater than the uncertainty in the concentration, $\sigma(G_i^*) / G_i^* \approx \sigma(G)_i / G_i$.

From Equation (A3.11), the variance in W_i may be written:

$$\sigma^2(W)_i = \sigma^2(\text{net makeup})_i + \sigma^2(\Delta)_i \qquad \text{(A3.17)}$$

In this expression, the variance of the net makeup is

$$\sigma^2(\text{net makeup})_i = \sum_j M_j^2 \sigma^2(C_{i,j}) \text{ samples returned}$$

$$+ \sum_j M_j^2 \sigma^2(C_{i,j}) \text{ samples removed} \qquad \text{(A3.18)}$$

since the relative error in the mass of the samples is much less than the relative error in the concentrations.

It was noted in Section A3.2.1 that the best values of the coolant concentration, $C_{i,j}$ in the equation for the net makeup (Equation (A3.12)) are determined by a least-square fit for all samples removed from the loop. However, the concentrations of samples returned to the loop during steady-state in Equation (A3.12) are determined by taking the average value for multiple (at least four) analyses of each individual sample returned. The statistical errors associated with the concentrations of the samples returned to the loop are calculated as the standard deviation of all the analyses of each sample from the average value for the sample, as shown in Equation (A3.19).

$$\sigma^2(C_{i,j}) \text{ return samples} = \frac{\sum_N (C_i - \bar{C}_i)_j^2}{(N-1)^2} \qquad \text{(A3.19)}$$

where

C_i is the concentration of the i^{th} component in the j^{th} sample determined in a single analysis

$\bar{C}_i$ is the average concentration of the i^{th} component in the j^{th} sample for N sample analyses

N is the number of separate VPC chromatograph analyses performed on the j^{th} sample

Because the term δM is small compared to the coolant mass in the loop, M_{loop}, in Equation (A3.14) and because the uncertainty in the concentration change, δC, is the same order of magnitude as the uncertainty in the concentration, the major source of uncertainty in the Δ correction is in the term, $M_{loop}(\delta C)$, in this equation. Therefore,

$$\frac{\sigma^2(\Delta)}{\Delta^2} \cong \frac{\sigma^2(M_{loop})}{M_{loop}^2} + \frac{\sigma^2(C_1-C_2)}{(C_1-C_2)^2} \qquad \text{(A3.20)}$$

where

C_1 = concentration of total terphenyl, terphenyl isomer, or HB, at the beginning of steady-state, weight fraction

C_2 = concentration of total terphenyl, terphenyl isomer, or HB, at the end of steady-state, weight fraction

In Appendix A2, it is shown that the maximum uncertainty in the circulating coolant mass in the loop is about ±300 grams, and for statistical analysis, it is assumed that one standard deviation in M_{loop} is 150 gms (about 2.7% of the total circulating coolant mass). The circulating coolant mass, therefore, is known to about ±3%, but where the concentration change during steady-state, $C_1 - C_2$, is small (0% to 3%), the relative uncertainty in the concentration change may be ±100%. To a good approximation, therefore,

$$\sigma^2(\Delta) = M_{loop,1}^2\sigma^2(C_1) + M_{loop,2}^2\sigma^2(C_2) \qquad \text{(A3.21)}$$

From Equations (A3.17), (A3.18), and (A3.19), it can be seen that the variance in the mass of terphenyl degraded is determined by the variance in the calculated concentration of terphenyl. By linear regression analysis, Hald (A3.1) has shown that the variance of the calculated value of the j^{th} sample is

$$\sigma^2(C_{i,j}) = \sigma^2(a_i') + \sigma^2(b_i)(X_j-\overline{X})^2 \qquad \text{(A3.22)}$$

where

$C_{i,j}$ = calculated concentration of the i^{th} component of the j^{th} sample determined by least-square-error analysis, weight fraction

$\sigma^2(a_i')$ = variance of the intercept, a_i'

$\sigma^2(b_i)$ = variance of the slope, b_i

X_j = independent variable, in this case, $(MWH)_j$

$\overline{X}$ = weighted mean of the X_j values

$a_i' = a_i + b_i\overline{X}$

As shown by Sawyer and Mason (A3.2), the weighting factor, W_j, for each data point is the reciprocal of the variance of the j^{th} data point from the calculated least-square fit.

$$W_j = \frac{1}{\sigma^2(Y_j)} \tag{A3.23}$$

where Y_j is a transformed concentration variable (see Section A3.3.2). For the correlation shown by Equation (A3.15), which is a zero kinetics order equation, this variable is simply the terphenyl concentration, $C_{i,j}$, and the weighting factor is the reciprocal of the variance of the measured concentration of the j^{th} sample from the least-square calculated concentration.

$$W_j = \frac{1}{\sigma^2(C_j)} \tag{A3.24}$$

The weighted mean of the X_j values is then

$$\overline{X} = \frac{\sum W_j X_j}{W_j} \tag{A3.25}$$

Sawyer and Mason (A3.2) describe a computer program, MNDEG, which has been used for the least-square error analysis of coolant samples removed from the loop, using another form of Equation (A3.22), as shown below.

$$\sigma^2(C_{i,j}) = \sigma^2(a_i) + X_j(X_j - 2\overline{X})\,\sigma^2(b_i) \tag{A3.26}$$

This computer program determines the constants a_i, b_i, $\sigma(a_i)$, $\sigma(b_i)$, $\overline{X}$, and the 95% confidence limits on $C_{i,j}$, calculated with the aid of Student's t for (N-2) degrees of freedom, where N is the total number

of individual analyses on the chromatograph for all samples in the least-square-error analysis (i. e., all samples removed from the loop during steady-state).

$$\text{confidence limits} = \pm tX(\text{standard deviation}) \qquad \text{(A3.27)}$$

It is apparent from Equation (A3.22) that the variance of the calculated concentration for the coolant is minimal at a sampling time corresponding to the weighted mean of the MWH range and is maximal at the extremes of the MWH range (the beginning and end of steady-state). This fact is illustrated in Figure A3.1 which shows all the individual VPC analyses for total omp concentration for samples removed from the loop during the steady-state period of Run 17. The least-square fit of these data, according to Equation (A3.15), is shown along with the 95% confidence limits on the calculated (least-square) concentration curve. Since the variance of the Δ correction as shown by Equation (A3.20) depends on the variance of the concentration at the beginning and end of steady-state, samples removed at these extremes are generally analyzed by vapor phase chromatography 10 to 20 times in order to reduce the uncertainties in the Δ correction. The statistical errors in the net makeup term in Equation (A3.17) are usually only 10-20% as large as the statistical errors in the Δ correction term for the degradation calculations of a typical M. I. T. steady-state run.

A3.3 Method of Calculating Degradation Rates for Transient Runs

A3.3.1 Method of Calculating the Rate Constants, K and K'

In a transient run, small (approximately 25 gram) samples are removed periodically (without organic makeup) in order to determine the coolant composition along the transient, resulting in a small decrease in the circulating coolant mass from the beginning to the end of the transient run as well as the decrease in terphenyl concentration. This different method of operation from the steady-state runs requires some modification of the data analysis and interpretation for transient irradiations from the procedure described in Appendix A3.2 for steady-state runs.

Since the G value is a function of terphenyl concentration and therefore changes continuously throughout a transient run, it is more

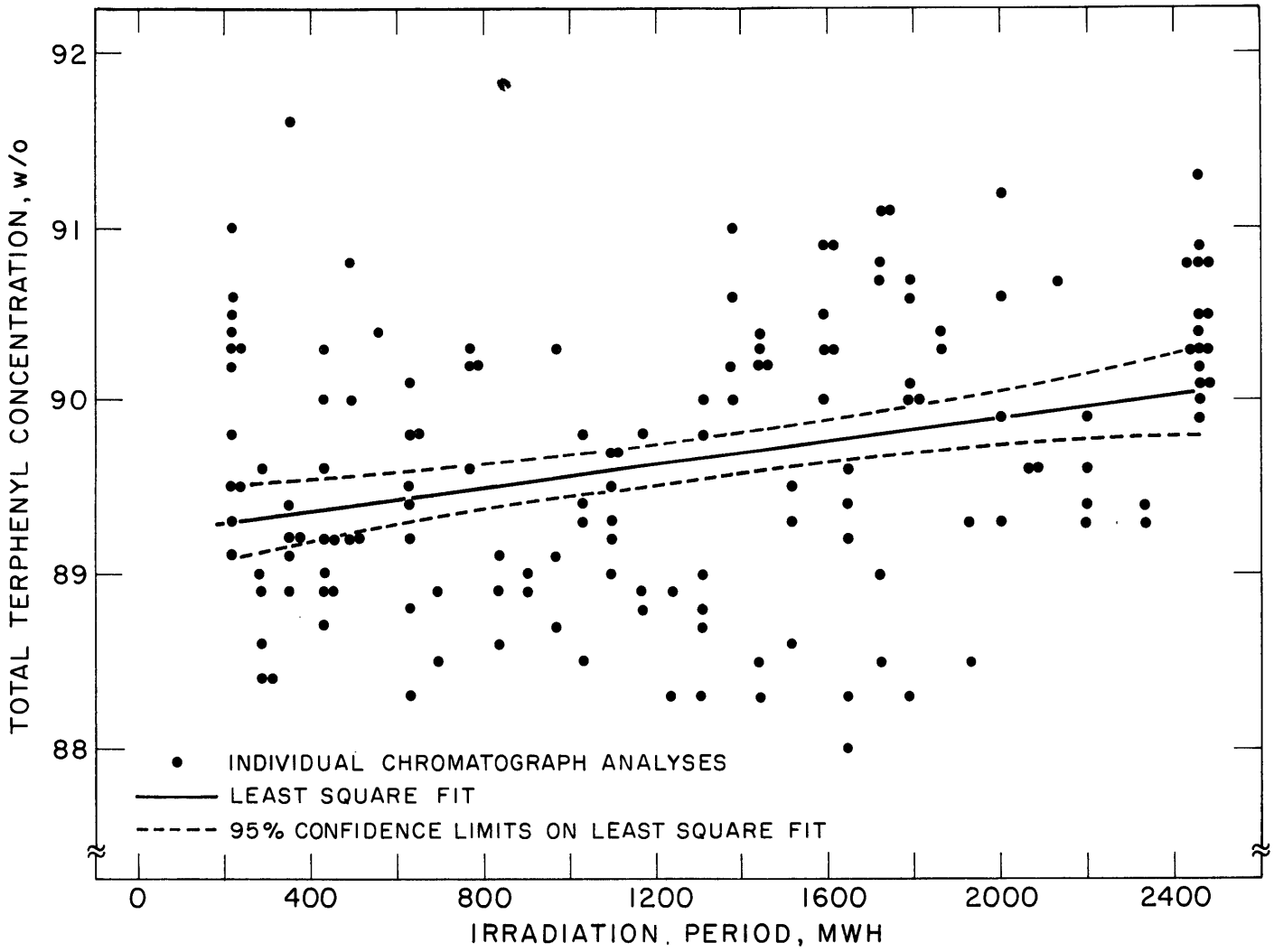

FIGURE A3.1 LEAST SQUARE FIT OF TERPHENYL CONCENTRATION VS MEGAWATT-HOURS RUN 17, STEADY-STATE-IRRADIATION CAPSULE AT 572°F (300°C)

convenient to describe the degradation results of transient irradiations by overall kinetics rate constants rather than by G values. The rate of terphenyl disappearance can be expressed as a function of radiation dose (watt-hr/gram) or time (hours), as shown below.

n^{th}-order kinetics

$$-\frac{dC_i}{d\tau} = K_{i,n}C_i^n \quad (\text{watt-hr/gm})^{-1} \tag{A3.28}$$

or

$$-\frac{dC_i}{dt} = K'_{i,n}C_i^n \quad (\text{hr})^{-1} \tag{A3.29}$$

where

$K_{i,n}$ = n^{th}-order overall rate constant for total terphenyl (or terphenyl isomer, i) disappearance based on radiation dose, $(\text{watt-hr/gm})^{-1}$

$K'_{i,n}$ = n^{th}-order overall rate constant for total terphenyl (or terphenyl isomer, i) disappearance based on irradiation time, $(\text{hr})^{-1}$

The overall rate constants for transient runs, $K_{i,n}$ and $K'_{i,n}$, are determined by a least-square fit of concentration versus specific dose or concentration versus time data, using the MNDEG computer program as described by Sawyer and Mason (A3.2). This computer program can (1) accept concentration versus specific dose or time data as input, or (2) accept concentration versus MWH data as input and then calculate the dose from Equation (A3.30),

$$\tau_{j+1} - \tau_j = \frac{\overline{F\rho}(MWH_{j+1} - MWH_j)}{M_j} \tag{A3.30}$$

where

$\overline{F}$ is the average dose rate factor for the in-pile section for the period $MWH_j + MWH_{j+1}$

$\bar{\rho}$ is the average density during this period, gms/cc

M_j is the mass of circulating coolant in the loop

j refers to the j^{th} sample

j+1 refers to the $j+1^{st}$ sample

The coolant densities in Equation (A3.30) are determined by MNDEG by interpolation using input density data, $\rho(MWH, T)$, using the values of $\rho(\%HB, T)$ shown in Chapter 3. The transient run data of other laboratories are usually published as concentrations versus specific dose and therefore the first method is used for these data. The M.I.T. transient run data are interpreted by the second method.

It has been a common practice of most laboratories to use correlations like Equations (A3.28) and (A3.29), assuming first- and second-order kinetics (n=1 and n=2), to smooth out the concentration versus dose curves for transient runs. It should be recognized that the first-order overall rate constant obtained from Equation (A3.28) is related to $G^*(-i)$ by

$$G^*(-i) = 11.65\ K_{i,1} \qquad \text{(A3.31)}$$

where $K_{i,1}$ is the first-order overall rate constant. $G^*(-i)$ values have been used by different laboratories to express the results of transient irradiations, since G^* for a transient run is a constant if the irradiation results are interpreted by first-order kinetics. As pointed out by Sawyer and Mason (A3.2) and shown in Section A3.4 of this report, it is generally impossible to show that either zero-, first-, or second-order kinetics (or some non-integer order) will provide the best correlation for transient irradiation data.

For low temperature irradiations (below 350°C) where radiolysis is the only phenomenon producing coolant degradation, it is clearly advantageous to correlate the transient irradiation results based on the dose, since at low temperature the overall rate constant, $K_{i,n}$, is identical to the rate constant for radiolysis $k_{R,i,n}$. However, for high temperature irradiations with low average dose rates, thermal decomposition (radiopyrolysis) can be the predominant form of coolant degradation, and it is useful to also correlate the transient irradiation results based on the time the coolant is irradiated at high temperature. Under these conditions (where radiolysis is a small contribution to the total coolant degradation rate), the overall rate constant, $K'_{i,n}$ $(hr)^{-1}$, approaches the average value of the radiopyrolysis rate constant, $k_{P,i,m}$, for the transient, when the same kinetics order is used to define both rate constants (i.e., n=m).

For irradiations at a constant average dose rate, $\bar{r}$, these different rate constants are related in the following manner.

$$\bar{r} = \frac{d\tau}{dt} \quad \text{(watts/gm)} \tag{A3.32}$$

$$K'_{i,n} = \bar{r} K_{i,n} \quad (\text{hr})^{-1} \tag{A3.33}$$

However, for Run 15, in which the average dose rate increased by a factor of about two during the irradiation (due to an increase in reactor power), no such simple conversion between K and K′ exists.

A3.3.2 Methods of Calculating Statistical Errors in Transient Runs

Equations (A3.28) and (A3.29), which are used to correlate the transient run results, can be integrated to yield

$$\begin{matrix} -K_{i,n}\tau + a_1 \\ \text{or} \\ -K'_{i,n}t + a_2 \end{matrix} = \begin{cases} \dfrac{C_i^{1-n}}{1-n} & n \neq 1 \\ \ln C_i & n = 1 \end{cases} \tag{A3.34}$$

where a_1 and a_2 are constants of integration. These linear relations between τ (or t) and a transformed concentration variable allow the experimental data to be treated by the method of weighted least-squares, as described by Sawyer and Mason (A1.2). In this least-square-error analysis, made by utilizing the MNDEG computer program, only statistical errors in the dependent variable (i. e., the transformed concentration variable) are considered. The dependent variable (specific dose τ, or irradiation time t) is considered to be exact in this computer analysis. This is a good approximation if the irradiation time is the independent variable, but it does not take into account statistical errors in the dose rate if τ is the independent variable.

The general form of the correlating equation is

$$Y = a + b\tau \tag{A3.35}$$

or

$$Y = a + bt \tag{A3.36}$$

where

Y is the transformed concentration variable

a is the intercept

b is the slope

The MNDEG computer program calculates the one standard deviation (σ) error limits on the constants a and b. For correlations based on concentration versus time data, the variance in the slope b is equal to the variance of K'.

$$\frac{\sigma^2(K')}{K'^2} = \frac{\sigma^2(b)}{b^2} \tag{A3.37}$$

By Equation (A3.37), the variance in K for the correlations based on concentration versus dose is

$$\frac{\sigma^2(K)}{K^2} = \frac{\sigma^2(\bar{r})}{\bar{r}^2} + \frac{\sigma^2(K')}{K'^2} \tag{A3.38}$$

The average dose rate, $\bar{r}$, is calculated from Equation (A3.39).

$$\bar{r} = \frac{F\rho P}{M_{loop}} \quad \text{watts/gm} \tag{A3.39}$$

where

F is the total in-pile dose rate factor, watt-cc/MW-gm

ρ is the coolant density at the irradiation capsule temperature, gm/cc

P is the reactor thermal power, megawatts

M_{loop} is the total circulating mass in the loop, grams

Since the relative errors in the density and reactor power are negligible compared to the relative errors in F and M_{loop},

$$\frac{\sigma^2(\bar{r})}{\bar{r}^2} \approx \frac{\sigma^2(F)}{F^2} + \frac{\sigma^2(M_{loop})}{M_{loop}^2} \tag{A3.40}$$

Combining Equations (A3.37), (A3.38), and (A3.40) gives for the variance of the overall rate constant, K,

$$\frac{\sigma^2(K)}{K^2} = \frac{\sigma^2(b)}{b^2} + \frac{\sigma^2(F)}{F^2} + \frac{\sigma^2(M_{loop})}{M_{loop}^2} \tag{A3.41}$$

In this equation, $\sigma(b)/b$ is found by the least-square-error analysis of the concentration variable (MNDEG computer correlation), $\sigma(F)/F$ is found by statistical error analysis of the dosimetry measurements (Appendix A1), and $\sigma(M_{loop})/M_{loop}$ is estimated from circulating coolant mass calculations based on tritium dilutions and volume calculations (Appendix A2).

A statistical parameter which is useful in comparing various curve fits is the correlation coefficient, R, defined as (A1.2)

$$R^2 = \frac{\sum W_j(Y_j-\bar{y})^2}{\sum W_j(y_j-\bar{y})^2} \qquad \text{(A3.42)}$$

where

Y_j is the least-square calculated value of the transformed concentration variable (see Equations (A3.35) and (A3.36)

y_j is the value of transformed concentration variable determined in a particular chromatograph analysis

$\bar{y}$ is the weighted mean of the transformed concentration variable, as shown in Equation (A3.43) with W_j defined by Equation (A3.23)

$$\bar{y} = \frac{\sum W_j y_j}{\sum W_j} \qquad \text{(A3.43)}$$

A3.4 Degradation Rates Measured in Fuel Position 20

The terphenyl degradation rates of Santowax WR measured in Fuel Position 20 are presented in this section, using the calculation methods described in Section A3.2 for steady-state runs and Section A3.3 for transient runs. The operating conditions and experimental results for these runs are summarized in Table A3.1.

For the transient runs, the experimental data and results for each run are presented in Tables A3.2 through A3.7 and Figures A3.2 through A3.8 which show terphenyl isomer concentrations versus irradiation time (MWH) and/or specific dose. Plots of the total omp concentration versus specific dose are shown in detail with the correlations by various kinetics orders shown for comparison. The overall rate constants, $K_{i,n}$ $(\text{watt-hr/gm})^{-1}$ and $K'_{i,n}$ $(\text{hr})^{-1}$, are summarized for each terphenyl

isomer and for total omp, using selected values of the kinetics order n between zero-order and second-order, depending on the irradiation temperature. For Run 13 (transient), only the overall rate constants, $K\ (wh/g)^{-1}$, were determined because this was a low temperature irradiation.

The results of steady-state runs are presented in Figures A3.9 through A3.12 as plots of terphenyl isomer and HB concentration versus irradiation time (MWH) for the steady-state period of the run. The degradation calculations of G and G^* values are given in Tables A3.8 through A3.11 along with the calculation of statistical error limits for these parameters.

Table A3.1

Summary of Operating Conditi tions and Experimental Results
For Santowax WR Irradiat ions in Fuel Position 20

Run No.	Date mo/day/yr	Type	Temperature °F	Temperature °C	Average Dose Rate watts/gm	% Coolant[a] Processed	% Coolant[a] Degraded	Concentration, w/o total omp	Concentration, w/o DP	Concentration, w/o HB	G(-i) or G(→HB) molecules/100 ev ortho	G(-i) or G(→HB) molecules/100 ev meta	G(-i) or G(→HB) molecules/100 ev para	G(-i) or G(→HB) molecules/100 ev total omp	G(-i) or G(→HB) molecules/100 ev HB	$G^*(-i)^b = G(-i)/C_i$ ortho	$G^*(-i)^b = G(-i)/C_i$ meta	$G^*(-i)^b = G(-i)/C_i$ para	$G^*(-i)^b = G(-i)/C_i$ total omp
14	7/15/65-9/30/65	SS	572	300	0.0066	80	10	84	16	11	0.034	0.115	0.010	0.163	0.151	0.226	0.180	0.200	0.195
16	10/29/65-2/24/66	SS	572	300	0.0158	31	10	63	37	29	0.019	0.074	0.011	0.100	0.091	0.195	0.151	0.265	0.159
17	2/28/66-4/1/66	SS	572	300	0.0158	175	11	90	10	6	0.037	0.126	0.016	0.181	0.168	0.253	0.179	0.340	0.202
18B	5/10/66-6/10/66	SS	800	427	0.0166	69	24	52	48	35	0.093	0.416	0.023	0.532	0.489	1.48	1.00	0.62	1.03
13	5/10/65-7/12/65	Tr	572	300	0.0061	—	8	92-84	6-16	5-11	—	—	—	—	—	0.216	0.179	0.230	0.189
15	10/5/65-10/28/65	Tr	800	427	0.0056-[c] 0.0118	—	25	82-57	18-43	11-30	—	—	—	—	—	2.24	1.56	1.33	1.64
18A	4/6/66-4/29/66	Tr	800	427	0.0161	—	36	90-54	10-46	6-35	—	—	—	—	—	1.54	1.04	0.49	1.07

[a] based on total coolant mass circulating in the loop

[b] $G^*(-i) = 11.65\ K_1(-i)$ for transient runs

[c] reactor power raised from 1.95 MW to 4.00 MW during this run

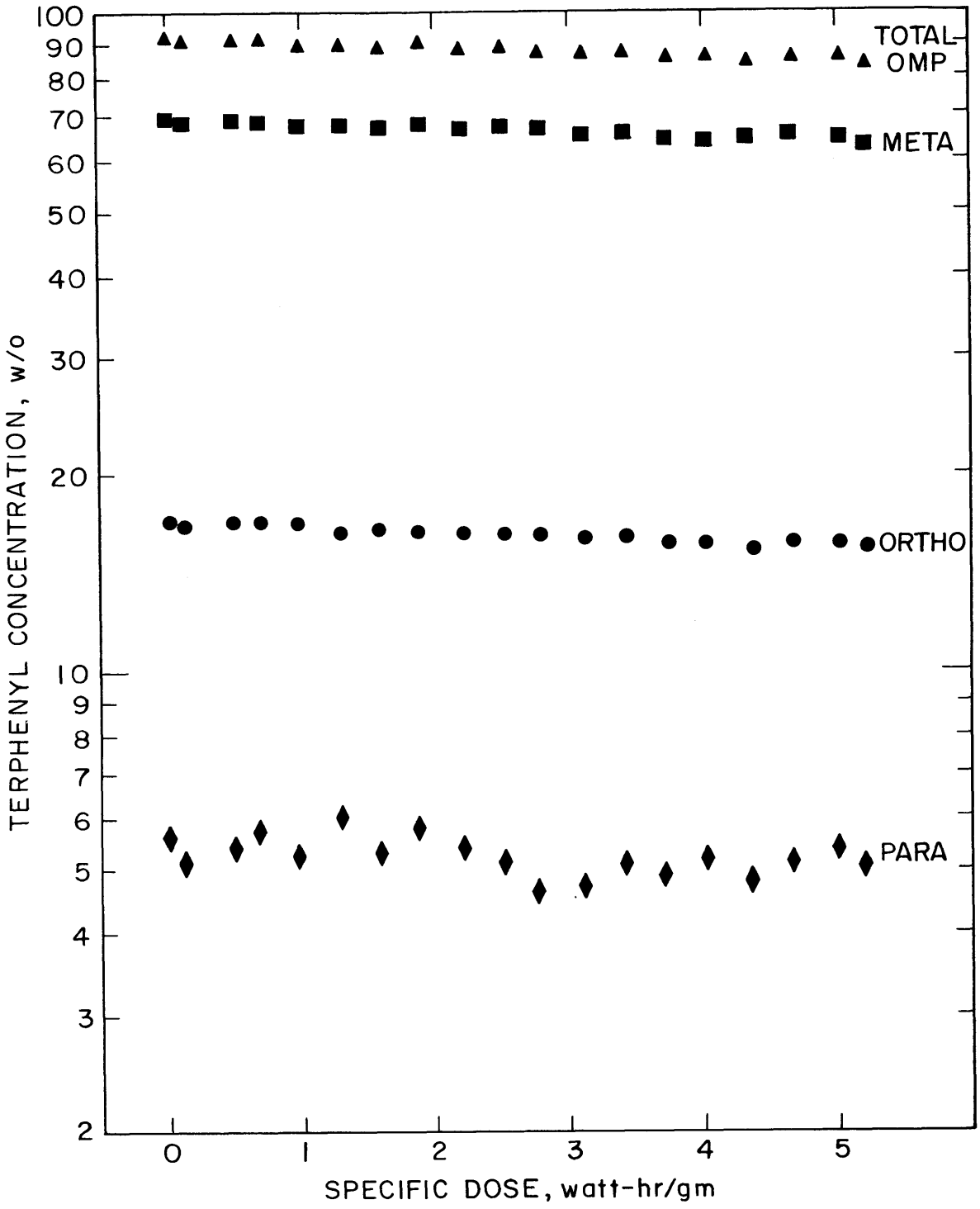

FIGURE A3.2 EFFECT OF SPECIFIC DOSE ON TERPHENYL CONCENTRATION IN LOOP DURING RUN 13, TRANSIENT - 572°F

Table A3.2

Summary of Data for Transient Run 13
Irradiation Capsule at 572°F (300°C)

Sample	Irradiation Period		Dose	Coolant Composition, wt fraction			
	MWH	Hours	watt-hr/gm	ortho terphenyl	meta terphenyl	para terphenyl	total terphenyl
13L-1	160	82	0.0	0.170	0.698	0.056	0.924
13L-2	196	100	0.11	0.168	0.684	0.051	0.903
13L-3	322	165	0.49	0.169	0.690	0.054	0.913
13L-4	388	199	0.69	0.169	0.686	0.057	0.912
13L-5	487	250	0.99	0.169	0.673	0.052	0.894
13L-6	584	300	1.29	0.161	0.677	0.060	0.898
13L-7	683	350	1.59	0.165	0.671	0.053	0.889
13L-8	783	401	1.90	0.163	0.680	0.058	0.901
13L-9	881	452	2.20	0.163	0.666	0.054	0.883
13L-10	978	501	2.50	0.163	0.673	0.051	0.887
13L-11	1072	550	2.80	0.162	0.668	0.046	0.876
13L-12	1172	602	3.11	0.160	0.656	0.047	0.863
13L-13	1274	654	3.43	0.160	0.657	0.051	0.868
13L-14	1367	700	3.72	0.157	0.648	0.049	0.854
13L-15	1466	752	4.04	0.157	0.644	0.052	0.853
13L-16	1566	803	4.37	0.153	0.641	0.048	0.842
13L-17	1666	855	4.69	0.156	0.658	0.051	0.865
13L-18	1768	906	5.02	0.156	0.644	0.054	0.854
13L-19	1829	939	5.21	0.155	0.632	0.051	0.838

[a]Reactor Power = 1.95 MW

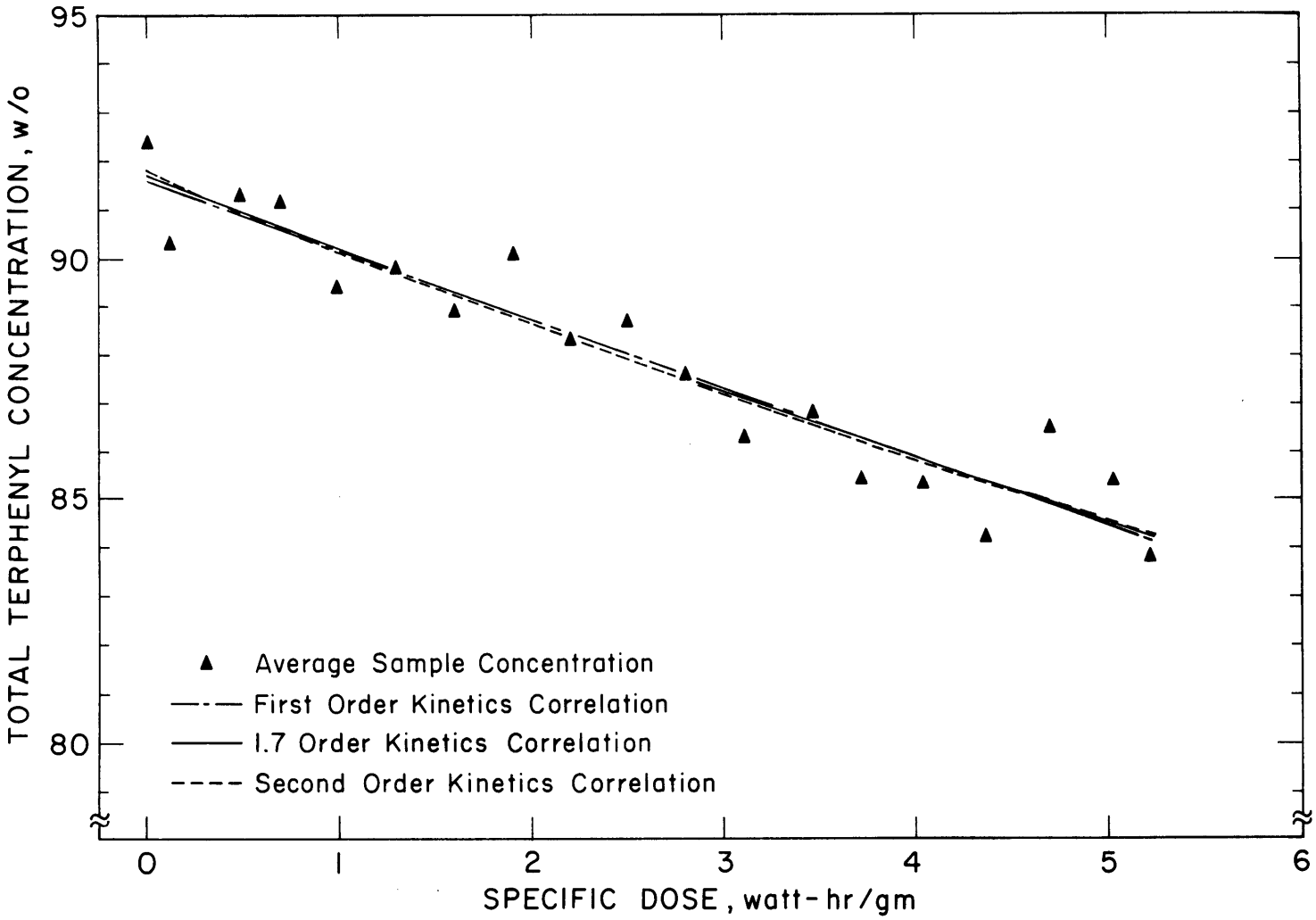

FIGURE A3.3 EFFECT OF SPECIFIC DOSE ON TOTAL TERPHENYL CONCENTRATION RUN 13, TRANSIENT- IRRADIATION CAPSULE AT 572°F (300°C)

Table A3.3

Summary of Data Analysis for Transient Run 13
Irradiation Capsule at 572°F (300°C)

Terphenyl Isomer	Overall Rate Constant,[a] $(wh/g)^{-1}$		
	K_1 (first order)	$K_{1.7}$ (1.7 order)	K_2 (second order)
ortho	0.0186 ±.0017	0.0666 ±.0057	0.115 ±.011
meta	0.0154 ±.0015	0.0204 ±.0020	0.0231 ±.0023
para	0.0198 ±.0089	0.1587 ±.0692	0.3868 ±.1671
total omp	0.0162 ±.0015	0.0177 ±.0016	0.0184 ±.0017
correlation coefficient (total omp)	0.947	0.947	0.947

[a] error limits are 1σ calculated by Equation (A3.28)

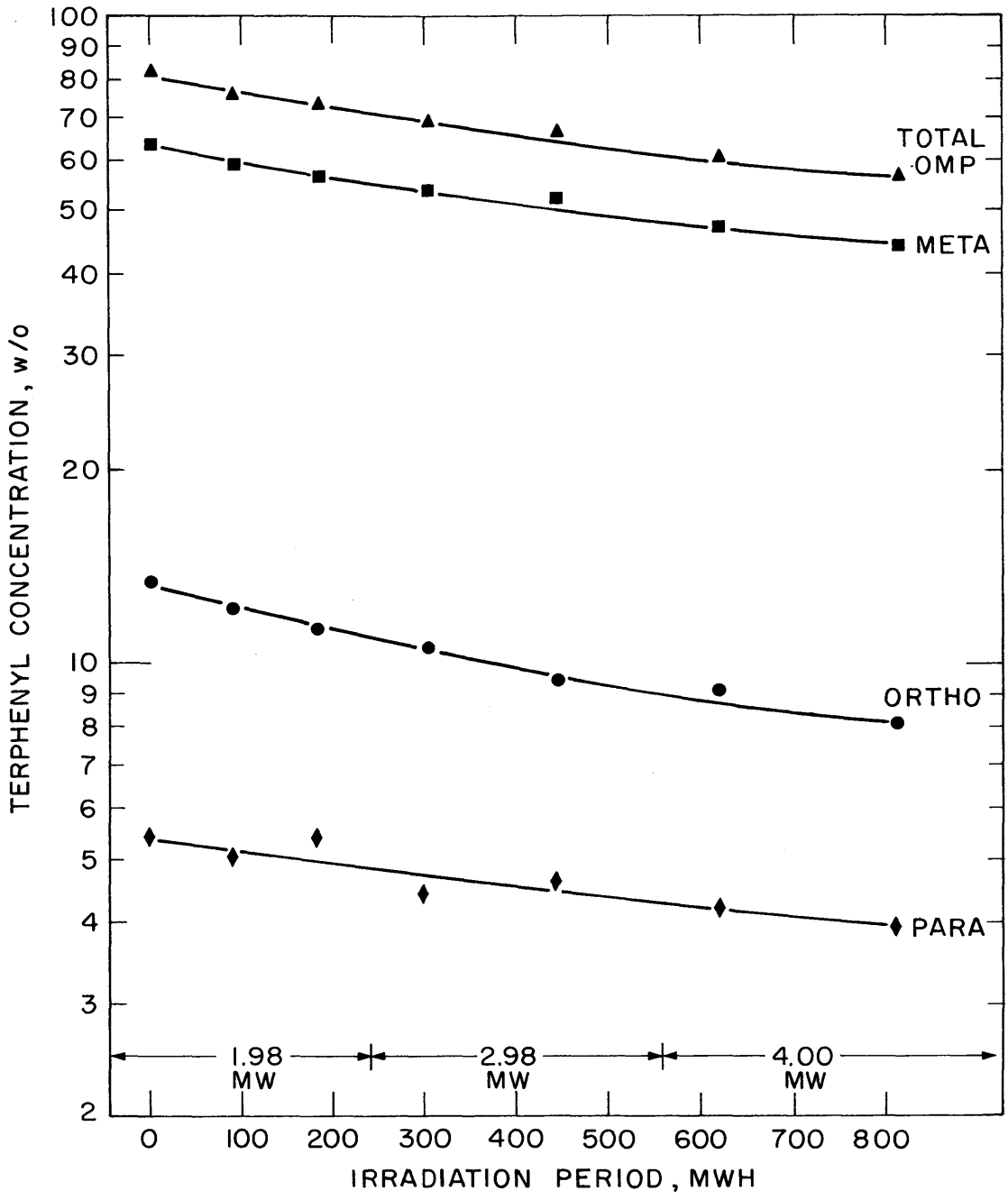

FIGURE A3.4 EFFECT OF IRRADIATION TIME ON TOTAL TERPHENYL CONCENTRATION - RUN 15, IRRADIATION CAPSULE AT 800°F (427°C)

Table A3.4

Summary of Data for Transient Run 15
Irradiation Capsule at 800°F (427°C)

Sample	Irradiation Period		Specific Dose[a]	Coolant Composition, wt fraction[b]				
	MWH	Hours	watt-hr/gm	biphenyl	ortho terphenyl	meta terphenyl	para terphenyl	total terphenyl
15L-1	0	0	0	0.007	0.134	0.635	0.054	0.823
15L-2	88	46	0.26	0.008	0.122	0.587	0.050	0.760
15L-3	180	95	0.53	0.021	0.114	0.561	0.054	0.731
15L-4	302	147	0.89	0.028	0.106	0.535	0.044	0.686
15L-5	443	195	1.31	0.032	0.095	0.523	0.046	0.661
15L-6	618	247	1.84	0.034	0.092	0.474	0.042	0.608
15L-7	810	296	2.42	0.039	0.082	0.449	0.040	0.571

[a] based on M_o = 5479 gms and F = 20.5 watt-cc/MW-gm

[b] average values based on at least four analyses per sample

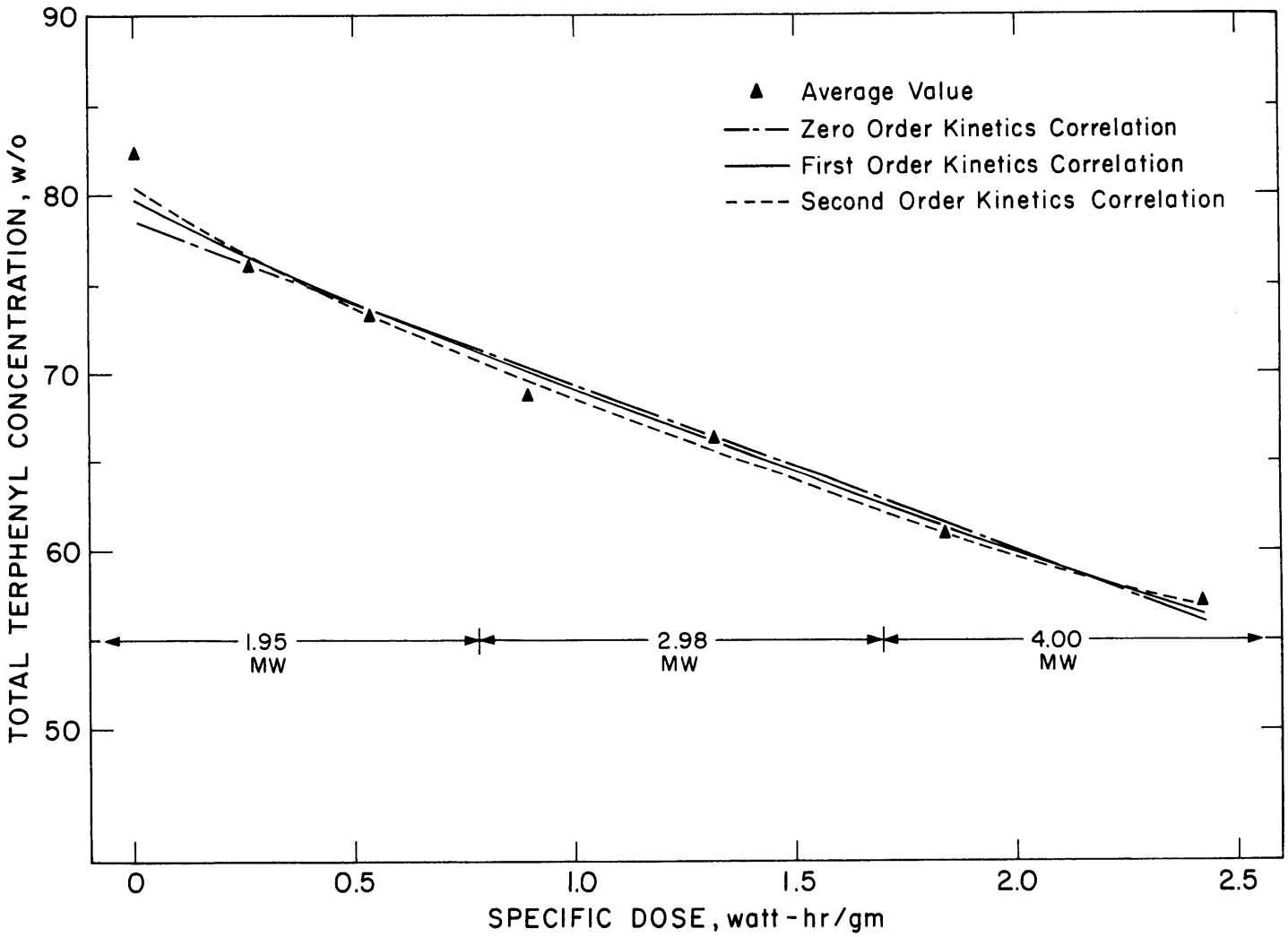

FIGURE A3.5 EFFECT OF SPECIFIC DOSE ON TOTAL TERPHENYL CONCENTRATION RUN 15, IRRADIATION CAPSULE AT 800°F (427°C)

Table A3.5

Summary of Data Analysis for Transient Run 15
Irradiation Capsule at 800°F

Terphenyl Isomer	Overall Rate Constant, $(wh/g)^{-1}$ [a]			Overall Rate Constant, $(hr)^{-1}$ [b]		
	K_0, (zero order)	K_1, (first order)	K_2, (second order)	K_0', (zero order) $(x10^3)$	K_1', (first order) $(x10^3)$	K_2', (second order) $(x10^3)$
ortho	0.0187 ±0.0010	0.192 ±0.011	1.91 ±0.10	0.166 ±0.005	1.61 ±0.04	15.34 ±0.42
meta	0.0688 ±0.0034	0.134 ±0.007	0.261 ±0.013	0.595 ±0.015	1.13 ±0.03	2.11 ±0.06
para	0.0049 ±0.0008	0.114 ±0.017	2.58 ±0.35	0.043 ±0.006	0.96 ±0.13	21.18 ±2.88
total omp	0.0919 ±0.006	0.141 ±0.007	0.213 ±0.011	0.803 ±0.017	1.19 ±0.02	1.74 ±0.04
correlation coefficient (total omp)	0.982	0.988	0.992	0.993	0.994	0.991

[a] error limits are 1σ calculated by Equation (A3.28)

[b] error limits are 1σ calculated by Equation (A3.24)

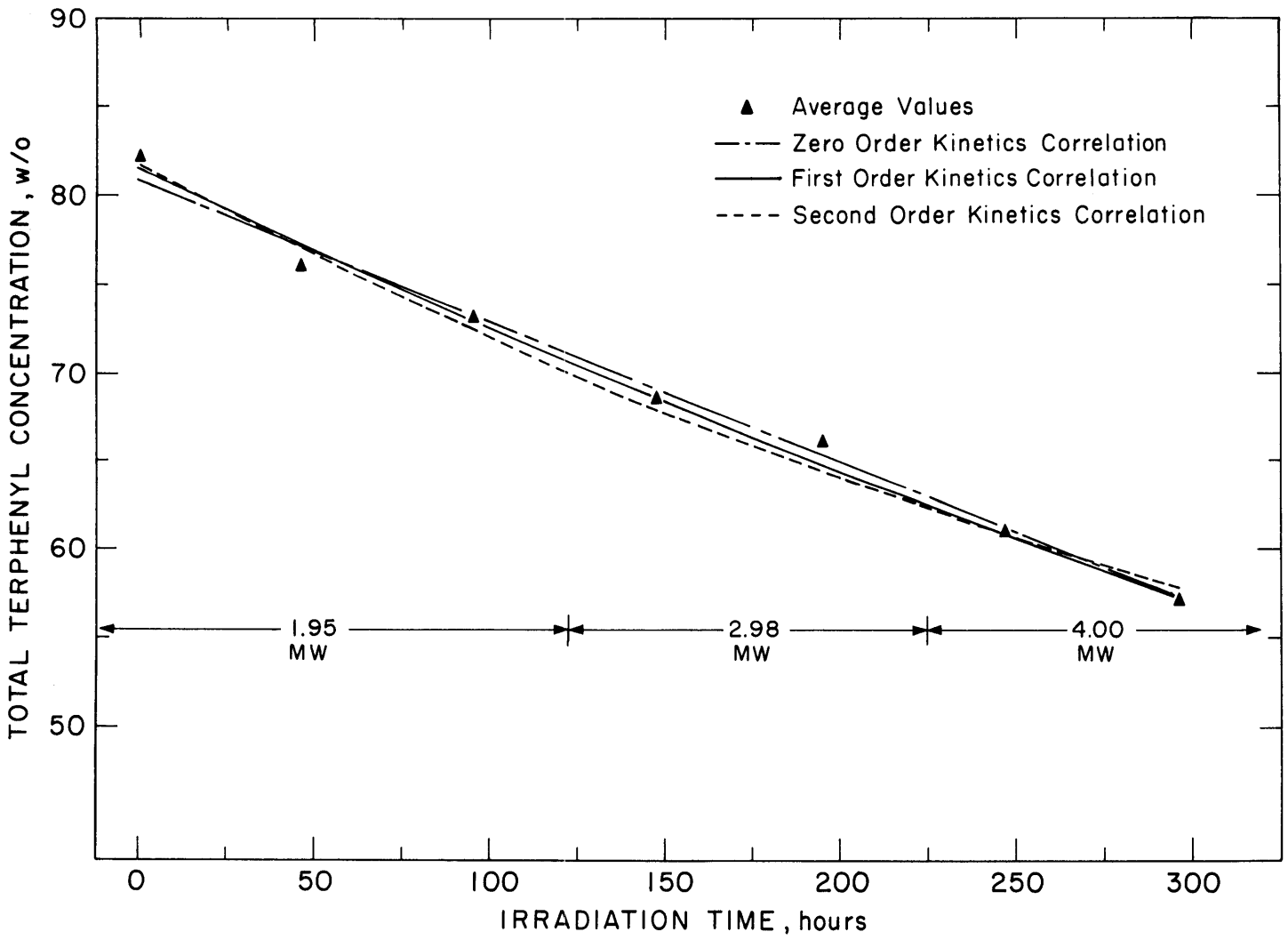

FIGURE A3.6 EFFECT OF IRRADIATION TIME ON TOTAL TERPHENYL CONCENTRATION RUN 15, IRRADIATION CAPSULE AT 800°F

Table A3.6

Summary of Data for Transient Run 18A
Irradiation Capsule at 800°F (427°C)

Sample	Irradiation Period		Specific Dose	Coolant Composition, wt fraction				
	MWH	Hours	watt-hr/gm	biphenyl	ortho terphneyl	meta terphenyl	para terphenyl	total terphenyl
17L-37	2470	0.0	0.0	0.0142	0.145	0.712	0.0488	0.906
18L-1	2680	45.3	0.64	0.0207	0.139	0.677	—	0.856
18L-2	2920	93.4	1.41	0.0273	0.122	0.618	0.0397	0.780
18L-3	3045	119.0	1.83	0.0302	0.118	0.609	0.0454	0.773
18L-4	3400	191.5	2.99	0.0351	0.099	0.546	0.0371	0.682
18L-5	3535	222.0	3.45	0.0362	0.093	0.522	0.0398	0.655
18L-6	4150	346.0	5.57	0.0516	0.071	0.434	0.0381	0.543

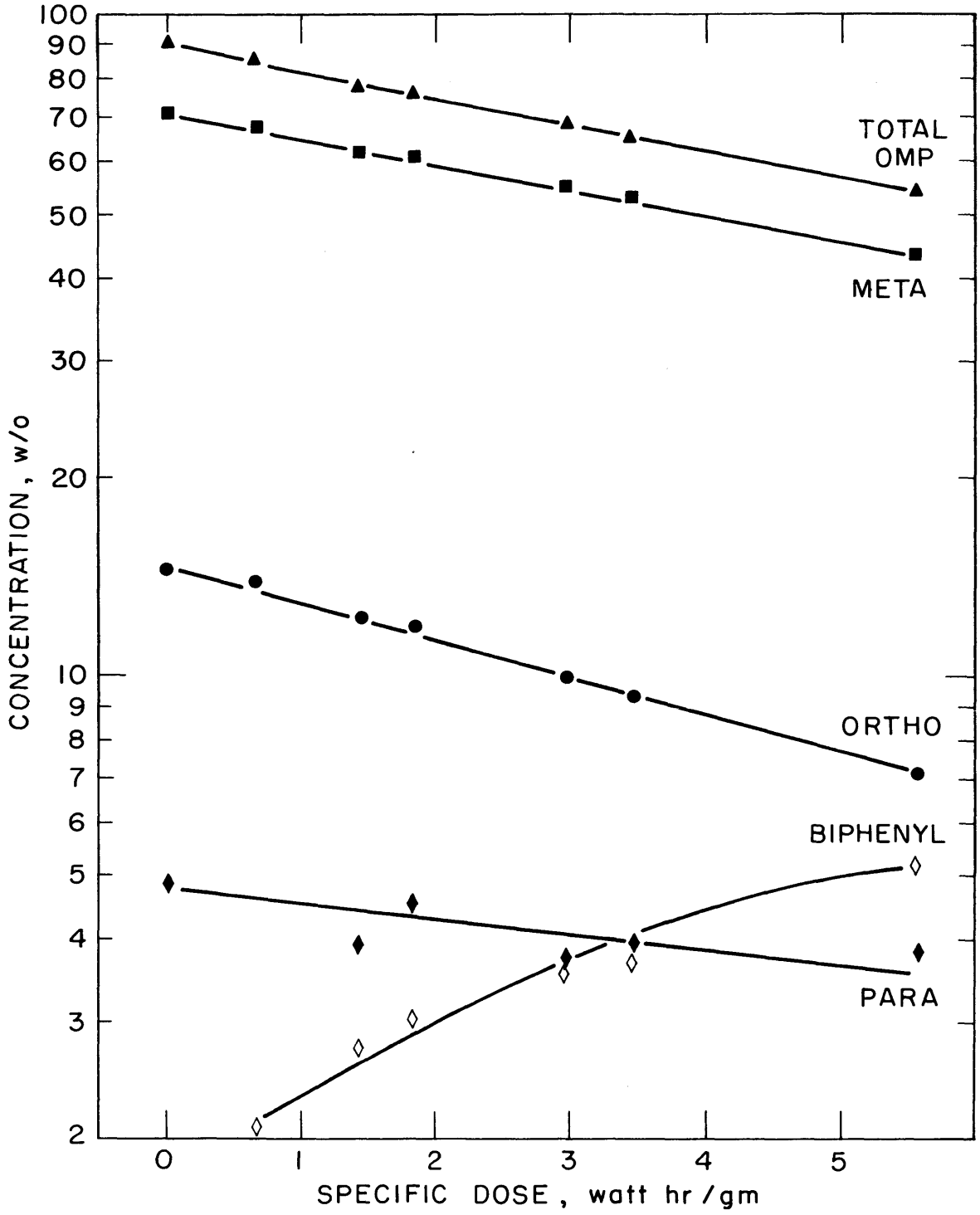

FIGURE A3.7 EFFECT OF SPECIFIC DOSE ON TERPHENYL CONCENTRATION - RUN 18A, TRANSIENT - 800°F

Table A3.7

Summary of Data Analysis for Transient Run 18A
Irradiation Capsule at 800°F

Terphenyl Isomer	Overall Rate Constant, $(wh/g)^{-1}$ [a]			Overall Rate Constant, $(hr)^{-1}$ [b]		
	K_0, (zero order)	K_1, (first order)	K_2, (second order)	K_0', (zero order) $(x10^3)$	K_1', (first order) $(x10^3)$	K_2', (second order) $(x10^3)$
ortho	0.0131 ±.0009	0.1322 ±.0066	1.238 ±.100	0.217 ±0.003	2.058 ±.031	18.32 ±0.61
meta	0.0487 ±.0029	0.0891 ±.0042	0.1576 ±.0092	0.808 ±0.010	1.422 ±.013	2.433 ±.045
para	0.0016 ±.0008	0.0419 ±.0185	1.073 ±0.432	0.0326 ±0.0055	0.813 ±.128	19.47 ±3.02
total omp	0.0633 ±.0041	0.0922 ±.0045	0.1297 ±.0075	1.053 ±0.015	1.475 ±.014	2.002 ±.037
correlation coefficient (total omp)	0.994	0.999	0.996	0.996	0.998	0.994

[a] error limits are 1σ calculated by Equation (A3.28)

[b] error limits are 1σ calculated by Equation (A3.24)

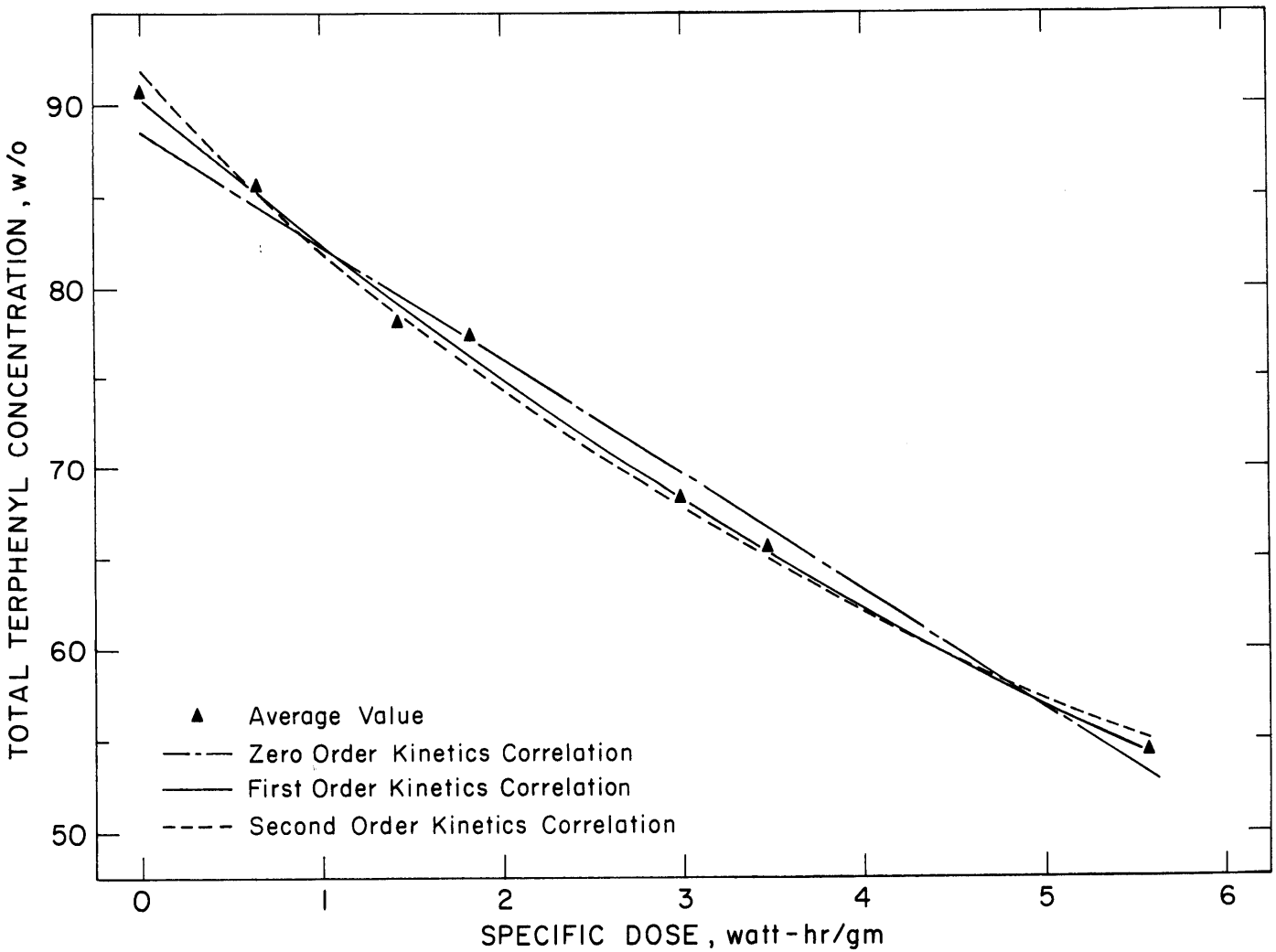

FIGURE A3.8 EFFECT OF SPECIFIC DOSE ON TOTAL TERPHENYL CONCENTRATION RUN 18A, IRRADIATION CAPSULE AT 800°F (427°C)

Table A3.8

Steady-State Run No. 14 Degradation Rate Calculations

Summary

Date: From 7/15/65 To 9/30/65

Irradiation Temp. 572°F Type of Distillation HB

Terphenyl Concentration 83.9 w/o HB Concentration 11.0 w/o

Terphenyl Degraded 536 gms Length of Run 2106 MWH

Average Dose Rate, $\bar{r}$ 0.0066 watts/gm ρ 0.89 gms/cc

In-Pile Dose Rate Factor, F_T^{SW} 20.5 watt-cc/MW-gm

Reactor Power 1.95 MW Fast Neutron Fraction, f_N 0.07

G(-omp) 0.163 σ(G) 0.008

Calculation of G:

	Total Coolant	o-$\emptyset_3$	m-$\emptyset_3$	p-$\emptyset_3$	Total omp	HB
1. Coolant Sample Average Concentration	1.000	0.150	0.638	0.050	0.837	0.110
2. Grams Removed	4320	648	2756	215	3615	-476
3. Return Sample Average Concentration	1.000	0.166	0.728	0.057	0.952	—
4. Grams Returned	4380	726	3789	251	4168	—
5. Net Makeup (4. - 2.)	60	78	433	36	553	-476
6. Initial Concentration, C_1	1.000	0.154	0.636	0.050	0.841	0.109
7. Initial Circulating Mass, M_1	5423	835	3449	271	4561	591
8. Final Concentration, C_2	1.000	0.146	0.639	0.050	0.835	0.112
9. Final Circulating Mass, M_2	5483	801	3504	274	4578	614

Table A3.8 (cont.)

Steady-State Run No. 14 Degradation Rate Calculations

Calculation of G:

	Total Coolant	o-ϕ_3	m-ϕ_3	p-ϕ_3	Total omp	HB
10. Δ Correction (7. - 9.)	-60	34	-55	-3	-17	-23
11. Total Mass Degraded, W (5. + 10.)		112	378	33	536	-499
12. G(-omp), G(-i), G(HB) $11.65/F\rho(MWH) = 3.033 \times 10^{-4}$		0.0340	0.115	0.0100	0.163	0.151
13. G*(-omp) = G(-omp)/C, G*(-i) = G(-i)C_i		0.226	0.180	0.200	0.195	——

Statistics of G Calculation:

MWH_1 = 0 MWH_2 = 2106 σ(F)/F 0.03

	o-ϕ_3	m-ϕ_3	p-ϕ_3	Total omp	HB
14. Intercept, a_i	0.154	0.636	0.0497	0.841	0.108
15. Slope, $b_i \times 10^5$	-0.377	0.122	0.001	-0.281	0.159
16. $\sigma(a_i)$	0.0004	0.001	0.0005	0.003	0.0008
17. $\sigma(b_i)$, $\times 10^4$	0.003	0.010	0.001	0.024	0.007
18. $\sigma^2(C_{initial})$, $\times 10^5$	0.0144	0.147	0.0208	0.726	0.0699
19. $\sigma^2(C_{final})$, $\times 10^5$	0.0188	0.176	0.0278	1.034	0.0728
20. σ^2(Δ correction)	9	89	13	482	39
21. σ^2(net makeup)	1	5	1	12	1
22. σ(W)/W	0.030	0.026	0.110	0.042	0.015
23. σ(G)/G	0.042	0.039	0.111	0.051	0.034
24. σ(G) (23. x 12.)	0.0013	0.0042	0.0011	0.008	0.005

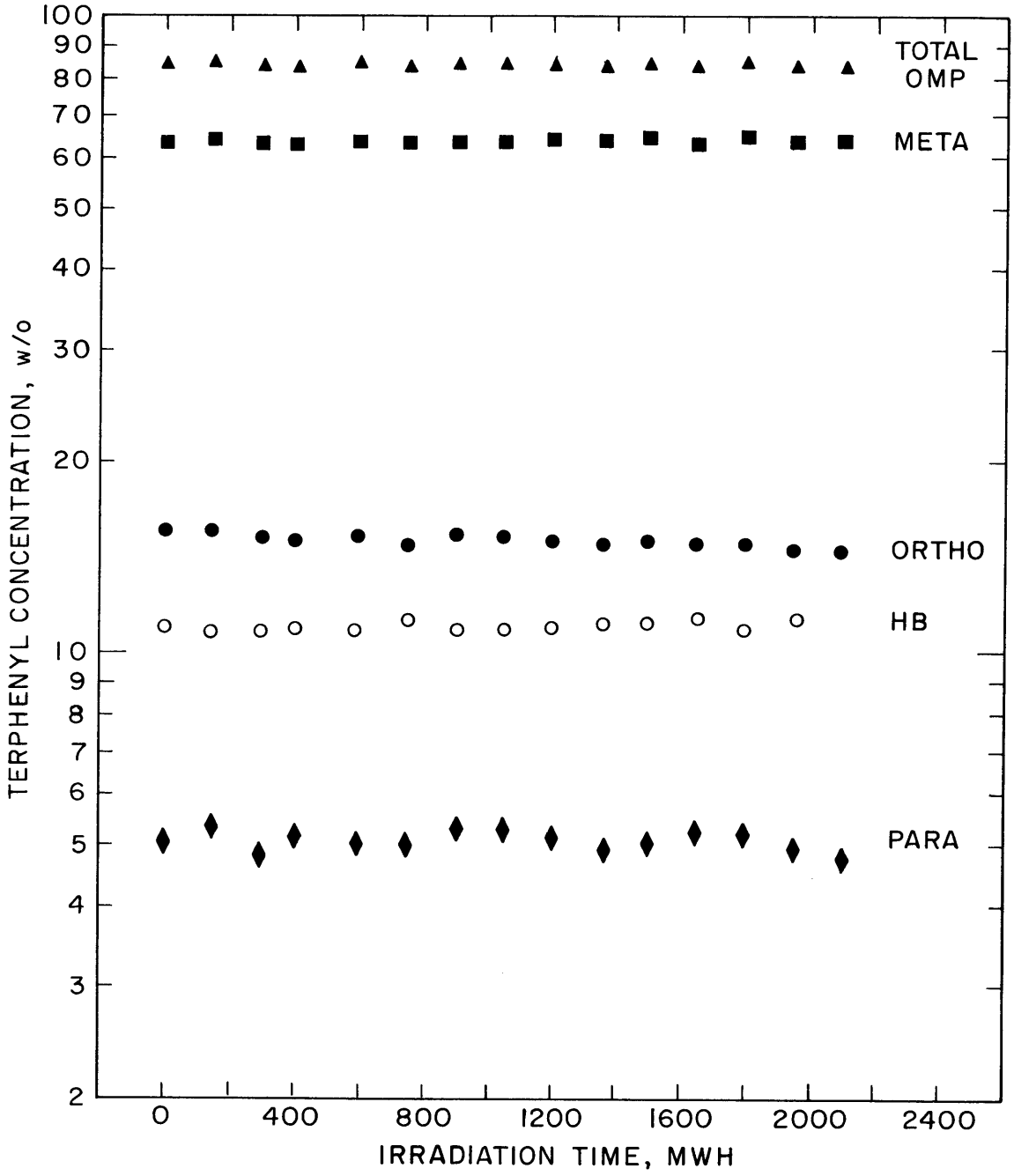

FIGURE A3.9 TERPHENYL AND HIGH BOILER CONCENTRATION DURING RUN 14—STEADY-STATE AT 572°F (300°C)

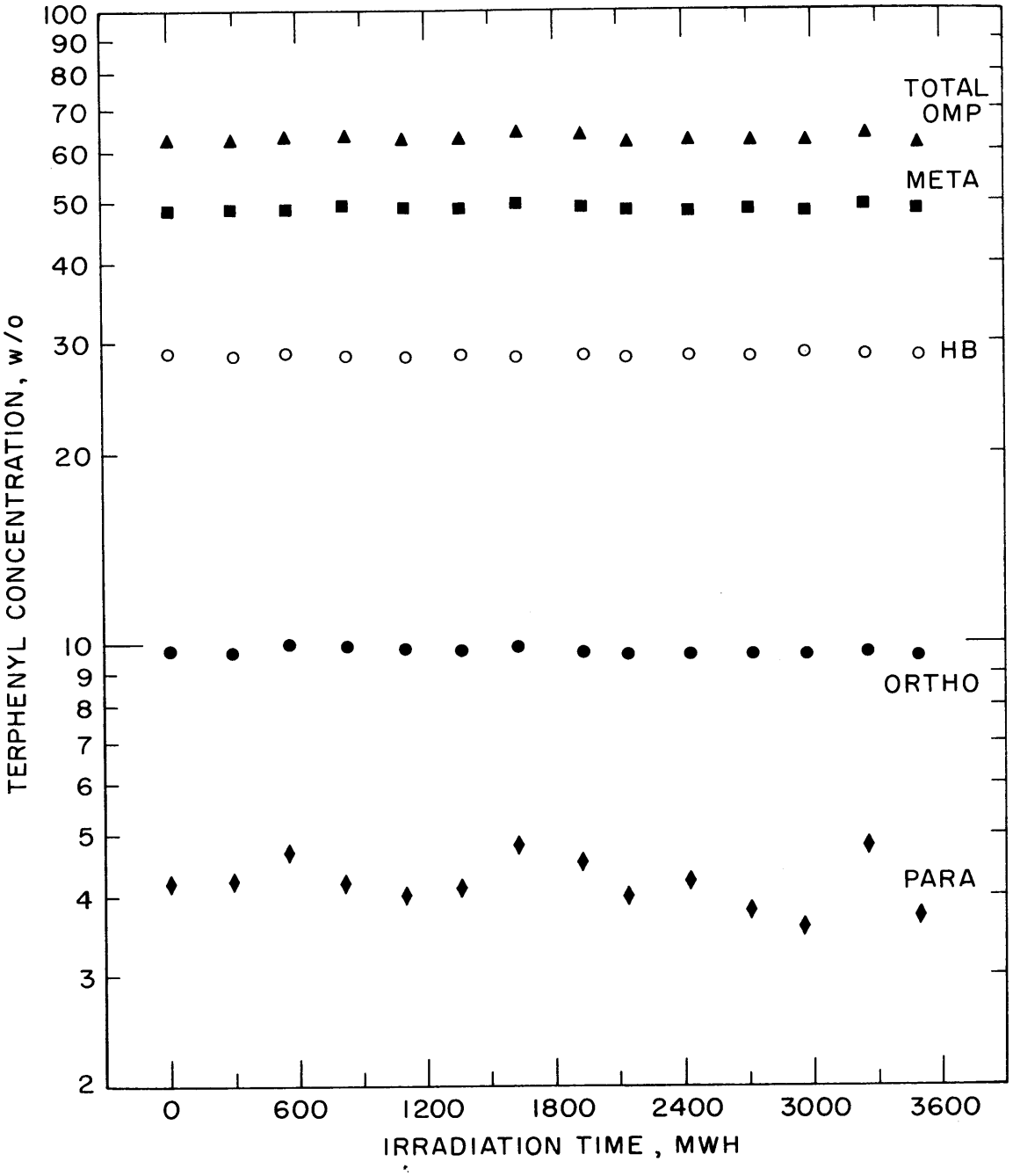

FIGURE A3.10 TERPHENYL AND HIGH BOILER CONCENTRATIONS DURING RUN 16-STEADY-STATE AT 572°F (300°C)

Table A3.9

Steady-State Run No. 16 Degradation Rate Calculations

Summary

Date: From 10/29/65 To 2/24/66

Irradiation Temp. 572°F Type of Distillation HB

Terphenyl Concentration 62.6 w/o HB Concentration 28.6 w/o

Terphenyl Degraded 566 gms Length of Run 3506 MWH

Average Dose Rate, $\bar{r}$ 0.0158 watts/gm ρ 0.91 gms/cc

In-Pile Dose Rate Factor, F_T^{SW} 20.5 watt-cc/MW-gm

Reactor Power 4.9 MW Fast Neutron Fraction, f_N 0.07

G(-omp) 0.0998 σ(G) 0.0038

Calculation of G:

	Total Coolant	o-$\emptyset_3$	m-$\emptyset_3$	p-$\emptyset_3$	Total omp	HB
1. Coolant Sample Average Concentration	1.000	0.097	0.488	0.040	0.626	0.286
2. Grams Removed	1807	175	881	73	1131	517
3. Return Sample Average Concentration	1.000	0.146	0.726	0.059	0.931	—
4. Grams Returned	1819	266	1321	108	1693	—
5. Net Makeup (4. - 2.)	12	91	440	35	562	-517
6. Initial Concentration, C_1	1.000	0.0986	0.486	0.0429	0.627	0.286
7. Initial Circulating Mass, M_1	5800	572	2819	249	3637	1656
8. Final Concentration, C_2	1.000	0.0956	0.489	0.0386	0.625	0.286
9. Final Circulating Mass, M_2	5812	556	2842	224	3633	1662

Table A3.9 (cont.)

Steady-State Run No. 16 Degradation Rate Calculations

Calculation of G:

	Total Coolant	o-ϕ_3	m-ϕ_3	p-ϕ_3	Total omp	HB
10. Δ Correction (7. - 9.)	-12	16	-23	25	4	-3
11. Total Mass Degraded, W (5. + 10.)	—	107	417	60	566	520
12. G(-omp), G(-i), G(HB) $11.65/F\rho(MWH) = 1.764 \times 10^{-4}$		0.0189	0.0736	0.0106	0.0998	0.0907
13. G*(-omp) = G(-omp)/C, G*(-i) = G(-i)C_i		0.195	0.151	0.265	0.159	—

Statistics of G Calculation:

MWH_1 = 0 MWH_2 = 3506 σ(F)/F 0.03

	o-ϕ_3	m-ϕ_3	p-ϕ_3	Total omp	HB
14. Intercept, a_i	0.0986	0.486	0.0429	0.627	0.287
15. Slope, $b_i \times 10^5$	-0.0853	0.0880	-0.123	-0.0786	0.002
16. $\sigma(a_i)$	0.0002	0.0010	0.0009	0.0016	0.0010
17. $\sigma(b_i) \times 10^4$	0.0010	0.049	0.043	0.078	0.0050
18. $\sigma^2(C_{initial}) \times 10^5$	0.0035	0.092	0.074	0.231	0.130
19. $\sigma^2(C_{final}) \times 10^5$	0.0042	0.104	0.077	0.265	0.129
20. σ^2(Δ correction)	4	66	51	167	87
21. σ^2(net makeup)	1	2	1	4	4
22. σ(W)/W	—	0.020	0.12	0.023	0.018
23. σ(G)/G	0.030	0.036	0.725	0.038	0.035
24. σ(G) (23. x 12.)	0.0006	0.0026	0.0013	0.0038	0.0032

Table A3.10

Steady-State Run No. 17 Degradation Rate Calculations

Summary

Date: From 2/28/66 To 4/1/66

Irradiation Temp. 572°F Type of Distillation HB

Terphenyl Concentration 89.7 w/o HB Concentration 6.2 w/o

Terphenyl Degraded 635 gms Length of Run 2244 gms

Average Dose Rate, $\bar{r}$ 0.0158 watts/gm ρ 0.89 gms/cc

In-Pile Dose Rate Factor, F_T^{SW} 20.5 watt-cc/MW-gm

Reactor Power 4.9 MW Fast Neutron Fraction, f_N 0.07

G(-omp) 0.181 σ(G) 0.006

Calculation of G:

	Total Coolant	o-ϕ_3	m-ϕ_3	p-ϕ_3	Total omp	HB
1. Coolant Sample Average Concentration	1.000	0.146	0.704	0.047	0.897	0.062
2. Grams Removed	9965	1450	7014	470	8938	621
3. Return Sample Average Concentration	1.000	0.157	0.755	0.052	0.965	—
4. Grams Returned	9936	1562	7499	520	9589	—
5. Net Makeup (4. - 2.)	-29	112	485	50	651	-621
6. Initial Concentration, C_1	1.000	0.147	0.698	0.048	0.893	0.065
7. Initial Circulating Mass, M_1	5672	833	3958	270	5066	369
8. Final Concentration, C_2	1.000	0.144	0.709	0.047	0.901	0.060
9. Final Circulating Mass, M_2	5643	.815	4002	264	5082	339

Table A3.10 (cont.)

Steady-State Run No. 17 Degradation Rate Calculations

Calculation of G:

	Total Coolant	o-ϕ_3	m-ϕ_3	p-ϕ_3	Total omp	HB
10. Δ Correction (7. - 9.)	29	18	-44	6	-16	30
11. Total Mass Degraded, W (5. + 10.)		130	441	56	635	-591
12. G(-omp), G(-i), G(HB) $11.65/F\rho(MWH) = 2.846 \times 10^{-4}$		0.037	0.126	0.016	0.181	0.168
13. $G^*(-omp) = G(-omp)/C$, $G^*(-i) = G(-i)C_i$		0.253	0.179	0.340	0.202	—

Statistics of G Calculation:

MWH_1 = 212 MWH_2 = 2456 σ(F)/F 0.03

	o-ϕ_3	m-ϕ_3	p-ϕ_3	Total omp	HB
14. Intercept, a_i	0.1471	0.6968	0.0476	0.8926	0.0656
15. Slope, $b_i \times 10^5$	-0.1117	0.5054	-0.0347	0.3231	-0.2557
16. $\sigma(a_i)$	0.0003	0.0011	0.0004	0.0012	0.0011
17. $\sigma(b_i)$, $\times 10^4$	0.0023	0.0080	0.0032	0.0086	0.0075
18. $\sigma^2(C_{initial})$, $\times 10^5$	0.0084	0.0960	0.0159	0.1109	0.0931
19. $\sigma^2(C_{final})$, $\times 10^5$	0.0146	0.1243	0.0198	0.1421	0.0844
20. σ^2(Δ correction)	7	71	11	81	57
21. σ^2(net makeup)	3	65	6	47	7
22. σ(W)/W	0.024	0.026	0.074	0.018	0.014
23. σ(G)/G	0.038	0.040	0.080	0.035	0.033
24. σ(G) (23. 12.)	0.001	0.005	0.001	0.006	0.006

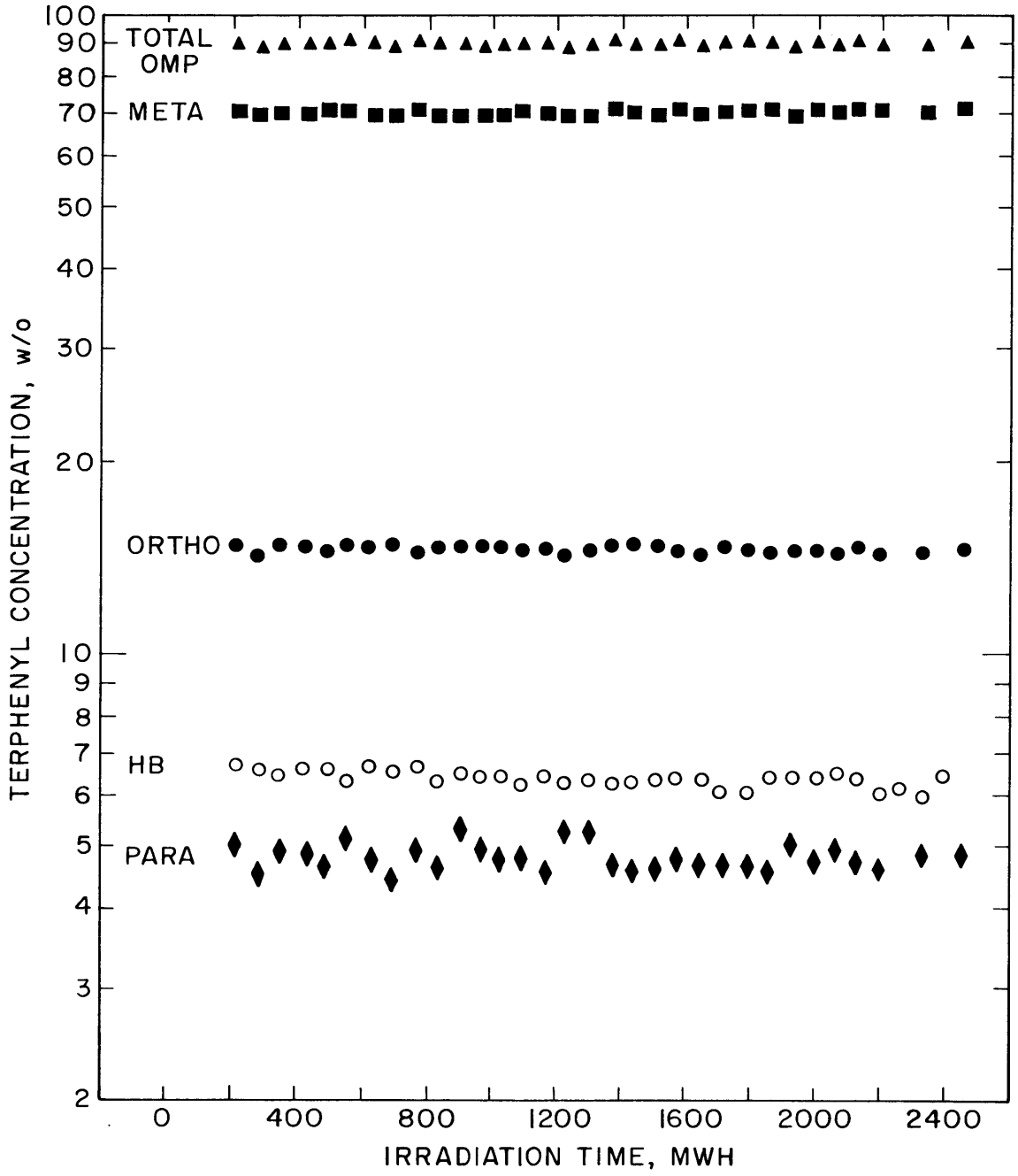

FIGURE A3.11 TERPHENYL AND HIGH BOILER CONCENTRATION DURING RUN 17—STEADY-STATE AT 572°F (300°C)

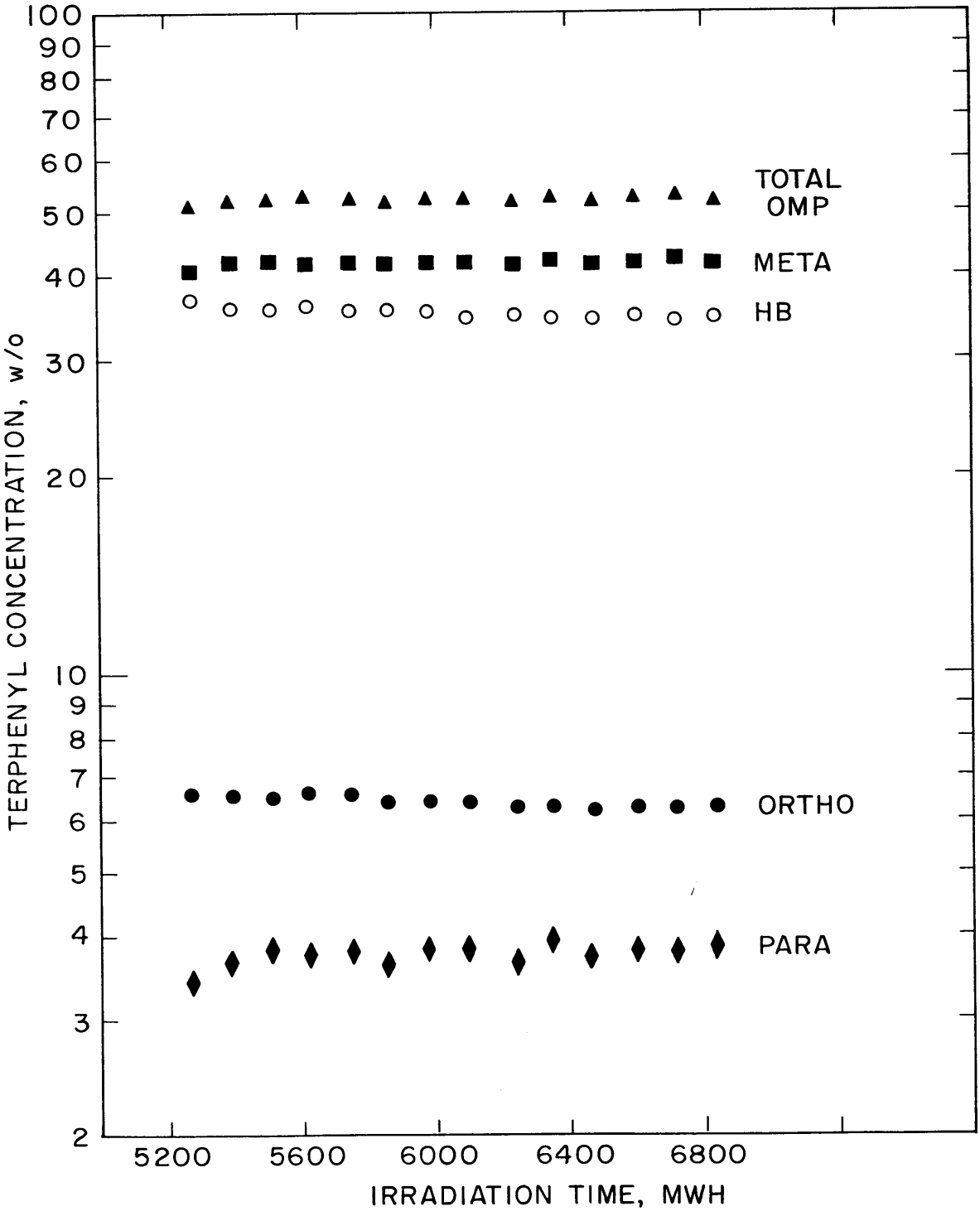

FIGURE A3.12 TERPHENYL AND HIGH BOILER CONCENTRATION DURING RUN 18B —STEADY-STATE, 800°F (427°C)

Table A3.11

Steady-State Run No. 18B Degradation Rate Calculations

Summary

Date: From 5/10/66 To 6/10/66

Irradiation Temp. 800°F Type of Distillation HB

Terphenyl Concentration 52 w/o HB Concentration 35

Terphenyl Degraded 1293 gms Length of Run 1555 gms

Average Dose Rate, $\bar{r}$ 0.0166 watts/gm ρ 0.89 gms/cc

In-Pile Dose Rate Factor, F_T^{SW} 20.5 watt-cc/MW-gm

Reactor Power 4.9 MW Fast Neutron Fraction, f_N 0.07

G(-omp) 0.532 σ(G) 0.017

Calculation of G:

	Total Coolant	o-$\emptyset_3$	m-$\emptyset_3$	p-$\emptyset_3$	Total omp	HB
1. Coolant Sample Average Concentration	1.000	0.063	0.417	0.037	0.517	0.349
2. Grams Removed	3720	236	1550	138	1923	1300
3. Return Sample Average Concentration	1.000	0.103	0.695	0.054	0.867	—
4. Grams Returned	3721	444	2587	202	3227	—
5. Net Makeup (4. - 2.)	1.000	208	1037	64	1304	-1300
6. Initial Concentration, C_1	1.000	0.0651	0.414	0.0360	0.516	0.361
7. Initial Circulating Mass, M_1	5379	350	2227	194	2776	1942
8. Final Concentration, C_2	1.000	0.0617	0.419	0.0379	0.518	0.340
9. Final Circulating Mass, M_2	5380	332	2254	204	2787	1829

Table A3.11 (cont.)

Steady-State Run No. 18B Degradation Rate Calculations

Calculation of G:

	Total Coolant	o-ϕ_3	m-ϕ_3	p-ϕ_3	Total omp	HB
10. Δ Correction (7. - 9.)		18	-27	-8	-11	113
11. Total Mass Degraded, W (5. + 10.)		226	1010	56	1293	1187
12. G(-omp), G(-i), G(HB) $11.65/F\rho(MWH) = 4.116 \times 10^{-4}$		0.093	0.416	0.023	0.532	0.489
13. $G^*(-omp) = G(-omp)/C$, $G^*(-i) = G(-i)C_i$		1.476	1.000	0.622	1.029	—

Statistics of G Calculation:

MWH_1 = 5275 MWH_2 = 6230 σ(F)/F 0.03

	o-ϕ_3	m-ϕ_3	p-ϕ_3	Total omp	HB
14. Intercept, a_i	0.0767	0.4000	0.0030	0.5074	0.4327
15. Slope, $b_i \times 10^5$	0.2197	0.2713	0.121	0.162	-1.361
16. $\sigma(a_i)$	0.0015	0.0081	0.0036	0.0106	0.0109
17. $\sigma(b_i)$, $\times 10^4$	0.0026	0.0135	0.0660	0.0176	0.0179
18. $\sigma^2(C_{initial})$, $\times 10^5$	0.0050	0.132	0.026	0.231	0.331
19. $\sigma^2(C_{final})$, $\times 10^5$	0.0060	0.163	0.033	0.276	0.313
20. σ^2(Δ correction)	3	85	17	147	186
21. σ^2(net makeup)	1	59	7	42	20
22. σ(W)/W	0.001	0.012	0.088	0.011	0.012
23. σ(G)/G	0.030	0.033	0.093	0.032	0.033
24. σ(G) (23. x 12.)	0.003	0.014	0.002	0.017	0.016

APPENDIX A4

DEGRADATION RATE CALCULATIONS FOR M.I.T. AUTOCLAVE PYROLYSIS EXPERIMENTS

Figures A4.1, A4.2, and A4.3 are plots of total terphenyl concentration versus time for M.I.T. autoclave pyrolysis tests. The various kinetics order correlations used to represent these data are shown on the plots. Tables A4.1, A4.2, and A4.3 give the results of the degradation calculations for these runs. The terphenyl isomer concentration versus pyrolysis time data were analyzed by least-square analysis (using the MNDEG computer program) assuming zero-, first-, and second-order kinetics. The correlation coefficient (see Equation (A3.42)) for the total terphenyl degradation rate by the various kinetics orders is also given.

The procedure and chronology of these pyrolysis tests is given in Chapter 2. A discussion of results of these experiments is presented in Chapter 5.

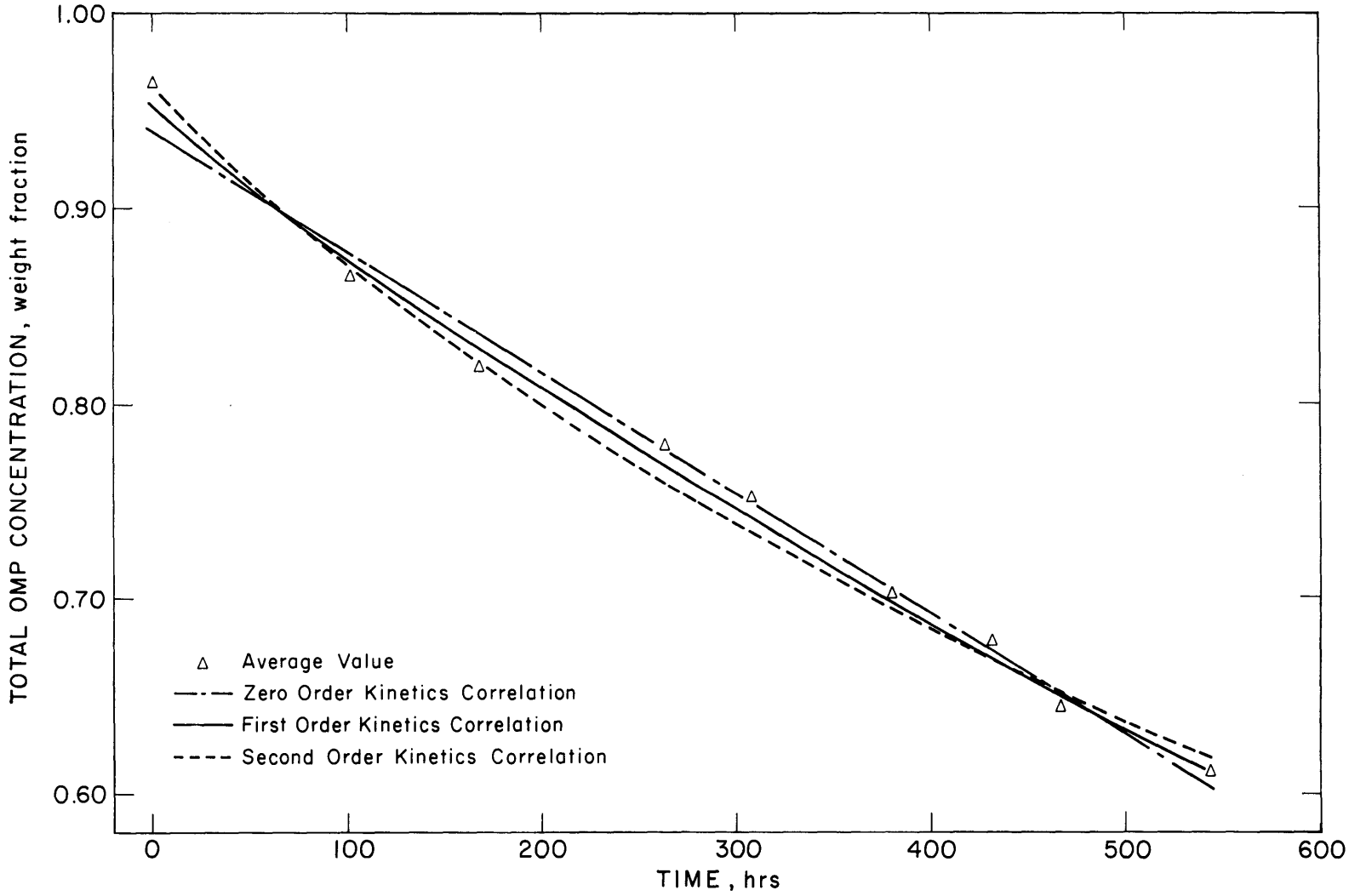

FIGURE A4.1 TOTAL TERPHENYL CONCENTRATION IN AUTOCLAVE DURING PYROLYSIS RUN PI-UNIRRADIATED SANTOWAX WR-780°F

Table A4.1

Summary of Results of Pyrolysis Run P1
Unirradiated Santowax WR - 780°F

Terphenyl Isomer	Degradation Rate Constant, $K'(hr)^{-1}$[a]		
	K_0' (zero order)	K_1' (first order)	K_2' (second order)
ortho	$1.77 \pm 0.02 \times 10^{-4}$	$1.03 \pm 0.01 \times 10^{-3}$	$5.82 \pm 0.12 \times 10^{-3}$
meta	$4.19 \pm 0.08 \times 10^{-4}$	$7.58 \pm 0.14 \times 10^{-4}$	$1.35 \pm 0.03 \times 10^{-3}$
para	$1.60 \pm 0.26 \times 10^{-5}$	$5.34 \pm 0.75 \times 10^{-4}$	$1.68 \pm 0.22 \times 10^{-2}$
total omp	$6.18 \pm 0.10 \times 10^{-4}$	$8.17 \pm 0.10 \times 10^{-4}$	$1.06 \pm 0.02 \times 10^{-3}$
correlation coefficient (total omp)	0.993	0.996	0.995

[a] error limits are 1σ

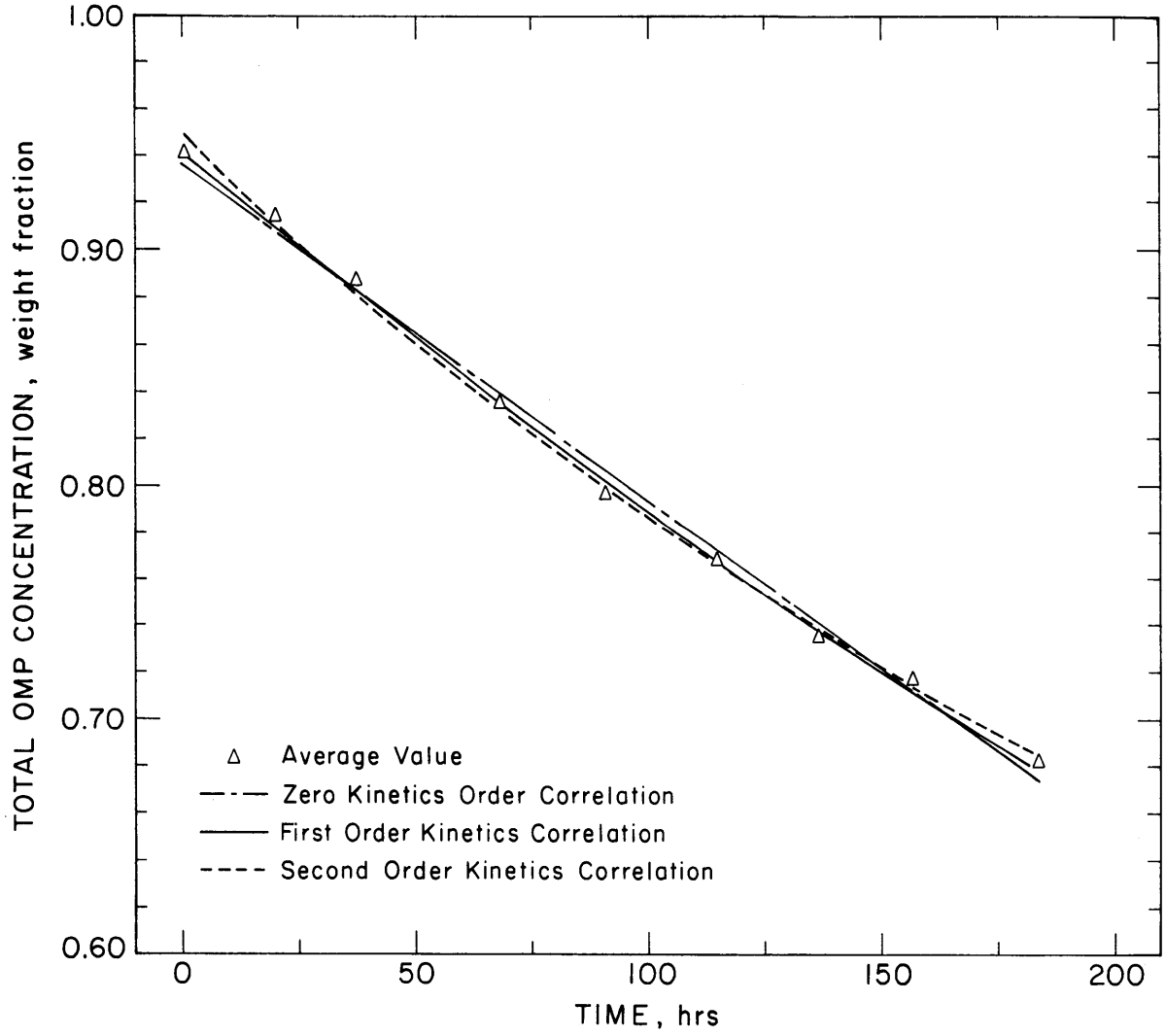

FIGURE A4.2 TOTAL TERPHENYL CONCENTRATION IN AUTOCLAVE DURING PYROLYSIS RUN P2-UNIRRADIATED SANTOWAX WR-800°F

Table A4.2

Summary of Results of Pyrolysis Run P2
Unirradiated Santowax WR - 800°F

Terphenyl Isomer	Degradation Rate Constant, $K'(hr)^{-1}$[a]		
	K'_0 (zero order)	K'_1 (first order)	K'_2 (second order)
ortho	$4.13 \pm 0.09 \times 10^{-4}$	$2.35 \pm 0.04 \times 10^{-3}$	$1.31 \pm 0.02 \times 10^{-2}$
meta	$9.52 \pm 0.20 \times 10^{-4}$	$1.62 \pm 0.03 \times 10^{-3}$	$2.72 \pm 0.05 \times 10^{-3}$
para	$6.23 \pm 0.71 \times 10^{-5}$	$1.71 \pm 0.21 \times 10^{-3}$	$4.58 \pm 0.64 \times 10^{-2}$
total omp	$1.42 \pm 0.03 \times 10^{-3}$	$1.78 \pm 0.03 \times 10^{-3}$	$2.21 \pm 0.04 \times 10^{-3}$
correlation coefficient (total omp)	0.993	0.995	0.995

[a] error limits are 1σ

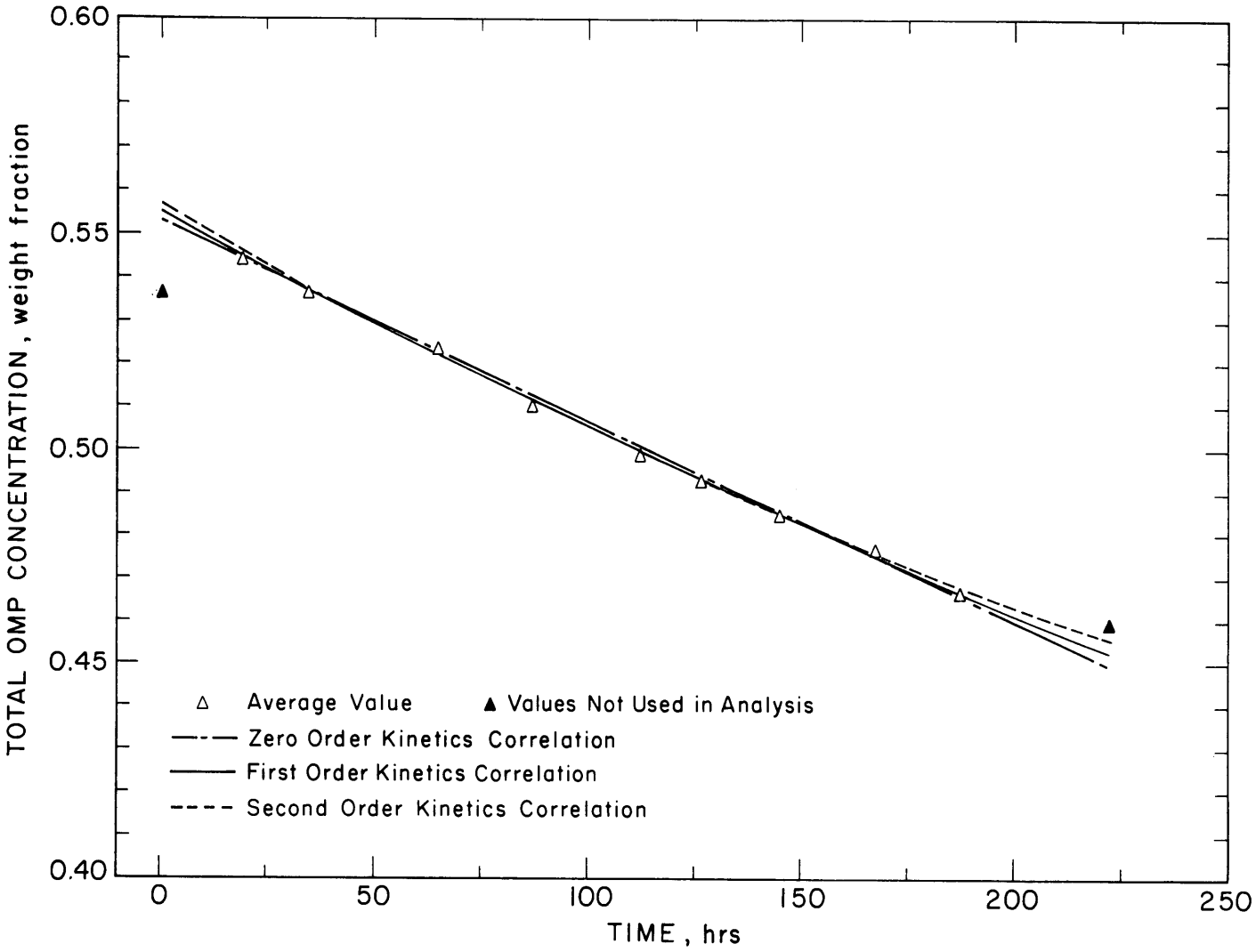

FIGURE A 4.3 TOTAL TERPHENYL CONCENTRATION IN AUTOCLAVE DURING PYROLYSIS RUN 18PI-IRRADIATED SANTOWAX WR - 780°F

Table A4.3

Summary of Results of Pyrolysis Run 18P1
Irradiated Santowax WR (Run 18B) - 780°F

Terphenyl Isomer	Degradation Rate Constant, $K'(hr)^{-1}$[a]		
	K'_0 (zero order)	K'_1 (first order)	K'_2 (second order)
ortho	$9.28 \pm 0.48 \times 10^{-5}$	$1.73 \pm 0.09 \times 10^{-3}$	$3.19 \pm 0.19 \times 10^{-2}$
meta	$3.66 \pm 0.18 \times 10^{-4}$	$8.81 \pm 0.43 \times 10^{-4}$	$2.11 \pm 0.10 \times 10^{-3}$
para	$1.20 \pm 0.62 \times 10^{-5}$	$3.95 \pm 1.82 \times 10^{-4}$	$1.25 \pm 0.54 \times 10^{-2}$
total omp	$4.64 \pm 0.14 \times 10^{-4}$	$9.19 \pm 0.28 \times 10^{-4}$	$1.82 \pm 0.06 \times 10^{-3}$
correlation coefficient (total omp)	0.992	0.992	0.992

[a] error limits are 1σ

APPENDIX A5

CALCULATION OF RADIOLYSIS AND RADIOPYROLYSIS RATE CONSTANTS FROM DATA OF M.I.T. AND OTHER LABORATORIES

A5.1 Radiolysis Rate Constants – 320°C

Table A5.1 gives the experimental conditions for low temperature irradiations of meta-rich coolants by Euratom, Atomics International (AI), Cal Research, AECL, and AERE, and presents the M.I.T. calculated values of the 1.7 order radiolysis rate constant for total terphenyl for these experiments. The results are correlated along with the M.I.T. low temperature irradiation results (presented in Chapter 4 and Appendix A3) in Figure 4.4. All experiments shown in Table A5.1 represent transient runs except the Euratom BLO4 loop data. For the Euratom steady-state runs, $k_{R,omp,1.7}$ was found by Equation (4.4), using the values of G(-omp) shown in Table 4.3, which were calculated by M.I.T. from the Euratom data. For transient runs, $k_{R,omp,1.7}$ was found by correlating total terphenyl concentration versus dose data by Equation (4.1a) (with $w_i = 0$ for transient runs), using the MNDEG least-square-error computer program, and assuming radiopyrolysis was negligible.

A5.2 Radiopyrolysis Rate Constants from Low-Average Dose Rate Runs

Table A5.2 presents the calculation of the first-order radiopyrolysis rate constants of total terphenyl in meta-rich coolants from M.I.T., Euratom, and Cal Research low-average dose rate runs. The $k_{P,omp,1}$ shown in this table are correlated in Figure 5.3 (M.I.T. runs only) and Figure 5.5 (all data). Equation (5.3) was used to calculate $k_{P,omp,1}$ for steady-state runs and Equation (5.8) was used to determine $k_{P,omp,1}$ for transient runs. For these high temperature irradiations, the radiolysis rate constant in Equations (5.3) and (5.8) were estimated from the correlation shown in Figure 4.4, assuming an activation energy of radiolysis ΔE_R = 1 k-cal/mole. The overall rate constant

for transient runs, K_1(-omp), in Table A5.2 was found by least-square error analysis (MNDEG computer program). Since concentration versus dose data were not available for the BLO2 runs, K_1(-omp) was calculated from the values of G^*(-omp) reported by Euratom using Equation (A3.31). It should be noted that the radiopyrolysis rate constants calculated in Table A5.2 for transient runs represent values at the terphenyl concentration, $\bar{C}_{omp}$, at which $-dC_{omp}/d\tau$ has the same value when calculated by first- and second-order kinetics (see Section 5.2.2).

A5.3 Radiolysis Rate Constants – AECL High Dose Rate Experiments

Tables A5.3 and A5.4 show the calculated values of the second-order radiolysis rate constants for AECL and AI (Scarborough) high dose rate runs. Second-order radiolysis kinetics was used (instead of 1.7 order) because recent AECL data (excluding the experiments at 0.1 and 0.3 watts/gram) were presented (A5.9) as initial G values, G^o(-i), determined by second-order kinetics. Terphenyl concentration versus dose data are not available at M.I.T. at this time to treat the data by other kinetics correlations. For these data, $k_{R,i,2}$ was found by

$$k_{R,i,2} = \frac{G^o(-i)}{11.65} \tag{A5.1}$$

where the reported G^o(-i) are already corrected for radiopyrolysis by AECL.

Since concentration versus dose data have been reported by AECL (A5.7) for the ortho, meta, and OM-2 irradiations at 0.1 and 0.3 watts/gram, M.I.T. has calculated first- and second-order overall rate constants for these runs. K_1(-i) and K_2(-i) were found by computer least-square-error analysis when several sample capsules were irradiated at a given temperature. In cases where only one sample was irradiated at a given temperature, the overall rate constants were found by

$$K_1(-i) = \frac{\ln C_i/C_o}{\tau} \tag{A5.2}$$

and

$$K_2(-i) = \frac{\frac{1}{C_i} - \frac{1}{C_o}}{\tau} \tag{A5.3}$$

where

C_i is the terphenyl concentration of component i after irradiation, weight fraction

C_o is the starting terphenyl concentration, weight fraction

τ is the dose, watt-hr/gram

The $k_{R,i,2}$ were then calculated for these AECL runs at 0.1 and 0.3 watts/gram by

$$k_{R,i,2} = \frac{1}{\bar{C}_i} K_1(-i) - \frac{k_{P,i,1}}{\bar{r}} \quad (\text{watt-hr/gm})^{-1} \tag{A5.4}$$

where

$$\bar{C}_i = \frac{K_1(-i)}{K_2(-i)} \tag{A5.5}$$

The first-order radiopyrolysis rate constants in Equation (A5.4) were estimated from Figures 5.6 and 5.7 for both meta-rich terphenyls (Table A5.3) and ortho-rich terphenyls (Table A5.4).

Scarborough (A5.16) published terphenyl concentration versus dose data for the AI electron irradiations of ortho terphenyl, and these data were reinterpreted by M.I.T., using least-square analysis to obtain $K_1(-i)$ and $K_2(-i)$. Since Scarborough reported that fourth-order kinetics gave the best correlation for these data, M.I.T. has analyzed both the entire transient and the first part of the transient (see Table A5.4). The first- and second-order overall rate constants for the entire transient are significantly lower than the values for the first part of the transient, indicating that a higher order kinetics correlation than second-order is needed to adequately fit these data. The second-order rate constants for the entire transient are plotted in Figure 6.2.

Table A5.1

Summary of Low Temperature Terphenyl Irradiation Data of Other Laboratories

Laboratory-Facility	Run No.	Terphenyl	Terphenyl Concentration	Temperature °F	Temperature °C	Average Dose Rate (milli watts/gm)	Fast Neutron Fraction	Author's Results	M.I.T. Correlation[a] $K_{R,1.7}$ (wh/g)$^{-1}$	Reference
Euratom (BL04)	C1-41-320	OM-2	0.746	608	320	~80	0.18	G(-omp) = 0.176	0.0246 ± 0.0018	(A5.6)
Euratom (BL04)	C2-42-320	OM-2	0.897	608	320	~145	0.28	G(-omp) = 0.282	0.0293 ± 0.0022	(A5.6)
			0.705	608	320			G(-omp) = 0.185	0.0294 ± 0.0021	
			0.619	608	320			G(-omp) = 0.149	0.0295 ± 0.0021	
Euratom (BL04)	C3-40-320	OM-2	0.892	608	320	~33	0.126	G(-omp) = 0.208	0.0211 ± 0.0016	(A5.6)
			0.704	608	320			G(-omp) = 0.134	0.0206 ± 0.0015	
Euratom (BL04)	C6-41-320	OM-2	0.921	608	320	~77	0.20	G(-omp) = 0.248	0.0239 ± 0.0019	(A5.6)
			0.706	608	320			G(-omp) = 0.168	0.0264 ± 0.0019	
Euratom (BL03)	B11	OM-2	1.00-0.86	608	320	17	0.16	K_1(-omp) = 2.35×10^{-2}	0.0246 ± 0.0008	(A5.10)
Euratom (BL03)	B12	OM-2	1.00-0.92	679	360	16	0.16	K_1(-omp) = 2.79×10^{-2}	0.0276 ± 0.0025	(A5.10)
AI (OGR)	—	SW-OMP	1.00-0.69	620	327	3	0.63	G^o(-omp) = 0.61	0.0457 ± 0.0040	(A5.12)
AI (CWRR)	—	ortho, meta para mixture	1.00-0.53	600-650	315-343	400	0.65	G^o(-omp) = 0.51	0.0429 ± 0.0038	(A5.11)
CalResearch (Susie neutron rich)	—	SW-OMP	1.00-0.71	425	219	10-15	0.95	b	0.0614 ± 0.0062	(A5.5)
CalResearch (Susie neutron rich)	—	SW-OMP	1.00-0.66	600	316	10-15	0.95	b	0.0704 ± 0.0055	(A5.5)
CalResearch (Susie gamma rich)	—	SW-OMP	1.00-0.90	425	219	10-15	0	b	0.0168 ± 0.0004	(A5.5)
CalResearch (Susie gamma rich)	—	SW-OMP	1.00-0.77	600	316	10-15	0	b	0.0194 ± 0.0066	(A5.5)
CalResearch (MTR gamma grid)	—	SW-OMP	1.00-0.71	425	219		0	b	0.0150 ± 0.0046	(A5.5)
CalResearch (MTR gamma grid)	—	SW-OMP	1.00-0.84	600	316		0	b	0.0240 ± 0.0017	(A5.5)
AECL (NRX E-3)	—	ortho and meta	1.00-0.60	212-572	100-300	100 and 300	0.50	K_1(-omp) = 0.0305-0.0408 K_2(-omp) = 0.0336-0.0454	0.0370 ± 0.0030	(A5.8)
AERE (BEPO)	Series 2	SW-R	0.99-0.90	572	300	8	0.54	G^o(→HB) = 0.51	0.0421	(A5.13)
AERE (Van de Graaff)	—	meta	0.99-0.79	572	300	6,000-80,000	0	G^o(→HB) = 0.19	0.0145 ± 0.0022	(A5.14) (A5.17)
AERE (Van de Graaff)	—	meta	0.99-0.54	662	350	6,000-80,000	0	G^o(→HB) = 0.19	0.0148 ± 0.0016	(A5.14) (A5.17)

[a] Error limits are 1σ. For the Euratom steady-state runs error limits include uncertainties in the dose rate. For all other transient runs error limits only include statistical errors in concentration vs dose curve fit.

[b] Results given for disappearance of individual isomers; see (A5.1) or (A5.5).

Table A5.2

Calculation of Radiopyrolysis Rate Constants from Low Dose Rate Runs
Meta-Rich Terphenyls (Assuming ΔE_R = 1 k-cal/mole)

Facility	Run No.	Terphenyl	Type	Temperature °F	Temperature °C	Avg. Dose Rate, $\bar{r}$ (watts/gm) [a]	f_N [a]	Author's Results (Reference)	M.I.T. Results (Reference)	$\bar{C}_{omp}$ (Range)	$k_{R,omp,1.7}$ [a] $(wh/g)^{-1}$	$k_{P,omp,1}$ [b] $(hr)^{-1}$
M.I.T. Loop	9	SW-WR	SS	800	427	0.0206	0.40 ±.02		G(-omp) = 0.91 + 0.03 (A5.1)	0.52	$4.07 + 0.13 \times 10^{-2}$	$2.56 + 0.18 \times 10^{-3}$
M.I.T. Loop	10	SW-WR	SS	800	427	0.0192	0.40 ±.02		G(-omp) = 1.06 + 0.04 (A5.1)	0.65	$4.07 + 0.13 \times 10^{-2}$	$2.10 + 0.16 \times 10^{-3}$
M.I.T. Loop	4	SW-WR	SS	780	416	0.0192	0.40 ±.02		G(-omp) = 0.53 + 0.03 (A5.1)	0.62	$4.03 + 0.13 \times 10^{-2}$	$8.60 + 1.92 \times 10^{-4}$
M.I.T. Loop	8 (tr #1)	SW-WR	Tr	780	416	0.0190	0.40 ±.02		K_1(-omp) = $(8.38 + 0.40) \times 10^{-2}$	0.61 (0.68-0.55)	$4.03 + 0.13 \times 10^{-2}$	$1.05 + 0.19 \times 10^{-3}$
	8 (tr #2)	SW-WR	Tr	780	416	0.0190	0.40 ±.02		K_1(-omp) = $(11.35 + 0.71) \times 10^{-2}$ (A5.1)	0.55 (0.60-0.51)	$4.03 + 0.13 \times 10^{-2}$	$1.74 + 0.34 \times 10^{-3}$
M.I.T. Loop	3	SW-WR	SS	750	399	0.0199	0.40 ±.02		G(-omp) = 0.34 + 0.014 (A5.1)	0.54	$3.96 + 0.13 \times 10^{-2}$	$6.50 + 0.96 \times 10^{-4}$
M.I.T. Loop	3 (tr #1)	SW-WR	Tr	750	399	0.0199	0.40 ±.02		K_1(-omp) = $(5.48 + 1.97) \times 10^{-2}$	0.75 (0.82-0.68)	$3.96 + 0.13 \times 10^{-2}$	$4.45 + 3.10 \times 10^{-4}$
	3 (tr #2)	SW-WR	Tr	750	399	0.0199	0.40 ±.02		K_1(-omp) = $(4.75 + 0.29) \times 10^{-2}$ (unreported)	0.55 (0.68-0.41)	$3.96 + 0.13 \times 10^{-2}$	$4.25 + 1.20 \times 10^{-4}$
M.I.T. Loop	6	SW-WR	SS	750	399	0.0184	0.40 ±.02		G(-omp) = 0.31 + 0.019 (A5.1)	0.69	$3.96 + 0.13 \times 10^{-2}$	$1.51 + 0.92 \times 10^{-4}$
M.I.T. Loop	7	SW-WR	SS	750	399	0.0182	0.40 ±.02		G(-omp) = 0.41 + 0.03 (A5.1)	0.74	$3.96 + 0.13 \times 10^{-2}$	$2.82 + 1.28 \times 10^{-4}$
M.I.T. Loop	2	SW-OMP	SS	750	399	0.0202	0.37 ±.02		G(-omp) = 0.32 + 0.02 (A5.2)	0.59	$3.74 + 0.13 \times 10^{-2}$	$4.20 + 1.16 \times 10^{-4}$
M.I.T. Loop	2 (tr #1)	SW-OMP	Tr	750	399	0.0202	0.37 ±.02		K_1(-omp) = $(3.95 + 0.30) \times 10^{-2}$	0.77 (0.90-0.63)	$3.74 + 0.13 \times 10^{-2}$	$1.72 + 1.20 \times 10^{-4}$
	2 (tr #2)	SW-OMP	Tr	750	399	0.0202	0.37 ±.02		K_1(-omp) = $(4.64 + 0.56) \times 10^{-2}$ (A5.2)	0.53 (0.66-0.41)	$3.74 + 0.13 \times 10^{-2}$	$4.55 + 2.22 \times 10^{-4}$
M.I.T. Loop	5	SW-WR	SS	700	371	0.0201	0.40 ±.02		G(-omp) = 0.20 + 0.01 (A5.1)	0.55	$3.86 + 0.13 \times 10^{-2}$	$1.48 + 0.64 \times 10^{-4}$
M.I.T. Loop	15	SW-WR	Tr	800	427	0.0056-0.0118 [d]	0.07 ±.005		K_1(-omp) [c] = $1.19 + 0.02 \times 10^{-3}$	0.68 (0.82-0.57)	$2.15 + 0.11 \times 10^{-2}$	$1.05 + 0.05 \times 10^{-3}$

[a] error limits are 1σ [b] error limits are 2σ [c] K_1(-omp) in $(hr)^{-1}$; first order rate constant based on irradiation time (hrs) instead of specific dose (wh/g)
[d] average value (0.0087) used in calculation of $k_{P,omp,1}$

Table A5.2 (cont.)

Calculation of Radiopyrolysis Rate Constants from Low Dose Rate Runs
Meta-Rich Terphenyls (Assuming ΔE_R = 1 k-cal/mole)

Facility	Run No.	Terphenyl	Type	Temperature °F	Temperature °C	Avg. Dose Rate, $\bar{r}$ (watts/gm)[a]	f_N[a]	Author's Results (Reference)	M.I.T. Results (Reference)	$\bar{G}_{omp}$ (Range)	$k_{R,omp,1.7}$[a] $(wh/g)^{-1}$	$k_{P,omp,1}$[b] $(hr)^{-1}$
M.I.T. Loop	18A	SW-WR	Tr	800	427	0.0161	0.07 ±.005		$K_1(-omp)$[c] = 1.48 ± 0.02 x 10^{-3}	0.74 (0.90-0.54)	2.15 ± 0.11 x 10^{-2}	1.20 ± 0.06 x 10^{-3}
M.I.T. Loop	18B	SW-WR	SS	800	427	0.0166	0.07 ±.005		G(-omp) = 0.53 ± 0.017	0.52	2.15 ± 0.11 x 10^{-2}	1.23 ± 0.06 x 10^{-3}
Euratom BL03 Loop	B6	OM-2	Tr	806	430	0.0152 ±.0011	0.16 ±.01	G*(-omp) = 2.20 $K_1(-omp)$ = 0.189 (A5.3)	$K_1(-omp)$ = 0.201 ± 0.005	0.85 (1.00-0.69)	2.74 ± 0.07 x 10^{-2}	2.68 ± 0.37 x 10^{-3}
Euratom BL03 Loop	B7	OM-2	Tr	842	450	0.0170 ±.0012	0.16 ±.01	G*(-omp) = 5.70 $K_1(-omp)$ = 0.489 (A5.3)	$K_1(-omp)$ = 0.487 ± 0.013	0.74 (0.98-0.53)	2.80 ± 0.07 x 10^{-2}	7.89 ± 1.10 x 10^{-3}
Euratom BL03 Loop	B8	OM-2	Tr	824	440	0.0147 ±.0010	0.16 ±.01	G*(-omp) = 3.86 $K_1(-omp)$ = 0.331 (A5.3)	$K_1(-omp)$ = 0.332 ± 0.008	0.81 (0.99-0.62)	2.76 ± 0.07 x 10^{-2}	4.52 ± 0.63 x 10^{-3}
Euratom BL03 Loop	B5	OM-2	Tr	788	420	0.018 ±.0012	0.16 ±.01	G*(-omp) = 1.47 $K_1(-omp)$ = 0.126 (A5.3)	$K_1(-omp)$ = 0.118 ± 0.004	0.87 (0.99-0.76)	2.71 ± 0.07 x 10^{-2}	1.68 ± 0.23 x 10^{-3}
Euratom BL03 Loop	B4 (first week)	OM-2	Tr	770	410	0.015 ±.0010	0.16 ±.01	G*(-omp) = 1.16 $K_1(-omp)$ = 9.96 x 10^{-2} (A5.3)	$K_1(-omp)$ = (9.52 ± 0.51) x 10^{-2}	0.91 (0.99-0.84)	2.68 ± 0.07 x 10^{-2}	1.05 ± 0.15 x 10^{-3}
Euratom BL03 Loop	B4 (second week)	OM-2	Tr	770	410	0.015 ±.0010	0.16 ±.01	G*(-omp)[e] = 1.19 $K_1(-omp)$ = 10.2 x 10^{-2} (A5.3)	corrected data not available	0.78 (0.82-0.73)	2.68 ± 0.07 x 10^{-2}	1.19 ± 0.17 x 10^{-3}
Euratom BL03 Loop	B3	OM-2	Tr	752	400	0.0166 ±.0012	0.16 ±.01	G*(-omp) = 0.70 $K_1(-omp)$ = 6.01 x 10^{-2} (A5.3)	data not available	0.91 (0.99-0.82)	2.64 ± 0.07 x 10^{-2}	5.86 ± 0.82 x 10^{-4}
Euratom BL03 Loop	B2	OM-2	Tr	716	380	0.0138 ±.0010	0.16 ±.01	G*(-omp) = 0.36 $K_1(-omp)$ = 3.09 x 10^{-2} (A5.3)	data not available	0.89 (0.99-0.80)	2.56 ± 0.07 x 10^{-2}	0.99 ± 0.20 x 10^{-4}
Euratom BL04 Loop	C5-41-420	OM-2	SS	788	423	0.071[f] ±.005	0.20 ±.01	G(-omp) = 0.58	data not available	0.87	2.94 ± 0.07 x 10^{-2}	2.17 ± 0.30 x 10^{-3}
	C5-41-420	OM-2	SS	788	423	0.071[f] ±.005	0.20 ±.01	G(-omp) = 0.44	data not available	0.64	2.94 ± 0.07 x 10^{-2}	2.66 ± 0.37 x 10^{-3}
Euratom BL02 Loop	A-22	OM-2	Tr	841	450	0.0391 ±.0028	0.18	G*(-omp) = 2.96 $K_1(-omp)$ = 0.254 (A5.4)	data not available	0.80[g]	2.91 x 10^{-2}	8.95 ± 1.25 x 10^{-3}
Euratom BL02 Loop	A-21	OM-2	Tr	823	440	0.0392 ±.0028	0.18	G*(-omp) = 1.50 $K_1(-omp)$ = 0.128 (A5.4)	data not available	0.80[g]	2.88 x 10^{-2}	4.04 ± 0.57 x 10^{-3}

[e] Euratom corrected values (A5.3) [f] assumed same as dose rate for Run C6-41-320 [g] terphenyl concentration range unknown at M.I.T.; $\bar{G}_{omp}$ = 0.80 is assumed value

Table A5.2 (cont.)

Calculation of Radiopyrolysis Rate Constants from Low Dose Rate Runs
Meta-Rich Terphenyls (Assuming ΔE_R = 1 k-cal/mole)

Facility	Run No.	Terphenyl	Type	Temperature °F	Temperature °C	Avg. Dose Rate, $\bar{r}$ (watts/gm) [a]	f_N [a]	Author's Results (Reference)	M.I.T. Results (Reference)	$\bar{G}_{omp}$ (Range)	$k_{R,omp,1.7}$ [a] $(wh/g)^{-1}$	$k_{P,omp,1}$ [b] $(hr)^{-1}$
Euratom BL02 Loop	A-20	OM-2	Tr	805	430	0.0385 ±.0027	0.18	G*(-omp) = 1.06 K_1(-omp) = 0.0910	data not available	0.80[g]	2.85×10^{-2}	$2.56 \pm 0.36 \times 10^{-3}$
Euratom BL02 Loop	A-17	OM-2	Tr	787	420	0.0416 ±.0030	0.18	G*(-omp) = 0.78 K_1(-omp) = 6.70×10^{-2} (A5.4)	data not available	0.80[g]	2.82×10^{-2}	$1.78 \pm 0.25 \times 10^{-3}$
Euratom BL02 Loop	A-12	OM-2	Tr	766	408	0.0396 ±.0028	0.18	G*(-omp) = 0.58 K_1(-omp) = 4.98×10^{-2} (A5.4)	data not available	0.80[g]	2.80×10^{-2}	$1.02 \pm 0.14 \times 10^{-3}$
Euratom BL02 Loop	A-18	OM-2	Tr	751	400	0.0411 ±.029	0.18	G*(-omp) = 0.48 K_1(-omp) = 4.12×10^{-2} (A5.4)	data not available	0.80[g]	2.75×10^{-2}	$7.24 \pm 1.00 \times 10^{-4}$
Euratom BL02 Loop	A-16	OM-2	Tr	715	380	0.0380 ±.0027	0.18	G*(-omp) = 0.33 K_1(-omp) = 2.83×10^{-2} (A5.4)	data not available	0.80[g]	2.70×10^{-2}	$1.86 \pm 0.26 \times 10^{-4}$
CRC Susie neutron rich - capsules	Samples 295 296 297 298 299 300	SW-OMP	Tr	750	399	0.015-0.019	0.95 ±.02	unreported for total omp disappearance	K_1(-omp) = $(12.68 \pm 0.38) \times 10^{-2}$ (A5.5)	0.67 (1.00-0.45)	6.87×10^{-2}	$1.27 \pm 0.30 \times 10^{-3}$
CRC Susie neutron rich - capsules	Samples 325 326 327 328 329 330	meta	Tr	750	399	0.0143-0.0186	0.95 ±.02	K_1(-m) = 11.81×10^{-2}	K_1(-m) = $(12.27 \pm 0.46) \times 10^{-2}$ (A5.5)	0.68 (0.96-0.45)	6.87×10^{-2}	$1.16 \pm 0.32 \times 10^{-3}$
CRC Susie neutron rich - capsules	Samples 343 344 345 346 347 348	meta in meta-para (50-50) mixture	Tr	750	399	0.013-0.014	0.95 ±.02	K_1(-m) = 9.26×10^{-2}	K_1(-m) = $(10.57 \pm 0.62) \times 10^{-2}$ (A5.5)	0.79 (1.00-0.59)	6.87×10^{-2}	$6.35 \pm 1.70 \times 10^{-4}$
CRC MTR Gamma Grid	Sample 111	meta	Tr	675	357	0.0078	0	K_1(-m) = 3.56×10^{-2} (A5.5)	K_1(-m) = 3.58×10^{-2}	0.81 (0.95-0.69)	1.69×10^{-2}	$1.48 \pm 0.24 \times 10^{-4}$
CRC MTR Gamma Grid	Samples 75 76 31 32	meta	Tr	750	399	0.0155-0.0185	0	K_1(-m) = 5.75×10^{-2} (A5.5)	K_1(-m) = $(5.00 \pm 0.47) \times 10^{-2}$ K_2(-m) = $(11.82 \pm 0.41) \times 10^{-2}$	0.62 (0.95-0.24)	1.77×10^{-2}	$6.38 \pm 1.60 \times 10^{-4}$ 1.03 ± 0.20[h] $\times 10^{-3}$
CRC MTR Gamma Grid	Samples 15 16 79 80	SW-OMP	Tr	750	399	0.0155-0.0181	0	unreported	K_1(-omp) = $(4.79 \pm 0.17) \times 10^{-2}$ K_2(-omp) = $(10.96 \pm 0.49) \times 10^{-2}$ (A5.5)	0.56 (1.00-0.25)	1.77×10^{-2}	$6.13 \pm 1.50 \times 10^{-4}$ 8.50 ± 1.70[h] $\times 10^{-4}$

[h] based on second-order kinetics correlation

Table A5.3

Calculation of Second-Order Radiolysis Rate Constants for AECL Irradiations of Meta-Rich Coolants

Facility	Run No.	Terphenyl	Type	Temperature °F	Temperature °C	Avg. Dose Rate, $\bar{r}$ (watts/gm)	f_N	Author's Results (Reference)	M.I.T. Results (Reference)	$\bar{G}_1$ (Range)	$k_{P,1,1}$ [a] $(hr)^{-1}$	$k_{R,1,2}$ $(wh/g)^{-1}$
AECL NRX E-3	Sample E-29	meta	Tr	840	447-449	0.1	0.50	G(-m) = 2.02 (integral value) (A5.7)	$K_1(-m) = 19.17 \times 10^{-2}$ $K_2(-m) = 21.23 \times 10^{-2}$	0.90 (1.00-0.82)	6.5×10^{-3}	14.1×10^{-2}
AECL NRX E-3	Sample E-102	meta	Tr	842	450	0.3	0.57	G(-m) = 1.61 (integral value) (A5.7)	$K_1(-m) = 15.05 \times 10^{-2}$ $K_2(-m) = 16.65 \times 10^{-2}$	0.90 (1.00-0.82)	6.5×10^{-3}	14.3×10^{-2}
AECL NRX E-3	Sample E-104	meta	Tr	831	444	0.3	0.57	G(-m) = 1.25 (integral value) (A5.7)	$K_1(-m) = 11.65 \times 10^{-2}$ $K_2(-m) = 12.8 \times 10^{-2}$	0.91 (1.00-0.84)	4.5×10^{-3}	11.2×10^{-2}
AECL NRX E-3	Sample E-103	meta	Tr	820	438	0.3	0.57	G(-m) = 1.23 (integral value) (A5.7)	$K_1(-m) = 11.74 \times 10^{-2}$ $K_2(-m) = 13.16 \times 10^{-2}$	0.89 (1.00-0.80)	3.8×10^{-3}	11.7×10^{-2}
AECL NRX E-3	Sample E-106	meta	Tr	771-779	411-415	0.3	0.57	G(-m) = 0.748 (integral value) (A5.7)	$K_1(-m) = 6.88 \times 10^{-2}$ $K_2(-m) = 7.42 \times 10^{-2}$	0.93 (1.00-0.86)	1×10^{-3}	7.1×10^{-2}
AECL NRX E-3	Sample E-96	meta	Tr	755-768	402-409	0.3	0.57	G(-m) = 0.762 (integral value) (A5.7)	$K_1(-m) = 6.93 \times 10^{-2}$ $K_2(-m) = 7.33 \times 10^{-2}$	0.94 (1.00-0.89)	7×10^{-4}	7.1×10^{-2}
AECL NRX E-3	Sample E-92	OM-2	Tr	748-755	398-402	0.3	0.57	G(-omp) = 0.600 (integral value) (A5.7)	$K_1(-omp) = 5.08 \times 10^{-2}$ $K_2(-omp) = 5.27 \times 10^{-2}$	0.96 (1.00-0.92)	4×10^{-4}	5.1×10^{-2}
AECL NRX E-3	Sample E-95	OM-2	Tr	751-769	400-410	0.3	0.57	G(-omp) = 0.648 (integral value) (A5.7)	$K_1(-omp) = 5.63 \times 10^{-2}$ $K_2(-omp) = 5.95 \times 10^{-2}$	0.95 (1.00-0.89)	6×10^{-4}	5.7×10^{-2}
AECL NRX E-3	Sample E-37	meta	Tr	669	354	0.1	0.50	G(-m) = 0.398 (integral value) (A5.7)	$K_1(-m) = 4.30 \times 10^{-2}$ $K_2(-m) = 5.48 \times 10^{-2}$	0.79 (1.00-0.63)	—	5.4×10^{-2}
AECL NRX E-3	Sample E-68	meta	Tr	667	353	0.1	0.50	G(-m) = 0.487 (integral value) (A5.7)	$K_1(-m) = 4.57 \times 10^{-2}$ $K_2(-m) = 5.05 \times 10^{-2}$	0.91 (1.00-0.83)	—	5.0×10^{-2}
AECL NRX E-3	Sample E-100	meta	Tr	673	356	0.3	0.57	G(-m) = 0.410 (integral value) (A5.7)	$K_1(-m) = 3.72 \times 10^{-2}$ $K_2(-m) = 3.95 \times 10^{-2}$	0.94 (1.00-0.88)	—	4.0×10^{-2}
AECL NRX X-rod		OM-2	Tr	581	305	0.33	0.30	(A5.8)	$K_1(-omp) = 2.65 \times 10^{-2}$ $K_2(-omp) = 3.10 \times 10^{-2}$ (A5.1)	0.86	—	3.1×10^{-2}
AECL NRX X-rod		OM-2	Tr	617	325	0.33	0.30	(A5.8)	$K_1(-omp) = 2.85 \times 10^{-2}$ $K_2(-omp) = 3.23 \times 10^{-2}$ (A5.1)	0.88	—	3.23×10^{-2}

[a] estimated from Figures 5.4 and 5.6

Table A5.3 (cont.)

Calculation of Second-Order Radiolysis Rate Constants for AECL Irradiations of Meta-Rich Coolants

Facility	Run No.	Terphenyl	Type	Temperature °F	Temperature °C	Avg. Dose Rate, $\bar{r}$ (watts/gm)	F_N	Author's Results (Reference)	M.I.T. Results (Reference)	$\bar{C}_1$ (Range)	$k_{P,i,1}$ [a] $(hr)^{-1}$	$k_{R,i,2}$ $(wh/g)^{-1}$
AECL NRX X-rod		OM-2	Tr	626	330	0.33	0.30	(A5.8)	$K_1(-omp) = 2.24 \times 10^{-2}$ $K_2(-omp) = 3.27 \times 10^{-2}$ (A5.1)	0.69	—	3.27×10^{-2}
AECL NRX X-rod		OM-2	Tr	536-617	280-325	0.33	0.30	(A5.8)	$K_1(-omp) = 2.05 \times 10^{-2}$ $K_2(-omp) = 2.94 \times 10^{-2}$ (A5.1)	0.70	—	2.94×10^{-2}
AECL NRX X-rod		OM-2	Tr	536	280	0.33	0.30	(A5.8)	$K_1(-omp) = 2.44 \times 10^{-2}$ $K_2(-omp) = 2.85 \times 10^{-2}$ (A5.1)	0.86	—	2.85×10^{-2}
AECL NRX Mk III Trans-former		meta	Tr	482	250	1.0	0.50	$G^o(-m) = 0.4$ [b] (A5.9)	—	—	—	3.44×10^{-2}
AECL NRX Mk III Trans-former		meta	Tr	725	385	1.0	0.50	$G^o(-m) = 0.44$ [b] (A5.9)	—	—	—	3.78×10^{-2}
AECL NRX Mk III Trans-former		meta	Tr	788	420	1.0	0.50	$G^o(-m) = 0.51$ [b] (A5.9)	—	—	—	4.37×10^{-2}
AECL Van de Graaff		meta	Tr	572	300	0.4 5.0	0	$G^o(-m) = 0.21$ [b] (A5.9)	—	—	—	1.8×10^{-2}
AECL Van de Graaff		meta	Tr	662	350	0.4 5.0	0	$G^o(-m) = 0.25$ [b] (A5.9)	—	—	—	2.1×10^{-2}
AECL Van de Graaff		meta	Tr	707	375	0.4		$G^o(-m) = 0.32$ [b] (A5.9)	—	—	—	2.7×10^{-2}
AECL Van de Graaff		meta	Tr	752	400	0.4		$G^o(-m) = 0.54$ [b] (A5.9)	—	—	—	4.6×10^{-2}
AECL Van de Graaff		meta	Tr	788	420	0.4	0	$G^o(-m) = 1.15$ [b] (A5.9)	—	—	—	9.9×10^{-2}
AECL Van de Graaff		meta	Tr	707	375	5	0	$G^o(-m) = 0.28$ [b] (A5.9)	—	—	—	2.4×10^{-2}
AECL Van de Graaff		meta	Tr	752	400	5	0	$G^o(-m) = 0.38$ [b] (A5.9)	—	—	—	3.3×10^{-2}
AECL Van de Graaff		meta	Tr	788	420	5	0	$G^o(-m) = 0.45$ [b] (A5.9)	—	—	—	3.9×10^{-2}
AECL Van de Graaff		meta	Tr	824	440	5	0	$G^o(-m) = 0.55$ [b] (A5.9)	—	—	—	4.7×10^{-2}
AECL NRX Cadmium Annulus		meta	Tr		360	0.2	0.01	$G^o(-m) = 0.3$ [b] (A5.9)	—	—	—	2.6×10^{-2}
AECL NRX Cadmium Annulus		meta	Tr		397	0.2	0.01	$G^o(-m) = 0.9$ [b] (A5.9)	—	—	—	7.7×10^{-2}
AECL NRX Cadmium Annulus		meta	Tr		455-458	0.2	0.01	$G^o(-m) = 1.7$ [b] (A5.9)	—	—	—	14.6×10^{-2}

[b] corrected for radiopyrolysis by AECL

Table A5.4

Calculation of Second-Order Radiolysis Rate Constants for AECL Irradiations of Ortho-Rich Coolants

Facility	Run No.	Terphenyl	Type	Temperature °F	Temperature °C	Avg. Dose Rate, $\bar{r}$ (watts/gm)	f_N	Author's Results (Reference)	M.I.T. Results (Reference)	σ_i (Range)	$k_{P,i,1}$ $(hr)^{-1}$	$k_{R,i,2}$ $(wh/g)^{-1}$
AECL NRX E-3	Sample E-23 to E-66	ortho	Tr	661-668	350-354	0.1	0.50	$G^o(-o)$ = [a] 0.67 - 1.0 (second order) (A5.7)	$K_1(-o)$ = 4.81×10^{-2} $K_2(-o)$ = 6.93×10^{-2}	0.69 (1.00-0.53)	—	6.93×10^{-2}
AECL NRX E-3	Sample E-8	ortho	Tr	746-752	397-400	0.1	0.50	G(-o) = 0.915 (integral value) (A5.7)	$K_1(-o)$ = 9.46×10^{-2} $K_2(-o)$ = 11.45×10^{-2}	0.83 (1.00-0.69)	5.8×10^{-4}	10.7×10^{-2}
AECL NRX E-3	Sample E-74	ortho	Tr	753	401	0.1	0.50	G(-o) = 2.51 (integral value) (A5.7)	$K_1(-o)$ = 23.44×10^{-2} $K_2(-o)$ = 25.00×10^{-2}	0.94	5×10^{-4}	26.1×10^{-2}
AECL NRX E-3	Sample E-14	ortho	Tr	780-782	416-417	0.1	0.50	G(-o) = 1.27 (integral value) (A5.7)	$K_1(-o)$ = 13.31×10^{-2} $K_2(-o)$ = 16.52×10^{-2}	0.81 (1.00-0.66)	1.4×10^{-3}	14.7×10^{-2}
AECL NRX E-3	Samples E-13 to E-60	ortho	Tr	794	424	0.1	0.50	$G^o(-o)$ = [a] 2.47 - 3.03 (second order) (A5.7)	$K_1(-o)$ = 14.93×10^{-2} $K_2(-o)$ = 22.60×10^{-2}	0.66 (1.00-0.46)	2.7×10^{-3}	18.5×10^{-2}
AECL NRX E-3	Samples E-21 to E-28	ortho	Tr	836-840	447-449	0.1	0.50	G(-o) = [a] 2.19 - 3.93 (integral values) (A5.7)	$K_1(-o)$ = 23.92×10^{-2} $K_2(-o)$ = 34.02×10^{-2}	0.70 (1.00-0.59)	7×10^{-3}	24.2×10^{-2}
AECL NRX E-3	Sample E-84	ortho	Tr	603-612	318-323	0.3	0.57	G(-o) = 0.495 (integral value) (A5.7)	$K_1(-o)$ = 4.63×10^{-2} $K_2(-o)$ = 5.07×10^{-2}	0.91 (1.00-0.83)	—	5.07×10^{-2}
AECL NRX E-3	Sample E-82	ortho	Tr	733-756	390-403	0.3	0.57	G(-o) = 1.38 (integral value) (A5.7)	$K_1(-o)$ = 12.88×10^{-2} $K_2(-o)$ = 14.08×10^{-2}	0.91 (1.00-0.84)	4×10^{-4}	14.0×10^{-2}
AECL NRX E-3	Sample E-85	ortho	Tr	759-766	404-408	0.3	0.57	G(-o) = 1.45 (integral value) (A5.7)	$K_1(-o)$ = 13.73×10^{-2} $K_2(-o)$ = 15.21×10^{-2}	0.90 (1.00-0.82)	6×10^{-4}	15.0×10^{-2}
AECL NRX E-3	Sample E-83	ortho	Tr	780-793	416-423	0.3	0.57	G(-o) = 1.71 (integral value) (A5.7)	$K_1(-o)$ = 16.46×10^{-2} $K_2(-o)$ = 18.65×10^{-2}	0.88 (1.00-0.78)	1.4×10^{-3}	18.2×10^{-2}
AECL NRX E-3	Sample E-78	ortho	Tr	800-805	427-430	0.3	0.57	G(-o) = 1.83 (integral value) (A5.7)	$K_1(-o)$ = 18.10×10^{-2} $K_2(-o)$ = 21.14×10^{-2}	0.86 (1.00-0.74)	2.1×10^{-3}	20.2×10^{-2}

[a] calculated individually for each sample

Table A5.4 (cont.)

Calculation of Second Order Radiolysis Rate Constants for AECL Irradiations of Ortho-Rich Coolants

Facility	Run No.	Terphenyl	Type	Temperature °F	Temperature °C	Avg. Dose Rate, $\bar{r}$ (watts/gm)	f_N	Author's Results (Reference)	M.I.T. Results (Reference)	$\bar{\sigma}_i$ (Range)	$k_{P,i,1}$ $(hr)^{-1}$	$k_{R,i,2}$ $(wh/g)^{-1}$
AECL NRX E-3	Sample E-79	ortho	Tr	821-825	439-441	0.3	0.57	G(-o) = 2.81 (integral value) (A5.7)	$K_1(-o) = 28.51 \times 10^{-2}$ $K_2(-o) = 34.10 \times 10^{-2}$	0.84 (1.00-0.71)	3.8×10^{-3}	32.4×10^{-2}
AECL NRX E-3	Sample E-76	ortho	Tr	836-845	447-452	0.3	0.57	G(-o) = 2.97 (integral value) (A5.7)	$K_1(-o) = 30.86 \times 10^{-2}$ $K_2(-o) = 38.11 \times 10^{-2}$	0.81 (1.00-0.66)	7×10^{-3}	35.2×10^{-2}
AECL NRX E-3	Sample E-11	ortho	Tr		253-259	0.1	0.50	G(-o) = 0.383 (integral value) (A5.7)	$K_1(-o) = 3.55 \times 10^{-2}$ $K_2(-o) = 3.87 \times 10^{-2}$	0.92 (1.00-0.84)	—	3.87×10^{-2}
AECL NRX E-3	Sample E-10	ortho	Tr		303	0.1	0.50	G(-o) = 0.443 (integral value)	$K_1(-o) = 4.11 \times 10^{-2}$ $K_2(-o) = 4.48 \times 10^{-2}$	0.92 (1.00-0.84)	—	4.48×10^{-2}
AECL NRX Mk III Trans-former		ortho	Tr		250	1.0	0.50	$G^o(-o) = 0.5$[b]	—	—	—	4.29×10^{-2}
AECL NRX Mk III Trans-former		ortho	Tr		350	1.0	0.50	$G^o(-o) = 0.75$[b]	—	—	—	6.44×10^{-2}
AECL NRX Mk III Trans-former		ortho	Tr		400	1.0	0.50	$G^o(-o) = 0.9$[b]	—	—	—	7.73×10^{-2}
AECL NRX Mk III Trans-former		ortho	Tr		450	1.0	0.50	$G^o(-o) = 1.3$	—	—	—	11.18×10^{-2}
AI Van de Graaff		ortho	Tr	752	402	0.82	0	$G^o(-o) = 2.14$[c] (A5.16)	$K_1(-o) = 7.69 \times 10^{-2}$ $K_2(-o) = 9.49 \times 10^{-2}$ (first part of transient)	0.81 (1.00-0.70)	6.5×10^{-4}	9.3×10^{-2}
									$K_1(-o) = 4.22 \times 10^{-2}$ $K_2(-o) = 6.66 \times 10^{-2}$ (entire transient)	0.63 (1.00-0.48)	1×10^{-3}	6.4×10^{-2}

[b] corrected for radiopyrolysis by AECL [c] estimated by graphical extrapolation

Table A5.4 (cont.)

Calculation of Second-Order Radiolysis Rate Constants for AECL Irradiations of Ortho-Rich Coolants

Facility	Run No.	Terphenyl	Type	Temperature °F	Temperature °C	Avg. Dose Rate, $\bar{r}$ (watts/gm)	f_N	Author's Results (Reference)	M.I.T. Results (Reference)	$\bar{\sigma}_1$ (Range)	$k_{P,i,1}$ $(hr)^{-1}$	$k_{R,i,2}$ $(wh/g)^{-1}$
AI Van de Graaff		ortho	Tr	802	429	0.72	0	$G^o(-o) = 4.05^c$ (A5.16)	$K_1(-o) = 15.2 \times 10^{-2}$ $K_2(-o) = 18.7 \times 10^{-2}$ (first part of transient)	0.81 (1.00-0.71)	2.5×10^{-3}	18.1×10^{-2}
									$K_1(-o) = 10.56 \times 10^{-2}$ $K_2(-o) = 16.4 \times 10^{-2}$	0.64 (1.00-0.45)	3.5×10^{-3}	15.5×10^{-2}
AI Van de Graaff		ortho	Tr	850	455	0.86	0	$G^o(-o) = 7.64^c$ (A5.16)	$K_1(-o) = 29.4 \times 10^{-2}$ $K_2(-o) = 38.1 \times 10^{-2}$	0.77 (1.00-0.67)	7×10^{-3}	36.2×10^{-2}
AECL NRX Cadmium Annulus		ortho	Tr		250	0.2	0.01	$G^o(-o) = 0.23^b$ (A5.9)	—	—	—	1.97×10^{-2}
AECL NRX Cadmium Annulus		ortho	Tr		350	0.2	0.01	$G^o(-o) = 0.72^b$ (A5.9)	—	—	—	6.2×10^{-2}
AECL NRX Cadmium Annulus		ortho	Tr		400	0.2	0.01	$G^o(-o) = 1.5^b$ (A5.9)	—	—	—	12.9×10^{-2}
AECL NRX Cadmium Annulus		ortho	Tr		450	0.2	0.01	$G^o(-o) = 5^b$ (A5.9)	—	—	—	43×10^{-2}

APPENDIX A6

REFERENCES

(1.1) Morgan, D. T., Mason, E. A., "Organic Moderator-Coolant In-Pile Irradiation Loop for the M.I.T. Nuclear Reactor, Part II, Equipment Design, Procedures and Results of Irradiation to October 5, 1961," MITNE-22, IDO-11,105, May, 1962.

(1.2) Sawyer, C. D., Mason, E. A., "The Effects of Reactor Irradiation on Santowax OMP at 610°F and 750°F," M.I.T., Cambridge, Massachusetts (September, 1963), MITNE-39, IDO-11,107.

(1.3) Timmins, T. H. Mason, E. A., Morgan, D. T., "Effect of Reactor Irradiation on Santowax WR: Irradiations from 425°F to 800°F at 40% Fast Neutron Fraction," M.I.T., Cambridge, Massachusetts (February, 1966), MITNE-68, MIT-334-34.

(1.4) Personal Communication from H. Hannaert, (Euratom) to E. A. Mason (M.I.T.) June, 1966.

(1.5) Boyd, A. W., Connor, H. W. J., Miller, O. A., "The Radiolysis of Ortho- and Meta-Terphenyl II: With Gamma Rays at Dose Rates of 0.15 - 0.2 Wg^{-1}," AECL, Chalk River, Ontario, AECL-2589, June, 1966.

(1.6) Mackintosh, W. D., Miller, O. A., "The Pyrolysis of the Potential Power Reactor Coolant, Santowax O-M," AECL, Chalk River, Ontario, AECL-2218, June, 1965.

(1.7) Houllier, A., "Interpretation des Resultats Experimentaux de Radiolyse au 31 Aout 1963 Obtenus Avec les Boucles a Liquide Organique No. 2 et No. 3 — Influence de la Pyrolyse sur la Vitesse de Decomposition du Terphenyle OM-2," Communication Euratom No. 589, Lyon, France, November, 1963.

(1.8) Juppe, G., Alvarenga, A., Hannaert, H., "The Pyrolytic Decomposition of Terphenyls," Euratom, EUR 1647.e, 1964.

(1.9) Marche d'Irradiation n° 117-63-4 ORGF (Rapport annuel) Periode du 1er Avril 1963 au 1er Avril 1964, Euratom.

(1.10) Bolt, R. O., et al., "Relative Effects of Fast Neutrons and Gamma Rays on the Radiolysis of Polyphenyls," California Research - AEC Report 23, June 30, 1963.

(1.11) Boyd, A. W., Connor, H. W. J., "The Radiolysis of Ortho and Meta Terphenyl I: With a Mixture of Fast Neutrons and Gamma Rays at Dose Rates of 0.1 and 0.3 W/g," AECL, Chalk River, Ontario, CRC-1219, AECL-2258, May, 1965.

(1.12) Personal Communication from S. R. Hatcher (AECL) to E. A. Mason (M.I.T.), Vienna, Austria, May, 1966, information understood to be contained in an AECL report in preparation, "The Radiolysis of Ortho- and Meta-Terphenyl III: With a Mixture of Fast Neutrons and Gamma Rays at a Dose Rate of 1 W/g."

(1.13) Scarborough, J. M., "Radiolytic and Pyrolytic Decomposition of Ortho Terphenyl at High Temperature," Atomics International, Canoga Park, California, NAA-SR-8277, June, 1964.

(2.1) Morgan, D. T., Mason, E. A., "Organic Moderator-Coolant In-Pile Irradiation Loop for the M.I.T. Nuclear Reactor, Part II, Equipment Design, Procedures and Results of Irradiation to October 5, 1961," MITNE-22, IDO-11,105, May, 1962.

(2.2) Sawyer, C. D., Mason, E. A., "The Effects of Reactor Irradiation on Santowax OMP at 610°F and 750°F," M.I.T., Cambridge, Massachusetts (September, 1963), MITNE-39, IDO-11,107.

(2.3) Timmins, T. H., Mason, E. A., Morgan, D. T., "Effect of Reactor Irradiation on Santowax WR: Irradiations from 425°F to 800°F at 40% Fast Neutron Fraction," M.I.T., Cambridge, Massachusetts (February, 1966), MITNE-68, MIT-334-34.

(3.1) Timmins, T. H. Mason, E. A., Morgan, D. T., "Effect of Reactor Irradiation on Santowax WR: Irradiations from 425°F to 800°F at 40% Fast Neutron Fraction," M.I.T., Cambridge, Massachusetts (February, 1966), MITNE-68, MIT-334-34.

(3.2) Swan, A. H., Mason, E. A., "Friction Factor and Heat Transfer Correlation for Irradiated Organic Coolants," M.I.T., Cambridge, Massachusetts (September, 1965), MIT-334-23.

(3.3) Morgan, D. T., Mason, E. A., "Organic Moderator – Coolant In-Pile Irradiation Loop for the M.I.T. Nuclear Reactor, Part II, Equipment Design, Procedures and Results of Irradiation to October 5, 1961," M.I.T., Cambridge, Massachusetts, MITNE-22, IDO-11,105, May, 1962.

(3.4) Sawyer, C. D., Mason, E. A., "The Effects of Reactor Irradiation on Santowax OMP at 610°F and 750°F," M.I.T., Cambridge, Massachusetts (September, 1963), MITNE-39, IDO-11,107.

(3.5) Mandel, H., "Heavy Water Organic Cooled Reactor, Physical Properties of Some Polyphenyl Coolants," AI-CE-15, April 15, 1966.

(3.6) Elberg, S., Fritz, G., "Physical Properties of Organic Nuclear Reactor Coolants," ORGEL Program, EUR-400.e (1963).

(3.7) Chavanel, et al., "Compilation des Mesures de Densite et Viscosite du Terphenyl OM-2 Irradie En Pile," ORGEL Program, Euratom Communication No. 673, April, 1964.

(3.8) Mason, E. A., "In-Pile Loop Irradiation Studies of Organic Materials," M.I.T., Cambridge, Massachusetts, MITNE-41, (1963).

(3.9) Bley, W. N., Mason, E. A., "The Nature of the High Boiler Degradation Products from Irradiated Santowax OMP," MITNE-55 (MIT-334-11), Department of Nuclear Engineering, M.I.T., Cambridge, Massachusetts, February 1, 1965.

(3.10) Personal Communications, R. C. Shepherd (Atomics International) to W. N. Bley (M.I.T.), April, 1966 and August, 1966.

(4.1) Timmins, T. H., Mason, E. A., and Morgan, D. T., "Effect of Reactor Irradiation on Santowax WR: Irradiations from 425°F to 800°F at 40% Fast Neutron Fraction," MIT-334-34 (MITNE-68), Cambridge, Massachusetts, February, 1966.

(4.2) Personal Communication, H. Hannaert (Euratom) to E. A. Mason, (M.I.T.), June, 1966.

(4.3) Sawyer, C. D. and Mason, E. A., "The Effects of Reactor Irradiation on Santowax OMP at 610°F and 750°F," IDO-11, 107 (MITNE-39), Cambridge, Massachusetts, September, 1963.

(4.4) Personal Communication from S. R. Hatcher (AECL) to E. A. Mason (M.I.T.), Vienna, Austria, May, 1966, information understood to be contained in an AECL report in preparation, "The Radiolysis of Ortho- and Meta-Terphenyl III: With a Mixture of Fast Neutrons and Gamma Rays at a Dose Rate of 1 W/g."

(4.5) Boyd, A. W., Connor, H. W. J., and Miller, O. A., "The Radiolysis of Ortho- and Meta-Terphenyl II: With Gamma Rays at Dose Rates of 0.15 - 0.2 Wg^{-1}," AECL-2589, Chalk River, Ontario, June, 1966.

(5.1) Timmins, T. H., Mason, E. A., Morgan, D. T., "Effect of Reactor Irradiation on Santowax WR: Irradiations from 425°F to 800°F at 40% Fast Neutron Fraction," M.I.T., Cambridge, Massachusetts (February, 1966), MITNE-68, MIT-334-34.

(5.2) Boyd, A. W. and Connor, H. W. J., "The Radiolysis of Ortho and Meta Terphenyl I: With a Mixture of Fast Neutrons and Gamma Rays at Dose Rates of 0.1 and 0.3 W/g," AECL-2258 (CRC-1219), Chalk River, Ontario, May, 1965.

(5.3) Personal Communication from S. R. Hatcher (AECL) to E. A. Mason (M.I.T.), Vienna, Austria, May 9, 1966, information understood to be in the following AECL report which is in preparation: "The Radiolysis of Ortho- and Meta-Terphenyl III: With a Mixture of Fast Neutrons and Gamma Rays at a Dose Rate of 1 W/g."

(5.4) Juppe, G., et al., "The Pyrolytic Decomposition of Terphenyls," EUR 1647.e, 1964.

(5.5) Personal Communication from H. Hannaert, Euratom, to E. A. Mason, M.I.T., June, 1966.

(5.6) Houllier, A., "Interpretation des Resultats Experimentaux de Radiolyse au 31 Aout 1963 Obtenus Avec les Boucles a Liquide Organique No. 2 et No. 3 – Influence de la Pyrolyse sur la Vitesse de Decomposition du Terphenyle OM-2," Communication Euratom No. 589, Category 1.2, Lyon, France, November, 1963.

(5.7) Mackintosh, W. D., Miller, O. A., "The Pyrolysis of the Potential Power Reactor Coolant, Santowax O-M," AECL, Chalk River, Ontario, June, 1965, AECL-2218.

(5.8) Bolt, R. O., et al., "Relative Effects of Fast Neutrons and Gamma Rays on the Radiolysis of Polyphenyls," California Research – AEC Report 23, June 30, 1963.

(5.9) Mackintosh, W. D., "The Electron Irradiation of the Potential Organic Coolant for Power Reactors, Santowax OM," paper presented at the Third Conference on Nuclear Reactor Chemistry, Gatlinburg, Tennessee, October, 1962.

(5.10) "Heavy Water Organic Cooled Reactor, 1000 Mwe Nuclear Power Plant Preliminary Conceptual Design," AI-CE-Memo 6, Volumes I and II, Combustion Engineering, Inc. and Atomics International, October 1, 1965.

(5.11) "Heavy Water Organic Cooled Reactor," Quarterly Technical Progress Report, Inception through June, 1965, AI-CE-3, Combustion Engineering, Inc. and Atomics International, August 15, 1965.

(5.12) Personal Communication from R. Stiens, Atomics International to T. H. Timmins, M.I.T., April 8, 1966.

(5.13) Personal Communication from R. S. Harding, Combustion Engineering, Inc., to W. N. Bley, M.I.T., March, 1966.

(6.1) Personal Communication from S. R. Hatcher (AECL) to E. A. Mason (M.I.T.), Vienna, Austria, May 9, 1966, information understood to be in the following AECL report which is in preparation: "The Radiolysis of Ortho- and Meta-Terphenyl III: With a Mixture of Fast Neutrons and Gamma Rays at a Dose Rate of 1 W/g."

(6.2) Mackintosh, W. D., "The Electron Irradiation of the Potential Organic Coolant for Power Reactors, Santowax OM," Paper presented at the Third Conference on Nuclear Reactor Chemistry, Gatlinburg, Tennessee, October, 1962.

(6.3) Terrien, J. F. and Mason, E. A., "Relative Roles of Pyrolysis and Radiolysis in the Degradation of Terphenyls," MITNE-48, Department of Nuclear Engineering, M.I.T., Cambridge, Massachusetts, June, 1964.

(6.4) Timmins, T. H., Mason, E. A., and Morgan, D. T., "Effect of Reactor Irradiation on Santowax WR: Irradiations from 425°F to 800°F at 40% Fast Neutron Fraction," MITNE-68, MIT-334-34, M.I.T., Cambridge, Massachusetts, February, 1966.

(6.5) "Effect of High Temperature on Radiolytic and Pyrolytic Damage of Polyphenyls," Excerpts from NAA-SR-8888, Annual Technical Progress Report, AEC Unclassified Program FY 63, Atomics International, Canoga Park, California.

(6.6) Scarborough, J. M., "Radiolytic and Pyrolytic Decomposition of Ortho Terphenyl at High Temperature," NAA-SR-8277, June 1, 1964.

(6.7) Boyd, A. W. and Connor, H. W. J., "The Radiolysis of Ortho and Meta Terphenyl, I: With a Mixture of Fast Neutrons and Gamma Rays at Dose Rates of 0.1 and 0.3 W/g," CRC-1219, AECL-2258, AECL, Chalk River, Ontario, May, 1965.

(6.8) "Heavy Water Organic Cooled Reactor, 750 Mwe Demonstration Plant," AI-CE Memo-25, Combustion Engineering, Inc. and Atomics International, March, 1966.

(6.9) Boyd, A. W., Connor, H. W. J., and Miller, O. A., "The Radiolysis of Ortho- and Meta-Terphenyl II: With Gamma Rays at Dose Rates of 0.15 - 0.2 Wg^{-1}," AECL-2589, Chalk River, Ontario, June, 1966.

(A1.1) Morgan, D. T., Mason, E. A., "Organic Moderator – Coolant In-Pile Irradiation Loop for the M.I.T. Nuclear Reactor, Part II, Equipment Design, Procedures and Results of Irradiation to October 5, 1961," MITNE-22, IDO-11,105, May, 1962.

(A1.2) Sawyer, C. D., Mason, E. A., "The Effects of Reactor Irradiation on Santowax OMP at 610°F and 750°F," M.I.T., Cambridge, Massachusetts (September, 1963), MITNE-30, IDO-11,107.

(A1.3) Timmins, T. H., Mason, E. A., Morgan, D. T., "Effect of Reactor Irradiation on Santowax WR: Irradiations from 425°F to 800°F at 40% Fast Neutron Fraction," M.I.T., Cambridge, Massachusetts (February, 1966), MITNE-68, MIT-334-34.

(A1.4) Mason, E. A., Timmins, T. H., Morgan, D. T., "Measurement of Dose Rates in the MITR Core: Adiabatic Calorimetry and Flux Measurements," MITNE-43 (MITNE-71), M.I.T., Cambridge, Massachusetts (Report in preparation).

(A1.5) Woodruff, G. L., Kaplan, I., and Thompson, T. J., "A Study of the Spatial Distributions of Fast Neutrons in Lattices of Slightly Enriched Uranium Rods Moderated by Heavy Water," M.I.T., Cambridge, Massachusetts (November, 1965), MITNE-67.

(A1.6) Rim, C. S., "Dosimetry of Reactor Radiation in the M.I.T. Reactor by Calorimetric Measurements," M.S. Thesis, M.I.T. Department of Nuclear Engineering (January, 1966), MIT-334-50.

(A1.7) Vidal, R., "Mesure des Integrales de Resonance d'Absorption," CEA-R-2486 (July, 1964).

(A1.8) Dahlberg, R., et al., "Measurements of Some Resonance Activation Integrals," J. Nuc. Eng., 14, No. 1, p. 53, April, 1961.

(A3.1) Hald, A., Statistical Theory with Engineering Applications, John Wiley and Sons, Inc., New York, Fourth Printing, 1960.

(A3.2) Sawyer, C. D., Mason, E. A., "The Effects of Reactor Irradiation on Santowax OMP at 610°F and 750°F," M.I.T., Cambridge, Massachusetts (September, 1963), MITNE-39, IDO-11,107.

(A3.3) Timmins, T. H., Mason, E. A., Morgan, D. T., "Effect of Reactor Irradiation on Santowax WR: Irradiations from 425°F to 800°F at 40% Fast Neutron Fraction," M.I.T., Cambridge, Massachusetts (February, 1966), MITNE-68, MIT-334-34.

(A5.1) Timmins, T. H., Mason, E. A., and Morgan, D. T., "Effect of Reactor Irradiation on Santowax WR, Irradiations from 425°F to 800°F at 40% Fast Neutron Fraction," (MITNE-68), MIT-334-34, M.I.T., Cambridge, Massachusetts, February, 1966.

(A5.2) Sawyer, C. D. and Mason, E. A., "The Effects of Reactor Irradiation on Santowax OMP at 610°F and 750°F," MITNE-39 (MIT-334-11), Department of Nuclear Engineering, M.I.T., Cambridge, Massachusetts, September, 1963.

(A5.3) Houllier, et al., March d'Irradiation Euratom – C.E.A. – Progil, No. 117-63-4 ORGF (Rapport Annual) Periode du 1er Avril, 1963 au 1er Avril, 1964.

(A5.4) Houllier, A., "Interpretation des Resultats Experimentaux de Radiolyse au 31 Aout 1963 Obtenus Avec les Boucles a Liquide Organique No. 2 et No. 3 – Influence de la Pyrolyse sur la Vitesse de Decomposition du Terphenyle OM-2," Communication Euratom No. 589, Category 1.2, Lyon, France, November, 1963.

(A5.5) Bolt, R. O., et al., "Relative Effects of Fast Neutrons and Gamma Rays on the Radiolysis of Polyphenyls," California Research – AEC Report No. 23, June 30, 1963.

(A5.6) Personal Communication H. Hannaert (Euratom) to E. A. Mason, (M.I.T.), June, 1966.

(A5.7) Boyd, A. W. and Connor, H. W. J., "The Radiolysis of Ortho and Meta Terphenyl, 1: With a Mixture of Fast Neutrons and Gamma Rays at Dose Rates of 0.1 and 0.3 W/g," CRC-1219, AECL-2258, AECL, Chalk River, Ontario, May, 1965.

(A5.8) Personal Communication, A. W. Boyd, AECL, Chalk River, Ontario, to E. A. Mason, M.I.T.

(A5.9) Personal Communication from S. R. Hatcher (AECL) to E. A. Mason (M.I.T.), Vienna, Austria, May, 1966, information understood to be contained in an AECL report in preparation, "The Radiolysis of Ortho- and Meta-Terphenyl III: With a Mixture of Fast Neutrons and Gamma Rays at a Dose Rate of 1 W/g."

(A5.10) Personal communication M. Van der Venne (Euratom) to E. A. Mason (M.I.T.), September, 1964.

(A5.11) Berg, S., et al., "Irradiations of Santowax OMP at the Curtiss-Wright Research Reactor, The Effect of Fast Neutrons on Organic Coolants," NAA-SR-5892, Atomics International, Canoga Park, California, January 3, 1961.

(A5.12) Zack, J. F. Jr., et al., "In-Pile Capsule Experiments to Determine the Effect of Fast Neutrons on the Radiolytic Decomposition Rate of Terphenyls," NAA-SR-7395, Atomics International, Canoga Park, California, June, 1959.

(A5.13) Bates, T. H., et al., "The Radiation and Thermal Stability of Some Potential Organic Moderator Coolants, Part V. Pile and Electron Irradiation of Biphenyl, Orthoterphenyl, Meta-terphenyl, and Pile Irradiation of Santowax R to High HBR Content," AERE-R3743, Chemistry Division, Atomic Energy Research Establishment, Harwell, Berkshire, March, 1962.

(A5.14) Bates, T. H., et al., "The Radiation and Thermal Stability of Some Potential Organic Moderator-Coolants, Part I. Electron Irradiation of Para-Terphenyl and Santowax R," AERE C/R2121, Chemistry Division, Atomic Energy Research Establishment, Harwell, Berkshire, 1957.

(A5.15) Burns, W. G., et al., "The Radiation and Thermal Stability of Some Potential Organic Moderator Coolants, Part VIII. Pile and Electron Irradiation of Various Polyphenyl Mixtures and Work with Additives," AERE R 4072, Chemistry Division, Atomic Energy Research Establishment, Harwell, Berkshire, 1963.

(A5.16) Scarborough, J. M., "Radiolytic and Pyrolytic Decomposition of Ortho Terphenyl at High Temperature," NAA-SR-8277, June 1, 1964.

APPENDIX A7

M.I.T. REPORT DISTRIBUTION LIST

U. S. Atomic Energy Commission
Savannah River Operations Office
P. O. Box A
Aiken, South Carolina 29801

2 Attn: R. J. Crosson, Acting
Director, HWOCR Division

1 Attn: R. G. Erdley, Chief
Patent Branch

1 Attn: N. Stetson, Manager SROO

U. S. Atomic Energy Commission
RDT Program Office (AI-CE)
CPAO
Canoga Park, California 91304

4 Attn: R. L. Morgan
RDT Sr. Site Representative

U. S. Atomic Energy Commission
RDT Site Office
P. O. Box 500
Windsor, Connecticut 06095

2 Attn: A. J. Alexander
RDT Sr. Site Representative

U. S. Atomic Energy Commission
RDT Site Office
P. O. Box A
Aiken, South Carolina 29801

1 Attn: J. H. Kruth
RDT Site Representative

USAEC Scientific Representative
Chalk River Liaison Office
c/o Atomic Energy of Canada, Ltd.
Chalk River, Ontario, Canada

3 Attn: M. N. Hudson, Jr.

USAEC Technical Representative
Whiteshell Branch, Chalk River Office
U. S. Atomic Energy Commission
c/o Whiteshell Nuclear Research Est., AECL
Pinawa, Manitoba, Canada

1 Attn: H. J. Reynolds

U. S. Atomic Energy Commission
Washington, D. C. 20545

1 Attn: R. M. Forssell, Chief
Advanced Development Branch
Division of Naval Reactors

2 Attn: A. N. Tardiff, Acting Chief
HWOCR Branch, RDT

1 Attn: J. W. Crawford
Asst. Director for Plant Engineering, RDT

1 Attn: G. M. Anderson, Chief
Components Branch, RDT

1 Attn: M. Booth, Chief
Systems Engineering Branch, RDT

1 Attn: M. Rosen, Chief
Applications of Facilities Branch, RDT

1 Attn: M. J. Whitman
Asst. Director for Reactor Engineering, RDT

1 Attn: K. A. Trickett, Chief
Core Design Branch, RDT

1 Attn: E. E. Sinclair
Asst. Director for Reactor Technology, RDT

1 Attn: W. H. McVey, Chief
Chemistry and Chemical Separations, RDT

1 Attn: F. Kerze
Fuels and Materials Branch, RDT

U. S. Atomic Energy Commission
Chicago Operations Office
9800 South Cass Avenue
Argonne, Illinois 60439

2 Attn: D. E. Simpson, Director

U. S. Atomic Energy Commission
Idaho Operations Office
P. O. Box 2108
Idaho Falls, Idaho 83401

1 Attn: Director, Nuclear Technology Division

U. S. Atomic Energy Commission
Oak Ridge Operations Office
P. O. Box E
Oak Ridge, Tennessee 37830

3 Attn: Division of Technical Information Extension

1 Attn: H. W. Behrman

1 Attn: R. L. Philippone

U. S. Atomic Energy Commission
Region III
Division of Compliance
Suite 410, Oakbrook Professional Bldg.
Oak Brook, Illinois 60523

1 Attn: H. D. Thornburg

U. S. Atomic Energy Commission
Brussels Office
U. S. Mission to the European Communities
APO, New York
New York 09667

1 Attn: T. J. Iltis
Acting Sr. USAEC Representative

HWOCR Program Office
c/o Atomics International
P. O. Box 309
Canoga Park, California 91304

1 Attn: C. L. Storrs

5 Attn: C. A. Trilling (for distribution)

Combustion Engineering, Inc.
Nuclear Division
P. O. Box 500
Windsor, Connecticut 06095

1 Attn: R. P. Varnes

1 Attn: R. S. Harding

1 Attn: W. Taylor

3 Attn: S. Visner (for distribution)

Atomics International
P. O. Box 309
Canoga Park, California 91304

4 Attn: R. T. Keen (for distribution)

1 Attn: R. A. Holroyd

1 Attn: R. Stiens

1 Attn: W. G. Smiley

Babcock and Wilcox Company
Atomic Energy Division
P. O. Box 1260
Lynchburg, Virginia 24505

3 Attn: W. N. Vannoy, Project Manager

Oak Ridge National Laboratory
Union Carbide Corporation
AEC Operations
P. O. Box X
Oak Ridge, Tennessee 37831

1 Attn: D. A. Douglas

1 Attn: D. E. Ferguson

1 Attn: J. A. Lane (ORNL P. O. Box Y)

1 Attn: I. Spiewak

Pacific Northwest Laboratory
P. O. Box 999
Richland, Washington 99352

1 Attn: J. J. Cadwell, Manager
Metallurgy Department

E. I. du Pont de Nemours and Company
Savannah River Laboratory
Aiken, South Carolina 29801

1 Attn: J. L. Crandall

2 Attn: S. W. O'Rear, Supv.
Technical Information Service

E. I. du Pont de Nemours and Company
Explosives Department
Wilmington, Delaware 19898

1 Attn: D. F. Babcock, Director
Reactor Engineering Section

Communaute Europeenne
de L'Energie Atomique
rue Belliard 51-53
Brussels, Belgium

1 Attn: J. Gueron

1 Hood Worthington
Devon Apartments, No. 1512
2401 Pennsylvania Avenue
Wilmington, Delaware 19806

Communaute Europeenne
de L'Energie Atomique
Ispra Research Center
Casella Postale No. 1
Ispra (Varese), Italy

4 Attn: H. Hannaert

1 W. G. Burns
Atomic Energy Research Est.
Radiation Chemistry Building 146
Harwell, Didcot
Berkshire, United Kingdom

1 P. A. Houllier
Laboratoire Central
de Recherches Progil
10 Quai du Commerce
(Boite Postale 105)
Lyon-Vaise, France

1 P. Leveque
Chef du Service de Physico-
Chimie Appliquee
CEA Centre d'Etudes Nucleaires de Saclay
Boite Postale No. 2
Gif-sur-Yvette (Seine-et-Oise)
France

1 J. R. Puig
CEA Centre d'Etudes Nucleaires de Saclay
Boite Postale No. 2
Gif-sur-Yvette (Seine-et-Oise)
France

1 E. Proksch
Reactorzentrum Seibersdorf
Lenaugasse 10
Wien VIII, Austria

1 R. Pointud
DPC/PCA
Centre d'Etudes Nucleaires de Grenoble
Boite Postale No. 269
Chemin des Martyrs 38
Grenoble, France

Chalk River Nuclear Laboratories
Atomic Energy of Canada, Ltd.
Chalk River, Ontario, Canada

2 Attn: W. M. Campbell

1 Attn: A. W. Boyd

1 Attn: S. R. Hatcher

Whiteshell Nuclear Research Est.
AECL
Pinawa, Manitoba, Canada

3 Attn: R. F. S. Robertson

1 Attn: M. Tomlinson

A7.6

1 G. Juppe
Chemistry Department
Euratom CCR
Casella Postale No. 1
Ispra (Varese), Italy

APPENDIX 8

NOMENCLATURE

A = constant.

A = inside surface area of test heater wall, ft^2.

A_i = atomic or molecular weight of species i.

a = constant.

a_i = constant.

B = per cent Bottoms, w/o.

b = constant.

b_i = constant.

C, C_i, C_{omp} = concentration of component i in a mixture, wt % or weight fraction. Subscript i refers most frequently to ortho-, meta-, para- or total terphenyl.

C_i^f, C_{omp}^f = concentration of component i or concentration of total terphenyl in the feed, weight fraction.

$C_{i,j}$ = concentration of component i in sample j, weight fraction or w/o.

$\overline{C}_{omp}$ = total terphenyl concentration near the mid-point of a transient determined as that concentration where both first- and second-order kinetics correlations give the same value for the total degradation rate, $-dC_{omp}/d_\tau$, weight fraction.

C_p = specific heat of material, cal/(gm)(°C).

c = constant.

DP = degradation products. That fraction of the irradiated coolant which is not terphenyls.

d = constant.

E = neutron energy, ev or Mev.

E_c = cadmium cutoff energy, ev.

E_{eff} = effective threshold energy of a threshold detector, Mev.

E_{th} = actual threshold energy of a threshold detector, Mev.

ΔE = activation energy, kcal/mole.

e = constant.

F, F_T = total in-pile dose rate factor, (watt)(hr)(cm^3)/(MWH)(gm).

F_N = in-pile dose rate factor due to fast neutron interactions, (watt)(hr)(cm^3)/(MWH)(gm).

F_γ = in-pile dose rate factor due to gamma-ray interactions, (watt)(hr)(cm^3)/(MWH)(gm).

f_N = fraction of absorbed dose due to fast neutron interactions.

f_γ = fraction of absorbed dose due to gamma-ray interactions.

$G_R(-i)$ = radiolytic decomposition yield of component i in the coolant, expressed as molecules of component i degraded/100 ev absorbed in the total coolant, where i refers to ortho-terphenyl (o-$\emptyset_3$), meta-terphenyl (m-$\emptyset_3$), para-terphenyl (p-$\emptyset_3$), or total terphenyl (omp).

$G(\rightarrow HB)$ = radiolytic production yield of HB in the coolant, expressed as equivalent molecules of omp degraded to form HB/100 ev absorbed in the total coolant.

$G(\rightarrow LIB)$ = radiolytic production yield of LIB in the coolant, expressed as equivalent molecules of omp degraded to form LIB/100 ev absorbed in the total coolant.

$G(-i)$ = total experimental G value, molecules of component i degraded/100 ev absorbed in the total coolant.

$G^*(-i) = G(-i)/C_i$.

$G_N(-i)$ = decomposition yield of component i in the coolant for fast neutron interactions.

$G_\gamma(-i)$ = decomposition yield of component i in the coolant for gamma-ray interactions.

$G^o_\gamma(-i)$ = initial decomposition yield of component i in the coolant for gamma-ray interactions (i.e., at 100% terphenyl concentration).

g_i = average fraction of neutron energy lost per collision with nuclide i, equal to $2A_i/(A_i + 1)^2$. Subscript i refers to hydrogen (H), carbon (C), beryllium (Be) or aluminum (Al).

HB = high boilers. Those fractions of irradiated coolant having higher boiling points than that of para-terphenyl.

h, h_f = film coefficient of convective heat transfer, Btu/(hr)(ft^2)(^oF).

h_s = scale coefficient of heat transfer, Btu/(hr)(ft^2)(^oF).

I_i = energy transfer integral for nuclide i, watts/atom. Subscript i refers to hydrogen (H), carbon (C), beryllium (Be) or aluminum (Al).

K = constant.

$K_n(-i)$, $K_{i,n}$ = overall rate constant for disappearance of component i in a transient run determined by n^{th} order kinetics, gms/watt-hr.

$K'_n(-i)$, $K'_{i,n}$ = overall rate constant for disappearance of component i in a transient run determined by n^{th} order kinetics, hr^{-1}.

k_R^o = constant.

k = thermal conductivity of the irradiated coolant, cal/(cm)(sec)(°C).

$k_{R,omp,n}$ = n^{th} order radiolysis reaction rate constant for total terphenyl (omp) in the coolant, gm/(watt)(hr).

$k_{R,i,a+b}$ = radiolysis reaction rate constant for component i (terphenyl isomer) for kinetics order a for component i and kinetics order a+b for total terphenyl, gms/watt-hr.

$k_{P,omp,m}$ = m^{th} order thermal decomposition reaction rate constant for total terphenyl (omp) in the coolant, hr^{-1}.

$k_{P,i,c+d}$ = thermal decomposition reaction rate constant for component i (terphenyl isomer) for kinetics order c for component i and kinetics order c+d for total terphenyl, hr^{-1}.

L = length of test heater, inches.

L_L = distance of the bottom of the in-pile capsule from the reactor core center, inches.

L_U = distance of the top of the in-pile capsule from the reactor core center, inches.

L_T = distance of the top of the in-pile assembly from the reactor core center, inches.

LIB = low and intermediate boilers. Those fractions of the irradiated coolant having boiling points equal to or less than those of the terphenyls (w/o DP - w/o HB = w/o LIB).

M = mass of coolant, grams.

M_j = mass of coolant in the j^{th} sample, grams.

M, M_L, M_{loop} = circulating mass of coolant in the loop, grams.

M_c = coolant mass in the reactor core, lbs.

M_N = coolant mass contained in Zone N of the coolant loop, lbs.

MW_N = number average molecular weight, grams/gram mole.

MWH = period of reactor operation, megawatt-hours.

m = kinetics order of pyrolysis or radiopyrolysis.

N = designated zone of the coolant loop.

N_i = number of atoms per gram of nuclide i.

Nu = Nusselt number = $h\hat{D}/k$.

n = kinetics order of radiolysis.

OMP, omp = ortho-, meta-, and para-terphenyl.

P, P_o = reactor power level, MW.

Pr = Prandtl number, $C_p\mu/k$.

p = constant.

Q_{in} = net heat input to coolant in a half section of a test heater, watts and Btu/hr.

q = constant.

q_c = fraction of the total thermal power of the reactor absorbed in the coolant.

R = universal gas constant, kcal/(gram mole)(^oR).

Re = Reynolds number, $DV\rho/\mu$.

R_T^j = total dose rate in material j, watts/gm. Subscript j refers to Santowax OMP (SW), polyethylene (PE), polystyrene (PS), carbon (C), beryllium (Be) or aluminum (Al).

R_N^j = fast neutron dose rate in material j, watts/gm.

R_γ^j = gamma ray dose rate in material j, watts/gm.

R_{th}^j = thermal neutron dose rate in material j, watts/gm.

R_{Cd} = cadmium ratio.

$\bar{r}$ = average dose rate, watts/gm = $d\tau/dt$.

S = conversion factor, 1.6×10^{-43} $(cm^2)(watt)(sec)/(barn)(ev)$.

T = termperature, ^oF and ^oR.

T_o = reference point temperature, ^oF, ^oR, ^oK.

T_B = bulk temperature of coolant in test heater, ^oF.

T_{lower} = lowest temperature in a variable temperature zone, N, of the coolant loop, ^oF.

$T_{w,i}$ = average inside wall surface temperature, ^oF.

t = time.

t = Student's t.

U = heat transfer coefficient, Btu/(hr)(ft^2)(^oF), from inside test heater wall to bulk coolant.

V = velocity, ft/sec.

W_T = total degradation rate for terphenyl, lbs/hr or gms/hr.

W_R = radiolysis degradation rate for terphenyl, lbs/hr or gms/hr.

W_P = radiopyrolysis degradation rate for terphenyl, lbs/hr or gms/hr.

W_i = total mass of terphenyl or terphenyl isomer degraded, or HB produced, grams or lbs.

w_i = organic coolant feed rate to the system, grams/hr or lbs/hr.

w/o = weight per cent.

X = volume per unit length of in-pile capsule, cc/inch.

X_j = j^{th} data point for independent variable.

$\overline{X}$ = weighted mean of X_j values.

y = surge tank gauge glass level, inches.

β = beta radiation.

γ = gamma radiation.

Δ = correction factor for G value calculations in steady-state-HB periods, grams.

δC = change in terphenyl concentration ($C_1 - C_2$) during steady-state, weight fraction.

δM = change in circulating coolant mass ($M_1 - M_2$) in the loop during steady-state, grams.

μ = viscosity, centipoises (cp).

μ_o = constant, cp.

μ_1 = constant, cp.

μ_B = bulk liquid coolant viscosity, cp.

μ_W = coolant viscosity measured at the inside test heater wall temperature, cp.

ρ = density, gm/cc.

Σ = summation sign.

σ, σ^2 = standard deviation and variance, respectively.

σ = neutron cross section, barns.

σ_s = elastic scattering neutron cross section, barns.

$\overline{\sigma_{eff}}$ = effective threshold neutron cross section, barns.

σ_{res} = resonance component of neutron cross section, barns.

$\sigma_{1/v}$ = 1/v component of neutron cross section, barns.

σ_{2200} = 2200 meter/sec neutron absorption cross section, barns.

τ = specific dose absorbed by irradiated coolant, watt-hr /gm coolant.

$\phi(E)$ = neutron flux per unit energy, $n/(cm^2)(sec)(ev)$.

$\phi(\geq E)$ = integrated fast neutron flux above energy E, $n/(cm^2)(sec)$.

ϕ_o = epithermal neutron flux constant, $n/(cm^2)(sec)$.

ϕ_{2200} = 2200 meter/sec neutron flux, $n/(cm^2)(sec)$.

~ = approximately.